Voraussetzungen und Variationen der Informationsintegration im menschlichen Gehirn – Verknüpfung von externen und internen Informationen zur Verbesserung der Mensch-Umwelt-Interaktion

Habilitationsschrift

zur Erlangung des akademischen Grades

Doctor rerum naturalium habilitatus (Dr.rer.nat.habil.)

Genehmigt durch die Fakultät für

Naturwissenschaften

der Otto-von-Guericke-Universität Magdeburg

von Dr. rer. nat. Stefan Dürschmid

geb. am 26.08.1979 Magdeburg

Gutachter

Prof. Dr. Hermann Hinrichs

Prof. Dr. Dirk Ostwald

Prof. Dr. Niko Busch

Magdeburg, den 29.06.22

Inhaltsverzeichnis

Vorbemerkung

Die vorliegende Habilitationsschrift gibt einen Überblick über eine Reihe von Studien, die sich im engeren bzw. weiteren Sinne mit den unterschiedlichen Mechanismen der Informationsintegration im menschlichen Gehirn beschäftigen. Betrachtet wird insbesondere, wie mit zunehmender Komplexität der Mensch-Umwelt-Interaktion Informationen aus unterschiedlichen externen und internen Informationsquellen integriert werden. Entscheidender Marker der Informationsintegration sind generell oszillatorische Prozesse und im Besonderen Muster hochfrequenter Aktivität (HFA) im menschlichen Gehirn. Dies erscheint besonders relevant, da das Verständnis von Informationsintegration Rückschlüsse auf die Funktionsweise zugrundeliegender Prozesse auf neuronaler Ebene ermöglicht. An der Entstehung der Originalarbeiten waren eine Reihe von Kolleginnen und Kollegen beteiligt, denen ich nachfolgend ganz herzlich danken möchte.

Zusammenfassung

Die Neurowissenschaften untersuchen Mechanismen, wie das Gehirn externe Umweltreize oder aber auch interne Signale (Ignacio Rebollo et al., 2018) verarbeitet. Bei den meisten, wenn nicht allen Ansätzen der neuronalen Informationsverarbeitung impliziert der Begriff der Verarbeitung, dass die unterschiedlichen Informationen in solcher Weise zu einer Einheit aufeinander abgestimmt werden (Integration), die es uns Menschen erlaubt optimal zu handeln. Dabei geht es in erster Linie um eine abstrakte Repräsentation durch die Assoziation unterschiedlicher Merkmale verschiedener Signale zu einem neuen Signal (Mudrik et al., 2016). Diese Informationsintegration findet sich auf einer Vielzahl von zeitlichen und räumlichen Skalen einerseits und kognitiven Ebenen andererseits wieder.

In der vorliegenden Habilitationsschrift werde ich exemplarisch zeigen, auf welchen neurophysiologischen und kognitiven Ebenen Informationsintegration stattfindet. Die Funktionsweise des menschlichen Gehirns beruht dabei auf der elektrischen Aktivität von Neuronen. Die HFA in makroskopischen Messungen wie dem MEG oder ECoG können als lokaler Index funktionaler selektiver Aktivität angesehen werden. Vor allem die HFA reflektiert die Fähigkeit des Gehirns zur Selbstorganisation, die es erlaubt Informationen optimal über die Zeit und unterschiedliche Kortexbereiche weiterzuleiten. Dies kann als Voraussetzung für die Informationsintegration gesehen werden. Diese Gehirnaktivität ist darüber hinaus essentiell für die Integration von Informationen, um optimale Entscheidungen zu treffen. Weiterhin wird in der Arbeit dargestellt, dass auf kortikaler und subkortikaler Ebene Vorhersagefehler generiert werden, die zeigen, dass das Gehirn durch Informationsintegration über die zeitliche Dimension ein internes Modell über die Umwelt generiert auf dessen Basis wiederum Vorhersagen getroffen werden. Kommen aktive motorische Handlungen, die mit den Umweltinformationen koordiniert werden müssen, dazu, kann in dieser Arbeit wiederum auf kortikaler und subkortikaler Ebene Integration von lokalen Informationen in funktionelle globale Netzwerke gezeigt werden, die mit den kognitiven Anforderungen variiert. Auf einer weiteren Ebene zeige ich in dieser Arbeit, wie Informationsintegration stattfindet, wenn zur Koordination von Umwelt und Handlungen noch selbst generierte Informationen, wie der Abruf von Gedächtnis während des *mind wanderings*, verarbeitet werden.

Zusammengenommen legen diese möglichen Einflussfaktoren nahe, dass die menschliche Informationsintegration ein multifaktorielles Geschehen ist, welches sich auf unterschiedlichen

Ebenen manifestiert und reziprok mit einer Vielzahl neuronaler Strukturen und Prozesse verbunden ist.

1. Einleitung

Die Menschen hätten nicht in diesem Maße die Welt gestalten können, wie wir sie heute kennen, wenn sie auf die Erfordernisse in der Umwelt nur im Nachhinein reagieren können: die Anpassung des Menschen wäre ein ausschließlich reflexiver Prozess. Jedoch haben sie gelernt Umweltereignisse so optimal zu verarbeiten, sie miteinander zu vergleichen und vorherzusehen, um schon im Vorfeld Handlungsoptionen zu überdenken, um sich optimal verhalten zu können. So reagieren wir schneller und genauer auf vorhersagbare Reize (Anllo-Vento, 1995; Desimone, 1995). Menschen müssen daher die Fähigkeit besitzen, Informationen zu einem bestimmten Zeitpunkt aus der Umwelt aufzunehmen aber auch Regelmäßigkeiten in der Umwelt fortlaufend zu erfassen und daraus Vorhersagen abzuleiten, um überleben zu können. Dabei können sich Regelmäßigkeiten in der Umwelt über zeitlich kurze (z.B. in Melodien innerhalb von wenigen Sekunden) als auch lange Intervalle (z. B. Veränderung über den Tag) erstrecken, die wir erfassen können. Menschen müssen, um mit der Umwelt optimal interagieren zu können, Informationen aufnehmen, verarbeiten, weiterleiten und mit bestehenden Informationen optimal verknüpfen. Dabei ist die Informationsintegration ein rekursiver Prozess, da jeder dieser Aspekte einerseits Integration voraussetzt und wiederum entscheidender Bestandteil der Informationsintegration ist.

In der vorliegenden Habilitationsschrift werden Prinzipien der Informationsintegration auf diesen unterschiedlichen Ebenen betrachtet und hinsichtlich ihrer Relevanz für menschliche Kognition beleuchtet. Zentraler Punkt hierbei ist, wie neuronale Aktivität, welche in allen Studien anhand hochfrequente Aktivität (80-250Hz) im menschlichen Kortex untersucht wird, diese Informationsintegration reflektiert. Dabei orientiert sich der Aufbau der Arbeit an den unterschiedlichen konzeptionellen Ebenen, auf welchen Informationsintegration im Gehirn zu finden ist. Am Anfang steht dabei die Frage, wie das menschliche Gehirn in Ruhe, ohne Einflüsse von außen Informationseinheiten zusammenfasst (geclustert) und weiterleitet (2.1 – Kritikalität). Danach wird der Frage nachgegangen, wie Informationen zu einer subjektiven Einschätzung verknüpft werden (2.2 – Delay Discounting) gefolgt von der Untersuchung, wie Informationen verknüpft werden, um zu einer objektiven Einschätzung über Regelmäßigkeiten in der Umwelt zu gelangen (2.3 – Erkennung von Abweichungen). Während die Experimente innerhalb der ersten Schwerpunktthemen keiner Reaktion auf die Umwelt bedürfen, geht es im Weiteren darum zu erfassen, wie Prozesse der Informationsintegration ablaufen, wenn wir auf die Umwelt bezugnehmen müssen (2.4 – motorisches Lernen) und wie diese Prozesse verändert sind, wenn sich das Gehirn auf sich selbst bezieht, obwohl es auf die Umwelt reagieren muss (2.5 – Mind Wandering). Das Konzept der Arbeit besteht also darin, zu zeigen welche Integrationsmechanismen bestehen, wenn zunehmend mehr Informationen aufeinander abgestimmt werden müssen: Ruhe – passive Verarbeitung von Umweltreizen – aktive Koordination von Bewegungen mit Umweltreizen – Kontrolle über

diese Koordination während die Gedanken abschweifen. Ein grundlegender Baustein in all diesen Studien ist dabei selbstreferentielle Kognition, die diese Integrationsmechanismen ermöglichen: Achtsamkeit – Selbst-Awareness – Vorhersagen aus einem internen Modell – Ausrichtung eigener motorischer Handlungen aus einem internen Modell – Verarbeitung von episodischen Gedächtnisinhalten. In den folgenden Kapiteln werden zunächst Prinzipien der Informationsintegration vorgestellt und mit welchen Messmethoden diese erfasst werden.

1.1 Formalisierung der Informationsintegration im Gehirn

Weiterleitung von Information über den Kortex

Im folgenden Abschnitt stelle ich eine Voraussetzung für effektive Informationsintegration – die Kritikalität – vor. Die Funktionsweise des menschlichen Gehirns beruht auf der elektrischen Aktivität von Milliarden von Neuronen, die über multiple räumliche und zeitliche Skalen koordiniert werden. Theoretische und experimentelle Arbeiten der Physik haben gezeigt, dass die Multiskalierungs-Dynamik komplexer Systeme durch räumliche und zeitliche Statistik z. B. von sich verzweigenden Lawine charakterisiert werden kann. Eine Lawine meint dabei das zusammenhängende ablaufende Auftreten von Events (z.B. Aktionspotentiale einzelner Neurone) über verschiedene Gehirnareale ohne eine zeitliche Unterbrechung. Diese Statistiken legen offen, ob ein System in einem zufälligen, geordneten oder *kritischen* Zustand ist. Letzteres bezeichnet einen komplexen Zustand an der Grenze zwischen Ordnung und Unordnung (Bak, 1996; Cocchi et al., 2017). Empirisch wurden kritische Lawinendynamiken in neuronalen Netzwerken zum ersten Mal in Zellkulturen und in vitro Schichten gezeigt (Beggs and Plenz, 2003). Am kritischen Punkt sind Netzwerkfunktionen hinsichtlich der Empfänglichkeit für Inputs, der dynamischen Bandbreite von Input/Output Beziehungen, Informationsübertragung und Informationskapazität (Shew and Yang, 2009; Shew, 2012) optimal. Neuronale Netzwerke werden dabei flexibler und adaptieren einfacher (Arcangelis and Herrmann, 2010). Somit wäre Informationsverarbeitung optimiert, wenn die Dynamik des Netzwerkes am kritischen Punkt operiert (Beggs and Timme, 2012).

Integration von zeitgleichen Handlungsoptionen

Um eine optimale Mensch-Umwelt-Interaktion zu erzielen, bedarf es in manchen Situationen einer optimalen Verknüpfung von Umweltereignissen, die gleichzeitig auftreten aber in gewisser Weise konkurrieren. Diese Verknüpfung von Informationen aus der Umwelt kann beson-

ders im Zusammenhang mit Entscheidungen untersucht werden, wobei ein Kompromiss zwischen dem Belohnungswert und dem Zeitpunkt, zu dem die Belohnung ausgezahlt wird, gefunden werden muss. Der Wert einer Belohnung sinkt mit der Zeit: je länger wir warten müssen, desto weniger ist uns die Belohnung wert. Daher verwandelt eine verzögerte Auszahlung einen objektiven Wert in einen wahrgenommen geringeren Wert. Das führt dazu, dass kleinere aber frühere Belohnungen (smaller sooner – SS) größeren aber späteren Belohnungen (larger later – LL) vorgezogen werden. Dies wird als *Delay Discounting* (DD) oder intertemporale Wahlmöglichkeiten bezeichnet. Impulsive Entscheidungen könnten durch die Tendenz begründet werden, dass SS gegenüber LL Belohnungen vorgezogen werden.

Integration von Wahrscheinlichkeiten von Umweltreizen.

Im nächsten Schritt stelle ich Arbeiten vor, die untersuchen, wie das menschliche Gehirn Informationen über längere Zeitintervalle zu einem internen Bild über die Umwelt integriert. *Predictive Coding* (PC) Theorien postulieren, dass neuronale Netzwerke im Gehirn Regularitäten in der Umwelt fortlaufend lernen. Aus diesen gelernten Regularitäten werden Vorhersagen abgeleitet, die dann mit den tatsächlichen Ereignissen in der Umwelt verglichen werden (Rao and Ballard, 1999). Stimmen Vorhersage und Umwelt zu einem Zeitpunkt nicht überein, sendet das Gehirn ein Fehlersignal (*predicition error; PE*), dass eine sensorische Abweichung stattgefunden hat (SanMiguel et al., 2013). Dieser Vorhersagefehler zeigt sich als Mismatch Negativity. Diese über das EEG definierte Komponente reflektiert den Unterschied in der relativen Wahrscheinlichkeit, wie häufig Ereignisse in der Umwelt in der Vergangenheit auftraten. Die Erforschung dieses internen Modells zielt deshalb häufig auf Gehirnprozesse ab, die die Integration von Wahrscheinlichkeit von bestimmten sensorischen Reizen über einen längeren Zeitraum widerspiegeln. Dabei stellt sich die Frage, ob und wie das Gehirn Vorhersagen trifft und wie diese neuronal verankert sind.

Diese Frage wird wissenschaftlich häufig mit dem sogenannten oddball-Paradigma untersucht. In der auditorischen Modalität wird ein sensorisches Gedächtnis für häufige Standardtöne aufgebaut, das wiederum durch zufällig eingestreute Devianten verletzt wird, die sich in der Tonhöhe (Frequenz) von den Standardtönen unterscheiden. Bei EKPS, die auf Devianten und Standards folgen, sieht man dabei eine Differenz zwischen der Amplitude, was als *Mismatch Negativity* (MMN) bezeichnet wird. Wie erwähnt, wird die MMN als Korrelat für die automatische Erkennung von Veränderungen in der akustischen Umwelt (Lindín et al., 2013) und als klassischer PE während des passiven Zuhörens gesehen (Näätänen et al., 1978). Die MMN ist als Differenzwelle definiert, wobei die Amplitudenmodulation auf den häufigen Standard von der erhöhten Amplitudenmodu-

lation der seltenen Devianten subtrahiert wird. Um eine Veränderung zu entdecken ist es notwendig, Informationen über die nähere Vergangenheit gesammelt zu haben oder einen Vergleich zwischen dem einkommenden Reiz und einer sensorischen Gedächtnisspur vorzunehmen. Als solche wird angenommen, das die MMN die Speicherung von Informationen im sensorischen Gedächtnis (Gaeta et al., 1999; Pekkonen et al., 2001) und die Geschwindigkeit der akustischen sensorischen Diskrimination (Engeland et al., 2002) reflektiert.

Integration von Umweltreizen und motorischen Handlungen

Auf einer höheren Komplexitätsstufe müssen Vorhersagen mit motorischen Handlungen verknüpft werden. Kopplung von Phase und Amplitude über unterschiedliche Frequenzbänder (Phase-amplitude cross-frequency coupling - PAC) von Oszillationen werden als effektiver Mechanismus angesehen, lokale Netzwerke zu rekrutieren, um funktionale globale Netzwerke zu formen und Informationen anzusteuern (Buzsaki and Draguhn, 2004; Canolty et al., 2006; Cohen et al., 2009; Staudigl et al., 2012). (Tort et al., 2008) zeigten transiente θ-Phase-HFA Kopplung im Striatum von Ratten während der Bewegung durch ein Labyrinth. Außerdem demonstrierten (Tort et al., 2009a) eine funktionelle Verbindung zwischen einer Leistungsverbesserung und der Stärke der θ-HFA Kopplung während des Lernens. Jedoch fehlt bisher der Nachweis, ob dieser Mechanismus auch bei Menschen zu beobachten ist. Darüber hinaus konnte PAC zwischen HFA (80-150Hz) und der θ (4-8Hz) Phase auch bei Menschen (Canolty et al., 2006) gezeigt werden. Desweiteren zeigen neuere klinische Studien eine Verbindung zwischen veränderter PAC und psychiatrischen und motorischen Störungen (Uhlhaas and Singer, 2010; Allen et al., 2011; Crowell et al., 2012; De Hemptinne et al., 2013). Außerdem tritt PAC bei Sprach- und motorischen Aufgaben auf (Canolty et al., 2006; Canolty and Knight, 2010) und die Frequenz der langsamen Oszillation ist aufgabenabhängig (Voytek et al., 2010). Jedoch außerhalb klinischer Studien sind Hinweise für eine funktionelle Rolle von PAC im Prozess der Organisation von Kognition und Verhalten von Menschen begrenzt auf die Domäne des Gedächtnisses. Axmacher et al (Axmacher et al., 2010b) berichteten, dass inter-individuelle Unterschiede in der Arbeitsgedächtnisleistung mit Unterschieden im PAC korrelieren, was eine funktionelle Relevanz von PAC für Gedächtnisprozesse unterstreicht. Tort et al (Tort et al., 2009b) untersuchten die dynamische Modifikation funktioneller Beziehungen zwischen Performanz und PAC im Hippocampus von Ratten und fanden, dass die Kopplungsstärke zwischen θ und γ (25-100Hz) mit dem Lernen im Labyrinth korreliert.

PAC beschreibt die Abhängigkeit der Amplitude einer hohen Frequenz von der Phase einer niedrigen Frequenz. Bei Ratten und Mäusen besteht eine enge Verbindung zwischen der Phase des theta Bandes (θ), des lokalen Feldpotentials (LFP) und Einzelzellaktivität (SUA – engl. Single unit

activity) (Chrobak and Buzsa, 1998; Sirota et al., 2003; Siapas et al., 2005) was es Neuronen vermutlich erlaubt, größere Neuronenverbände durch transiente Kopplung zu bilden (Chrobak and Buzsa, 1998). Diese Studien legen nahe, dass die Interaktion zwischen dem PFK und dem HC über PAC stattfindet. (O'Donnell and Grace, 1995) zeigten, dass die hippocampale Hyper- und Depolarisation zur Hyper- und Depolarisation des Nucleus Accumbens (NAcc) führt. Während der Depolarisation steigt die Wahrscheinlichkeit, dass Neuronen des NAcc als Antwort auf PFK Stimulation feuern (French and Totterdell, 2002; Goto and Grace, 2008). Dies liefert Hinweise für PAC mit einer Erhöhung der HFA an den Senken der θ Aktivität.

Integration von Umweltinformationen während des Mind Wanderings

Zusätzlich zu alle diesen Integrationsprozessen haben Menschen die Tendenz während des Alltages mit Gedanken zu episodischen Gedächtnisinhalten zu wandern. Wie schafft es aber das Gehirn entgegen diesen zusätzlichen Informationen Informationsintegration fortzuführen, obwohl wir während einer experimentellen Aufgabe mit unseren eigenen Gedanken beschäftigt sind und damit in einen Zustand erhöhten Bewusstseins für uns selbst übergehen? Diese Frage ist besonders wichtig, da während der Zeit des Mind-Wanderings bestimmte Verhaltensmasse eine Verschlechterung zeigen. Diese Phasen der Bewusstseinsschwankungen müssen daher überwunden werden. Bisherige Studien gehen davon aus, dass die Aufmerksamkeit auf externe Reize und damit einhergehend sensorische Antworten reduziert werden. Jedoch ist dies bisher nicht explizit getestet worden. Hierbei benutzen wir ein klassisches Paradigma, das eine EEG Komponente erzeugt, die in einer Vielzahl von vorherigen Studien als Indikator für räumliche Aufmerksamkeitsverlagerung gefunden wurde.

1.2 Untersuchungsmethoden

In dieser Habilitationsschrift werden unterschiedliche Originalarbeiten vorgestellt, in denen unterschiedliche Messmethoden zum Einsatz gekommen sind. Dabei wurden sowohl nichtinvasive als auch invasive Aufnahmetechniken bei unterschiedlichen Probandengruppen eingesetzt und analysiert.

Nicht-invasive Messungen

Magnet- und Elektroenzephalographie

Das MEG detektiert Veränderungen im magnetischen Feld von Neuronen, welche durch neuronale Aktivität entstehen, die durch Ionen generiert wird, die einem Gradienten innerhalb des neuronalen Dipols folgen (Hämäläinen et al., 1993). Der elektrische Fluss generiert ein elektrisches Potential vertikal zum Dipol, dessen Veränderungen mit dem EEG gemessen werden können. Gleichzeitig entsteht ein magnetisches Feld horizontal zum Dipol, dessen Veränderungen mit dem MEG gemessen werden können. Aktivierung des neuronalen Dipols verändert den Ionenstrom innerhalb des Dipols und darum das elektrische Potential und das begleitende Magnetfeld außerhalb des Dipols. Sowohl MEG als auch EEG zeichnen sich im Vergleich mit dem fMRT durch eine hohe zeitliche Auflösung auf. Beide haben zudem eine hohe spektrale Auflösung. Jedoch erfasst das MEG im Wesentlichen tangential orientierte Dipole, die in den Sulci liegen, während das EEG zusätzliche radiale Dipole erfasst. Anders als beim EEG tragen Volumenströme kaum zum gemessenen Signal im MEG bei, was zu einer höheren räumlichen Auflösung führt aus der sich auch eine größere Sensitivität für die HFA ergibt. Der Vorteil des EEG liegt in der Tatsache, dass es transportabel ist und wesentlich billiger in der Anschaffung ist. Der grundlegende Mechanismus des MEG besteht darin, dass es schwache magnetische Felder des Gehirns erfassen kann. Die Signale des Gehirns, die mehr als eine Milliarde mal kleiner als die Stärke des Erdmagnetfeldes sind, werden mit sogenannten Superconducting Quantum Interference Devices (SQUIDs) erfasst. Die SQUIDs sind in eimem Helm fest integriert und werden mit flüssigem Helium gekühlt, um die Supraleitfähigkeit herzustellen. Die vom Gehirn erzeugten Magnetfeldänderungen induzieren einen elektrischen Strom im SQUID, ähnlich wie in einer Spule. Die Sensorfelder, die jeweils aus einem Magnetometer und zwei Gradiometern bestehen, sind systematisch über dem gesamten Helm verteilt, sodass eine Rekonstruktion der Signalquellen möglich ist. Dieses Triple-Sensor Design erhöht das Signal-zu-Rauschen Verhältnis und ermöglicht die Aufnahme von hochfrequenter Aktivität.

Invasive Messungen

Elektrokortikographie (ECoG) und Tiefe-Hirnstimulation (DBS)

Im Kontext von invasiven Messungen sind die untersuchten Gruppen von Studienteilnehmern durch die Ziele der klinischen Diagnose und Therapie vordefiniert, da invasive Aufnahmen nur im klinischen Kontext durchgeführt werden können und somit Teil einer Behandlung von Erkrankungen des Gehirns sind. ECoG Messungen werden daher vorrangig bei Patienten mit Epilepsie erhoben. Bei der Epilepsie handelt es sich um eine neurologische Erkrankung, die sich durch rezidivierende epileptische Anfälle auszeichnet. Liegt bei einem Patienten eine medikamentöse Therapieresistenz vor (zwei passende Medikamente in angemessener Dosierung bringen keine Anfallsfreiheit) vor, ist die Abklärung einer möglichen epilepsiechirurgischen Behandlung schnellstmöglich indiziert. Bei der können in bestimmten Situationen mittels intrakraniellem EEG (iEEG) EEG-Elektroden in einem stereotaktisch-neurochirurgischen Eingriff direkt entweder subdural auf den Kortex (ECoG) oder in tiefere Areale (Tiefenelektroden) in das Gehirn gebracht werden. Auf diese Weise ist es möglich, Aktivierungen von Neuronenpopulationen mittels Makroelektroden mit einer höheren Auflösung als beim herkömmlichen EEG zu messen. Bei einem solchen Eingriff handelt es sich um ein invasives Verfahren mit dem Risiko von Komplikationen, die allerdings durch die wachsende Erfahrung mit den Eingriffen über die letzten Jahre seltener werden und häufig zeitnah sistieren (Gonzalez-Martinez et al., 1982, 2014). Subdurale Elektroden sind in Grids angeordnet, also Streifen mit mehreren Elektroden in meist einer oder zwei Reihen, die in einer dünnen Schicht aus speziellem Silikon eingebettet sind (Önal et al., 2003).

Bei Epilepsiepatienten werden also Elektrodengitter implantiert, um den Fokus des pathologischen Gewebes zu lokalisieren. Dies wird getan, um im Anschluss das neuronale Gewebe, dessen abnormale Aktivität für die Entstehung des klinischen Bildes, das die Patienten zeigen, verantwortlich ist, zu resezieren. In der Regel befinden sich die Patienten für eine Dauer von zwei
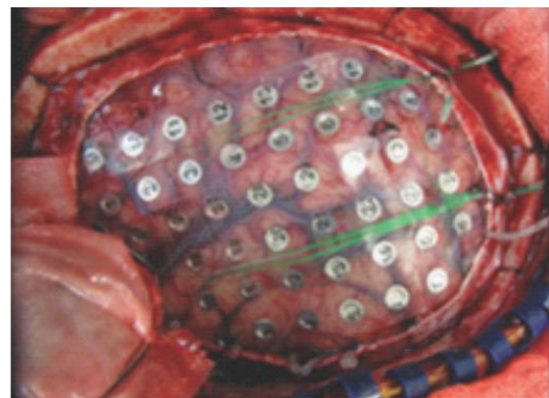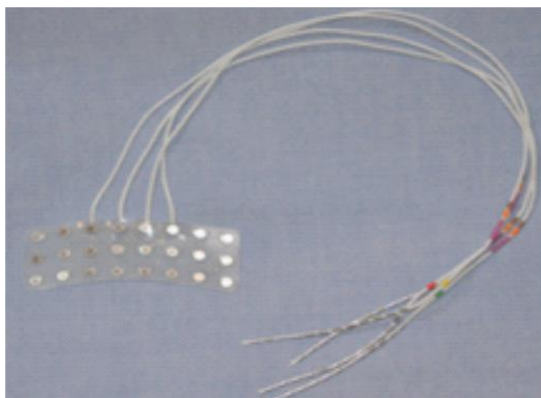

Abbildung 1. Intrakranielle Elektrophysiologie. (A) Beispiel eines 3 x 8 Grids mit Elektroden für subdurale Implantation. (B) Einsatz eines Grids intraoperativ bei Kraniotomie.

Wochen in stationärer Behandlung. Während dieser Zeit können die implantierten Elektroden genutzt werden, um die Aktivitätsveränderung von Neuronengruppen als Antwort auf experimentelle Bedingungen zu untersuchen.

Ein weiterer Ansatz ist die Tiefe-Hirnstimulation (deep brain stimulation – DBS), die bei unterschiedlichen neurologischen und psychiatrischen Störungen, wie der Epilepsie, Morbus Parkinson (Machado et al., 2012) oder Depression (Bewernick et al., 2010) eingesetzt wird. Die Stimulation des NAcc hat zum Beispiel den Effekt eines Antidepressivums und führt zu positiven Veränderungen klinischer Symptome (Bewernick et al., 2010). Ein therapeutischer Effekt der DBS lässt sich auch bei der Behandlung der Parkinson-Erkrankung (Parkinson disease – PD) finden. Bradykinesia als ein Symptom der PD konnte in früheren Studien durch die Stimulation des Ncl. Subthalamicus reduziert werden (Okun et al., 2012). Wie oben dargestellt können einige Patienten mit pharmakoresistenter Epilepsie mittels einer Resektion pathologischen Gewebes behandelt werden. Jedoch gibt es eine Gruppe von ungefähr 4% dieser Patienten, die keinen Behandlungserfolg durch diese Art von Behandlung zeigen, da der zu resezierende Fokus nicht lokalisiert werden kann (Ellis and Stevens, 2008). Bei diesen Patienten ist eine DBS von großer Bedeutung. Postoperativ können die Elektroden externalisiert werden, um sowohl elektrische Teststimulation mit unterschiedlichen Parametern aber auch die Aufzeichnung von Aktivität an den Kontakten während experimentalpsychologischer Aufgaben zu ermöglichen.

Diskussion der Messmethoden

Bei beiden invasiven Aufnahmetechniken, ECoG und DBS, ist die Datenaufzeichnung, während den Patienten ein experimentelles Paradigma präsentiert wird, ein nachrangiges Ziel. Daher ist bei dieser Art von Studien einerseits die Anzahl an Probanden reduziert und andererseits die untersuchten Gehirnregionen nach ihrem klinischen Interesse und nicht nach experimentellen Erwägungen ausgerichtet. Eine standardisierte Evaluation von Gruppeneffekten wie in EEG Studien ist daher nicht im gleichen Maße möglich, da alle Patienten unterschiedliche Elektrodenpositionen haben. Außerdem ist die räumliche Information knapp, da nicht der gesamte Kortex mit Elektroden erfasst werden kann. Dagegen ist die räumliche Auflösung im ECoG gegenüber dem EEG und MEG in dem umschriebenen Areal, in dem das Elektrodengitter liegt, sehr viel höher.

Die Vorteile von nicht-invasiven Aufnahmetechniken sind einerseits die größeren Gruppen von Probanden, die genutzt werden können und andererseits verfügen EEG und MEG über ein höheres Maß an Standardisierung, da Elektroden und Sensoren in vordefinierten Mustern über den Kortex verteilt sind (Jasper H H, 1958). Die invasiven Messmethoden können durch die di-

rekte Messung von Gehirnaktivität und geringer Überlagerung unterschiedlicher Quellen eine höhere spektrale Auflösung erzielen. Bei den nicht-invasiven Methoden dominieren die niedrigen Frequenzen, wogegen die hohen nur sehr selten erfasst werden können (Pfurtscheller and Cooper, 1975). Daher sind hohe Frequenzen wie Aktivitätsmuster zwischen 80-250 Hz am besten mit subduralen Aufnahmen auf Kosten kleinerer Probandengruppen zu erfassen. Jedoch sind EEG und MEG nicht gleichermaßen eingeschränkt. Während das EEG elektrische Potentiale erfasst, nimmt das MEG magnetische Signale des menschlichen Gehirns auf. Okada et al. (Okada et al., 1999) berichteten, dass zumindest oberflächennahe Quellen im MEG relativ unbeeinflusst durch den Schädel sind, sodass im MEG höhere Frequenzen besser erfasst werden als im EEG. Außerdem sind Lokalisationsfehler im MEG geringer als im EEG, da das EEG sowohl kortikale als auch subkortikale Quellen, wogegen das MEG vorzugsweise kortikale Quellen erfasst. Zusammengenommen kann man sagen, dass alle Messmethoden sehr verschiedene Vorteile haben, die durch eine optimale Kombination ausgenutzt werden können. Ein gemeinsames Merkmal all dieser Aufnahmetechniken ist, dass es sich hierbei um Zeitreihen handelt, die einen Gehirnzustand an aufeinanderfolgenden Zeitpunkten in hoch aufgelöster Weise definieren. Diese Messmethoden erfassen Gehirnprozesse mit hoher zeitlicher Auflösung. Sie eignen sich daher ideal, unterschiedliche Maße zu extrahieren, die den Grad an Informationsintegration definieren.

2. Wissenschaftliche Originalarbeiten

Im Detail zeigen die sich anschließenden Kapitel, welchen wissenschaftlichen Beitrag die einzelnen Studien leisten. Im ersten Teil wird untersucht, ob das Gehirn als ein sich selbst organisierendes System zu verstehen ist, das es ermöglicht, Informationen optimal zu verarbeiten. Informationsintegration meint dabei die Dynamik, mit der neuronale Aktivität über den Kortex weitergeleitet wird und verschiedene Kortexbereiche Aktivitätsmuster bündeln. Diese Ergebnisse wurden in *Dürschmid et al., 2020b (PLoS One)* veröffentlicht und zeigen, dass sich das Gehirn an einem optimalen Punkt für Informationsintegration befindet, wenn sich Menschen in einem Zustand hoher Achtsamkeit befinden.

Im zweiten Teil wird untersucht, wie aus objektiven Informationen über Belohnungen und deren Auszahlungszeitpunkt ein subjektiver Wert entsteht. Informationsintegration meint dabei, ob und wie der Wert und die Zeit innerhalb von Netzwerken gleichermaßen repräsentiert werden. Die Ergebnisse aus drei Studien wurden in *Dürschmid et al., 2020a (J Neurosci)* publiziert und zeigen, dass diese Netzwerkrepräsentation dann zu finden ist, wenn Menschen vor dem Hintergrund hoher Selbstwahrnehmung handeln.

Im dritten Teil werden Studien über die Erkennung von Abweichungen in der Umwelt zusammengefasst. Informationsintegration meint dabei das Erfassen von Wahrscheinlichkeitsverteilungen von Reizen in der Umwelt über die Zeit, welches erlaubt, dass wir Vorhersagen über die Auftretenswahrscheinlichkeit von zukünftigen Reizen treffen können. Ergebnisse über die Informationsintegration von Umweltreizen auf subkortikaler Ebene wurden in *Dürschmid et al. 2016 (Cerebral Cortex)* als auch in *Dürschmid et al. 2017 (EJN)* veröffentlicht. Diese Studien zeigen, dass subkortikale Areale Vorhersagefehler kodieren und an den Kortex weiterleiten und dass die richtige Funktionsweise subkortikaler Areale entscheidend für das sensorische Gedächtnis ist. Weiterhin konnten wir in *Dürschmid et al. 2016 (PNAS)* und *Dürschmid et al. 2019 (Cerebral Cortex)* anhand von kortikalen Aktivitätsmustern zeigen, dass eine zeitliche Informationsintegration zur Vorhersage von Umweltreizen im Gehirn repräsentiert ist, was als Voraussetzung für optimale Ausrichtung von Handlungen auf die Umwelt gewertet werden kann.

Im darauf folgenden vierten Schwerpunkt geht es um die Integration von Informationen aus der Umwelt mit motorischen Handlungen, die es erlaubt, zunehmend effektiver zu handeln. Vor dem Hintergrund motorischen Lernens wurde untersucht, wie neuronale Informationsintegration, wie die Kopplung zwischen unterschiedlichen Frequenzen, mit dem Lernen kovariiert. In *Dürschmid et al. 2014 (PLoS ONE)* und *Dürschmid et al. 2013 (Front Hum Neurosci)* zeigen wir, dass die Frequenzkopplung als ein wesentliches Maß für Informationsintegration mit dem Lernen variiert und zustandsabhängig ist.

Im letzten Schritt wird dargestellt, ob Informationsintegration weiterhin besteht, obwohl wir während einer experimentellen Aufgabe mit unseren eigenen Gedanken beschäftigt sind und damit in einen Zustand erhöhten Bewusstseins für uns selbst übergehen. Die Studienergebnisse sind in **Wienke et al. 2021 (Cerebral Cortex Communications)** veröffentlicht worden und zeigen, dass Informationsintegration dynamisch an Bewusstseinszustände angepasst wird. Diese Artikel geben zusammengenommen einen Überblick, welche Mechanismen der Informationsintegration im Gehirn zu finden sind und werden im Folgenden detailliert vorgestellt.

2.1 Kritikalität – Achtsamkeitsmeditation moduliert Gehirndynamik

Ob Kritikalität geeignet ist, um kognitive Gehirnfunktionen zu beschreiben ist noch nicht klar. Unterschiedliche Marker der Kritikalität, wie weitreichende Korrelationen in spontaner niederfrequenter (10 und 20 Hz) EEG Aktivität, wurden am Menschen untersucht (Linkenkaer-hansen et al., 2001). Beim Menschen wurde Kritikalität neuronaler Lawinen vergleichbar mit der Weiterleitung von Aktionspotentialen nur verlässlich im Ruhezustand gezeigt. Shriki et al. (Shriki et al., 2013) zeigten, dass makroskopische Lawinen über das gesamte Gehirn, die durch Senken und Spitzen der Breitband-MEG-Aktivität definiert werden, keine charakteristische Skalierung haben. Dies ist typisch für einen Systemzustand nahe dem kritischen Punkt. Jedoch bleibt die Physiologie neuronaler Lawinen auf einer makroskopischen Ebene unklar. Da Spitzen und Senken im MEG/EEG unterschiedliche Phasen von räumlich und zeitlich ausgedehnten oszillatorischen Generatoren reflektieren können, sollte die Rekonstruktion von Lawinen auf makroskopischer Ebene die Polarität und die Frequenz von Gehirnsignalen in Betracht ziehen, um überlagerte Quellen auseinanderzuhalten. Vor allem ist die funktionelle Relevanz der Kritikalität und ihre Rolle in der Kognition noch immer eine offen Frage.

Die meisten experimentellen Studien bei wachen, gesunden Probanden wurden unter Ruhe (resting) durchgeführt, da aufgabenbezogene Aktivität Nichtstationarität und Überlagerung von reiz- und antwortgetriebener Aktivität (Fagerholm et al., 2015) impliziert, für welche gegenwärtige statistische Analysen der Kritikalität nicht gut geeignet sind. Jedoch können menschliche Studienteilnehmer verbal instruiert werden, anhaltend ihre Dynamik des Ruhezustandes durch Selbstregulation zu verändern. Eine bekannte Selbstregulationstechnik ist die Achtsamkeitsmeditation, welche vermutlich Kritikalität induzieren kann. Während der Meditation wird die achtsame fokussierte Aufmerksamkeit (mindful focused attention – MFA) benötigt, um den Fokus über eine längere Zeit auf die Wahrnehmung zu richten. Dies reduziert den negativen Einfluss von Ablenkungen, während zur gleichen Zeit kognitive Kontrolle benötigt wird, um Phasen von Mind-Wandering (MW siehe unten) zu detektieren. Achtsamkeit (Meditation) und MW (Ruhezustand) können als gegensätzliche stationäre Hintergrundzustände angesehen werden, die von Aufmerksamkeitsnetzwerken beziehungsweise vom Default Mode Network vermittelt werden (Brewer et al., 2011). Bei der Untersuchung ist es wichtig, *state* und *trait* Veränderungen zu unterscheiden (Lazar et al., 2005; Pagnoni and Cekic, 2007). Bei trainierten Meditierenden könnte die Mediation weniger Mühe verlangen, was eine Veränderung hin zu einer subkritischen Dynamik erklären würde oder Meditationserfahrene könnten Schwierigkeiten dabei empfinden, während einer Ruhephase nicht zu meditieren (Cahn and Polich, 2009).

Im Folgenden werden frequenz- und polaritätsspezifische Analysen neuronaler Lawinen-dynamik zwischen Achtsamkeit und Ruhezustand verglichen. Um die zuvor genannten möglichen Konfundierenden zu vermeiden, wurde eine einfache Achtsamkeitsaufgabe bei Novizen genutzt. Da der menschliche Ruhezustand Kritikalität zeigt (Shriki et al., 2013) und MFA die Aufmerksamkeitskontrolle erhöht (Slagter et al., 2007; van Leeuwen et al., 2012), wurde der Hypothese nachgegangen, dass die Modulation der top-down Aufmerksamkeit während der Achtsamkeit – im Gegensatz zur bottom-up Aufmerksamkeit (Fagerholm et al., 2015) – neuronale Netzwerke näher an den kritischen Punkt bringt. Spezifisch wurde der Hypothese nachgegangen, dass die räumlich-zeitliche Lawinendynamik in diesen Zuständen unterschiedliche kortikale
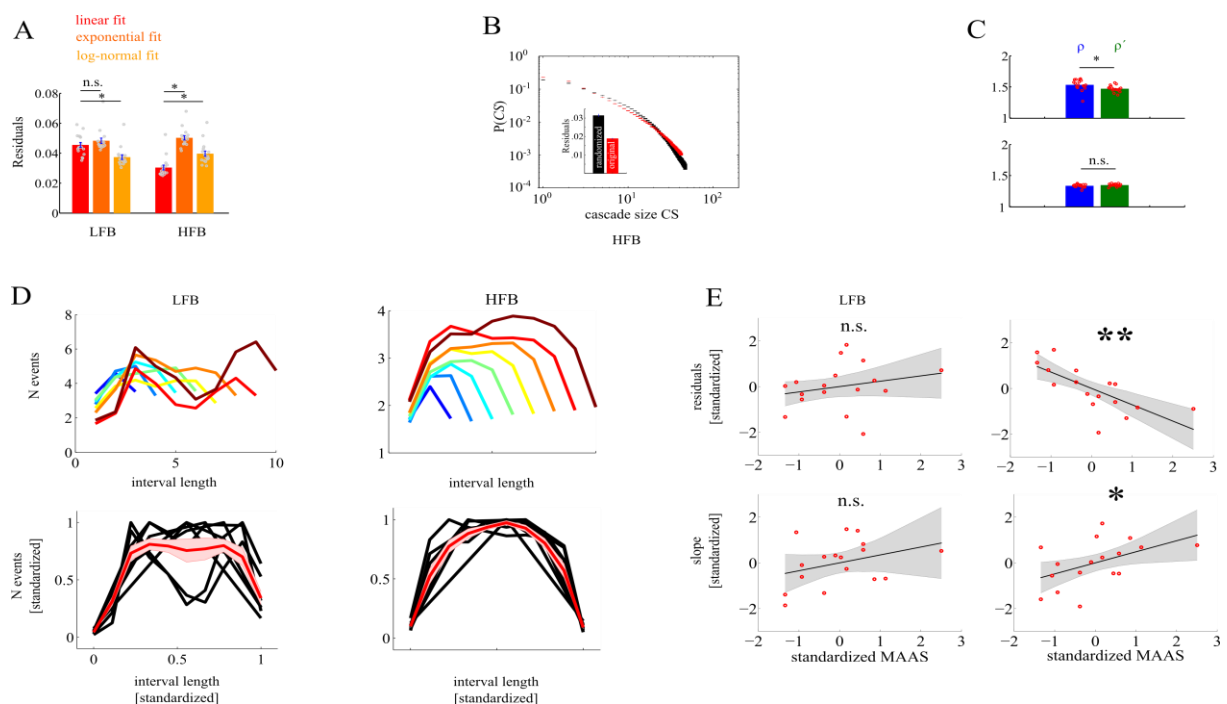
Abbildung 2 Darstellung der Kaskadengrößenverteilung über die Frequenzen. *A Der lineare Fit ist am besten in der HFA. B die gemessenen Daten werden besser durch einen linearen Fit erklärt als randomisierte Daten. C Das Verhältnis von Kaskadengröße und –dauer entspricht dem der Anstiege von Kaskadengröße und –dauer in HFA. D die HFA zeigt vergleichbare Kaskadenformen für unterschiedlichen Kaskadenlängen E MAAS scores sind mit dem Anstiegsparameter des linearen fits korreliert.*

Regionen involviert, da angenommen wird, dass MFA und Ruheaktivität von unterschiedlichen neuronalen Netzwerken vermittelt werden (Kucyi et al., 2013; Mittner et al., 2014; Zhou and Lei, 2018).

Dabei konnte gezeigt werden (Dürschmid et al., 2020b), dass Spitzen und Senken im Breit-band MEG hinsichtlich ihrer Phase an Oszillationen im niedrigen (<50) und hohen Frequenzbe-reich (>100Hz) gebunden sind. Parallel dazu zeigte eine lineare Regression niedrige Residuen und fast kritische Exponenten in einem niedrigen (LFB: 9-37 Hz) und hohen Frequenzband (HFA: 170-275 Hz). Klare Hinweise auf Kritikalität wurde nur im HFA Frequenzband gefunden: die Güte der

Regression war signifikant besser als für einen exponentiellen Fit. Zudem war die Beziehung der Exponenten zwischen der Verteilung von Kaskadengröße und –dauer, was als Zeichen für Kritikalität angesehen wird, nur im HFA- aber nicht im LFA-Band gegeben. Außerdem waren zeitliche Profile von Lawinen unterschiedlicher Größe power-law skalierte Versionen der gleichen Parabelform und konnten nach Skalierung übereinandergelegt werden. Dieser Indikator von Kritikalität konnte nur für das HFA- aber nicht das LFA-Band gefunden werden. Außerdem führt die Achtsamkeitsmeditation zu topographischen Veränderungen der Lawinen verglichen mit Ruheaktivität.

Zusammenfassend hat diese Untersuchung ergeben, dass hochfrequente Aktivität, die stellvertretend für neuronale Aktivität untersucht wurde, eine kritische Dynamik zeigt, die die physiologische Grundlage für optimale Informationsintegration bildet. Im nächsten Kapitel wird untersucht, inwiefern diese Gehirnantworten externe Informationen zu subjektiven Bewertungen zusammenfassen können.

Dürschmid S., Reichert C., Walter N., Hinrichs H., Heinze H.J., Ohl F.W., Tononi G., Deliano M. Self-regulated critical brain dynamics originate from high frequency-band activity in the MEG. PLoS ONE, 2020.

2.2 Delay Discounting – Selbstwahrnehmung reduziert Impulsivität

Der Wert einer Belohnung sinkt mit der Zeit: je länger wir warten müssen, desto weniger ist uns die Belohnung wert. Daher verwandelt eine verzögerte Auszahlung einen objektiven Wert in einen wahrgenommen geringeren Wert. Das führt dazu, dass kleinere aber frühere Belohnungen (smaller sooner – SS) größeren aber späteren Belohnungen (larger later – LL) vorgezogen werden. Dies wird als *Delay Discounting* (DD) oder intertemporale Wahlmöglichkeit bezeichnet. Impulsive Entscheidungen könnten durch die Tendenz begründet werden, dass SS gegenüber LL Belohnungen vorgezogen werden. Bisherige Studien der funktionellen Magnetresonanztomographie fokussierten auf neuroanatomische Korrelate der subjektiven Bewertung und Interaktionen multipler unabhängiger Bewertungssysteme im ventromedialen Präfrontalkortex (vmPFC) und dorsolateralen Präfrontalkortex (dlPFC) (McClure et al., 2004, 2007). Dort korreliert der Wert eines Ziels mit der Aktivität im vmPFC und die Höhe der Selbstkontrolle mit der Aktivität im dlPFC (Hare et al., 2009). Impulsivität könnte aber auch daraus resultieren, dass wir nur unzureichend die objektiven Alternativen beachten (Ainslie, 1975; Myerson et al., 2003; Olson et al., 2007), die in einen subjektiven Wert übersetzt werden müssen (Mazur, 1987; Green and Myerson, 2004). Diese Ansicht legt nahe, dass geringe Aufmerksamkeit für objektive Werte zu stärkerem DD führen kann.
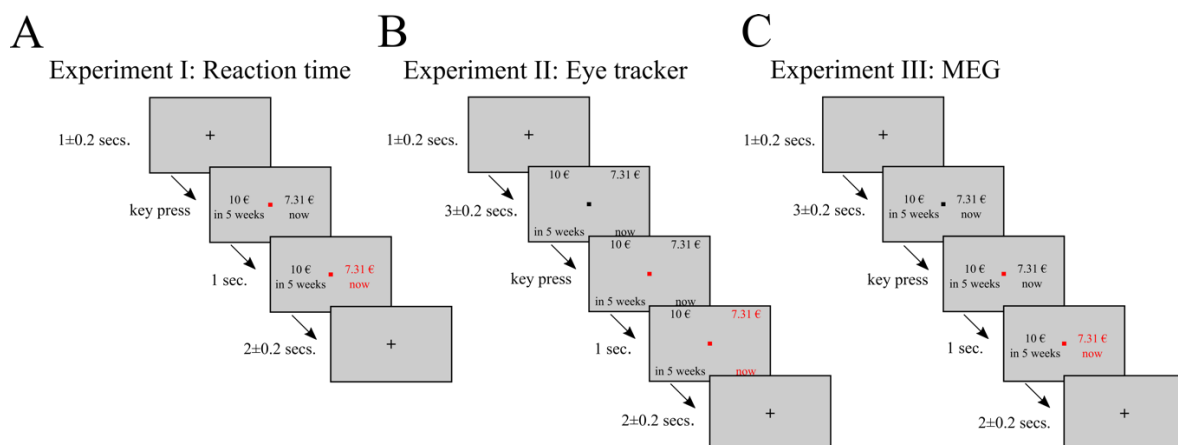
Abbildung 3 Darstellung der Belohnungsoptionen. **A:** *Reaktionszeitexperiment. **B:** Augenbewegungsmessung. **C:** MEG-Experiment. Im ersten Experiment testeten wir, ob es Unterschiede hinsichtlich der Zeit, die für eine Entscheidung benötigt wurde, gab. **B-C:** Sowohl im Augenbewegungs- als auch im MEG-Experiment wurden den Probanden die Wahlmöglichkeiten zusammen mit der Aufforderung die Entscheidung erst nachdem der Fixationspunkt seine Farbe wechselte anzuzeigen, präsentiert. **B:** Während des Augenbewegungsexperiments wurden die Wahlmöglichkeiten mit größerem Abstand zum Fixationspunkt präsentiert.*

Unterschiede des DD zwischen Studienteilnehmern könnten auch in der unzureichenden Repräsentation von Wahlmöglichkeiten im Arbeitsgedächtnis (Fuster, 1990; Baddeley, 1992; Goldman-

Rakic, 1992), bevor eine Option selektiert wird, begründet liegen. Wichtig dabei ist, dass Selbstwahrnehmung den Unterschieden im DD entgegenwirkt (Peters and Büchel, 2010). Diese Beobachtung legt nahe, dass Wahlmöglichkeiten, bei denen Selbstwahrnehmung vernachlässigt wird, zu stärkerem DD führt, wobei zwei Beiträge noch immer diskutiert werden. Erstens, wie Aufmerksamkeitsmechanismen und der Grad der neuronalen Repräsentation zu Entscheidungen in diesen intertemporalen Wahlmöglichkeiten beitragen, ist noch nicht klar. Zweitens, ob und wie diese Mechanismen qualitativ durch subjektives Bewusstsein moduliert werden, ist nicht klar. Es kann angenommen werden, dass aufmerksamkeitsbezogene Selektion und neuronale Repräsentation mehr Anstrengung benötigen, wenn man die Entscheidung für sich selbst trifft, was in prosozialen Entscheidungen reduziert ist (Lockwood et al., 2017). In Übereinstimmung mit früheren Studien (Lockwood et al., 2017) kann getestet werden, wie die Übernahme der Perspektive einer anderen Person die Anstrengung zur aufmerksamkeitsbezogenen Selektion und die neuronale Repräsentation verändert. Dabei liegt der experimentelle Kontrast auf der Übernahme der Perspektive des besten Freundes (das Vorgeben sich für den besten Freund zu entscheiden), was eine Grundvoraussetzung für prosoziale Handlungen ist und per Definition Selbstwahrnehmung reduziert.

Im Folgenden wurden mit Hilfe von Augenbewegungsmessungen (Eye tracking – ET) und MEG Mustern die aufmerksamkeitsbezogene Evaluation und neuronale Repräsentation von objektiven Werten im DD Paradigma in zwei Bedingungen miteinander verglichen. In einer Bedingung entschieden die Studienteilnehmer über ihre eigene Belohnung, während sie in einer zweiten, anonymen prosozialen Bedingung vorgaben, sich für ihren vorgestellten besten Freund zu entscheiden. Daher unterschieden sich die Bedingungen nur hinsichtlich der subjektiven Wahrnehmung der Belohnung für die Studienteilnehmer. Dabei wurde die Hypothese getestet, dass Studienteilnehmer sich in prosozialen Entscheidungen impulsiver entscheiden, selbst dann, wenn die Entscheidung komplett anonym war, da sich die Studienteilnehmer ihren besten Freund nur vorstellten (Lockwood et al., 2017). Dabei wurde der Hypothese nachgegangen, dass objektive Handlungsalternativen weniger berücksichtigt werden und daher auch weniger im Gehirn repräsentiert werden, wenn Entscheidungen für Andere gemacht werden. Augenbewegungen sind ein sensitiver Indikator für Aufmerksamkeitsverlagerungen und daher kann der Zeitverlauf des Aufmerksamkeitsfokus über die Augenbewegungen untersucht werden und weniger Aufmersamkeit bei Entscheidungen für Andere vorhergesagt werden. Mit dem MEG wurde erstens untersucht, ob frequenzspezifische Aktivität Wahlmöglichkeiten integriert und zweitens, ob Unterschiede in den Wahloptionen (Belohnung und Verzögerung in
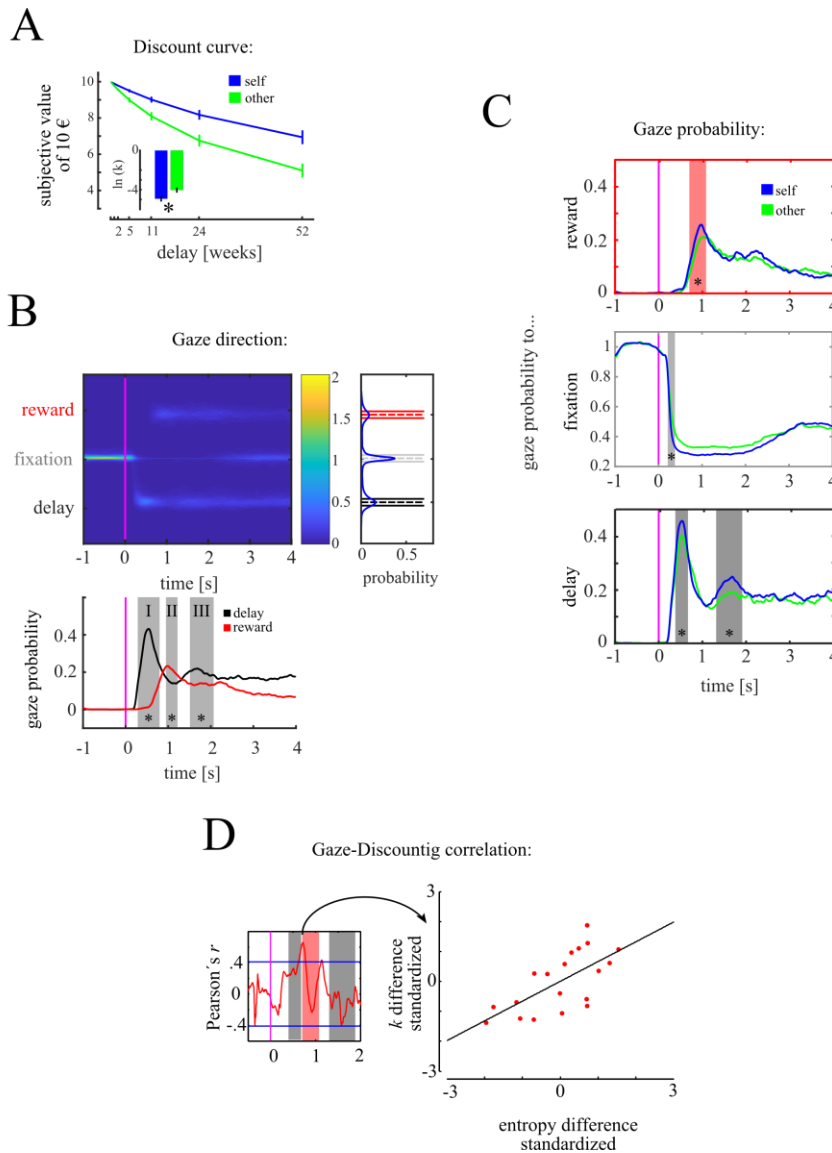
Abbildung 4 Augenbewegungsmessung. *A zeigt stärkeres Discounting in der prosozialen Bedingung. B Farbkodierte Blickrichtungswahrscheinlichkeit in Abhängigkeit von der Zeit. C zeigt die zeitabhängige Variation der Blickbewegung zur Belohnung (oben), zum Fixationskreuz (Mitte) und zum Delay (unten) für beide Bedingungen. D zeigt die Korrelation der Blickrichtungsstabilität und Unterschiede der Discountparameter.*

den beiden Bedingungen) innerhalb des Aufmerksamkeitsfokus zu Unterschieden in der Gehirnaktivierung führen.

In den drei vorgestellten Experimenten mussten sich die Probanden zwischen einem LL von 10€ mit einer variablen Auszahlungszeit *D* (1,2,5,11,24 oder 52 Wochen) und SS Wert entscheiden, die beide hypothetisch waren. Der SS Wert war dabei hyperbolisch von dem LL Wert abhängig. Im ersten Experiment wurde untersucht, ob sich die Probanden hinsichtlich der Entscheidungszeit zwischen den beiden Bedingungen unterscheiden. Im zweiten und dritten Experiment

wurden die Probanden gebeten, erst zu antworten, wenn das Fixationskreuz die Farbe wechselt (nach 3s ± 200ms). Das war ausreichend länger als die Entscheidungszeit, die in Experiment 1 ermittelt wurde und minimiert Einflüsse motorischer Handlungen, was besonders für das MEG Experiment wichtig ist. Daher konnten ET und MEG Aktivität zeitaufgelöst miteinander verglichen werden.

Dabei zeigt sich, dass die Studienteilnehmer über unterschiedliche Gruppen hinweg impulsivere Entscheidungen (weniger DD wenn sie sich für sich selbst entschieden, verglichen mit der prosozialen Bedingung) trafen, auch wenn die Zeit, die sie für die Entscheidung benötigten, vergleichbar war (Dürschmid et al., 2020a). Im ET-Experiment führte die erhöhte

räumliche Distanz zu mehr Anstrengung die Augen zu bewegen. Diese war in der prosozialen Bedingung gegenüber der Selbstwahrnehmungsbedingung reduziert, was als soziale Apathie bezeichnet werden kann (Lockwood et al., 2017). Es zeigt sich, dass Intervalle der Aufmerksam-keitsverlagerung zur Beloh-nungshöhe und -verzögerung im ET mit Intervallen der Repräsentation von Beloh-nungshöhe und -verzögerung im MEG in der HFA über-einstimmten. Diese Ergebnisse legen nahe, dass Unterschiede im Discounting aus den Unter-schieden in der Evaluation der Wahlmöglichkeiten resultiert. In der MEG Studie zeigte sich, dass die über fronto-temporale MEG Sensoren verteilte HFA (175-250Hz) ausschließlich in der Bedingung der Selbstwahr-nehmung durch die Wahlmög-lichkeiten moduliert wurde. Dabei waren das Discountverhalten zwischen den beiden Bedingungen korreliert, was für eine individuelle Disposition des DD spricht.
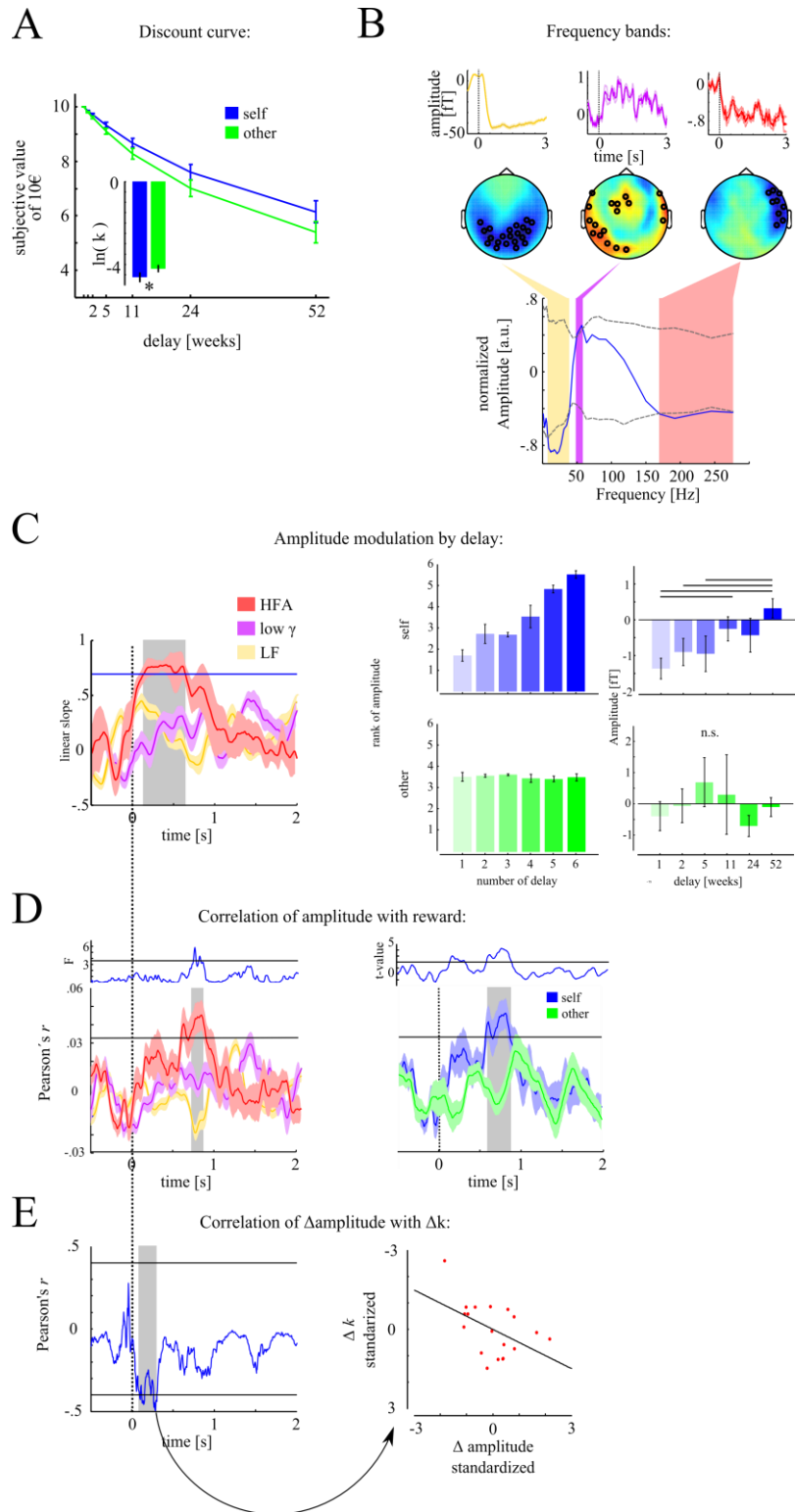
Abbildung 5 MEG Ergebnisse. **A** *Verhaltensergebnisse.* **B** *zeigt die Amplitudenmodulation in drei unterschiedlichen Frequenzbändern und deren topographische Verteilung.* **C** *nur die HFA zeigt eine Korrelation mit dem Delay.* **D** *in einem sich anschließenden zeitlichen Interval zeigte sich eine signifikante Korrelation mit der Belohnungsinformation in der HFA.*

Zusammenfassend kann gesagt werden, dass Informationen in der Umwelt zu einem subjektiven Wert integriert werden. Dabei handelte es sich in dieser Studie um zu einem Zeitpunkt präsentierte Handlungsoptionen. Wie das menschliche Gehirn Informationen über die Zeit integriert, um vor dem Hintergrund des so gewonnenen Wissens über die Regelhaftigkeit in der Umwelt Vorhersagen über diese zu treffen, wird im anschließenden Kapitel dargestellt.

Dürschmid S, Maric A, Kehl MS, Robert T Knight RT, Hinrichs H, Heinze HJ. Fronto-temporal cortex regulation of subjective valence to suppress impulsivity in intertemporal choices. Journal of Neuroscience, 2021.

2.3 Erkennen von Abweichungen – Wie wir ein internes Modell erstellen und Vorhersagen ableiten

2.3.1 Subkortikale Verarbeitung

Vorhersagefehler im Nucleus Accumbens

Die Detektion von unerwarteten Umweltereignissen ist eine fundamentale Eigenschaft von Säugetieren, die darauf beruht, dass wir langzeitliches kontextuelles Wissen einsetzen, um unser Verhalten zu lenken (Rao and Ballard, 1999; Heilbron and Chait, 2018). Das erlaubt es, vorhersagbare Komponenten des Inputsignals zu entfernen und Redundanz zu reduzieren. Auf einem neurophysiologischen Level wird angenommen, dass mit zeitlicher Regularität Rückwärtsverbindungen gestärkt und gleichzeitig die Stärke von Vorwärtsverbindungen reduziert werden (Kumar et al., 2011). Damit werden stabile sensorische Gedächtnisrepräsentationen hergestellt, wenn keine PE auftreten.

Eine subkortikale Region, die bei der Generierung eines PE involviert ist, ist der Nucleus Accumbens (NAcc). Dies ist eine Region, die in zielgerichtetem Verhalten involviert ist (Goto and Grace, 2008) und bekannt dafür ist, sensitiv für Neuheit (Wood et al., 2004), kontextuelle Abweichung (Axmacher et al., 2010a), aversive Reize (Becerra et al., 2001; Baliki et al., 2010) und Belohnungs-PE bei Menschen (Abler et al., 2006; Spicer et al., 2007) zu sein. Diese Befunde zeigen, dass der NAcc eine kritische Rolle bei der Abweichungserkennung spielen könnte. Jedoch sind die neuronalen Grundlangen, die im menschlichen NAcc während der Abweichungserkennung und der Erzeugung eines PE beteiligt sind, unklar.

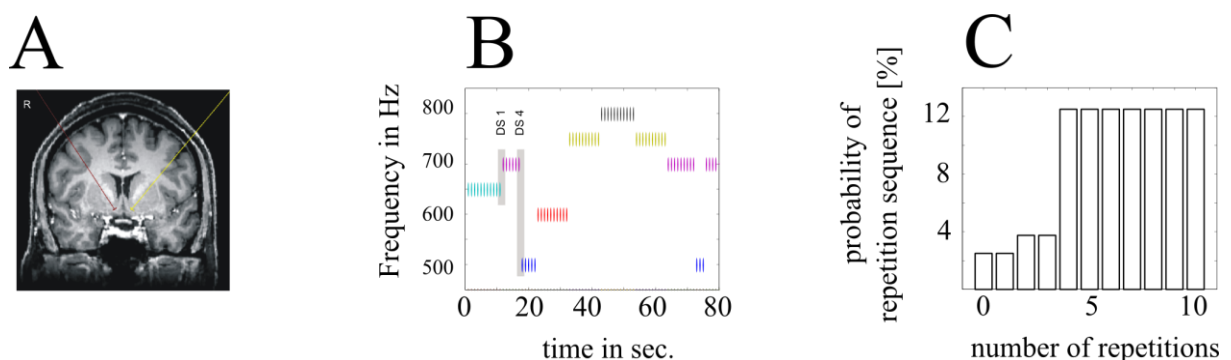*Abbildung 6 A zeigt die anatomische Region der bilateralen NAcc Tiefenelektroden. B Sieben unterschiedliche Töne wurden definiert, die sich nur in der Tonhöhe (500-800Hz) unterschieden. C die Anzahl an Wiederholungen variierte zwischen 0 und 10.*

Im Folgenden wurde bei fünf Patienten, die an einem Experiment teilgenommen haben (Garrido et al., 2008), das eine detaillierte Analyse der graduellen Stärke der sensorischen Diskrepanz (mismatch) und der Erwartung erlaubt, direkt aus dem NAcc abgeleitet. Dabei wurde vorhergesagt, dass der NAcc neue Informationen dahingehend gewichtet, ob sie in den fortlaufenden sensorischen Kortex passen und Informationen über Abweichungen an Regionen in der kortikalen Hierarchie übermittelt. Dabei wurden die Hypothesen aufgestellt, dass (i) der NAcc ein sensorisches Mismatch-Signal evoziert, (ii) dass das Mismatch-Signal in Abhängigkeit von der Stärke der Abweichung variiert und (iii) dass die NAcc MMN zur späteren Entstehung der kortikalen Mismatch-Komponenten beiträgt, die in Verhaltensanpassung involviert sind.

Dabei wurde beobachtet, dass der NAcc die Statistik der lokalen auditorischen Szene verlässlich nachverfolgt und dass dessen Aktivität spätere kortikale Aktivität vorhersagt. Weiterhin wurde gefunden, dass die Stärke der Abweichung stärker im NAcc kodiert wurde, wenn sie nach vielen Wiederholungen der Standards auftraten. Dass Probanden in dieser Studie passiv einem Audiostream zuhörten, unterstreicht den schnellen prä-attentionalen und automatischen Prozess, der im NAcc-Signal repräsentiert ist (Dürschmid et al., 2016b).

Dürschmid S, Zaehle T, Hinrichs H, Heinze HJ, Voges J, Garrido MI, Dolan RJ, Knight RT. Sensory Deviancy Detection Measured Directly Within the Human Nucleus Accumbens. Cereb Cortex. 2016
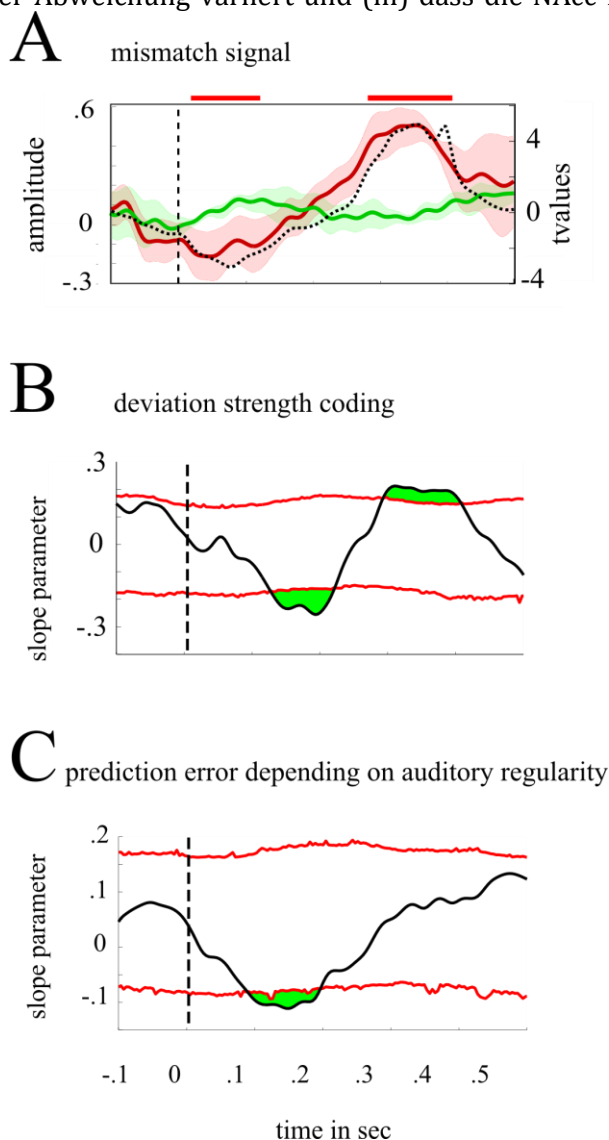
Abbildung 7 A der NAcc zeigt eine Mismatch Antwort nach der Präsentation des Devianten. B die Stärke der Abweichung ist im NAcc kodiert. Die Amplitude nach einem Devianten nimmt in Abhängigkeit von DS erst ab und nimmt dann in einem späteren Intervall zu. C die Amplitudenmodulation im NAcc variiert in Abhängigkeit von der Anzahl an vorherigen Standards.

Sensorisches Gedächtnis im Nucleus basalis von Meynert

Dass die MMN einen basalen Gedächtnisprozess widerspiegelt, zeigt sich an deren Reduktion bei Patienten mit Alzheimerscher Krankheit (AD). AD ist mit einer fortschreitenden Verschlechterung von Gedächtnis und kognitiven Funktionen assoziiert und ist die häufigste Ursache für Demenz in der mittleren und späten Lebensspanne aufgrund einer organischen Erkrankung (Terry and Davies, 1980). Frühere Studien zeigten, dass bei AD Patienten Neurone im Nucleus Basalis (NB) massiv degenerieren (Whitehouse et al., 1982). Der NB ist eng mit einer Vielzahl von kortikalen und subkortikalen Strukturen vernetzt und ist die größte Quelle cholinerger Innervation zum Neokortex (Mesulam et al., 1983) mit Projektionen zum frontalen, parietalen, zingulären und temporalen Kortex (Gratwicke et al., 2013). Acetylcholin (ACh) ist ein wichtiger Neuromodulator, der im Kortex ausgeschüttet wird, durch den neuronale Plastizität erhöht wird (Rasmusson, 2000) und der bei vielen kognitiven Funktionen wie Aufmerksamkeit (Voytko et al., 1994; McGaughy et al., 1996; Sarter and Bruno, 1999; Furey et al., 2008; Kole et al., 2008) und Lernen und Gedächtnis (Miasnikov et al., 2001, 2008; Thiel et al., 2002; Warburton et al., 2003; Weinberger, 2003; Froemke et al., 2007; Kole et al., 2008) beteiligt ist. Der ACh-Rezeptorblocker Scopolamin führt, vermutlich durch eine Verhinderung der Aufnahme neuer Information und Speicherung dieser im Gedächtnis, zu einer spezifischen Einschränkung im Lernen (Aggelopoulos et al., 2011). Pharmakologische Erhöhung zerebraler ACh-Konzentration (durch Acetylcholinesterasehemmer) wird als Behandlung fortgeschrittener Demenz eingesetzt. Bei AD Patienten könnte also die abnehmende cholinerge Innervation des Kortex aufgrund der NB-Degeneration die Ursache für den fortschreitenden Gedächtnisverlust sein.

Neben pharmakologischen Ansätzen wird die Tiefe-Hirnstimulation (DBS, engl. für Deep Brain Stimulation) als potentielle therapeutische Option betrachtet. Die Überlegung dabei ist, die verbleibende cholinerge Übertragung durch Stabilisierung oszillatorischer Aktivität in gedächtnisrelevanten Kreisläufen zu unterstützen und somit kognitive Funktionen zu verbessern (Kuhn et al., 2015; Hardenacke et al., 2016). NB-DBS ist eine experimentelle, in seltenen Fällen therapeutisch effektive, nicht-lädierende Behandlungsmethode in Form von Verabreichung von Stromimpulsen in dysfunktionalen Gehirnstrukturen mittels dauerhaft implantierter Elektroden. NB-DBS wird bei der Behandlung von Bewegungsstörungen eingesetzt. Ob sie auch das Potential hat, sensorische Gedächtnisfunktionen bei AD Patienten zu verbessern, ist unklar.

Bei AD Patienten nimmt die Amplitude der MMN in Abhängigkeit vom Inter-Stimulus-Interval (ISI) stärker ab als bei gesunden Kontrollprobanden. Dies legt nahe, dass die Gedächtnisspur bei AD Patienten schneller abnimmt als bei Probanden gleichen Alters (Pekkonen et al., 1994).

Übereinstimmend mit Verhaltensveränderung ist die MMN in hohem Maße bei AD Patienten beeinträchtigt. Cheng et al. (Cheng et al., 2012) und Hsiao et al. (Hsiao et al., 2014) berichteten größere Amplituden und kürzere Latenzen bis zum Maximum der rechtsseitig gemessenen temporalen MMN bei jungen im Vergleich zu älteren und AD Patienten. Ebenso fanden Lindín et al. (Lindín et al., 2013) eine reduzierte MMN bei Patienten mit einer leichten kognitiven Störung (mild cognitive impairment – MCI) aber nicht bei Kontrollprobanden. Wichtig bei diesen Studien ist, dass die MMN sogar dann erhalten bleibt, wenn Aufmerksamkeit auf die Stimuli nicht notwendig ist. Engeland et al. (Engeland et al., 2002) fanden, dass Nikotin, ein cholinerger Agonist, eine Reihe von kognitiven Prozessen erhöht, die MMN Latenz verkürzt und prä-attentionale zeitliche Verarbeitung erhöht. Scopolamin, ein zentral ansetzender cholinerger Antagonist, reduzierte dagegen die MMN Amplitude (Pekkonen et al., 2001). Frühere Studien zeigten, dass die Amplitude der P50 Komponente bei Patienten mit MCI oder bei früher AD im Vergleich zu gesunden Kontrollprobanden erhöht ist (Polich et al., 1990; Golob and Starr, 2000; Golob et al., 2007; Cheng et al., 2012). Eine stärkere P50 bei AD Patienten könnte die beobachteten Unterschiede in der MMN erklären. Eine stärkere Amplitude könnte eine Störung der prä-attentionalen Hemmung repetitiver auditorischer Inputs indizieren (Cheng et al., 2012). Dabei ist unklar, ob eine Amplitudenmodulation bei AD oder MCI eine Pathologie kortikaler Neurone ist oder stattdessen eine funktionelle Konsequenz einer Pathologie entfernterer Systeme, so wie dem NB.

Im Folgenden wurden Gehirnantworten auf wiederholte Reize in einem auditorischen Oddball Paradigma bei Patienten mit AD untersucht, die mit NB-DBS behandelt wurden, und mit Gehirnantworten von altersübereinstimmenden gesunden Kontrollprobanden verglichen. Die erste Hypothese dabei war, dass Patienten Unterschiede in der MMN mit und ohne NB-DBS zeigen würden und dass diese Unterschiede nicht, wie in der Kontrollgruppe, der wiederholten auditorischen Stimulation zugeschrieben werden können. Weiterhin wurde die Hypothese untersucht, dass Antworten auf Standardtöne im Besonderen bei AD Patienten ohne NB-DBS, möglicherweise aufgrund der Amplitudenmodulation des P50/N1 Komplexes, verändert sind. Dafür wurden die neuronalen Antworten von AD Patienten mit und ohne NB-DBS auf Standards und Devianten in einem auditorischen Oddball Paradigma untersucht, um den Effekt der elektrischen Stimulation auf die auditorische Verarbeitung zu beleuchten. Eine Gruppe von altersübereinstimmenden gesunden Kontrollprobanden wurde dabei in die Studie einbezogen, um den Effekt wiederholter, auditorischer Stimulation im selben Paradigma zu quantifizieren. Die Überlegung dabei war, dass Veränderungen in der Patientengruppe zwischen OFF und ON NB-DBS, die nicht parallel mit der wiederholten auditorischen Stimulation in der Kontrollgruppe laufen, der DBS aber nicht der Wiederholung des gleichen Paradigmas zuzuschreiben sind. Dabei zeigte sich, dass die MMN signifikant eher ohne NB-DBS kam als mit DBS und verglichen zu der Kontrollgruppe in beiden Blöcken.
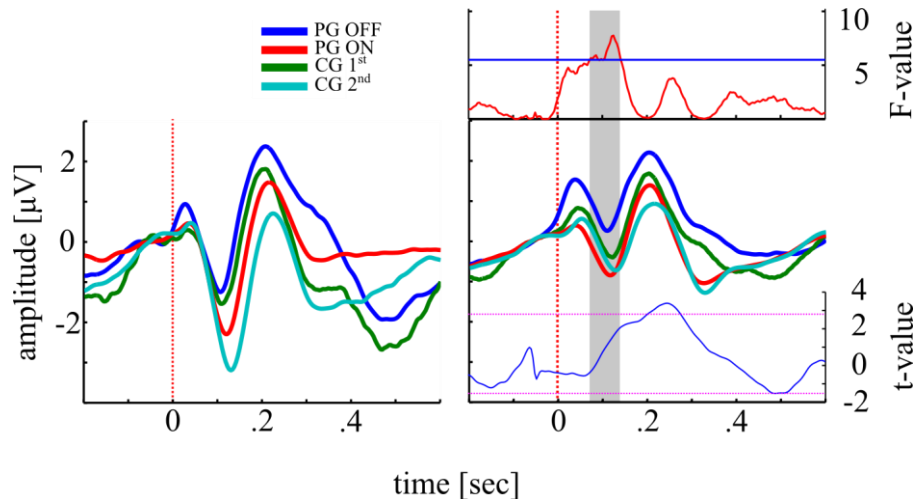
Abbildung 8 *Abbildung der Gehirnantworten auf die Reize für jede Gruppe und jeden Block. Es zeigte sich ein signifikanter Interaktionseffekt zwischen Patienten und Kontrollen der auf einen Unterschied zwischen den Blöcken bei den Patienten hindeutet, aber nicht bei den Kontrollprobanden. Während der NB-DBS normalisierte sich die Antwort auf die Standardtöne bei den Patienten, während sie bei den Kontrollen über die Blöcke gleich blieb.*

Diese frühe MMN ist sehr wahrscheinlich abhängig von der veränderten Antwort auf Standardreize, wenn keine NB-DBS vorgenommen wurde.

In der Tat fand sich eine veränderte Antwort auf Standardtöne in der Patientengruppe, wenn die NB-DBS ausgeschaltet wurde. Hier konnte ein stärkerer positiver Ausschlag im P50 Intervall überlappend mit der reduzierten N1 Komponente beobachtet werden. Unter NB-DBS Stimulation ähnelte die Antwort der der altersübereinstimmenden Kontrollgruppe. Im Gegensatz dazu fand sich dieses Muster in den Antworten auf die abweichenden Stimuli (Devianten)(Dürschmid et al., 2017).

Dürschmid S, Reichert C, Kuhn J, Freund HJ, Hinrichs H, Heinze HJ. Deep Brain stimulation of the Nucleus Basalis of Meynert attenuates early EEG components associated with defective sensory gating in patients with Alzheimer disease – a two-case study. EJN.

2.3.2 Kortikale Verarbeitung

Repräsentation von globalen und lokalen Abweichungen

Wie bereits erwähnt, ergibt sich die Fähigkeit unerwartete Umweltereignisse zu detektieren aus dem Vergleich des aktuellen Zustands der sensorischen Welt mit den Vorhersagen aus unmittelbarem und langzeitlichem kontextuellem Wissen. Dabei wird ein Vorhersagefehler generiert, sobald es eine Diskrepanz zwischen beiden gibt. Wichtig ist, dass niederfrequente Kopfoberflächenaufzeichnungen, wie die MMN, nicht das gesamte Spektrum der neuronalen Antworten auf Vorhersageverletzungen zeigen. Während die Aufzeichnung von HFA mit Kopfoberflächen EEG aufgrund des schlechten Signal-zu-Rauschen Verhältnisses ein großes methodisches Problem darstellt (Yuval-Greenberg et al., 2008; Muthukumaraswamy, 2013), haben eine Vielzahl von elektrokortikographischen (ECoG; abgeleitet von der kortikalen Oberfläche) Studien HFA Antworten als einen lokalen Index funktionaler selektiver Aktivität gezeigt (Crone et al., 1998; Miller
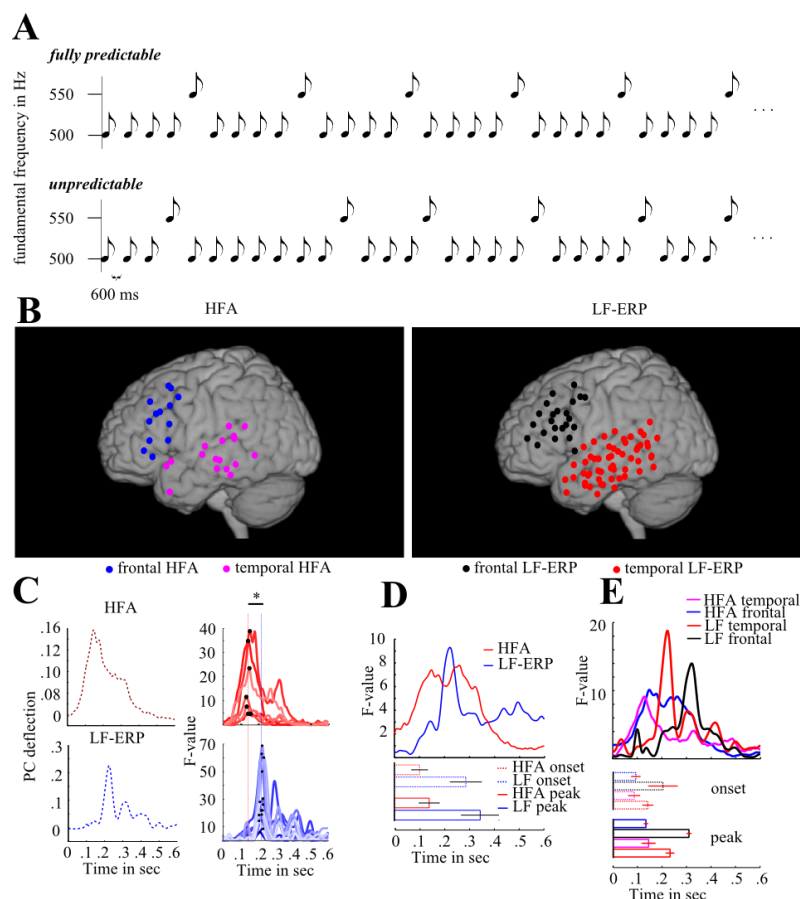

Abbildung 9 A *Darstellung des Paradigmas.* **B** *Darstellung der Gehirnregionen mit einer signifikanten Antwort auf die Stimuli für das nieder- und hochfrequente Band.* **C** *zeigt eine frühere Mismatchantwort in der HFA mit früherem Beginn und Maximum (D). E Darstellung der Mismatchantworten getrennt nach kortikalen Regionen.*

et al., 2007). Dabei ist nicht klar, ob kortikale neuronale Aktivität, die verantwortlich für die Erkennung von Abweichungen ist, am besten durch niedrige oder hohe Frequenzanteile repräsentiert wird. Diese Unterscheidung ist allerdings notwendig, da HFA andere Antwortcharakteristika zeigt als NF-EKPs (Crone et al., 2006). Intrakranielle Aufzeichnungen zeigten, dass sowohl niederfrequente ereigniskorrelierte Potentiale (NF-EKP) als auch HFA im temporalen Kortex bei der Generierung von PE eine Rolle spielen (Berger et al., 2005; Fishman and Steinschneider, 2012), wobei die HFA eher ansteigt als die Amplitude der NF-EKPs (Edwards et al., 2014). Im inferioren Frontalkortex zeigten sich in früheren ECoG Studien (Edwards et al., 2014; El Karoui et al., 2015) keine Hinweise auf frontal HFA als Antwort auf lokale Abweichungen (im Gegensatz zu globalen (El Karoui et al., 2015) obwohl NF-EKP Effekte in einigen (Liasis et al., 2001; Rosburg et al., 2005), aber nicht allen Studien (Baudena et al., 1995) diskutiert wurden.

Aufgrund der Schwierigkeit HFA mit EEG abzuleiten, fokussierten frühere PE Studien auf niederfrequente ereigniskorrelierte Potentiale. Die Mismatch Negativität (MMN) wird als klassisches PE Signal betrachtet, das hervorgerufen wird, während Probanden passiv Töne hören, die vom Kontext abweichen, der durch repetitive Standardstimuli generiert wird (Näätänen et al., 1978). Hinweise verdichten sich, dass die MMN interagierende Generatoren im sekundären auditorischen Kortex und dem superioren temporalen Kortex aber genauso im frontalen Kortex hat (Deouell, 2007; Shalgi and Deouell, 2007). Jedoch sind die unterschiedlichen Beiträge dieser einzelnen Regionen, besonders die des frontalen Kortex, nicht bekannt. Neuropsychologische EKP und bildgebende Studien unterstützen die Ansicht einer zentralen Rolle des Präfrontalkortex (PFK) bei kontextueller Verarbeitung (MacDonald et al., 2000; Fogelson et al., 2009).
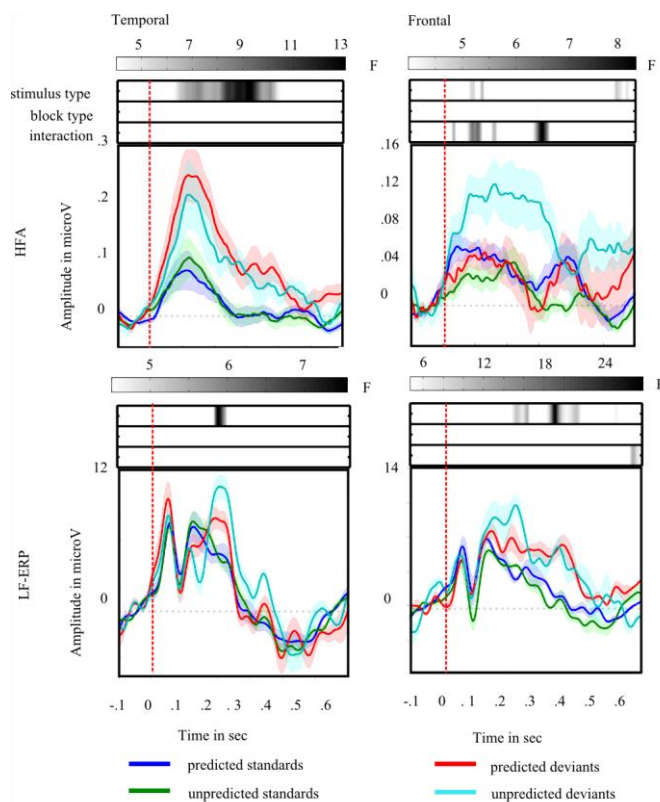
Abbildung 10 *Frontale und temporale Aktivitätsmuster variieren mit der Vorhersagbarkeit von Stimuli. Balken über den farbigen Abbildungen zeigen den Verlauf von F-werten über die Zeit. Nur die HFA im frontalen Kortex zeigt einen signifikanten Interaktionseffekt.*

Im Folgenden wurden frontale und temporale kortikale Muster von NF-EKPs und HFA verglichen. Dabei unterschieden sich, wie oben beschrie-

ben, die Bedingungen in der Vorhersagbarkeit der Abweichung von der Hintergrundstimulation (vorhersagbar: vier Standards vor jedem Devianten; nicht vorhersagbar: Devianten sind zufällig eingebettet). Der Vorhersagefehler wurde als Differenz zwischen der Antwort auf die Devianten und Standards operationalisiert. Abweichungen vom auditorischen Kontext modulierte sowohl die HFA als auch die NF-EKPs, die typischerweise mit MMN im EEG assoziiert sind. Der PE zeigte sich eher in der HFA als in den NF-EKPs und war sowohl im temporalen als auch frontalen Kortex evident. Jedoch nur die HFA im FK differenzierte zwischen vorhersagbaren und nicht vorhersagbaren Abweichungen, was die Schlüsselrolle des FK beim PE hervorhebt (Dürschmid et al., 2016a).

Dürschmid S, Edwards E, Reichert C, Dewar C, Hinrichs H, Heinze HJ, Kirsch HE,Dalal SS, Deouell LY, Knight RT. Hierarchy of prediction errors for auditory events in human temporal and frontal cortex. Proc Natl Acad Sci U S A. 2016

Repräsentation von Vorhersagen

Hieraus ergibt sich die Frage, ob dieses von der Umwelt generierte Bild für Vorhersagen genutzt werden kann. Mehrere Studien haben die Frage einer proaktiven Vorhersage zu beantworten versucht, in dem zum Beispiel kein abweichender Stimulus präsentiert wurde, sondern die Präsentation des Reizes ausgelassen wurde (Heilbron and Chait, 2018). Die meisten neuronalen Antworten auf Auslassungen können als Verletzung einer allgemeinen Vorhersage des zeitlichen Auftretens eines Stimulus betrachtet werden. SanMiguel et al. (SanMiguel et al., 2013) ließen die Probanden Umweltgeräusche produzieren, indem diese einen Knopf drückten. Die Hypothese besteht in diesem Experiment darin, dass die Erwartung eines Tones die vorhergesagte Aktivität der Tonrepräsentation im auditorischen Kortex auslöst. Wenn keine Vorhersage gemacht wird, dann sollte auf die Präsentation des Tones auch keine auditorisch sensorische Antwort zu finden sein. Gehirnantworten auf eine Auslassung sollten deshalb nur eine direkte Konsequenz der Vorhersageaktivität sein. Antworten auf gelegentliche Tonauslassungen wurden nur dann gefunden, wenn der gleiche Ton wiederholt durch den Knopfdruck hervorgerufen wurde und somit vorhersagbar war, da die Probanden den Ton selber generierten. In einer passiven Aufgabe mit visueller Ablenkung präsentierten Bendixen et al. (Bendixen et al., 2015) in schneller Reihenfolge sequentielle Tonpaare. Innerhalb eines Paares waren die Töne identisch, wogegen die Frequenzen zwischen den Paaren variierten. Antworten auf Auslassungen wurden gefunden, wenn der Ton vorhergesagt werden kann (da es der zweite Ton innerhalb eines Paares war), nicht aber, wenn nur vorhergesagt werden konnte, wann der Stimulus kommt nicht aber welcher es ist (da es der erste Ton eines Paares war). Jedoch hätten die Probanden die Paare als auditorische Objekte wahrnehmen können und die Auslassung des zweiten Tones innerhalb des Paares, der die kritische Auslassungsantwort hervorrief, könnte eher eine post-hoc Antwort auf die Veränderung der Dauer sein, als eine antizipatorische Antwort.

In der folgenden Studie wurde deshalb nicht auf die Antworten nach der Stimuluspräsentation oder nach einer Auslassung geschaut. Vielmehr wurde direkt das Intervall vor dem Stimulus untersucht. Dies ist das Zeitfenster, in welchem eine Aktivitätsmodulation einem Vorhersagefehler zuzuschreiben ist, da noch kein Fehler berechnet werden kann. In gleicher Weise wurde aus dem MEG die Orientierung eines visuellen Streifenmusters dekodiert, das durch einen vorausgehenden auditorischen Reiz vorhergesagt werden kann (valider visueller Stimulus) oder nicht (in-
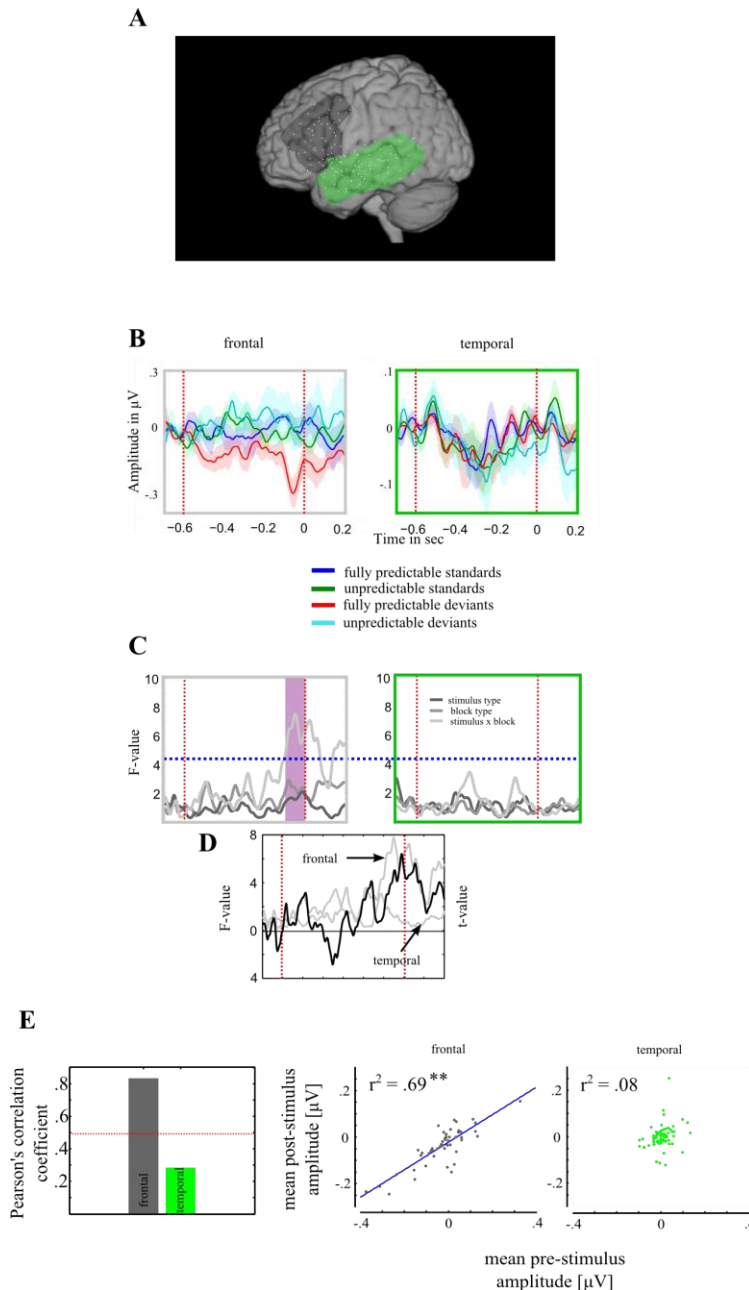
Abbildung 11 Zeitaufgelöste Varianzanalyse. **A** Darstellung der frontalen und temporalen Regionen, wobei nur die erste eine HFA Modulation vor den vorhersagbaren Devianten zeigt (**B**) was durch einen signifikanten Interaktionseffekt gekennzeichnet ist (**C**), der in der frontalen Region größer als in der temporalen ist (**D**). **E** Je größer die Prä-stimulus-modulation, desto geringer ist der Vorhersagefehler in frontalen aber nicht in temporalen Elektroden.

valider visueller Stimulus). Die Subtraktion des Signals eines valide von einem invalide angekündigten Streifenmuster zeigte eine Differenz vor der Stimuluspräsentation. Dies legt den Schluss einer vorzeitigen Aktivierung eines antizipatorischen sensorischen Schemas nahe. Grisoni et al (Grisoni et al., 2017) fanden mittels EEG Hinweise auf prä-stimulus antizipatorische Bewegungsvorbereitung auf spezifische Handlungsverben, die durch bedeutungsvolle Sätze vorhergesagt wurden. Jedoch ist nicht klar, ob es sich hierbei um einen automatischen Prozess handelt, da die Probanden mit großer Wahrscheinlichkeit die Sätze angehört haben. Während diese Studien übereinstimmende Hinweise für eine pro-aktive Vorhersage im MEG und EEG gefunden haben, bleiben die Quelle und die Art des Signals dieser prädiktiven Aktivität noch unklar. Um diese Frage zu klären, wurde der Vorteil des hohen Signal-zu-Rausch Verhältnisses und die verbesserte räumliche Auflösung von ECoG Daten genutzt.

Im Folgenden sollte nun gemessen werden, wie das Gehirn spektral und anatomisch Vorhersagen repräsentiert. Fünf Epilepsiepatienten, bei denen ein prächirurgisches Monitoring mit subduralen Elektroden durchgeführt wurde, nahmen an der Studie teil. Ihnen wurden Reize präsentiert, die 180 ms lange, harmonische Töne mit einer Grundfrequenz von 500 oder 550 Hz und den 3 jeweils ersten Harmonischen waren. Die Probanden schauten eine ablenkende visuelle Stimulation an, während die Tonsequenzen präsentiert wurden. Die Tonsequenzen bestanden aus sehr wahrscheinlichen Standardtönen (P = .8; f_0 = 500 Hz) gemischt mit Devianten mit niedriger Wahrscheinlichkeit (P = .2; f_0 = 550 Hz). In den Blöcken war die Reihenfolge entweder zufällig, mit einem Minimum von 3 Standards zwischen zwei Devianten, oder völlig vorhersagbar, so dass jeder fünfte Ton ein Deviant war. Dabei zeigte sich eine HFA Modulation, die den regulären und somit vorhersagbaren Devianten vorausging. Dieses Muster fand sich nur im lateralen Frontalkortex (Dürschmid et al., 2019). Im nächsten Schritt wurde untersucht, ob die prä-stimulus Modulation einen Einfluss auf die Hirnantwort auf den Stimulus hat. Dabei zeigte sich, dass die prä-stimulus HFA im Frontalkortex mit der post-stimulus HFA korreliert war. Dieses Muster zeigte sich allerdings nicht im Temporalkortex (Dürschmid et al., 2019).

Dürschmid S, Reichert C, Hinrichs H, Heinze HJ, Kirsch HE, Knight RT, Deouell LY. Direct evidence for prediction signals in frontal cortex independent of prediction error. Cereb Cortex. 2019. https://doi.org/10.1093/cercor/bhy331

2.4 Motorisches Lernen – Integration von Umweltinformationen und motorischen Handlungen

Im folgenden Kapitel werden zwei Studien vorgestellt, die sich mit der Integration von Information aus hochfrequenter Aktivität in niederfrequente Netzwerke auf neurophysiologischer Ebene befassen. Ähnlich wie im vorangegangenen Kapitel wird zunächst die Kopplung von Frequenzen auf subkortikaler, gefolgt von dem gleichen Phänomen auf kortikaler Ebene beschrieben.

2.4.1 Informationsintegration im Nucleus Accumbens

Der Nucleus Accumbens (NAcc) ist Teil des ventralen Striatums und spielt eine zentrale Rolle bei der Informationsintegration (Goto and Grace, 2008) des limbischen System, insbesondere dem Präfrontalkortex (PFK) und dem Hippocampus (HC). Der NAcc wird als Schnittstelle, durch welche der HC Input zum PFK ansteuert, angesehen (French and Totterdell, 2002). Bei Ratten konvergieren sowohl der PFK als auch der HC auf einzelne NAcc Neurone (Finch, 1996; Goto and Grace, 2008) und die PFC-NAcc und HC-NAcc Verbindungen sind wechselseitig voneinander abhängig. So zum Beispiel zieht eine Langzeitpotenzierung der HC-NAcc Assoziation eine Langzeitdepression der PFC-NAcc Assoziation nach sich (Grace et al., 2007). Es wird angenommen, dass die selektive Stärkung der HC-NAcc Verbindung wichtig für die schnelle Erleichterung zielgerichteten Verhaltens und Unterstützung automatisierter Handlung ist (Goto and Grace, 2005; Belujon and Grace, 2008). Solche automatisierten Handlungen sind besonders evident in Aufgaben des Bewegungslernens, in welchen der NAcc Informationen für die Planung von Bewegungen integriert (Mogenson et al., 1980; Grace, 2000). Münte et al. (Münte et al., 2008) spekulierten, dass der menschliche NAcc Information für die Anpassung von Antwortstrategien evaluiert. Dementsprechend limitieren Läsionen im NAcc die Flexibilität, die für Verhaltensänderungen während des Lernens benötigt werden (Grace et al., 2007). Jedoch ist Wissen über die spezifischen neuronalen Mechanismen, die für die Informationsintegration von PFK und HC im Gehirn benutzt werden, noch immer begrenzt.
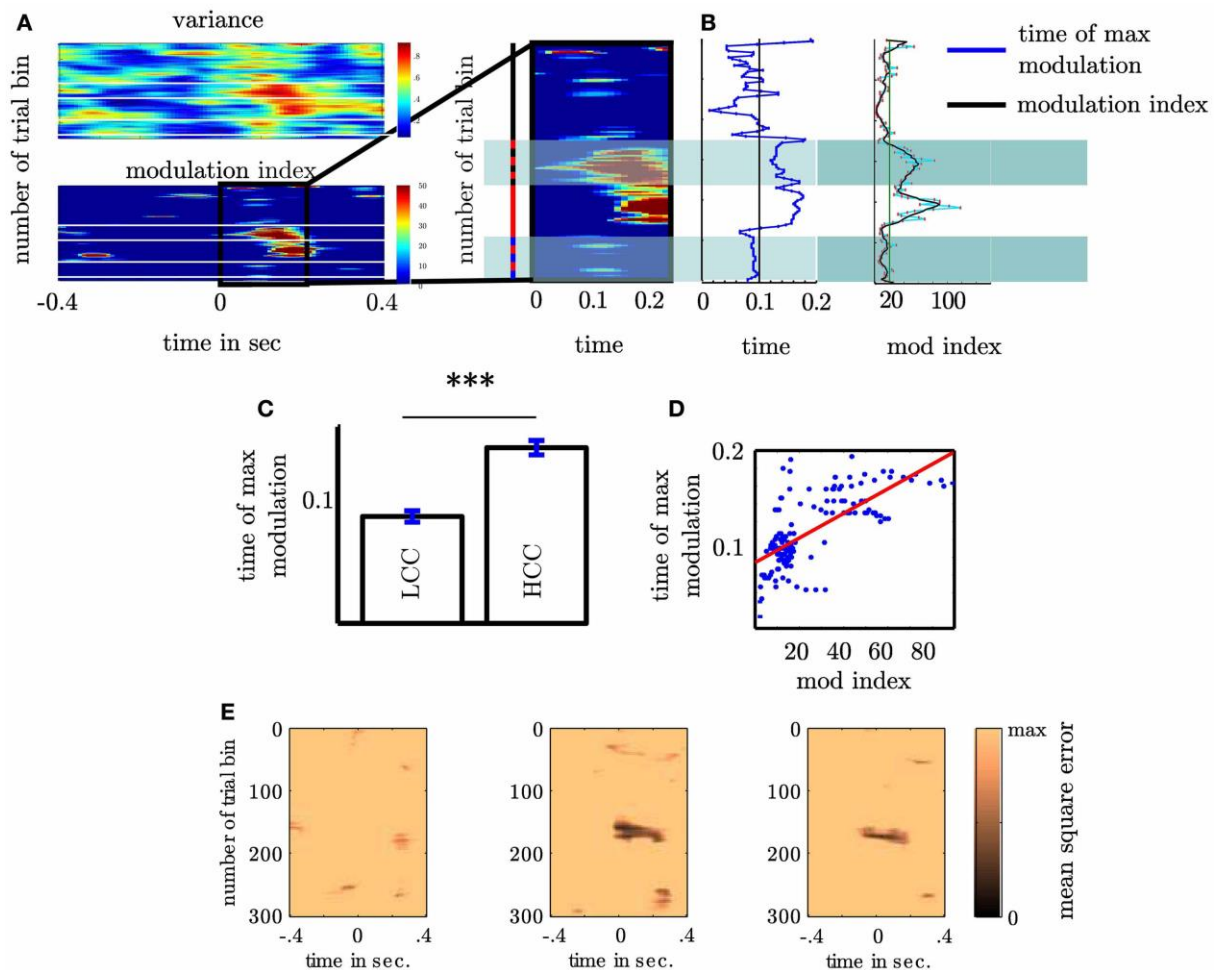
Abbildung 12 Darstellung der Variation der Kopplungsstärke.
*Die Kopplung zwischen der θ Phase und der HFA ist groß, wenn die kognitive Belastung besonders hoch ist. Dies ist am Anfang des Experiments und während dem Verfolgen der zufälligen Sequenz der Fall (**A,B**). Die Kopplung tritt in Durchgängen mit niedriger kognitiver Belastung eher auf (**C**), wobei der Zeitpunkt der Kopplung von der Modulationsstärke abhängig ist (**D**). **E** zeigt die Kopplungsstärke für jeden Teilnehmer.*

Kopplung von Phase und Amplitude über unterschiedliche Frequenzbänder (Phase-amplitude cross-frequency coupling - PAC) von Oszillationen werden als effektiver Mechanismus angesehen, lokale Netzwerke zu rekrutieren, um funktionale globale Netzwerke zu formen und Informationen anzusteuern (Buzsaki and Draguhn, 2004; Canolty et al., 2006; Cohen et al., 2009; Staudigl et al., 2012). Eine transiente θ-Phase-HFA Kopplung während des Bewegungslernens durch ein Labyrinth konnte bereist im Striatum von Ratten gezeigt werden (Tort et al., 2008) (Tort et al., 2009a). Jedoch wurde bisher nicht festgestellt, ob der NAcc PAC zwischen θ und HFA in einer funktionell spezifischen Art und Weise beim Menschen zeigt. Dies würde darauf hindeuten, dass Informationsintegration innerhalb des NAcc auf der transienten Kopplung zwischen Frequenzen beruht.

Im Folgenden wurde direkt die NAcc Aktivität bei drei Patienten mittels subkortikaler Elektroden gemessen. Dabei wurden die Probanden gebeten, eine Sequenz auf dem Bildschirm zu

verfolgen und auf sie mit einem Tastendruck zu reagieren (SRTT - (Nissen and Bullemer, 1987).

Die numerischen Reize der Sequenz konnten dabei entweder in fester oder zufälliger Abfolge prä-

sentiert werden, was zu Unterschieden in der kognitiven Kontrolle führt. Tort et al. (Tort et al.,

2009a) folgend, kann angenommen werden, dass PAC transient im NAcc auftritt und durch das

Maß an eingesetzter kognitiver Kontrolle moduliert wird. Dabei wurde getestet, ob es (i) PAC im

NAcc gibt, ob (ii) PAC zwischen hoher und niedriger kognitiver Kontrolle diskriminiert, und ob

(iii) PAC systematisch mit Verhaltensleistung über das Experiment variiert.

Dabei zeigte sich, dass im NAcc kontralateral zur Bewegung die θ Phase die HFA (100-

140Hz) nach der motorischen Antwort moduliert. Dabei stieg die PAC im menschlichen NAcc mit

der kognitiven Kontrolle und sagte die Verhaltensadaptation (Reduktion der Fehlerrate) vorher.

Die stärkste PAC wurde im ersten Teil gefunden, in dem die Probanden auf die vorhersagbare aber

noch unbekannte Sequenz antworteten und während sie auf die Reize in der zufälligen Sequenz,

die hohe kognitive Kontrolle erforderte, antworteten. Im Gegensatz dazu war PAC reduziert, wenn

die Probanden auf die bereits gelernten Stimuli oder wenn sie mit selbstgewähltem Tastendrü-

cken antworten mussten. Diese Ergebnisse zeigen eine Erhöhung der PAC, nachdem eine Ent-

scheidung getroffen wurde. Somit zeigen diese Daten, dass die PAC ein Mechanismus der Infor-

mationsintegration ist, da sie während der Phase hoher kognitiver Kontrolle auftritt. Das unter-

stützt die Hypothese, dass PAC einen effektiven Mechanismus liefert, über den lokale Netzwerke

rekrutiert werden, um funktionelle globale Netzwerke zu formen, mit dem Ziel, Informationen

bereitzustellen (Dürschmid et al., 2013).

Dürschmid S, Zaehle T, Kopitzki K, Voges J, Schmitt FC, Heinze HJ, Knight RT, Hinrichs H. Phase-amplitude cross-frequency coupling in the human nucleus accumbens tracks action monitoring during cognitive control. Front Hum Neurosci. 2013.

2.4.2 Phasen-Amplituden-Kopplung als zentraler Mechanismus für Mensch-Umwelt-Interaktion

Wie bereits erwähnt, sind jenseits klinischer Studien Hinweise für eine funktionelle Rolle von PAC im Prozess der Organisation von Kognition und Verhalten von Menschen begrenzt auf die Domäne des Gedächtnisses. Eine stärkere Verbindung zwischen PAC und menschlichem Verhalten würde durch eine Korrelation zwischen PAC und trial-by-trial Variationen in der Performanz gezeigt werden können. Um sich damit zu befassen, wurde im Folgenden die Beziehung zwischen PAC und Verbesserung der motorischen Leistung untersucht. Dafür wurde bei 6 Patienten die kortikale Aktivität (ECoG) erhoben während diese motorische Fertigkeiten lernten. Um die Verbindung zwischen PAC und Verhalten zu untersuchen, wurden Veränderungen im PAC mit Veränderungen der motorischen Performanz während der Aneignung von motorischen Fertigkeiten verglichen.

Dabei wurden drei motorische Experimente durchgeführt (Serial Reaction time task, Go/No-Go task und auditorisch-motorische Koordination), wobei jeder Patient an nur einem Experiment teilnahm. Alle Paradigmen erforderten die Koordination von Tastendrücken auf einer Computertastatur mit einem externen Stimulus. Alle Probanden führten die Aufgaben mit der Hand kontralateral zu dem implantierten Elektrodengitter aus.
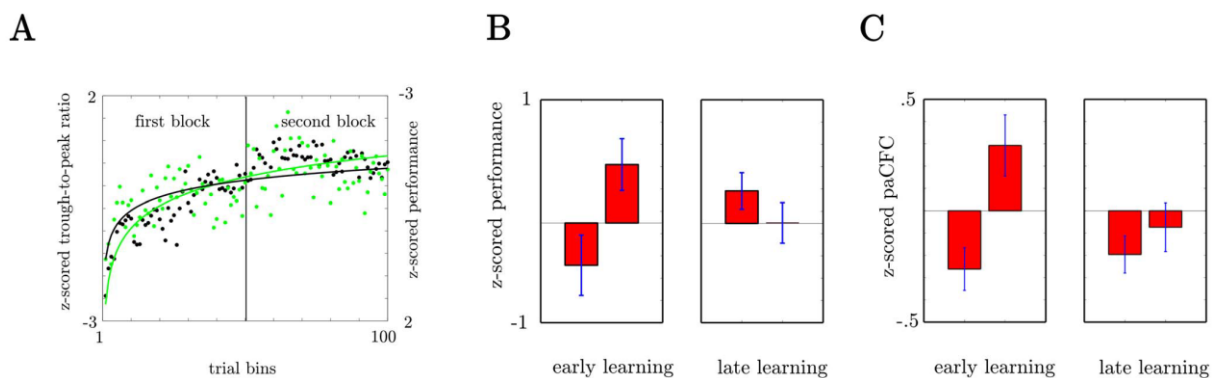
Abbildung 13 *Darstellung der Variation der Frequenzkopplung mit der Performanz gemittelt über alle Teilnehmer über den Verlauf des Experiments zeigen eine gleiche Dynamik (**A**). In **B** und **C** sind die Performance und Frequenzkopplungswerte gemittelt über die frühe und späte Phase dargestellt.*

Während der Verbesserung der motorischen Leistung zeigte sich eine klare Entwicklung der Kopplung. Diese konvergierte in der Stärke, wenn die Verhaltensverbesserung konvergierte. Damit konnte gezeigt werden, dass die PAC Dynamik adaptives motorisches Verhalten reflektiert. Trotz der Unterschiede in den Aufgaben konnten vergleichbare kortikale Regionen, die mit Verhaltensverbesserung assoziiert sind, identifiziert werden. Außerdem konnte gezeigt werden,

dass, obwohl sich die Phase der Kopplung nicht verändert, das Aktivitätsmuster beider Frequenzen mit Verhaltensveränderungen variiert (Dürschmid et al., 2014).

Dürschmid S, Quandt F, Krämer UM, Hinrichs H, Heinze HJ, Schulz R, Pannek H, Chang EF, Knight RT. Oscillatory dynamics track motor performance improvement in human cortex. PLoS One. 2014.

2.5 Mind Wandering – Erhöhung der Informationsintegration während der Selbstreflektion

Abhängig davon wie lange wir wach sind und von der Menge an Erfahrungen, die wir in Phasen der Wachheit machen, geht das Gehirn in schlafähnliche Zustände über, die sich als langsame Oszillationen mit hoher Amplitude (slow wave activity – SWA) und kurzer Minderung neuronaler Aktivität (Vyazovskiy et al., 2011) zeigen. Dies wird auch als lokaler Schlaf (LS) bezeichnet. Das Auftreten dieser OFF Phasen in verhaltensrelevanten kortikalen Arealen wie dem Motorkortex kann zu Verhaltensfehlern führen (Vyazovskiy et al., 2011). Auf phänomenologischer Ebene wird angenommen, dass LS zu Phasen des Mind Wanderings (MW) führt (Andrillon et al., 2019), während derer Aufmerksamkeit zu episodischen Inhalten wandert, die nichts mit der aktuellen Umgebungsinformation zu tun haben (Andrillon et al., 2019). MW umfasst dabei, dass wir episodisches Gedächtnis abrufen, während wir mit einer anderen Aufgabe befasst sind und dass wir uns dieser Inhalte bewusst werden. Jedoch ist das Bewusstsein für etwas nicht gleichbedeutend mit der Aufmerksamkeitsausrichtung darauf. In der Praxis ist die Trennung zwischen beiden jedoch sehr schwierig. Daraus ergibt sich die Frage, wie eng Bewusstsein und Aufmerksamkeit gekoppelt sind und ob Aufmerksamkeit ausgerichtet werden kann während wir uns anderer Dinge bewusst werden.

Andrillon et al. (Andrillon et al., 2019) schlugen vor, dass LS in Aufmerksamkeitsnetzwerken zu deren Deaktivierung und zur Rekrutierung des Default Mode Netzwerks führt und in Kombination zur MW führt. Ob LS aber tatsächlich zu MW führt ist nicht klar. Jedoch sind diese OFF Phasen potentiell gefährlich, vor allem, wenn das Bedürfnis des Gehirns nach Ruhe dann auftritt, wenn Aufmerksamkeit flexibel eingesetzt werden muss. Daher stellt sich die Frage, wie die Fähigkeit des Gehirns, Aufmerksamkeit während der OFF Phasen (LS und MW) zu verschieben, variiert und ob MW tatsächlich zu einer aufmerksamkeitsbezogenen Entkopplung von der Umwelt führt.

Im Folgenden wurde anhand der N2pc, die eine etablierte elektrophysiologische Antwort darstellt, die der Fokussierung von visueller Aufmerksamkeit auf Zielreize zwischen Distraktoren zugeschrieben wird (Luck and Hillyard, 1994; Eimer, 1996; Girelli et al., 1997; Hopf, 2000; Mazza et al., 2009), untersucht, wie sich räumliche Aufmerksamkeit während des MW verändert. Theoretisch sind zwei Szenarien möglich, wobei entweder die N2pc während des MW absinkt (Aufmerksamkeitsentkopplung) oder aber zunimmt, da MW als Ablenkung wahrgenommen wird und bekannt ist, dass die N2pc mit zunehmenden ablenkenden Reizen auch zunimmt (Mazza et al., 2009). Die Aufgabe der Pobanden dabei war es nach einem farbdefiniertem Zielreiz zwischen

aufgabenirrelevanten Distraktoren zu suchen. Dabei wurde die Hypothese untersucht, dass wenn MS mit LS assoziiert ist, dann finden sich während des MW mehr Phasen der SWA und Indikatoren für neuronale Ruhephasen. Letzteres könnte in einer Reduktion der HFA zu finden sein, was als Korrelat für die Feuerrate von Zellpopulationen gesehen wird (Friston et al., 2005; Liu and Newsome, 2006; Manning et al., 2009; Miller et al., 2009; Ray and Maunsell, 2011).
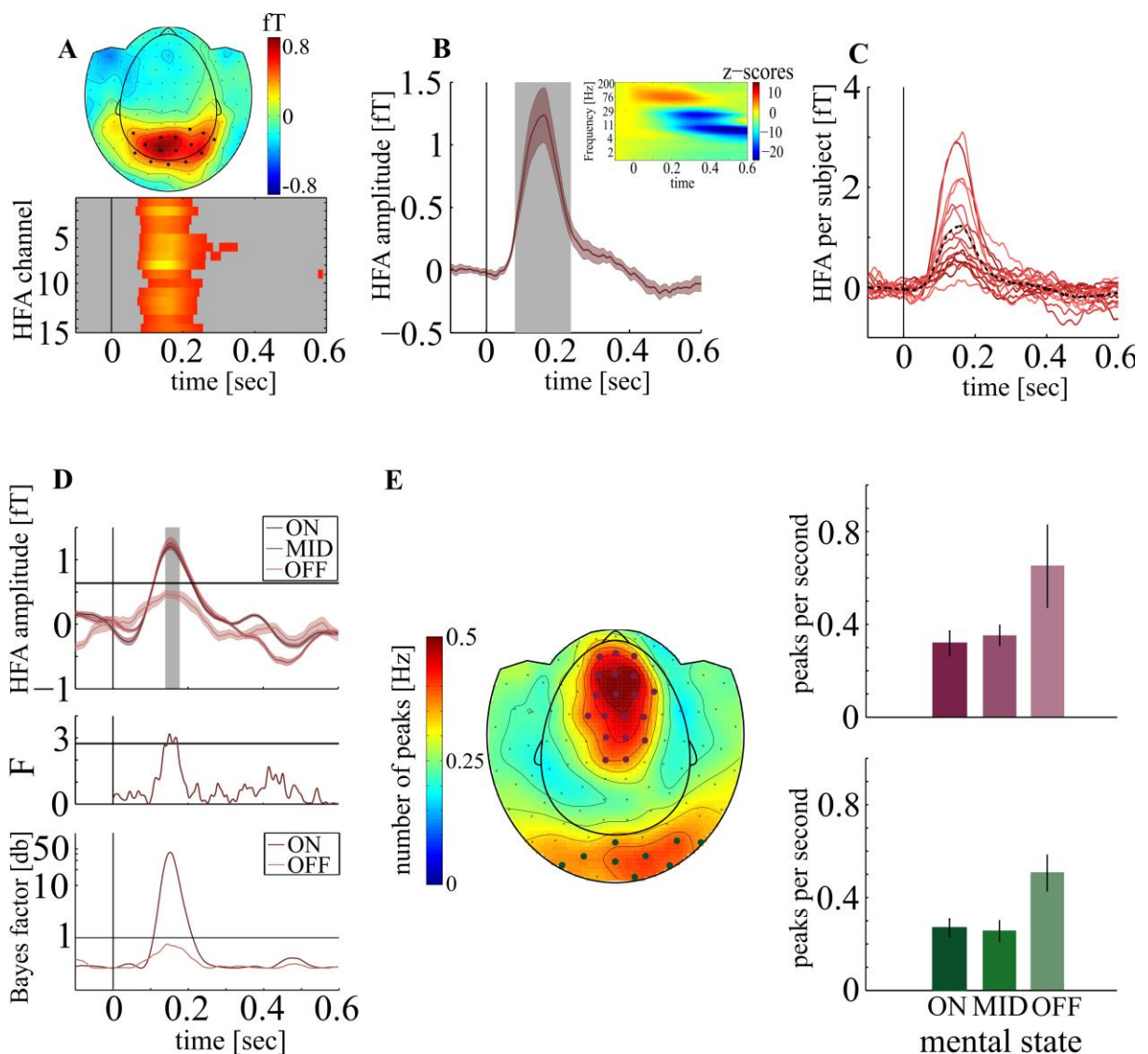
Abbildung 14 A *zeigt die HFA Antwort für die 15 MEG Sensoren mit einer signifikanten Antwort auf das Suchdisplay zwischen 81 und 234 ms (**B**) welche über allen Teilnehmern einen vergleichbaren Verlauf zeigt (**C**). Während des Mind Wanderings war diese reduziert (**D**) und Slow Wave Oszillationen traten vermehrt auf.*
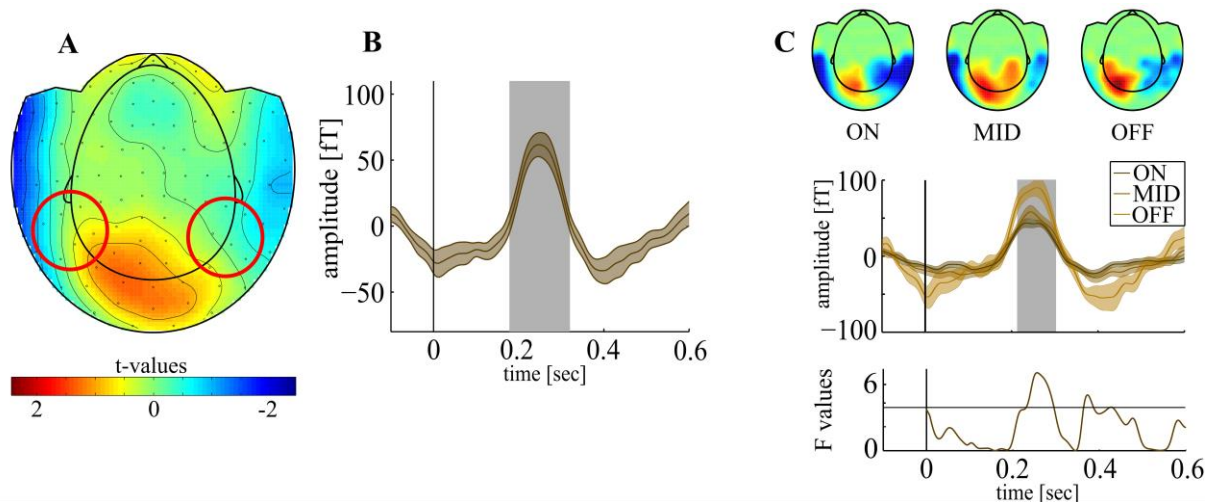
Abbildung 15 A *Darstellung des ereigniskorrelierten magnetischen Feldes (1-30Hz) gemittelt über Versuchs-durchgänge zwischen 200 und 300 ms.* **B** *Zeitverlauf der N2pc.* **C** *zeigt die magnetische Feldverteilung für die drei unterschiedlichen mentalen Zustände. Die N2pc ist während des Mind Wanderings erhöht.*

In diesem Experiment konnten sowohl eine verlässliche HFA Antwort in okzipitalen MEG Sensoren gefunden werden als auch einer sich anschließenden N2pc, die aufmerksamkeitsbezogene Zielreizselektion reflektiert. Der Onset der HFA stieg in okzipitalen MEG Sensoren um die 90 ms an und war davon abhängig, wie fokussiert die Studienteilnehmer waren. Spezifisch unter MW war die HFA stark abgesenkt (kein signifikanter Unterschied von der baseline). Parallel dazu nahm die Anzahl an SWA Perioden mit MW zu. Wie erwartet wurde die Leistung unter MW schlechter und die Reaktionszeiten nahmen zu. Im Kontrast dazu waren neurale Marker der Aufmerksamkeitsselektion stärker während MW und eng mit Verhaltensantworten verbunden. Das heißt, dass obwohl die Performanz generell niedrig war, zeigten Probanden mit einer hohen N2pc bessere Leistungen als Probanden mit weniger ausgeprägter N2pc. Allgemein waren Prozesse der attentionalen Zielreizselektion, die durch die N2pc indiziert werden, während des MW eher erhöht, um möglicherweise die mentale Ablenkung durch MW zu kompensieren.

Wienke C, Bartsch M V., Vogelgesang L, Reichert C, Hinrichs H, Heinze H-J, *Dürschmid S.* Local sleep during mind-wandering enhances processes of spatial attention allocation. Cerebral Cortex Communications, *2021; 2(1)*

3. Zusammenfassende Diskussion und Ausblick

Menschen sind in der Lage Informationen zu verarbeiten, diese in für die jeweilige Person sinnvoller Weise zusammenzufassen um aus den gewonnenen Informationen ein Bild von der Umwelt zu erzeugen, anhand dessen sie ihre Handlungen ausrichten. In dieser Habilitationsschrift gebe ich einen Überblick über die Mechanismen, von denen angenommen wird, dass sie zur Informationsintegration beitragen. Diese Mechanismen sind komplex und notwendigerweise so divers wie die Anforderung, die die Umwelt auf der einen Seite stellt und wie die Handlungen, mit denen wir auf die Umwelt reagieren, auf der anderen Seite sind. Um Informationsintegration in der tatsächlichen Breite möglichst umfänglich zu erfassen, sind Messmethoden eingesetzt worden, die die jeweilige Fragestellung am besten erfassen. Invasive Messmethoden sind dabei Garant subkortikale Aktivität überhaupt und neuronale Aktivität ohne verzerrende Filtereffekte etwa durch den Schädel erfassen zu können. Diese Art der Messmethoden ergänzen die nicht-invasiven Methoden wie EEG und MEG in logischer Weise. Ein einheitliches Merkmal all dieser Messmethoden ist, dass sie Gehirnprozesse in ihrer tatsächlichen zeitlichen Skala am besten abbilden können.

Wir konnten in der ersten hier vorgestellten Studie zeigen, dass das menschliche Gehirn einen kritischen Punkt erreichen kann, an dem es sich an der Grenze zwischen Ordnung und Chaos befindet, bei dem man davon ausgeht, dass dieser die Grundlage für optimale Informationsintegration bildet. Dieser Punkt kann durch ein einfaches meditatives Training erreicht werden, das, wie in der Literatur beschrieben, zu einem verbesserten Einsatz der Aufmerksamkeitsressourcen führt. Jedoch wird der Zusammenhang in der bestehenden Literatur immer noch kontrovers diskutiert. Ein ausgereifter Konsens ist allerdings schon allein aufgrund nur wenigen Untersuchungen nicht wahrscheinlich. Nur wenige Studien haben die Beziehung zwischen Meditation und Kritikalität untersucht. Irrmischer et al. (Irrmischer et al., 2018) zeigten eine Reduktion langer zeitlicher Korrelationen während der MFA und vertraten die Hypothese, dass Aufmerksamkeit am kritischen Punkt ausbalanciert ist, was sowohl einen transienten Fokus als auch einen schnellen Wechsel zwischen Aufmerksamkeitsressourcen erlaubt. Argumentiert wurde in dieser Studie, dass der Aufmerksamkeitsfokus die Informationsweiterleitung reduziert, was im Kontrast zu unseren Ergebnissen steht. Diese können aber auch durch die Unterschiede in der Messtechnik (MEG bei uns, EEG bei Irrmischer et al.) liegen. Außerdem war es unser Ziel, Informationsintegration unabhängig von Umweltinformationen zu untersuchen, weshalb wir nicht stimulusgetriebene (zum Vergleich (Fagerholm et al., 2015)) sondern selbstregulierte Modulation der top-down Aufmerksamkeit untersuchten. Die Kritikalität stellt daher eine Voraussetzung für die Informationsintegration dar.

Wichtig ist dabei, dass die selbstorganisierte Kritikalität mit einer Verringerung der Amplitude der hochfrequenten Aktivität in rechten fronto-temporalen Kortexregionen einhergeht. Ein gleiches räumliches wie auch spektrales Muster findet sich auch dann, wenn wir Probanden baten sich zwischen einer frühen aber kleinen und einer späten dafür aber größeren Belohnung zu entscheiden. MEG Sensoren über dieser fronto-temporalen Region zeigten eine Integration von Belohnungswert und deren Auszahlungszeitpunkt. Integration im Sinne des Delay Discountings meint, dass eine Region gleiche Umweltreize kodiert. Eine Neuheit an der Studie ist, dass wir direkt untersucht haben, ob der subjektive Wert Impulsivität entgegenwirkt. Bisherige Studien konnten dabei nicht den Zeitverlauf der Repräsentation von Wahlmöglichkeiten in der zeitlichen Dimension (Millisekunden bis Sekunden), in der dieser stattfindet, auflösen. Der subjektive Wert wurde dabei durch den Kontrast zwischen Wahlmöglichkeiten für einen selbst oder in einer prosozialen Bedingung operationalisiert. Eine Frage die sich dabei stellt ist, ob Menschen tatsächlich prosozial handeln. Vorherige Studien zeigen, dass Probanden weniger Anstrengungsbereitschaft zeigten, wenn sie sich für andere entscheiden sollten (Lockwood et al., 2017). Daher nahmen wir an, dass die Bereitschaft, Wahlmöglichkeiten in ihrer Tiefe zu evaluieren, sich zwischen den beiden experimentellen Bedingungen unterschied. Um die zeitlichen Entwicklung der Integration der Optionen zu untersuchen, verglichen wir Muster der Aufmerksamkeitsverlagerung (Eye Tracker) und der Integration von Handlungsoptionen auf neuronaler Ebene (MEG). Bei Letzterem zeigt sich, dass Aktivität in MEG Sensoren über fronto-temporalen Regionen diese Integration reflektiert. Frühere intrakranielle Aufzeichnungen hochfrequenter Aktivität haben unser Verständnis über die kortikale Informationsintegration erweitert, wobei gezeigt wurde, dass die HFA als Index lokaler kortikaler Berechnung dient. Diese Studien zeigen, dass die Voraussetzungen für optimale Informationsintegration durch kritische Gehirndynamik gegeben sind und dass Informationen aus der Umwelt tatsächlich integriert werden.

In der Umwelt treten jedoch bestimmte Ereignisse mit unterschiedlicher Häufigkeit auf. Diese Häufigkeitsverteilung erfasst das Gehirn über die Zeit, was es erlaubt, Vorhersagen über die Auftretenswahrscheinlichkeit von Umweltreizen zu treffen. Im NAcc zeigt sich dabei eine doppelte Integration, da auf anatomischer Ebene Informationen aus dem Hippocampus und dem PFC einerseits und über die Auftretenswahrscheinlichkeit von Umweltreizen andererseits integriert werden. Der NAcc trägt dabei zur Kodierung der Statistik der auditorischen Umwelt bei, was sich durch eine graduelle Variation der Amplituden des LFP manifestiert. Diese Ergebnisse zeigen die Bedeutung des NAcc hinsichtlich der automatischen Integration sensorischer Informationen. Die Beziehung zwischen dem NAcc und der P300 liefert Hinweise auf die Rolle in Gedächtnisprozessen, da möglicherweise neuronale Aktivität, die zwischen dem medialen Temporallappen und dem dopaminergen Mittelhirn geteilt werden, verbunden werden. Die Korrelation der NAcc Aktivität mit der P300 ist zentral für die Annahme einer Verhaltensrelevanz des NAcc – was sich an

der Kreuzkorrelation zwischen den Frequenzen während des motorischen Lernens zeigt. Die P300 ist verbunden mit Gedächtnisspeicherung und der Detektion verhaltensrelevanter Zielreize (Knight, 1996, 1998; Polich and Criado, 2006; Polich, 2007). In unserer Studie benutzten wir nur schwache Abweichreize, die typischerweise nur die zentro-parietale P3 Antwort aktivieren. Dies könnte bedeuten, dass die Detektion kontextueller Abweichung im hippocampalen-NAcc Netzwerk stattfindet. Diese integrierte Information wird benutzt, um die Aktivierung eines breiten Aufmerksamkeitsnetzwerks auszulösen, dass sich als P3 Antwort manifestiert.

Dass diese Integration von Umweltinformationen über die Zeit eine wichtige Ressource des Gehirns ist, zeigt vor allem die Modulation der Detektion von kontextuellen Abweichungen bei Alzheimer Patienten, deren Fähigkeit sensorischer Bahnung auditorischer Informationen in sensorisches Gedächtnis eingeschränkt ist. Die Hypothese in dieser Studie war, dass wir eine Veränderung der Gehirnantworten zwischen der auditorischen Stimulation ohne und mit NB-DBS finden, die sich nicht durch eine wiederholte Stimulation bei den gesunden Kontrollprobanden finden lässt. In dem Fall würden Unterschiede allein der Stimulation aber nicht der Wiederholung zugeschrieben werden können. Wir fanden, dass ohne DBS die MMN früher war, was durch eine stärkere P50 erklärt werden kann, welche eine Beeinträchtigung der präattentiven Hemmung wiederholten auditorischen Inputs widerspiegelt. Die P50 ist altersabhängig mit stärkerer Amplitude bei älteren Probanden und der Anstieg indiziert ein Defizit in der Filterung bekannter Informationen. Das vorrangige Ziel der Studie war es, einen möglichen vorteilhaften Effekt der NB-DBS auf die sensorische Integration zu untersuchen. Trotz der begrenzten Generalisierbarkeit aufgrund der geringen Anzahl an Patienten handelt es sich hier um einen wichtigen Hinweis, vor allem vor dem Hintergrund nur weniger Publikationen zu dem Thema. Bei dieser sehr seltenen Gelegenheit der Aufzeichnung von Gehirnprozessen zeigte sich, dass die Fähigkeit der Informationsintegration über die Zeit bei AD Patienten verloren geht, diese aber durch DBS wieder hergestellt werden kann. Die Frage der Integration von Information über die Zeit an sich konnte in dieser Studie und in vorherigen Studien bereits positiv beantwortet werden. Allein die Relevanz der Informationsintegration ist damit noch nicht gezeigt. Eine Veränderung eines Vorhersagefehlers, wie ihn die MMN anzeigt in Abhängigkeit von der Vorhersagbarkeit von Devianten, würde dagegen zeigen, dass Umweltinformationen über die Zeit tatsächlich genutzt werden und zu einem schlüssigen Bild über die Umwelt integriert werden. EEG und MEG sind nicht geeignet, eng umschriebene Gehirnareale aufzulösen. Außerdem ist es zumindest im EEG nicht möglich, die HFA aufgrund des schlechten Signal-zu-Rauschen Verhältnisses zu erfassen. Funktionelle MRT Studien deuten auf sowohl temporale als auch präfrontale Aktivität hin. Nur mögliche Unterschiede in den Antwortprofilen können damit nicht aufgelöst werden. In unserer ECoG Studie zeigte sich sowohl im frontalen als auch im temporalen Kortex eine Antwort auf die auditorischen

Reize. Die Dissoziation von Antwortmustern auf vorhersagbare und nicht vorhersagbare zwischen beiden Kortexregionen zeigt Unterschiede in der Informationsverarbeitung und Integration auf. Diese Unterscheidung ist vor allem durch die HFA möglich. Dabei fügt die HFA Information über unterschiedliche zeitliche Dimensionen zusammen. Alle Devianten können als lokale Abweichungen gesehen werden. Darüber hinaus sind die Devianten in den nicht vorhersagbaren Blöcken auch globale Devianten. Aber nur die globalen Devianten führen zu einem PE im frontalen Kortex. Diese Studie zeigt im Gegensatz zu früheren Studien, in denen der deviante Ton ein Zielreiz war, bei dessen Auftreten ein Knopf gedrückt werden musste, dass die Umweltinformationen automatisch erfasst werden: also auch dann, wenn eine Reaktionen nicht zwingend notwendig ist.

Im anschließenden Schritt konnten wir direkte Hinweise zeigen, dass der frontale Kortex Vorhersagesignale unabhängig vom PE zeigt. Predictive Coding Theorien gehen davon aus, dass das Gehirn kontinuierlich verfügbare Informationen integriert, um auf Grundlage dessen zukünftige Ereignisse vorherzusagen. Jedoch kamen Hinweise darauf auf Veränderungen des Vorhersagefehlers und waren damit nur indirekt. Diese Studie lieferte Hinweise, dass der frontale Kortex, nicht jedoch der temporale Kortex die Statistik der Umwelt integriert und automatisch proaktive, antizipatorische Vorhersagen generiert. Dieses Muster stimmt mit einer so genannten *hazard function* überein, innerhalb derer ein bevorstehendes Ereignis wahrscheinlicher wird, je länger es nicht aufgetreten ist. Dies kann nur gelingen, in dem das Gehirn automatisch und ohne Verhaltensrelevanz komplexe Regularitäten über die Zeit integriert und basierend darauf Vorhersagen generiert. Jedoch ist nicht klar, ob die prästimulus HFA Modulation in unserer Studie die gleichen Vorhersagesignalen repräsentiert wie jene, die in PC Theorien formuliert sind oder ob sie ein Ergebnis von Vorhersagesignale sind. In der Summe zeigt sich, dass Informationsintegration aufwärts und abwärts in der kortikalen Hierarchie nicht so simpel ist wie zuvor angenommen. Globale Regularitäten zu erfassen ermöglicht es dem PFC, Aufmerksamkeit auf unerwartete Ereignisse zu lenken. Die Detektion von lokalen Abweichungen ist dagegen auch vorteilhaft, nämlich dann wenn es darum geht, den auditorischen Input in bedeutungsvolle Stücke zu zergliedern. Beide Aspekte sind für die Informationsintegration unerlässlich, da diese erst die Voraussetzung ist, damit wir auf Umwelt optimal reagieren können. Dies zeigt sich an der Kontrolle von motorischen Bewegungen in Abstimmung mit Umweltreizen.

Ein vielfach beschriebenes Phänomen dabei ist die Kopplung von θ und HFA, die sich übereinstimmend mit der Verhaltensverbesserung verändert. Dieses Kopplungsmuster ermöglicht adaptives Verhalten, was Resultat von kontinuierlicher Informationsintegration ist. Trotz der Unterschiede zwischen den motorischen Aufgaben, die die Probanden durchführen mussten, zeigten sich übereinstimmende kortikale Regionen, die mit Verhaltensverbesserung und zufälliger Leis-

tungsvariation assoziiert sind. In unserer Studie konnten wir außerdem zeigen, dass sich das Aktivitätsmuster trotz Phasenstabilität mit den Verhaltensveränderungen verändert. Verhaltensverbesserung während des Übens wird durch verteilte θ-Netzwerke – die während des Wachseins hochreguliert werden – ermöglicht. Diese integrieren oder koordinieren lokale Aktivität. Hierbei meint das Konzept der Informationsintegration, dass θ oszillatorische Aktivität die Ergebnisse aus lokaler Verarbeitung, die durch die HFA im (prä-)motorischen Kortex reflektiert werden, akkumuliert. Dabei kann angenommen werden, dass Informationen über die Planung von motorischen Antworten durch PAC ins Gedächtnis integriert werden. Dies zeigt sich besonders eindrucksvoll an der Frequenzkopplung im NAcc, der wechselseitig von Hippocampus und PFC-Aktivität abhängig ist. Die komplexe Verbindung limbischer, präfrontaler und motorischer Aktivität macht den NAcc zu einer idealen Region für Informationsintegration, was man wiederum an der Veränderung der Frequenzkopplung in dieser Region sehen kann. Bemerkenswert dabei ist, dass das Kopplungsmuster abhängig von der kognitiven Kontrolle und damit zustandsabhängig ist. Dies untermauert die Hypothese, das PAC ein Mechanismus ist, um Informationen zu integrieren. Frühere Studien legen nahe, dass unterschiedlichen Phasen im θ Zyklus unterschiedliche funktionelle Bedeutung haben. Vorallem die abfallende Flanke ist wichtig für den Gedächtnisabruf und die Senke für das Enkodieren neuer Informationen.

In den vorangegangen Studien konnte gezeigt werden, dass Informationen integriert werden und dass es sich dabei vermutlich um einen automatischen Prozess handelt, der im Hintergrund abläuft. Auch wenn dieses nicht explizit getestet wurde, kann angenommen werden, dass dies auch dazu führt, dass wir während des Mind Wanderings nicht komplett den Bezug zur Umwelt verlieren. Es kann angenommen werden, dass das Gehirn detektiert, dass wichtige Informationen durch lokalen Schlaf nicht weiter integriert werden und dadurch Aufmerksamkeitsressouren hochgefahren werden, um der mentalen Ablenkung während des MW entgegenzuwirken. Integration muss dabei auf zwei Ebenen stattfinden. Informationen über interne Prozesse werden integriert, um anhand derer den Einsatz kognitiver Ressourcen zu vermitteln, um eine optimale Integration von externen Informationen wieder zu gewährleisten.

Zusammengenommen demonstrieren die vorgelegten Arbeiten die Wichtigkeit einer breiten Perspektive in der Erforschung komplexer Integrationsprozesse. Die Interaktion mit der Umwelt wird durch eine Vielzahl an internen und externen Faktoren bestimmt und zeigt uns so, welche Komponenten zum Verständnis der grundlegenden Fähigkeit zur Verhaltenskontrolle und Verhaltenssteuerung wichtig sind, wenn wir lernen oder mental abgelenkt sind.

4. Relevante Publikationen des Autors

Dürschmid S., Reichert C. , Walter N., Hinrichs H., Heinze H.J., Ohl F.W., Tononi G., Deliano M. Self-regulated critical brain dynamics originate from high frequency-band activity in the MEG. PLoS ONE, 2020.
https://doi.org/10.1371/journal.pone.0233589

Dürschmid S, Maric A, Kehl MS, Robert T Knight RT, Hinrichs H, Heinze HJ. Fronto-temporal cortex regulation of subjective valence to suppress impulsivity in intertemporal choices. Journal of Neuroscience, 2021.

Dürschmid S, Zaehle T, Hinrichs H, Heinze HJ, Voges J, Garrido MI, Dolan RJ, Knight RT. Sensory Deviancy Detection Measured Directly Within the Human Nucleus Accumbens. Cereb Cortex. 2016 Mar;26(3):1168-1175.

Dürschmid S, Reichert C, Kuhn J, Freund HJ, Hinrichs H, Heinze HJ. Deep Brain stimulation of the Nucleus Basalis of Meynert attenuates early EEG components associated with defective sensory gating in patients with Alzheimer disease – a two-case study. EJN. 2017

Dürschmid S, Edwards E, Reichert C, Dewar C, Hinrichs H, Heinze HJ, Kirsch HE,Dalal SS, Deouell LY, Knight RT. Hierarchy of prediction errors for auditory events in human temporal and frontal cortex. Proc Natl Acad Sci U S A. 2016 Jun 14;113(24):6755-60. IF: 10.4 (5y)

Dürschmid S, Reichert C, Hinrichs H, Heinze HJ, Kirsch HE, Knight RT, Deouell LY. Direct evidence for prediction signals in frontal cortex independent of prediction error. Cereb Cortex. 2019. https://doi.org/10.1093/cercor/bhy331

Dürschmid S, Zaehle T, Kopitzki K, Voges J, Schmitt FC, Heinze HJ, Knight RT, Hinrichs H. Phase-amplitude cross-frequency coupling in the human nucleus accumbens tracks action monitoring during cognitive control. Front Hum Neurosci. 2013 Oct 7;7:635.

Dürschmid S, Quandt F, Krämer UM, Hinrichs H, Heinze HJ, Schulz R, Pannek H, Chang EF, Knight RT. Oscillatory dynamics track motor performance improvement in human cortex. PLoS One. 2014 Feb 27;9(2).

Wienke C, Bartsch M V., Vogelgesang L, Reichert C, Hinrichs H, Heinze H-J, ***Dürschmid S.*** Local sleep during mind-wandering enhances processes of spatial attention allocation. Cerebral Cortex Communications, *2021; 2(1)*

Vollständige Publikationsliste des Autors

Artikel, die nach der Dissertation publiziert wurden, sind mit ***** gekennzeichnet

Erst- oder Seniorautorenschaften

* 1. Wienke C, Bartsch M V., Vogelgesang L, Reichert C, Hinrichs H, Heinze H-J, *Dürschmid S.* Local sleep during mind-wandering enhances processes of spatial attention allocation. Cerebral Cortex Communications, *in press* *****

* 2. *Dürschmid S, Maric A,* Kehl MS, Robert T Knight RT, Hinrichs H, Heinze HJ. Fronto-temporal cortex regulation of subjective valence to suppress impulsivity in intertemporal choices. Journal of Neuroscience, in press 2020.

* 3. Reichert C, Tellez Ceja IF, Sweeney-Reed CM, Heinze HJ, Hinrichs H, *Dürschmid S.* Impact of stimulus features on the performance of a gaze-independent brain-computer interface based on covert spatial attention shifts. Frontiers in Neuroscience, 2020. https://doi.org/10.3389/fnins.2020.591777

* 4. Vogelgesang L, Reichert C, Hinrichs H, Heinze, HJ, *Dürschmid S.* Early Shift of Attention is Not Regulated by Mind-Wandering in Visual Search. Frontiers in Human Neuroscience, 2020. https://doi.org/10.3389/fnins.2020.552637

* 5. *Dürschmid S.,* Reichert C. , Walter N., Hinrichs H., Heinze H.J., Ohl F.W., Tononi G., Deliano M. Self-regulated critical brain dynamics originate from high frequency-band activity in the MEG. PLoS ONE, 2020. https://doi.org/10.1371/journal.pone.0233589

* 6. *Dürschmid S*, Reichert C, Hinrichs H, Heinze HJ, Kirsch HE, Knight RT, Deouell LY. Direct evidence for prediction signals in frontal cortex independent of prediction error. Cereb Cortex. 2019. https://doi.org/10.1093/cercor/bhy331

* 7. *Dürschmid S*, Reichert C, Kuhn J, Freund HJ, Hinrichs H, Heinze HJ. Deep Brain stimulation of the Nucleus Basalis of Meynert attenuates early EEG components associated with defective sensory gating in patients with Alzheimer disease – a two-case study. EJN.https://doi.org/10.1111/ejn.13749

* 8. Stenner MP, *Dürschmid S**, Rutledge RB, Zaehle T, Schmitt FC, Kaufmann J, Voges J, Heinze HJ, Dolan RJ, Schoenfeld MA. Perimovement decrease of alpha/beta oscillations in the human nucleus accumbens. J Neurophysiol. 2016 Oct 1;116(4):1663-1672. https://doi.org/10.1152/jn.00142.2016

* 9. *Dürschmid S*, Edwards E, Reichert C, Dewar C, Hinrichs H, Heinze HJ, Kirsch HE,Dalal SS, Deouell LY, Knight RT. Hierarchy of prediction errors for auditory events in human temporal and frontal cortex. Proc Natl Acad Sci U S A. 2016 Jun 14;113(24):6755-60. IF: 10.4 (5y) https://doi.org/10.1073/pnas.1525030113

* 10. *Dürschmid S*, Zaehle T, Hinrichs H, Heinze HJ, Voges J, Garrido MI, Dolan RJ, Knight RT. Sensory Deviancy Detection Measured Directly Within the Human Nucleus Accumbens. Cereb Cortex. 2016 Mar;26(3):1168-1175. https://doi.org/10.1093/cercor/bhu304

* 11. *Dürschmid S*, Quandt F, Krämer UM, Hinrichs H, Heinze HJ, Schulz R, Pannek H, Chang EF, Knight RT. Oscillatory dynamics track motor performance improvement in human cortex. PLoS One. 2014 Feb 27;9(2). https://doi.org/10.1371/journal.pone.0089576

*12. **Dürschmid S**, Zaehle T, Kopitzki K, Voges J, Schmitt FC, Heinze HJ, Knight RT, Hinrichs H. Phase-amplitude cross-frequency coupling in the human nucleus accumbens tracks action monitoring during cognitive control. Front Hum Neurosci. 2013 Oct 7;7:635. https://doi.org/10.3389/fnhum.2013.00635

Ko-Autorenschaften

*1. Krüger J, Reichert C, **Dürschmid S**, Krauth R, Vogt S, Huchtemann T, Lindquist S, Lamprecht J, Sailer M, Heinze H-J, Hinrichs H, Sweeney-Reed CM. Rehabilitation nach Schlaganfall: Durch Gehirn-Computer-Schnittstelle vermittelte funktionelle Elektrostimulation. Klinische Neurophysiologie, 2020. https://doi.org/10.1055/a-1205-7467

*2. Reichert C, **Dürschmid S**, Bartsch M, Hopf JM, Heinze H-J, Hinrichs H. Decoding the covert shift of spatial attention from electroencephalographic signals permits reliable control of a brain-computer interface. Journal of Neural Engineering, 2020. https://doi.org/10.1088/1741-2552/abb692

*3. Reichert C, **Dürschmid S**, Hinrichs H. EEG as a Control Signal: Decoding of Brain Activity and ist Efficient Application as Communication Channel for Patients with Motor Deficits. Klinische Neurophysiologie, 2020. https://doi.org/10.1055/a-1135-3782

*4. Beck AK, Sandmann P, **Dürschmid S**, Schwabe K, Saryyeva A, Krauss JK. Neuronal activation in the human centromedian-parafascicular complex predicts cortical responses to behaviorally significant auditory events. *Neuroimage*. 2020. IF: 5.8 https://doi.org/10.1016/j.neuroimage.2020.116583

*5. Reichert C, **Dürschmid S**, Kuhn J, Freund HJ, Hinrichs H, Heinze HJ. A Comparative Study on the Detection of Covert Attention in Event-related EEG and MEG Signals to Control a BCI. Frontiers in Human Neuroscience. IF: 3.2. https://doi.org/10.3389/fnins.2017.00575

*6. Reichert C, **Dürschmid S**, Kruse R, Hinrichs H. An Efficient Decoder for the Recognition of Event-Related Potentials in High-Density MEG Recordings. Computers. 2016.https://doi.org/10.1186/s12868-016-0283-6

*7. Mikutta C, **Dürschmid S**, Bean N, Lehne M, Lubell J, Altorfer A, Parvizi J, Strik WK, Knight RT, Koelsch S, Amygdala and Orbitofrontal engagement in breach and resolution of expectancy - a case study. Psychomusicology: Music, Mind and Brain, 2015. https://doi.org/10.1037/pmu0000121

8. Quandt F, Reichert C, Schneider B, **Dürschmid S**, Richter D, Rieger JW. Fundamentals and Application of Brain-Machine Interfaces (BMI). Klinische Neurophysiologie June 2012 43(2):158-167. https://doi.org/10.1055/s-0032-1308970

9. Busch NA, **Dürschmid S**, Herrmann CS. ERP effects of change localization, change identification, and change blindness. Neuroreport. 2010 Mar 31;21(5):371-5. IF: 1.3 https://doi.org/10.1097/WNR.0b013e3283378379

Buchkapitel

C.S. Herrmann, ***S. Dürschmid***. Von Libet zu einer Neuen Willensfreiheit: Bewusste versus unbewusste Handlungsabsichten. In: T. Fuchs, G. Schwarzkopf (Hrsg.) Verantwortlichkeit – nur eine Illusion?, 127-146, Universitätsverlag Heidelberg, 2010

Referenzen

Abler B, Walter H, Erk S, Kammerer H, Spitzer M (2006) Prediction error as a linear function of reward probability is coded in human nucleus accumbens. Neuroimage 31:790–795.

Aggelopoulos NC, Liebe S, Logothetis NK, Rainer G (2011) Cholinergic control of visual categorization in macaques. Front Behav Neurosci.

Ainslie G (1975) Specious reward: a behavioral theory of impulsiveness and impulse control. Psychol Bull 82:463–496.

Allen EA, Liu J, Kiehl KA, Gelernter J, Pearlson GD, Perrone-Bizzozero NI, Calhoun VD (2011) Components of cross-frequency modulation in health and disease. Front Syst Neurosci.

Andrillon T, Windt J, Silk T, Drummond SPA, Bellgrove MA, Tsuchiya N (2019) Does the Mind Wander When the Brain Takes a Break? Local Sleep in Wakefulness, Attentional Lapses and Mind-Wandering. Front Neurosci 13:1–10.

Anllo-Vento L (1995) Shifting attention in visual space: The effects of peripheral cueing on brain cortical potentials. Int J Neurosci 80:353–370.

Arcangelis L De, Herrmann HJ (2010) Learning as a phenomenon occurring in a critical state.

Axmacher N, Cohen MX, Fell J, Haupt S, Dümpelmann M, Elger CE, Schlaepfer TE, Lenartz D, Sturm V, Ranganath C (2010a) Intracranial EEG Correlates of Expectancy and Memory Formation in the Human Hippocampus and Nucleus Accumbens. Neuron 65:541–549.

Axmacher N, Henseler MM, Jensen O, Weinreich I, Elger CE, Fell J (2010b) Cross-frequency coupling supports multi-item working memory in the human hippocampus. Proc Natl Acad Sci U S A 107:3228–3233.

Baddeley A (1992) Working Memory: The Interface between Memory and Cognition. J Cogn Neurosci 4:281–288.

Bak P (1996) How Nature Works, 2nd ed. copernicus.

Baliki MN, Geha PY, Fields HL, Apkarian AV (2010) Predicting Value of Pain and Analgesia: Nucleus Accumbens Response to Noxious Stimuli Changes in the Presence of Chronic Pain. Neuron 66:149–160.

Baudena P, Halgren E, Heit G, Clarke JM (1995) Intracerebral potentials to rare target and distracter auditory and visual stimuli. III. Frontal cortex. Electroencephalogr Clin Neurophysiol 94:251–264.

Becerra L, Breiter HC, Wise R, Gonzalez RG, Borsook D (2001) Reward circuitry activation by noxious thermal stimuli. Neuron 32:927–946.

Beggs JM, Plenz D (2003) Neuronal Avalanches in Neocortical Circuits. J Neurosci 23:11167–11177.

Beggs JM, Timme N (2012) Being critical of criticality in the brain. Front Physiol 3 JUN:1–14.

Belujon P, Grace AA (2008) Critical role of the prefrontal cortex in the regulation of

hippocampus-accumbens information flow. J Neurosci 28:9797–9805.

Bendixen A, Schwartze M, Kotz SA (2015) Temporal dynamics of contingency extraction from tonal and verbal auditory sequences. Brain Lang 148:64–73.

Berger MS, Deouell LY, Knight RT, Edwards E, Soltani M (2005) High Gamma Activity in Response to Deviant Auditory Stimuli Recorded Directly From Human Cortex. J Neurophysiol 94:4269–4280.

Bewernick BH, Hurlemann R, Matusch A, Kayser S, Grubert C, Hadrysiewicz B, Axmacher N, Lemke M, Cooper-Mahkorn D, Cohen MX, Brockmann H, Lenartz D, Sturm V, Schlaepfer TE (2010) Nucleus Accumbens Deep Brain Stimulation Decreases Ratings of Depression and Anxiety in Treatment-Resistant Depression. Biol Psychiatry 67:110–116.

Brewer JA, Worhunsky PD, Gray JR, Tang Y, Weber J, Kober H (2011) Meditation experience is associated with differences in default mode network activity and connectivity. 108.

Buzsaki G, Draguhn A (2004) Neuronal Oscillations in Cortical Networks. Science (80-) 304:1926–1929 Available at: http://science.sciencemag.org/.

Cahn BR, Polich J (2009) Meditation (Vipassana) and the P3a event-related brain potential. Int J Psychophysiol 72:51–60 Available at: http://dx.doi.org/10.1016/j.ijpsycho.2008.03.013.

Canolty RT, Edwards E, Dalal SS, Soltani M, Nagarajan SS, Kirsch HE, Berger MS, Barbaro NM, Knight RT (2006) High Gamma Power Is Phase-Locked to Theta Oscillations in. 313:1626–1629.

Canolty RT, Knight RT (2010) The functional role of cross-frequency coupling. Trends Cogn Sci 14:506–515.

Cheng CH, Wang PN, Hsu WY, Lin YY (2012) Inadequate inhibition of redundant auditory inputs in Alzheimer's disease: An MEG study. Biol Psychol 89:365–373.

Chrobak JJ, Buzsa G (1998) Gamma Oscillations in the Entorhinal Cortex of the Freely Behaving Rat. 18:388–398.

Cocchi L, Gollo LL, Zalesky A, Breakspear M (2017) Criticality in the brain: A synthesis of neurobiology, models and cognition. Prog Neurobiol 158:132–152.

Cohen MX, Axmacher N, Lenartz D, Elger CE, Sturm V, Schlaepfer TE (2009) Good vibrations: Cross-frequency coupling in the human nucleus accumbens during reward processing. J Cogn Neurosci 21:875–889.

Crone NE, Miglioretti DL, Gordon B, Lesser RP (1998) Functional mapping of human sensorimotor cortex with electrocorticographic spectral analysis II . Event-related synchronization in the gamma band. :2301–2315.

Crone NE, Sinai A, Korzeniewska A (2006) High-frequency gamma oscillations and human brain mapping with electrocorticography. Prog Brain Res 159:275–295 Available at: http://dx.doi.org/10.1016/S0079-6123(06)59019-3.

Crowell AL, Ryapolova-Webb ES, Ostrem JL, Galifianakis NB, Shimamoto S, Lim DA, Starr PA

(2012) Oscillations in sensorimotor cortex in movement disorders: An electrocorticography study. Brain 135:615–630.

De Hemptinne C, Ryapolova-Webb ES, Air EL, Garcia PA, Miller KJ, Ojemann JG, Ostrem JL, Galifianakis NB, Starr PA (2013) Exaggerated phase-amplitude coupling in the primary motor cortex in Parkinson disease. Proc Natl Acad Sci U S A 110:4780–4785.

Deouell LY (2007) The frontal generator of the mismatch negativity revisited. J Psychophysiol 21:188–203.

Desimone R (1995) Neural Mechanisms of Selective Visual Attention. Annu Rev Neurosci 18:193–222.

Dürschmid S, Edwards E, Reichert C, Dewar C, Hinrichs H, Heinze H-J, Kirsch HE, Dalal SS, Deouell LY, Knight RT (2016a) Hierarchy of prediction errors for auditory events in human temporal and frontal cortex. Proc Natl Acad Sci U S A 113.

Dürschmid S, Maric A, Kehl MS, Knight RT, Hinrichs H, Heinz H-J (2020a) Fronto-temporal regulation of subjective value to suppress impulsivity in intertemporal choices. J Neurosci:JN-RM-1196-20.

Dürschmid S, Quandt F, Krämer UM, Hinrichs H, Heinze H-J, Schulz R, Pannek H, Chang EF, Knight RT (2014) Oscillatory dynamics track motor performance improvement in human cortex. PLoS One 9.

Dürschmid S, Reichert C, Hinrichs H, Heinze HJ, Kirsch HE, Knight RT, Deouell LY (2019) Direct Evidence for Prediction Signals in Frontal Cortex Independent of Prediction Error. Cereb Cortex 29:4530–4538.

Dürschmid S, Reichert C, Kuhn J, Freund H-J, Hinrichs H, Heinze H-J (2017) Deep brain stimulation of the nucleus basalis of Meynert attenuates early EEG components associated with defective sensory gating in patients with Alzheimer disease - a two-case study. Eur J Neurosci.

Dürschmid S, Reichert C, Walter N, Hinrichs H, Heinze H-J, Ohl FW, Tononi G, Deliano M (2020b) Self-regulated critical brain dynamics originate from high frequency-band activity in the MEG. PLoS One 15.

Dürschmid S, Zaehle T, Hinrichs H, Heinze H-J, Voges J, Garrido MI, Dolan RJ, Knight RT (2016b) Sensory Deviancy Detection Measured Directly Within the Human Nucleus Accumbens. Cereb Cortex 26.

Dürschmid S, Zaehle T, Kopitzki K, Voges J, Schmitt FC, Heinze H-J, Knight RT, Hinrichs H (2013) Phase-amplitude cross-frequency coupling in the human nucleus accumbens tracks action monitoring during cognitive control. Front Hum Neurosci 7:635 Available at: http://www.pubmedcentral.nih.gov/articlerender.fcgi?artid=3791425&tool=pmcentrez&rendertype=abstract.

Edwards E et al. (2014) High Gamma Activity in Response to Deviant Auditory Stimuli Recorded

Directly From Human Cortex High Gamma Activity in Response to Deviant Auditory Stimuli Recorded Directly From Human Cortex.

Eimer M (1996) The N2pc component as an indicator of attentional selectivity. Electroencephalogr Clin Neurophysiol 99:225–234.

El Karoui I, King JR, Sitt J, Meyniel F, Van Gaal S, Hasboun D, Adam C, Navarro V, Baulac M, Dehaene S, Cohen L, Naccache L (2015) Event-related potential, time-frequency, and functional connectivity facets of local and global auditory novelty processing: An intracranial study in humans. Cereb Cortex 25:4203–4212.

Ellis TL, Stevens A (2008) Deep brain stimulation for medically refractory epilepsy. Neurosurg Focus 25.

Engeland C, Mahoney C, Mohr E, Ilivitsky V, Knott V (2002) Nicotine and sensory memory in Alzheimer's disease: an event-related potential study. Brain Cogn 49:232–234.

Fagerholm ED, Lorenz R, Scott G, Dinov M, Hellyer XPJ, Mirzaei N, Leeson C, Carmichael XDW, Sharp DJ, Shew WL, Leech X (2015) Cascades and Cognitive State : Focused Attention Incurs Subcritical Dynamics. 35:4626–4634.

Finch DM (1996) Neurophysiology of converging synaptic inputs from the rat prefrontal cortex, amygdala, midline thalamus, and hippocampal formation onto single neurons of the caudate/putamen and nucleus accumbens. Hippocampus 6:495–512.

Fishman YI, Steinschneider M (2012) Searching for the mismatch negativity in primary auditory cortex of the awake monkey: Deviance detection or stimulus specific adaptation? J Neurosci 32:15747–15758.

Fogelson N, Shah M, Scabini D, Knight RT (2009) Prefrontal cortex is critical for contextual processing: Evidence from brain lesions. Brain 132:3002–3010.

French SJ, Totterdell S (2002) Hippocampal and prefrontal cortical inputs monosynaptically converge with individual projection neurons of the nucleus accumbens. J Comp Neurol 446:151–165.

Friston KJ et al. (2005) Coupling Between Neuronal Firing, Field Potentials, and fMRI in Human Auditory Cortex. Science (80-) 309:951–954.

Froemke RC, Merzenich MM, Schreiner CE (2007) A synaptic memory trace for cortical receptive field plasticity. Nature 450:425–429.

Furey ML, Pietrini P, Haxby J V., Drevets WC (2008) Selective effects of cholinergic modulation on task performance during selective attention. Neuropsychopharmacology 33:913–923.

Fuster JM (1990) Behavioral electrophysiology of the prefrontal cortex of the primate. Prog Brain Res 85:313–314.

Gaeta H, Friedman D, Ritter W, Cheng J (1999) Changes in sensitivity to stimulus deviance in Alzheimer's disease: An ERP perspective. Neuroreport 10:281–287.

Garrido MI, Friston KJ, Kiebel SJ, Stephan KE, Baldeweg T, Kilner JM (2008) The functional

anatomy of the MMN: A DCM study of the roving paradigm. Neuroimage 42:936–944.

Girelli M, McDermott M, Luck S, Ford M (1997) Bridging the gap between monkey neurophysiology and human perception: an ambiguity resolution theory of visual selective attention. Cogn Psychol 33:64–87.

Goldman-Rakic PS (1992) Working memory and the mind. Sci Am 267:110–117.

Golob EJ, Irimajiri R, Starr A (2007) Auditory cortical activity in amnestic mild cognitive impairment: Relationship to subtype and conversion to dementia. Brain 130:740–752.

Golob EJ, Starr A (2000) Effects of stimulus sequence on event-related potentials and reaction time during target detection in Alzheimer's disease. Clin Neurophysiol 111:1438–1449.

Gonzalez-Martinez J, Mullin J, FAU - Vadera S, Vadera S, FAU - Bulacio J, Bulacio J, FAU - Hughes G, Hughes G, FAU - Jones S, Jones S, FAU - Enatsu R, Enatsu R, FAU - Najm I, Najm I (2014) Stereotactic placement of depth electrodes in medically intractable epilepsy. - J Neurosurg.

Gonzalez-Martinez J, Vadera S, Mullin J, Enatsu R, Alexopoulos A V., Patwardhan R, Bingaman W, Najm I (1982) Robot-assisted stereotactic laser ablation in medically intractable epilepsy: Operative technique. Neurosurgery 10:167–172.

Goto Y, Grace AA (2005) Dopamine-dependent interactions between limbic and prefrontal cortical plasticity in the nucleus accumbens: Disruption by cocaine sensitization. Neuron 47:255–266.

Goto Y, Grace AA (2008) Limbic and cortical information processing in the nucleus accumbens. Trends Neurosci 31:552–558.

Grace AA (2000) Gating of information flow within the limbic system and the pathophysiology of schizophrenia. Brain Res Rev 31:330–341.

Grace AA, Floresco SB, Goto Y, Lodge DJ (2007) Regulation of firing of dopaminergic neurons and control of goal-directed behaviors. Trends Neurosci 30:220–227.

Gratwicke J, Kahan J, Zrinzo L, Hariz M, Limousin P, Foltynie T, Jahanshahi M (2013) The nucleus basalis of Meynert: A new target for deep brain stimulation in dementia? Neurosci Biobehav Rev 37:2676–2688.

Green L, Myerson J (2004) A discounting framework for choice with delayed and probabilistic rewards. Psychol Bull 130:769–792.

Grisoni L, Miller TMC, Pulvermüller F (2017) Neural correlates of semantic prediction and resolution in sentence processing. J Neurosci 37:4848–4858.

Hämäläinen M, Hari R, Ilmoniemi RJ, Knuutila J, Lounasmaa O V. (1993) Magnetoencephalography Theory Instrumentation Application to noninvasive studies of the working human brain. :93 Available at: papers2://publication/uuid/A82B6765-D36B-44DF-8E1D-47B7E8C626CF.

Hardenacke K, Hashemiyoon R, Visser-Vandewalle V, Zapf A, Freund HJ, Sturm V, Hellmich M, Kuhn J (2016) Deep Brain Stimulation of the Nucleus Basalis of Meynert in Alzheimer's

Dementia: Potential Predictors of Cognitive Change and Results of a Long-Term Follow-Up in Eight Patients. Brain Stimul 9:799–800.

Hare TA, Camerer CF, Rangel A (2009) Self-control in decision-making involves modulation of the vmPFC valuation system. Science 324:646–648.

Heilbron M, Chait M (2018) Great Expectations: Is there Evidence for Predictive Coding in Auditory Cortex? Neuroscience 389:54–73 Available at: http://dx.doi.org/10.1016/j.neuroscience.2017.07.061.

Hopf J-M (2000) Neural Sources of Focused Attention in Visual Search. Cereb Cortex 10:1233–1241.

Hsiao FJ, Chen WT, Wang PN, Cheng CH, Lin YY (2014) Temporo-frontal functional connectivity during auditory change detection is altered in Alzheimer's disease. Hum Brain Mapp 35:5565–5577.

Ignacio Rebollo, Anne-Dominique Devauchelle, Benoît Béranger, Catherine Tallon-Baudry (2018) Stomach-brain synchrony reveals a novel, delayed-connectivity resting-state network in humans. Elife 7.

Irrmischer M, Houtman SJ, Mansvelder HD, Tremmel M, Ott U (2018) Controlling the Temporal Structure of Brain Oscillations by Focused Attention Meditation. :1825–1838.

Jasper H H (1958) The ten twenty electrode system of the International Federation. Electroencephalogr Clin Neurophysiol 10:371–375.

Knight RT (1996) Contribution of human hippocampal region to novelty detection. Nature 383:256–259.

Knight RT (1998) Electrophysiology and behavior converge in human extrastriate cortex. Nat Neurosci 1:546.

Kole MHP, Herrero JL, Letzkus JJ, Roberts MJ, Stuart GJ, Delicato LS, Gieselmann MA, Dayan P, Thiele A (2008) Acetylcholine contributes through muscarinic receptors to attentional modulation in V1. Nature 454:1110–1114 Available at: papers2://publication/doi/10.1038/nature07141.

Kucyi A, Salomons T V., Davis KD (2013) Mind wandering away from pain dynamically engages antinociceptive and default mode brain networks. Proc Natl Acad Sci 110:18692–18697.

Kuhn J, Hardenacke K, Shubina E, Lenartz D, Visser-Vandewalle V, Zilles K, Sturm V, Freund HJ (2015) Deep brain stimulation of the nucleus basalis of meynert in early stage of Alzheimer's dementia. Brain Stimul 8:838–839.

Kumar S, Sedley W, Nourski K V, Kawasaki H, Oya H, Patterson RD, Iii MAH, Friston KJ, Griffiths TD (2011) Predictive Coding and Pitch Processing in the Auditory Cortex. :3084–3094.

Lazar SW, Kerr CE, Wasserman RH, Gray JR, Greve DN, Treadway MT, McGarvey M, Quinn BT, Dusek JA, Benson H, Rauch SL, Moore CI, Fischl B (2005) Meditation experience is associated with increased cortical thickness. Neuroreport 16:1893–1897.

Liasis a., Towell a., Alho K, Boyd S (2001) Intracranial identification of an electric frontal-cortex response to auditory stimulus change: A case study. Cogn Brain Res 11:227–233.

Lindín M, Correa K, Zurrón M, Díaz F (2013) Mismatch negativity (MMN) amplitude as a biomarker of sensory memory deficit in amnestic mild cognitive impairment. Front Aging Neurosci 5.

Linkenkaer-hansen K, Nikouline V V, Palva JM, Ilmoniemi RJ (2001) Long-Range Temporal Correlations and Scaling Behavior in Human Brain Oscillations. 21:1370–1377.

Liu J, Newsome WT (2006) Local field potential in cortical area MT: Stimulus tuning and behavioral correlations. J Neurosci 26:7779–7790.

Lockwood PL, Hamonet M, Zhang SH, Ratnavel A, Salmony FU, Husain M, Apps MAJ (2017) Prosocial apathy for helping others when effort is required. Nat Hum Behav 1:1–23.

Luck SJ, Hillyard SA (1994) Spatial filtering during visual search: Evidence from human electrophysiology. J Exp Psychol Hum Percept Perform 20:1000–1014.

MacDonald AW, Cohen JD, Stenger A V, Carter CS (2000) Dissociating the Role of the Dorsolateral Prefrontal and Anterior Cingulate Cortex in Cognitive Control. Science (80-) 288:1835–1838 Available at: http://www.sciencemag.org/cgi/content/abstract/288/5472/1835.

Machado AG, Deogaonkar M, Cooper S (2012) Deep brain stimulation for movement disorders: Patient selection and technical options. Cleve Clin J Med 79.

Manning JR, Jacobs J, Fried I, Kahana MJ (2009) Broadband shifts in local field potential power spectra are correlated with single-neuron spiking in humans. J Neurosci 29:13613–13620.

Mazur JE (1987) An adjusting procedure for studying delayed reinforcement. (M. L. Commons J. E. Mazur JAN& HR, ed). Hillsdale, NJ: Erlbaum.

Mazza V, Turatto M, Caramazza A (2009) Attention selection, distractor suppression and N2pc. Cortex 45:879–890.

McClure SM, Ericson KM, Laibson DI, Loewenstein G, Cohen JD (2007) Time discounting for primary rewards. J Neurosci 27:5796–5804.

McClure SM, Laibson DI, Loewenstein G, Cohen JD (2004) Separate neural systems value immediate and delayed monetary rewards. Science (80-) 306:503–507 Available at: http://dx.doi.org/10.1126/science.1100907.

McGaughy J, Kaiser T, Sarter M (1996) Behavioral vigilance following infusions of 192 IgG-saporin into the basal forebrain: Selectivity of the behavioral impairment and relation to cortical AChE-positive fiber density. Behav Neurosci 110:247–265.

Mesulam M -Marsel, Mufson EJ, Levey AI, Wainer BH (1983) Cholinergic innervation of cortex by the basal forebrain: Cytochemistry and cortical connections of the septal area, diagonal band nuclei, nucleus basalis (Substantia innominata), and hypothalamus in the rhesus monkey. J Comp Neurol 214:170–197.

Miasnikov AA, Chen JC, Weinberger NM (2008) Specific auditory memory induced by nucleus

basalis stimulation depends on intrinsic acetylcholine. Neurobiol Learn Mem 90:443–454.

Miasnikov AA, McLin D, Weinberger NM (2001) Muscarinic dependence of nucleus basalis induced conditioned receptive field plasticity. Neuroreport 12:1537–1542.

Miller KJ, Leuthardt EC, Schalk G, Rao RPN, Anderson NR, Moran DW, Miller JW, Ojemann JG (2007) Spectral changes in cortical surface potentials during motor movement. J Neurosci 27:2424–2432.

Miller KJ, Sorensen LB, Ojemann JG, Den Nijs M (2009) Power-law scaling in the brain surface electric potential. PLoS Comput Biol 5.

Mittner M, Boekel W, Tucker AM, Turner BM, Heathcote A, Forstmann BU (2014) When the Brain Takes a Break: A Model-Based Analysis of Mind Wandering. J Neurosci 34:16286–16295.

Mogenson GJ, Jones DL, Yim CY (1980) From motivation to action: Functional interface between the limbic system and the motor system. Prog Neurobiol 14:69–97.

Mudrik L, Faivre N, Koch C (2016) Information integration without awareness. Trends Cogn Sci 20:559.

Münte TF, Heldmann M, Hinrichs H, Marco-Pallares J, Krämer UM, Sturm V, Heinze HJ (2008) Nucleus accumbens is involved in human action monitoring: Evidence from invasive electrophysiological recordings. Front Hum Neurosci 1.

Muthukumaraswamy SD (2013) High-frequency brain activity and muscle artifacts in MEG/EEG: A review and recommendations. Front Hum Neurosci 7:1–11.

Myerson J, Green L, Hanson J. Scott Holt, D. D, Estle SJ (2003) Discounting delayed and probabilistic rewards: Processes and traits. J Econ Psychol.

Näätänen R, Gaillard AWK, Mäntysalo S (1978) Early selective-attention effect on evoked potential reinterpreted. Acta Psychol (Amst) 42:313–329.

Nissen MJ, Bullemer P (1987) Attentional requirements of learning: Evidence from performance measures. Cogn Psychol 19:1–32.

O'Donnell P, Grace AA (1995) Synaptic interactions among excitatory afferents to nucleus accumbens neurons: Hippocampal gating of prefrontal cortical input. J Neurosci 15:3622–3639.

Okada YC, Lahteenmäki A, Xu C (1999) Experimental analysis of distortion of magnetoencephalography signals by the skull. Clin Neurophysiol 110:230–238.

Okun MS et al. (2012) Subthalamic deep brain stimulation with a constant-current device in Parkinson's disease: An open-label randomised controlled trial. Lancet Neurol 11:140–149 Available at: http://www.embase.com/search/results?subaction=viewrecord&from=export&id=L5180 8606%5Cnhttp://dx.doi.org/10.1016/S1474-4422(11)70308-8%5Cnhttp://sfx.library.uu.nl/utrecht?sid=EMBASE&issn=14744422&id=doi:10.1016%2F

S1474-4422%2811%2970308-8&atitle=Subthalamic+deep.

Olson EA, Hooper CJ, Collins P, Luciana M (2007) Adolescents' performance on delay and probability discounting tasks: contributions of age, intelligence, executive functioning, and self-reported externalizing behavior. Pers Individ Dif 43:1886–1897.

Önal Ç, Otsubo H, Araki T, Chitoku S, Ochi A, Weiss S, Logan W, Elliott I, Snead OC, Rutka JT (2003) Complications of invasive subdural grid monitoring in children with epilepsy. J Neurosurg 98:1017–1026.

Pagnoni G, Cekic M (2007) Age effects on gray matter volume and attentional performance in Zen meditation. Neurobiol Aging 28:1623–1627.

Pekkonen E, Hirvonen J, Jääskeläinen IP, Kaakkola S, Huttunen J (2001) Auditory sensory memory and the cholinergic system: Implications for Alzheimer's disease. Neuroimage 14:376–382.

Pekkonen E, Pekkonen E, Jousmäki V, KÖnÖnen M, Reinikainen K, Partanen J (1994) Auditory sensory memory impairment in alzheimer's disease: An event-related potential study. Neuroreport 5:2537–2540.

Peters J, Büchel C (2010) Episodic future thinking reduces reward delay discounting through an enhancement of prefrontal-mediotemporal interactions. Neuron 66:138–148 Available at: http://dx.doi.org/10.1016/j.neuron.2010.03.026.

Pfurtscheller G, Cooper R (1975) Frequency dependence of the transmission of the EEG from cortex to scalp. Electroencephalogr Clin Neurophysiol 38:93–96.

Polich J (2007) Updating P300: An integrative theory of P3a and P3b. Clin Neurophysiol 118:2128–2148.

Polich J, Criado JR (2006) Neuropsychology and neuropharmacology of P3a and P3b. Int J Psychophysiol 60:172–185.

Polich J, Ladish C, Bloom FE (1990) P300 assessment of early Alzheimer's disease. Electroencephalogr Clin Neurophysiol Evoked Potentials 77:179–189.

Rao RPN, Ballard DH (1999) Predictive coding in the visual cortex : a functional interpretation of some extra-classical receptive-field effects. :79–87.

Rasmusson DD (2000) The role of acetylcholine in cortical synaptic plasticity. Behav Brain Res 115:205–218.

Ray S, Maunsell JHR (2011) Different origins of gamma rhythm and high-gamma activity in macaque visual cortex. PLoS Biol 9.

Rosburg T, Trautner P, Dietl T, Korzyukov O a., Boutros NN, Schaller C, Elger CE, Kurthen M (2005) Subdural recordings of the mismatch negativity (MMN) in patients with focal epilepsy. Brain 128:819–828.

SanMiguel I, Saupe K, Schröger E (2013) I know what is missing here: Electrophysiological prediction error signals elicited by omissions of predicted "what" but not "when." Front

Hum Neurosci.

Sarter M, Bruno JP (1999) Cortical cholinergic inputs mediating arousal, attentional processing and dreaming: Differential afferent regulation of the basal forebrain by telencephalic and brainstem afferents. Neuroscience 95:933–952.

Shalgi S, Deouell LY (2007) Direct evidence for differential roles of temporal and frontal components of auditory change detection. Neuropsychologia 45:1878–1888 Available at: http://dx.doi.org/10.1016/j.neuropsychologia.2006.11.023.

Shew WL (2012) Neuroscientist The Functional Benefits of Criticality in the Cortex.

Shew WL, Yang H (2009) Neuronal Avalanches Imply Maximum Dynamic Range in Cortical Networks at Criticality.

Shriki O, Alstott J, Carver F, Holroyd T, Henson RNA, Smith ML, Coppola R, Bullmore E, Plenz D (2013) Neuronal avalanches in the resting MEG of the human brain. J Neurosci 33:7079–7090.

Siapas AG, Lubenov E V., Wilson MA (2005) Prefrontal phase locking to hippocampal theta oscillations. Neuron 46:141–151.

Sirota A, Csicsvari J, Buhl D, Buzsáki G (2003) Communication between neocortex and hippocampus during sleep in rodents. Proc Natl Acad Sci U S A 100:2065–2069.

Slagter HA, Lutz A, Greischar LL, Francis AD, Nieuwenhuis S, Davis JM, Davidson RJ (2007) Mental training affects distribution of limited brain resources. PLoS Biol 5:1228–1235.

Spicer J, Galvan A, Hare TA, Voss H, Glover G, Casey B (2007) Sensitivity of the nucleus accumbens to violations in expectation of reward. Neuroimage 34:455–461.

Staudigl T, Zaehle T, Voges J, Hanslmayr S, Esslinger C, Hinrichs H, Schmitt FC, Heinze HJ, Richardson-Klavehn A (2012) Memory signals from the thalamus: Early thalamocortical phase synchronization entrains gamma oscillations during long-term memory retrieval. Neuropsychologia 50:3519–3527.

Terry R, Davies P (1980) Dementia of the Alzheimer type. Annu Rev Neurosci 35:447.

Thiel CM, Bentley P, Dolan RJ (2002) Effects of cholinergic enhancement on conditioning-related responses in human auditory cortex. Eur J Neurosci 16:2199–2206.

Tort ABL, Komorowski RW, Manns JR, Kopell NJ, Eichenbaum H (2009a) Theta – gamma coupling increases during the learning of item – context associations. 106:2–7.

Tort ABL, Komorowski RW, Manns JR, Kopell NJ, Eichenbaum H (2009b) Theta-gamma coupling increases during the learning of item-context associations. Proc Natl Acad Sci U S A 106:20942–20947.

Tort ABL, Kramer MA, Thorn C, Gibson DJ, Kubota Y, Graybiel AM, Kopell NJ (2008) Dynamic cross-frequency couplings of local field potential oscillations in rat striatum and hippocampus during performance of a T-maze task. 105:20517–20522.

Uhlhaas PJ, Singer W (2010) Abnormal neural oscillations and synchrony in schizophrenia. Nat

Rev Neurosci 11:100–113.

van Leeuwen S, Singer W, Melloni L (2012) Meditation increases the depth of information processing and improves the allocation of attention in space. Front Hum Neurosci 6:1–16.

Voytek B, Canolty RT, Shestyuk A, Crone NE, Parvizi J, Knight RT (2010) Shifts in gamma phase-amplitude coupling frequency from theta to alpha over posterior cortex during visual tasks. Front Hum Neurosci 4.

Voytko M Lou, Olton DS, Richardson RT, Gorman LK, Tobin JR, Price DL (1994) Basal forebrain lesions in monkeys disrupt attention but not learning and memory. J Neurosci 14:167–186.

Vyazovskiy V V., Olcese U, Hanlon EC, Nir Y, Cirelli C, Tononi G (2011) Local sleep in awake rats. Nature 472:443–447 Available at: http://dx.doi.org/10.1038/nature10009.

Warburton EC, Koder T, Cho K, Massey P V., Duguid G, Barker GRI, Aggleton JP, Bashir ZI, Brown MW (2003) Cholinergic neurotransmission is essential for perirhinal cortical plasticity and recognition memory. Neuron 38:987–996.

Weinberger NM (2003) The nucleus basalis and memory codes: Auditory cortical plasticity and the induction of specific, associative behavioral memory. Neurobiol Learn Mem 80:268–284.

Whitehouse PJ, Price DL, Struble RG, Clark AW, Coyle JT, DeLong MR (1982) Alzheimer's disease and senile dementia: Loss of neurons in the basal forebrain. Science (80-) 215:1237–1239.

Wood DA, Kosobud AEK, Rebec G V. (2004) Nucleus accumbens single-unit activity in freely behaving male rats during approach to novel and non-novel estrus. Neurosci Lett 368:29–32.

Yuval-Greenberg S, Tomer O, Keren AS, Nelken I, Deouell LY (2008) Transient Induced Gamma-Band Response in EEG as a Manifestation of Miniature Saccades. Neuron 58:429–441.

Zhou X, Lei X (2018) Wandering Minds with Wandering Brain Networks. Neurosci Bull 34:1017–1028 Available at: https://doi.org/10.1007/s12264-018-0278-7.

Auflistung der Lehrtätigkeit

	Art der Lehrveranstaltung	Studiengang	Anzahl SWS
SoSe 17	Seminar Biologische Psychologie	Bachelor	2
WiSe 17/18	Experimentelles Praktikum	Bachelor	4
SoSe 18	Seminar Biologische Psychologie	Bachelor	2
	Grundlagenmodul Kognitive Neurowissenschaft I – I.2: Kognition	Master	2
	Allgemeine Psychologie Vorlesung Motivation	Master	2
WiSe 18/19	Biologische Psychologie II (Seminar) -Modul I –	Bachelor	2
	Allgemeine Psychologie II Seminar	Bachelor	2
SoSe 19	Allgemeine Psychologie Seminar Kognition	Master	2
WiSe 19/20	Experimentelles Praktikum	Bachelor	4
SoSe 20	Allgemeine Psychologie Seminar Kognition	Master	2
WS 20/21	Forschungskolloquium Kognitive Neurowissenschaften	Master	2

1. Relevante Publikationen des Autors

Dürschmid S., Reichert C. , Walter N., Hinrichs H., Heinze H.J., Ohl F.W., Tononi G., Deliano M. Self-regulated critical brain dynamics originate from high frequency-band activity in the MEG. PLoS ONE, 2020.

Dürschmid S, Maric A, Kehl MS, Robert T Knight RT, Hinrichs H, Heinze HJ. Fronto-temporal cortex regulation of subjective valence to suppress impulsivity in intertemporal choices. Journal of Neuroscience, in press 2020.

Dürschmid S, Zaehle T, Hinrichs H, Heinze HJ, Voges J, Garrido MI, Dolan RJ, Knight RT. Sensory Deviancy Detection Measured Directly Within the Human Nucleus Accumbens. Cereb Cortex. 2016 Mar;26(3):1168-1175.

Dürschmid S, Reichert C, Kuhn J, Freund HJ, Hinrichs H, Heinze HJ. Deep Brain stimulation of the Nucleus Basalis of Meynert attenuates early EEG components associated with defective sensory gating in patients with Alzheimer disease – a two-case study. EJN. 2017

Dürschmid S, Edwards E, Reichert C, Dewar C, Hinrichs H, Heinze HJ, Kirsch HE,Dalal SS, Deouell LY, Knight RT. Hierarchy of prediction errors for auditory events in human temporal and frontal cortex. Proc Natl Acad Sci U S A. 2016 Jun 14;113(24):6755-60. IF: 10.4 (5y)

Dürschmid S, Reichert C, Hinrichs H, Heinze HJ, Kirsch HE, Knight RT, Deouell LY. Direct evidence for prediction signals in frontal cortex independent of prediction error. Cereb Cortex. 2019.

Dürschmid S, Zaehle T, Kopitzki K, Voges J, Schmitt FC, Heinze HJ, Knight RT, Hinrichs H. Phase-amplitude cross-frequency coupling in the human nucleus accumbens tracks action monitoring during cognitive control. Front Hum Neurosci. 2013 Oct 7;7:635.

Dürschmid S, Quandt F, Krämer UM, Hinrichs H, Heinze HJ, Schulz R, Pannek H, Chang EF, Knight RT. Oscillatory dynamics track motor performance improvement in human cortex. PLoS One. 2014 Feb 27;9(2).

Wienke C, Bartsch M V., Vogelgesang L, Reichert C, Hinrichs H, Heinze H-J, **Dürschmid S.** Local sleep during mind-wandering enhances processes of spatial attention allocation. Cerebral Cortex Communications, *2021; 2(1)*

Vollständige Publikationsliste des Autors
Artikel, die nach der Dissertation publiziert wurden, sind mit ***** gekennzeichnet

Erst- oder Seniorautorenschaft.

* 1. Wienke C, Bartsch M V., Vogelgesang L, Reichert C, Hinrichs H, Heinze H-J, ***Dürschmid S.*** Local sleep during mind-wandering enhances processes of spatial attention allocation. Cerebral Cortex Communications, *in press* *****

* 2. ***Dürschmid S, Maric A,*** Kehl MS, Robert T Knight RT, Hinrichs H, Heinze HJ. Fronto-temporal cortex regulation of subjective valence to suppress impulsivity in intertemporal choices. Journal of Neuroscience, in press 2020.

* 3. Reichert C, Tellez Ceja IF, Sweeney-Reed CM, Heinze HJ, Hinrichs H, ***Dürschmid S.*** Impact of stimulus features on the performance of a gaze-independent brain-computer interface based on covert spatial attention shifts. Frontiers in Neuroscience, 2020. https://doi.org/10.3389/fnins.2020.591777

* 4. Vogelgesang L, Reichert C, Hinrichs H, Heinze, HJ, ***Dürschmid S.*** Early Shift of Attention is Not Regulated by Mind-Wandering in Visual Search. Frontiers in Human Neuroscience, 2020. https://doi.org/10.3389/fnins.2020.552637

* 5. ***Dürschmid S.,*** Reichert C. , Walter N., Hinrichs H., Heinze H.J., Ohl F.W., Tononi G., Deliano M. Self-regulated critical brain dynamics originate from high frequency-band activity in the MEG. PLoS ONE, 2020. https://doi.org/10.1371/journal.pone.0233589

* 6. ***Dürschmid S***, Reichert C, Hinrichs H, Heinze HJ, Kirsch HE, Knight RT, Deouell LY. Direct evidence for prediction signals in frontal cortex independent of prediction error. Cereb Cortex. 2019. https://doi.org/10.1093/cercor/bhy331

* 7. ***Dürschmid S***, Reichert C, Kuhn J, Freund HJ, Hinrichs H, Heinze HJ. Deep Brain stimulation of the Nucleus Basalis of Meynert attenuates early EEG components associated with defective sensory gating in patients with Alzheimer disease – a two-case study. EJN.https://doi.org/10.1111/ejn.13749

* 8. Stenner MP, ***Dürschmid S****, Rutledge RB, Zaehle T, Schmitt FC, Kaufmann J, Voges J, Heinze HJ, Dolan RJ, Schoenfeld MA. Perimovement decrease of alpha/beta oscillations in the human nucleus accumbens. J Neurophysiol. 2016 Oct 1;116(4):1663-1672. https://doi.org/10.1152/jn.00142.2016

* 9. ***Dürschmid S***, Edwards E, Reichert C, Dewar C, Hinrichs H, Heinze HJ, Kirsch HE,Dalal SS, Deouell LY, Knight RT. Hierarchy of prediction errors for auditory events in human temporal and frontal cortex. Proc Natl Acad Sci U S A. 2016 Jun 14;113(24):6755-60. IF: 10.4 (5y) https://doi.org/10.1073/pnas.1525030113

* 10. ***Dürschmid S***, Zaehle T, Hinrichs H, Heinze HJ, Voges J, Garrido MI, Dolan RJ, Knight RT. Sensory Deviancy Detection Measured Directly Within the Human Nucleus Accumbens. Cereb Cortex. 2016 Mar;26(3):1168-1175. https://doi.org/10.1093/cercor/bhu304

* 11. ***Dürschmid S***, Quandt F, Krämer UM, Hinrichs H, Heinze HJ, Schulz R, Pannek H, Chang EF, Knight RT. Oscillatory dynamics track motor performance improvement in human cortex. PLoS One. 2014 Feb 27;9(2). https://doi.org/10.1371/journal.pone.0089576

12. **Dürschmid S**, Zaehle T, Kopitzki K, Voges J, Schmitt FC, Heinze HJ, Knight RT, Hinrichs H. Phase-amplitude cross-frequency coupling in the human nucleus accumbens tracks action monitoring during cognitive control. Front Hum Neurosci. 2013 Oct 7;7:635. https://doi.org/10.3389/fnhum.2013.00635

Ko-autorenschaft

* 1. Krüger J, Reichert C, **Dürschmid S**, Krauth R, Vogt S, Huchtemann T, Lindquist S, Lamprecht J, Sailer M, Heinze H-J, Hinrichs H, Sweeney-Reed CM. Rehabilitation nach Schlaganfall: Durch Gehirn-Computer-Schnittstelle vermittelte funktionelle Elektrostimulation. Klinische Neurophysiologie, 2020. https://doi.org/10.1055/a-1205-7467

* 2. Reichert C, **Dürschmid S**, Bartsch M, Hopf JM, Heinze H-J, Hinrichs H. Decoding the covert shift of spatial attention from electroencephalographic signals permits reliable control of a brain-computer interface. Journal of Neural Engineering, 2020. https://doi.org/10.1088/1741-2552/abb692

* 3. Reichert C, **Dürschmid S**, Hinrichs H. EEG as a Control Signal: Decoding of Brain Activity and ist Efficient Application as Communication Channel for Patients with Motor Deficits. Klinische Neurophysiologie, 2020. https://doi.org/10.1055/a-1135-3782

* 4. Beck AK, Sandmann P, **Dürschmid S**, Schwabe K, Saryyeva A, Krauss JK. Neuronal activation in the human centromedian-parafascicular complex predicts cortical responses to behaviorally significant auditory events. *Neuroimage.* 2020. IF: 5.8 https://doi.org/10.1016/j.neuroimage.2020.116583

* 5. Reichert C, **Dürschmid S**, Kuhn J, Freund HJ, Hinrichs H, Heinze HJ. A Comparative Study on the Detection of Covert Attention in Event-related EEG and MEG Signals to Control a BCI. Frontiers in Human Neuroscience. IF: 3.2. https://doi.org/10.3389/fnins.2017.00575

* 6. Reichert C, **Dürschmid S**, Kruse R, Hinrichs H. An Efficient Decoder for the Recognition of Event-Related Potentials in High-Density MEG Recordings. Computers. 2016.https://doi.org/10.1186/s12868-016-0283-6

* 7. Mikutta C, **Dürschmid S**, Bean N, Lehne M, Lubell J, Altorfer A, Parvizi J, Strik WK, Knight RT, Koelsch S, Amygdala and Orbitofrontal engagement in breach and resolution of expectancy - a case study. Psychomusicology: Music, Mind and Brain, 2015. https://doi.org/10.1037/pmu0000121

2. Quandt F, Reichert C, Schneider B, **Dürschmid S**, Richter D, Rieger JW. Fundamentals and Application of Brain-Machine Interfaces (BMI). Klinische Neurophysiologie June 2012 43(2):158-167. https://doi.org/10.1055/s-0032-1308970

3. Busch NA, **Dürschmid S**, Herrmann CS. ERP effects of change localization, change identification, and change blindness. Neuroreport. 2010 Mar 31;21(5):371-5. IF: 1.3
https://doi.org/10.1097/WNR.0b013e3283378379

Buchkapitel

C.S. Herrmann, **_S. Dürschmid_**. Von Libet zu einer Neuen Willensfreiheit: Bewusste versus unbewusste Handlungsabsichten. In: T. Fuchs, G. Schwarzkopf (Hrsg.) Verantwortlichkeit – nur eine Illusion?, 127-146, Universitätsverlag Heidelberg, 2010

Self-regulated critical brain dynamics originate from high frequency-band activity in the MEG

Stefan Dürschmid[1,2]*, Christoph Reichert[1,3,4], Nike Walter[5], Hermann Hinrichs[1,2,3,4,6], Hans-Jochen Heinze[1,2,3,4,6], Frank W. Ohl[6,7,8], Giulio Tononi[9,10], Matthias Deliano[1]*

1 Department of Behavioral Neurology, Leibniz Institute for Neurobiology, Magdeburg, Germany, **2** Department of Neurology, Otto-von-Guericke University, Magdeburg, Germany, **3** Forschungscampus STIMULATE, Otto-von-Guericke University, Magdeburg, Germany, **4** CBBS—center of behavioral brain sciences, Otto-von-Guericke University, Magdeburg, Germany, **5** Research Section Applied Consciousness Science, Department of Psychosomatic Medicine, University Medical Center, Regensburg, Germany, **6** German Center for Neurodegenerative Diseases (DZNE), Magdeburg, Germany, **7** Dept. Systems Physiology of Learning (SPL), Leibniz Institute for Neurobiology (LIN), Magdeburg, Germany, **8** Institute of Biology (IBIO), Otto-von-Guericke University, Magdeburg, Germany, **9** Department of Psychiatry, University of Wisconsin-Madison, Madison, Wisconsin, United States of America, **10** Center for sleep and consciousness, University of Wisconsin-Madison, Madison, Wisconsin, United States of America

* stefan.duerschmid@googlemail.com (SD); matthias.deliano@lin-magdeburg.de (MD)

Abstract

Brain function requires the flexible coordination of billions of neurons across multiple scales. This could be achieved by scale-free, critical dynamics balanced at the edge of order and disorder. Criticality has been demonstrated in several, often reduced neurophysiological model systems. In the intact human brain criticality has yet been only verified for the resting state. A more direct link between the concept of criticality and oscillatory brain physiology, which is strongly related to cognition, is yet missing. In the present study we therefore carried out a frequency-specific analysis of criticality in the MEG, recorded while subjects were in a defined cognitive state through mindfulness meditation. In a two-step approach we assessed whether the macroscopic neural avalanche dynamics is scale-free by evaluating the goodness of a power-law fits of cascade size and duration distributions of MEG deflections in different frequency bands. In a second step we determined the closeness of the power-law exponents to a critical value of -1.5. Power-law fitting was evaluated by permutation testing, fitting of alternative distributions, and cascade shape analysis. Criticality was verified by defined relationships of exponents of cascade size and duration distributions. Behavioral relevance of criticality was tested by correlation of indices of criticality with individual scores of the Mindful Attention Awareness Scale. We found that relevant scale-free near-critical dynamics originated only from broad-band high-frequency (> 100 Hz) MEG activity, which has been associated with action potential firing, and therefore links criticality on the macroscopic level of MEG to critical spike avalanches on a microscopic level. Whereas a scale-free dynamics was found under mindfulness meditation and rest, avalanche dynamics shifted towards a critical point during meditation by reduction of neural noise. Together with our finding that during mindfulness meditation avalanches show differences in topography relative to rest, our results show that self-regulated attention as

required during meditation can serve as a control parameter of criticality in scale-free brain dynamics.

Significance statement

Our study bridges the gap between criticality, brain physiology and cognition. We show that scale-free critical dynamics in the MEG can be observed in the broad-band high-frequency (>100 Hz) activity that has been associated with action potential firing. Our study provides a link between critical avalanche dynamics at a macroscopic MEG and spike avalanches at a microscopic level. We show that mindfulness meditation shifts scale-free dynamics towards the critical point by reducing neural noise. In contrast to a state of rest, mindful focused attention requires detection and inhibition of mind-wandering, and the refocusing of breath, and therefore relies on constant monitoring and executive control, particularly in novices. This could be implemented by brain states balanced at an instable critical point between order and disorder allowing for flexibly focusing and shifting attention. Self-regulated attention might thereby serve as a control parameter of criticality in the scale-free brain dynamics.

Introduction

The proper functioning of the human brain rests on the electrical activity of billions of neurons coordinated across multiple scales. Theoretical and experimental work in physics has shown that the multi-scale dynamics of a complex system can be characterized by the spatial and temporal statistics of avalanches branching through the system. These statistics reveal whether the system is in a fully random or a fully ordered state, or whether it is in a critical state, i.e. in a complex state at the edge between order and disorder [1,2]. Empirically, critical avalanche dynamics in neuronal networks has been first demonstrated in cell cultures and slices in vitro by the seminal work of [3]. Further in vitro studies have shown that at the critical point, network functions are optimized with respect to the susceptibility of inputs, dynamic range of input/output relationships, information transmission, and information capacity [4,5], neural networks can become highly flexible, display meta-stable patterns, and adapt more easily to different rules through Hebbian plasticity [6]. Thus, information processing functions would be optimized if the network dynamics operates at its critical point [7].

However, being a concept derived from physics, criticality still needs to be empirically linked to cognitive brain functions in awake subjects, more directly. Different markers of criticality like long-range correlation in spontaneous low frequency (10 and 20Hz) EEG activity in humans have been studied [8]. In humans, criticality of neural avalanches comparable to unit firing propagation has only been demonstrated reliably for the resting state condition. Shriki et al. [9] showed that macroscopic whole brain avalanches defined by peaks and troughs of broad-band MEG activity in awake humans at rest have no characteristic scale, typical for a system state close to a critical point. However, the physiological nature of neural avalanches on a macroscopic level remains unclear. Since peaks and troughs in the MEG/EEG can reflect different phases of spatially and temporally extended oscillatory generators, reconstruction of avalanches on a macroscopic level should take into account the polarity and the frequency of the brain signals to disentangle superimposed sources. Most importantly, the functional relevance of criticality and its role in cognition is still an open question.

Most experimental studies in awake healthy subjects have been carried out under resting conditions, as task related activity implies non-stationarity and superposition of stimulus- and

response-driven activities [10], for which current statistical analyses of criticality are not well suited. However, human subjects can be verbally instructed to constantly alter their resting state dynamics through self-regulation switching into a different, stationary operational mode. A prominent self-regulation technique is mindfulness meditation, which we hypothesize is purportedly suited to induce changes in criticality, i.e. how close the system is as to its critical point. During meditation, mindful focused attention (MFA) is required to maintain focus on sensations over an extended period of time, which reduces distractor noise while at the same time cognitive control is required to detect phases of mind wandering [11–14] during which attention is directed elsewhere, as it occurs during an uninstructed resting state. In fact, mindfulness (meditation) and mind wandering (resting state) can be considered as opposing stationary background states, mediated by attentional subnetworks and the default mode network, respectively [15]. Irrmischer et al. [16] hypothesized that focused attention is balanced at a critical point of instability between order and disorder allowing for both, transient focus and swift change of attentional resources. They have shown that criticality is reduced in trained practitioners, i.e. when the meditation task becomes a habit. This would suggest that during MFA in contrast to the resting state, brain dynamics is tuned closer to a critical point. However, Irrmischer et al. show [16] that criticality is reduced in trained practitioners during MFA compared to rest. In trained practitioners, meditation might therefore require less effort, which could explain the observed shift towards a subcritical dynamics, or, as suggested by other studies, trained practitioners might experience difficulties in refraining from meditation practice during rest [17]. Thus, it is important to differentiate state from trait changes [18,19]. In our study we combined a frequency and polarity specific analysis of the macroscopic neural avalanche dynamics with a variation of the internal cognitive state by comparing a group of subjects performing mindfulness meditation with a group under rest. To avoid the aforementioned possible confounds between meditation-induced state and trait changes, we employed a simple mindful breathing task in novices. As human resting-state activity displays criticality [9], and MFA enhances attentional control [14,20], we hypothesize that top-down attention– in contrast to bottom-up attention [10]–modulation during mindfulness training tunes neural networks closer towards the critical point. Specifically, since it is assumed that MFA and resting activity are mediated by different neuronal networks [21–23], we further hypothesize that spatio-temporal avalanche dynamics will involve different cortical regions in these states.

Methods

Participants and paradigm

Seventeen healthy participants (eleven females; mean age 28.3±7.5 SD years, two left-handed), with no history of neurological disorders participated in group MFA. MEG activity was recorded while subjects were at rest or had to apply MFA (**Fig 1A**). Specifically, subjects started with a resting period, followed by an instructed meditation, and finally were asked to rest again without MFA. The whole experiment consisted of a sequence of five blocks: Rest (5min)–MFA (5min)–MFA (5min)–MFA (5min)–Rest (5min). Each block was initiated by the instruction either to rest or to apply MFA. Instructions (see S1 Data) were recorded in advance and spoken by an experienced meditator (extensive training in Vipassana-meditation [24] with an overall of 2500 hours of experience during a time period of 5 years and prior experience as a meditation teacher). In sum, preceding the first MFA phase, subjects were instructed to concentrate on the breathing cycle as the primary object of awareness. Following the first MFA block another audio file was played, reminding the participants to refocus on their breathing whenever they caught their mind wandering. Then the second MFA phase started. Thereafter a third audio file was presented as a reminder to continue with the task of
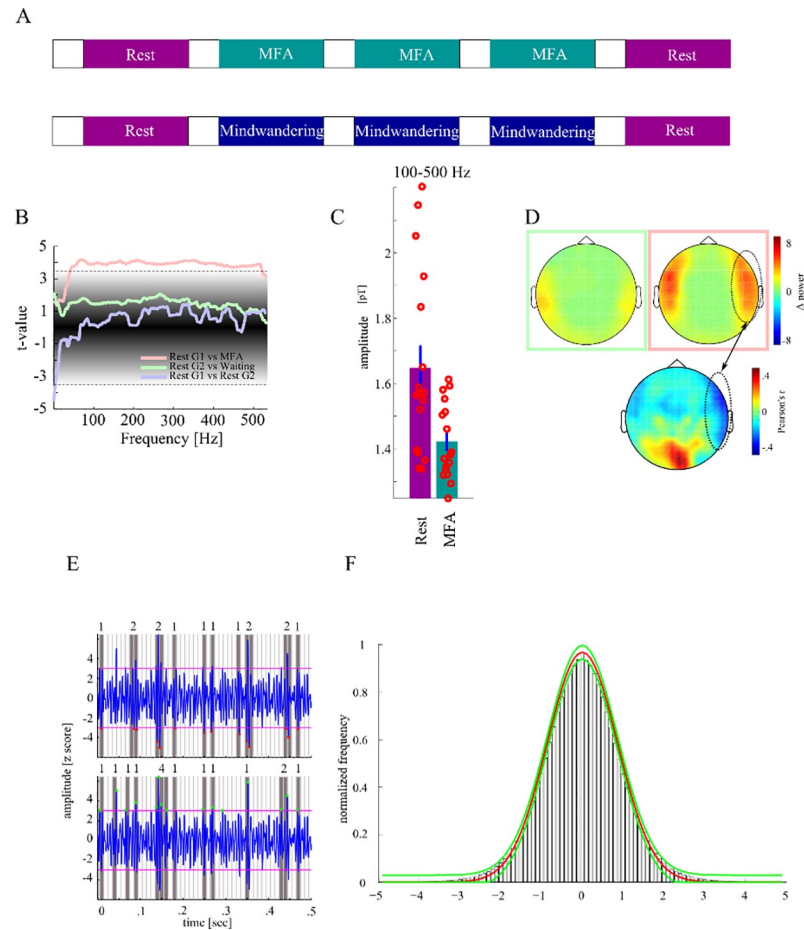
Fig 1. Procedure of the experiment. *A* The mindful focused attention (MFA) experiment conducted with group 1 consisted of five blocks each 5 min long and initiated by an instruction either to rest or to meditate with the breath as the primary object of awareness while in intermediate blocks in group 2 short stories were read from the same speaker and subjects had to wait for 5 min afterwards. *B* Power spectral density was compared between rest, mindful focused attention and in the mind-wandering condition of group 1 (G1) and group 2 (G2), respectively. Colored lines show difference in power values (t-values) as a function of frequency, within each group between the first resting block, and the MFA- (pink line), W- (green line) and final resting blocks (violet line), respectively. The black shaded area gives the surrogate distribution against which each t-value was compared. The horizontal lines give the confidence interval. *C* We observed a significant decrease of power between rest and MFA across a wide frequency spectrum covering the gamma and high frequency activity range. *D* shows the topographical distribution of differences in power in the high frequency band. The green and pink square correspond with the green and pink line in *C*, respectively. MEG magnetometers showing the strongest difference in power were located bilaterally over a fronto-temporal region. The lower panel shows correlation of individual MAAS scores with power difference between rest and MFA. Only in sensors covering the right frontal cortex we found both power difference between rest and MFA and correlation of these power differences with MAAS score. *E* shows MEG activity with trough (upper panel) and peak (lower panel) events showing different patterns of clustering yielding different likelihood distribution of cascade sizes. *F* shows Gaussian fit to histogram of trough and peak events (red line mean, green line lower and upper confidence interval of estimated Gaussian fits.

https://doi.org/10.1371/journal.pone.0233589.g001

focussing on the breathing cycle. A third MFA phase lasting another 5 min was recorded that ended with another audio stimulus to initialize a following measurement of resting state activity for 5 minutes. The participants kept their eyes closed during the whole procedure; the volume of the audio stimuli was adjusted individually before the MEG recording to a comfortable level. Another group of ten subjects with no history of neurological disorders forming the mind wandering (MW) control group (mean age 26±2.75 SD years, one left-handed) carried

out the same experiment with the difference that instead of listening to the MFA instruction, short stories (excerpts from the book "Let me tell you a story: Tales along the road to happiness" written by Jorge Bucay) were read by the same speaker (**Fig 1B**). After each short story participants were asked to wait until the next one to be narrated. In essence, we recorded five blocks of rest, which is characterized by mind-wandering. For a better comparison with group 1 we tagged intermediate blocks as blocks of MW: Rest (5min)–MW (5min)–MW (5min)–MW (5min)–Rest (5min). Additionally, the trait Mindful Attention Awareness Scale (MAAS [25]), a 15-item scale designed to assess a core characteristic of mindfulness, was answered by all subjects of both groups. Higher scores reflect higher levels of dispositional mindfulness. All participants gave their written informed consent prior to recordings and were compensated financially for their time. MAAS scores were compared between groups with an unpaired t-test. The study was approved by the local ethics committee ("Ethical Commitee of the Otto-von-Guericke University Magdeburg").

Data acquisition

The subjects were seated in a magnetically shielded room in which magnetoencephalographic activity (MEG) was recorded while the subjects performed the experiment. Electrooculographic (EOG) activity was recorded to reconstruct vertical and horizontal eye movements. Electrode impedance was kept below 10 kΩ. For data acquisition a whole-head, 102-sensor element array (Elekta Neuromag® TRIUX^TM) was used. Each of the 102 sensor elements was equipped with one magnetometer measuring the normal field component and two orthogonally oriented planar gradiometers for measuring the gradient components. The participants sat in an upright position underneath the MEG "helmet". MEG data were sampled at 2000 Hz and low-pass filtered with 660 Hz cutoff frequency.

Preprocessing

We used Matlab 2013b (Mathworks, Natick, USA) for all offline data processing. Only magnetometers were involved in our analyses. All filtering (see below) was done using zero phase-shift IIR filters (filtfilt.m in Matlab). First, we used an absolute threshold of 300 fT to discard signal epochs of excessive, non-physiological amplitude. We then visually inspected all data, excluded epochs exhibiting excessive muscle activity, as well as time intervals containing artifactual signal distortions, such as signal steps or pulses. We refrained from applying artifact reduction procedures that affect the dimensionality and/or complexity of the data like independent component analysis.

Analysis

We estimated the power spectral density (PSD) for different blocks and groups. Specifically, for each subject we calculated PSD as a function of frequency for the first and the last rest block across the entire 5 min interval using Welch's method based on the FFT [26]. Afterwards, the spectra were averaged yielding one mean spectrum for each subject of group 1 for the rest condition. The same was done for the three blocks of MFA. In the second group the power spectra of both blocks of resting were similarly calculated and averaged. Then the power spectra of all 3 MW blocks were calculated and averaged. Across the two groups this yields four PSD frequency spectra: rest of group 1, MFA of group 1, rest of group 2, and MW of group 2. In planned comparisons we tested (i) whether the PSD (coefficient of each frequency) differed between groups in the rest block, (ii) MFA differs from rest within group 1, and (iii) MW from rest within group 2. We hypothesized that rest does not differ between both groups while potentially MFA results in an altered PSD compared to rest. Hence, for each

frequency we conducted three t-tests using log power values: rest vs. MFA within group 1, rest vs. MW within group 2, and rest group 1 vs. rest group 2. To correct the significance threshold for multiple comparisons resulting t-values were compared against a single surrogate distribution which was constructed by randomly reassigning labels (i.e. rest group 1, rest group 2, MFA, MW) to the values of subjects in 10,000 runs [27]. In each iteration we randomly picked two (out of four) labels and assigned randomly the values of subjects. This results in 10,000 surrogate t-values from which we determined a two-sided 99.9% confidence interval as significance threshold.

Phase spectral analysis of peaks and troughs in the broad-band signal

We then analyzed whether the local minima of negative excursions (troughs) or local maxima of positive excursions (peaks) of the broad-band signal are sufficiently sensitive events to detect certain phases of oscillations in narrow frequency bands (see **Fig 1E** for difference between troughs–local minima in negative excursions–and peaks–local maxima in positive excursions). Hence, we asked whether events represent only certain phases at *certain* frequencies, or certain phases of *all* frequencies. This is important if peaks and troughs of the broad-band signal are actually generated by band-limited processes. We tested this in the following way. The raw signal was filtered between 1 and 275 Hz. A notch filter was applied to remove line noise (±2Hz around the first 5 harmonics).

We then discretized the broad-band signal largely following the procedure proposed by [9]. Epochs in which amplitudes exceeded ± 5 SD were marked as artefacts and excluded. Then, the time series of all blocks in group 1 were z-transformed individually for all five blocks (rest 1, MFA1, MFA2, MFA3, rest 2), separately for each magnetometer. Positive and negative excursions exceeding the chosen threshold of ±3 SDs [9] from the mean for each magnetometer were identified (see **Fig 1E & 1F**). A single peak event was identified as local maximum within each positive excursion, and a single trough event as local minimum within each negative excursion. We extracted cascades across our set of MEG magnetometers by first binning the whole time series in 10 ms windows which is the average bin duration in previous studies [9] and then summing up all events found within each bin for each magnetometer.

Peak time points (TP_{peak}) and trough time points (TP_{trough}) were stored. We then filtered the broad-band signal in 39 narrow frequency bands with exponentially spaced center-frequencies between 6 and 250 Hz each with a bandwidth of 10% (IIR Filter of order 4) around the center-frequency. Note that frequency bands around line noise and harmonics can be assessed since filtered frequency bands are broader than notch filters applied. In each frequency we extracted the instantaneous phase angle (Hilbert function in Matlab). Both, at all TP_{peak} and TP_{trough} we estimated the phase of each of 39 narrow frequencies. This results in two phase angle distributions for each narrow frequency band–one at the time point of the broad-band troughs and one at the broad-band peaks. For each distribution, we calculated the concentration coefficient κ (reciprocal value to variance).

$$\kappa = \frac{1}{\varsigma^2}$$

across all phase angles in each frequency band. A low κ represents an equal likelihood of all possible phases (-π to +π), which means that the phase of specific frequency is unrelated to the peak or trough event. A higher κ, on the other hand indicates that, a certain phase is overrepresented within the phase distribution, i.e. that the oscillation at the corresponding frequency is time- and phase-locked to the broad-band peak or trough event. To determine significance, we compared frequency specific κ values against a surrogate distribution. In 10,000 runs we

draw 10,000 random phase values from the phase angle distributions across all frequency and calculated surrogate κ values and determined the 99% confidence interval of the resulting surrogate distribution.

To investigate criticality features in the MEG data, we performed the following analysis steps. In short, we first assessed spectral differences between the experimental conditions rest, MFA and MW within and between groups. In the next step we analyzed whether peaks and troughs in the broad-band signal are associated with certain phases of oscillations in narrower frequency bands. Then we carried out a first frequency- and polarity-specific analysis of criticality across all conditions by fitting a truncated power-law to each cascade size and duration distribution, and by assessing the closeness of its exponent α to a critical value of α = -1.5. We thereby systematically follow a two-step approach: Before interpreting the exponent, we always assessed the goodness of the power-law fit, as an insufficient goodness of fit would leave the estimated exponent uninterpretable. The frequency specific analysis of criticality allowed us to determine candidate frequency bands of the critical dynamics. Then we carried out a more detailed analysis of criticality with MEG signals filtered in these candidate bands, including comparisons of alternative fitting distributions, shuffling tests, evaluation of exponent relationships between cascade size and duration distributions, a shape analysis of temporal cascade profiles, as well as a correlation analysis between individual power-law fits (exponents and residuals) and MAAS scores. This initial analysis then allowed us to specifically analyze changes in criticality with experimental conditions by statistically comparing goodness of power-law fit and exponents within and between groups under conditions of MFA, MW, and rest. Finally, we assessed the topographical origin of the branching dynamics, and across which cortical regions cascades extend during rest vs. MFA to assess similarity and overlap of the involved networks.

Frequency-specific analysis of criticality

In the next step we assessed whether the brain exhibits criticality and if this is a frequency-specific phenomenon. We assessed this in the following way as outlined in [3,9]. We filtered the broadband signal in 39 narrow frequency bands with exponentially spaced center-frequencies between 6 and 250 Hz, each with a bandwidth of 10% (IIR Filter of order 4) around the center-frequency in each of the five blocks. We then discretized the bandpass filtered signal in the same way as the broad-band signal (see above, and **Fig 1E & 1F**). Separately for peak and trough events, we extracted cascades across our set of MEG magnetometers by first binning the whole time series in 10 ms windows which is the average bin duration in previous studies [9] and then summing up all events found within each bin for each magnetometer. The same analysis was repeated for the frequency bands but different bin durations ranging from 5 to 20 ms. A cascade was defined as a continuous sequence of time bins in which there was an event on any magnetometer, ending with a time bin with no events on any magnetometer. The sum of events across all magnetometers in a cascade was defined as the cascade size as it has been described in previous studies [3,9]. To avoid double dipping in the selection of frequency bands displaying criticality, we did not make use of differences in meditative state for selecting the bands. Thus, cascades were pooled across all blocks of a group including both rest and MFA/MW conditions. Using a power mass function we determined the likelihood of each cascade size (CS) within the set of all cascades. The exponent of the likelihood distribution of the cascade size (CSLD) was determined by the slope of a linear regression line fitted to the log-log representation of the CSLD in each subject. Here we used the first 2/3 of each single log-log CSLD to exclude the sharply dropping likelihood for the longest cascades.

The residuals of the linear fit to the CSLD quantify the deviation of the CSLD from power-law scaling, and thus from a critical regime. In each frequency band we compared the residuals

for trough cascades with the residuals for the peak cascades by calculating t-values across subjects.

To correct the significance threshold for multiple comparisons, the resulting 39 t-values were individually compared against the same surrogate distribution [27]. In 10,000 runs we randomly assigned the residual of our participants to peak and trough cascades. This yields a surrogate distribution of 10,000 t-values for each frequency band. We then estimated the probability of each observed t-value of each frequency band within the surrogate distribution of the given frequency band. For assessing the frequency characteristics of criticality, we constructed the surrogate distribution of CSLD exponents in the following way. We randomly permuted CSLDs in each subject and for each frequency, and estimated the slopes of their log-log representation, again. The dispersion of the surrogate distribution was used to determine a confidence interval around a hypothesized exponent of α = -1.5, which according to theoretical considerations indicates critical systems behavior [9]. Frequency bands with a mean CSLD exponent α across subjects lying within the confidence interval were considered showing critical behavior since it did not deviate from theoretically assumed criticality parameter (α = -1.5). As further control, time series of each magnetometer was shifted in time separately by a randomly chosen number of samples ($N_{permutations}$ = 10,000) leading to new cascades with unsystematic spatial spread. Both, an exponent closer to -1.5 and/or smaller residuals in the original compared to the surrogate data would be indicative for criticality in the original data.

In addition to linear regression, we tested whether cascade size distributions can be better described by an exponential fit or a log-normal fit, which would indicate a different non-critical systems state. To this end we compared residuals of the linear fit with residuals of the exponential fit and log-normal fit. T-values were compared against a surrogate distribution. This surrogate distribution was constructed in the following way. In 10,000 runs we randomly swapped labels (linear vs. exponential vs. log-normal) and calculated new t-values yielding a surrogate distribution of 10,000 t-values against which we compared the observed t values.

Additionally, we compared the ratio of the exponents of the cascade size distribution (α) and cascade duration distribution (τ) with the exponent ρ of the cascade size vs. cascade duration distribution [28]. The ratio ρ' is given by $\frac{\alpha-1}{\tau-1}$. We compared ρ and ρ' values in paired t tests both for the LFB and the HFB. In a critical state, the relation ρ is not different from ρ' [28].

Avalanche shape collapse

If a neural system is in a critical state, in addition to exhibiting power-law size and duration distributions, the mean temporal profiles of avalanches should be identical across scales [28,29] meaning that long duration avalanches should have the same scaled mean shape as short avalanches (shape collapse). Shapes were produced by averaging the temporal profiles (number of events in consecutive time bins) of all avalanches of a particular duration. We then scaled shapes to a uniform duration and scaled the minimal and maximal numbers of events constituting a cascade between 0 and 1.

External validity

To assess the behavioral relevance of criticality, we tested whether mindfulness correlates with the goodness of the linear fit in the critical frequency bands as an indicator of power-law scaling and thus of criticality. For this, we correlated the residuals with the summed MAAS scores.

Differences between mindful focused attention and rest

The previous analysis informed us which frequency bands show criticality. We then filtered the signals in the frequency bands (to anticipate, a low frequency (9-37Hz) and a high

frequency band (170-275Hz) showing exponents close to criticality α = -1.5). Separately for the three blocks of MFA and the two blocks of resting activity, we discretized the resulting bandpass filtered signal and extracted the cascades as outlined above. Then we estimated the CSLD for both conditions and compared exponents in planned comparisons with a t-test. In the second step we separately determined the CSLD exponent for each of the five blocks of group 1 to test the specific hypotheses that *(i)* brain dynamics were regulated towards criticality from the first block (rest) to the second block (mindful focused attention), *(ii)* remained at a constant critical level throughout the following two blocks of mindful focused attention and *(iii)* rebound from critical dynamics in the last block when mindful focused attention is suspended (rest). Each t-value resulting from the pairwise comparisons were compared against a surrogate distribution to test for significance. In 10,000 runs we randomly assigned condition labels (rest vs. MFA) to the CSLD exponent values across subjects and calculated a t-value between rest and MFA from these surrogate data. This yields 10,000 new t-values against which we compared the observed t-values. Finally, we tested whether waiting and rest differed in the control group comparing exponent values with a paired t-test.

Topographic analysis of avalanche propagation

We further characterized the topographic spread of the avalanches. First, we evaluated where cascades typically started and hence most likely triggered the avalanches. This was assessed in the frequency bands showing criticality according to the previous analysis steps. To this end, we determined the likelihood of each magnetometer to show an event in the first time bin of each cascade. We did this only for cascades longer than 10 time bins. We hypothesized that shorter cascades cannot spread fast enough allowing for a comparison between trigger zones on the one hand and regions where cascades typically propagate on the other hand. If cascades systematically spread away from the trigger zone then this is most likely detectable in longer cascades. The likelihood of each magnetometer in the first time bin yielded a topographic distribution of avalanche starting points, separately for rest and MFA in each subject. In each MEG magnetometer we compared the likelihood during rest and MFA across subjects with a t-test yielding a t-value for each MEG magnetometer. Regions of MEG magnetometers with a significant negative t-value mark those regions where cascades during MFA originate from more frequently. Conversely, regions of MEG magnetometers with a significant positive t-value denote those regions where cascades originate more often during rest than during MFA. Second, to reveal cortical regions across which cascades extend, we determined for each cascade all MEG magnetometers involved. Then we calculated for each MEG magnetometer the likelihood to be involved in any cascade. This was done for each subject both in the MFA and the rest condition. The likelihood of each MEG magnetometer to be involved was compared between MFA and rest across subjects yielding a t-value for each MEG magnetometer. Regions of MEG magnetometers with a significant negative t-value mark those regions where cascades during MFA frequently originate from. To correct the significance threshold for multiple comparisons, t-values of each MEG sensor were compared against a surrogate distribution. In 10,000 runs we randomly assigned condition labels (rest vs. MFA) to the CSLD exponent values across subjects and calculated a t-value between rest and MFA from these surrogate data. This yields 10,000 new t-values against which we compared the observed t-values.

Results

MAAS score for trait mindfulness

The two experimental groups did not differ with respect to the score of the trait Mindful Attention Awareness Scale (MAAS: M_{group1} = 4.32; SD = 0.49; M_{group2} = 4.41; SD = 0.56; t_{25} = .44;

p = 0.7). Thus, potential differences in brain dynamics are not due to different levels of mindfulness.

Spectral power differences

We compared PSD spectra between rest, MFA and MW in planned comparisons to assess whether these conditions differ regarding oscillatory activity (**Fig 1B**). We found a difference in PSD within group 1 between rest and MFA from 42 to 520 Hz as indicated by t-values exceeding the upper boundary of the 99.9% confidence interval of a surrogate distribution ($ci_{99.9}$ = [-3.37 3.48]) corresponding to a decrease of high frequency activity during MFA compared to rest (**Fig 1C**). The maximal t-value was 4.16 (p = .00004) at 72 Hz. In contrast, we did not find significant differences between rest and MW within the second group, nor in the rest condition between group 1 and group 2. MEG magnetometers showing the strongest difference in power were located bilaterally over a fronto-temporal region (**Fig 1D**, *upper panels*). Furthermore, individual MAAS scores were significantly correlated with a high frequency power decrease in a right set of fronto-temporal magnetometers and an increase in mid-occipital magnetometers (**Fig 1D**, *lower panel*) indicating that activity modulation in these regions predicts subjective mindfulness. In summary, we found a selective decrease in power of high frequency activity during MFA (**Fig 1C***). The comparison with the MW control condition (**Fig 1B**) suggests that this modulation of the high frequency activity was not due to changes in arousal over recording time but was truly related to meditation.

Neural oscillations associated with broad-band peaks and troughs

In previous studies, neural avalanches have been defined on the basis of troughs and peaks in the broad-band signal of magnetometers, which have been used as basic events for reconstructing avalanches [3,9]. However, the broad-band signal can be split into narrow frequency bands which are associated with different psycho-physiological processes. By phase spectral analysis we determined, whether peaks and troughs in the broad-band signal were associated with certain phase angle of band-limited oscillations. Particularly, instantaneous phase angle at the time point of each peak or trough event were determined by a Hilbert transform of 39 narrow frequency band signals (exponentially spaced center-frequencies between 6 and 250 Hz each with a bandwidth of 10%) obtained by digitally filtering the broad-band signal (IIR Filter of order 4). Phase angle distributions were calculated across all TP_{peak} and TP_{trough} of all conditions in the experimental group, respectively, separately for each of the 39 narrow frequency bands. From these distributions, concentration κ (reciprocal value to standard deviation) was calculated for peaks and troughs in each frequency band, respectively. Phase distributions in the *alpha*, *beta*, *gamma* (LFB: low frequency band) and *high-frequency* range (HFB: high frequency band) have a biased oval while frequencies around 50 Hz have more symmetric, circular form (**Fig 2A**) and showed significant κ values (κ_{crit} = .55; LFB: κ_{max} = .87, p < .0001; HFB: κ_{max} = .88, p < .0001). Thus, peaks and troughs were associated with specific oscillatory phases of low-frequency oscillations (*alpha*, *beta*, *gamma*) and of high-frequency activity, but not of mid-frequency oscillations.

Frequency bands displaying critical brain dynamics

To assess whether criticality has to be considered as a global or a band-limited phenomenon, we investigated the frequency-characteristics of the critical avalanche dynamics by fitting truncated power-laws to cascade size distributions derived from narrow-band filtered MEG signals (**Fig 2B and 2C**). Whether the dynamics is scale-free can be assessed by the goodness of the power-law fit, and how close it is to the critical point by the value of the power-law exponent.
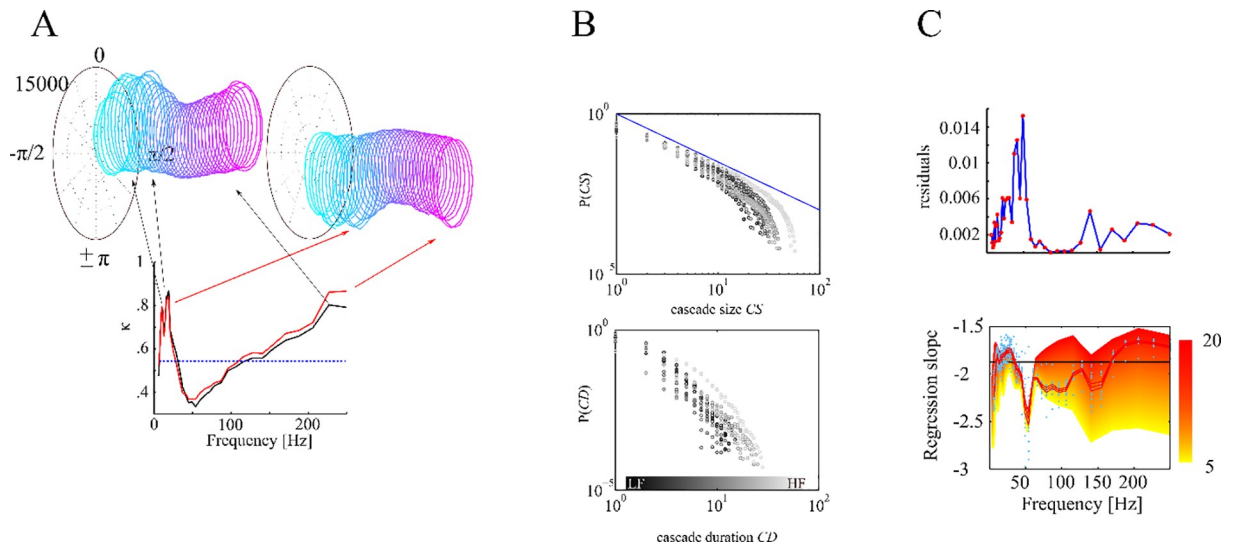
Fig 2. Depiction of trough and peak cascades. *A* We extracted the peaks (black) and troughs (red) of the broad band signal. At these time points we estimated the phase distribution of all 39 narrow frequency bands. Each ring represents the phase distribution of one frequency band ranging from low (cyan) to high frequencies (pink). We calculated the phase concentration κ for each of the frequencies (lower panel). The phase distributions in the alpha, beta, gamma and high-frequency range have an oval (corresponding with high κ) while frequencies around 50 Hz have more circular form (corresponding with low κ). *B* shows cascade size and cascade duration likelihood distributions for one subject for the different frequency bands in a log-log representation. Low frequencies are shown in darker shades. *C* We found systematically lower residuals (better linear fit) for 9–37 Hz (LFB) and 170–275 Hz (HFB) frequency bands and slopes not different from the critical value α = -1.5. Red line shows average across subjects (individual values shown by blue dots) and standard errors for 10 ms time bins.

https://doi.org/10.1371/journal.pone.0233589.g002

Power-law fits to trough cascade size distributions displayed significantly smaller residuals than for peak-cascades at low frequencies between 6 and 34Hz, at 66Hz, and between 104 and 206Hz with an average p-value of .013. This result indicates that trough cascades yielded a better power-law fit than the peak cascades in a low (<35 Hz) and a high frequency band (> 100Hz). As we have argued in the introduction, including both, peaks and troughs as events into the analysis, might bias cascade size and duration distributions. We therefore continued our analysis only with the better fitting trough-cascades.

For the trough cascade size distributions (**Fig 2B**, *upper panel*), we found low residuals (**Fig 2C**, *upper panel*) and near-critical exponents (**Fig 2C**, *lower panel*) that were not statistically different ($p>.05$) from a critical value of α = -1.5 at low (9–37 Hz) and high frequencies (170–275 Hz), as determined by a permutation test. In all other frequency bands α differed significantly from the theoretically assumed critical exponent value of -1.5 demonstrating that networks in these frequency bands did not display near-critical dynamics. We also systematically varied the bin duration used for cascade reconstruction (**Fig 2B**, *lower panel*). Near-critical exponents were only found for longer bin durations (**Fig 2C**, *lower panel*). Shorter bin durations only yielded exponents significantly more negative (supercritical) than the critical value of α = -1.5 across all frequencies.

A more detailed analysis of criticality was then carried out in two candidate frequency bands determined from the frequency-specific analysis above, i.e. for a low frequency band (LFB: 9–37 Hz) and a high frequency band (HFB: 170–275 Hz). We chose a bin duration of 10 ms since this is the mean bin duration in previous studies (see for example [9]), and, depending on frequency, shows low residuals of power-law fitting and near-critical exponents in our data. First, we fitted truncated power-laws to the cascade size distributions derived from these two bands. In the HFB, the power-law yielded significantly better goodness of fit than an exponential (**Fig 3A**, res_{exp} = .051, res_{lin} = .031; t_{16} = 16; $p < .0001$), and a log-normal function

(res$_{lognorm}$ = .04; t$_{16}$ = 6; p < .0001), but not in the LFB (res$_{exp}$ = .046; res$_{lin}$ = .049; t$_{16}$ = 1.05; p>.05) where the log-normal fit was better than the linear fit (res$_{lognorm}$ = .038; t$_{16}$ = 3.5; p = .003). Thus, only in the HFB cascade size distributions were better explained by a truly scale-free distribution than by other heavy-tailed distributions. Next, we compared in the HFB the goodness of fit and the estimated exponents with those obtained from surrogate MEG-signals time-shifted across magnetometers, in which the temporal relation across magnetometers was perturbed while the temporal succession of events within each MEG magnetometer was maintained. Residuals of the power-law fits were significantly larger in the HFB surrogate than in the original data (t$_{16}$ = 12.8; p < .0001; see **Fig 3B**). This shows that in the HFB cascade sizes better fit to a scale-free distribution than the randomly permuted surrogate data. Residuals in the LFB were generally larger than in the HFB, and did not significantly differ from the residuals of the surrogate data (t_{16} = 2.2; p>.05). To further evaluate criticality, we tested whether the ratio $\rho' = \frac{\alpha-1}{\tau-1}$. derived from the exponent α of the cascade size distribution (A) and the exponent τ of the cascade duration distribution (B) differed from the exponent ρ of the average size distribution over fixed cascade durations (C) for the LFB and the HFB, respectively. The confidence interval (t$_{ci}$ = ±2.5) was exceeded only in the LFB (t$_{16}$ = 3.8; ρ'_{LFB} = 1.53; ρ_{LFB} = 1.47) indicating a significant difference between ρ' and ρ for the LFB, but not for the HFB (t$_{16}$ = 2.1; ρ'_{HFB} = 1.33; ρ_{HFB} = 1.34; see **Fig 3C**). The observed relation ρ'_{HFB} = ρ_{HFB} [28] can be regarded as a genuine sign for criticality in the HFB. Criticality for the LFB, instead, could not be verified by this test, as $\rho'_{LFB} \neq \rho_{LFB}$.
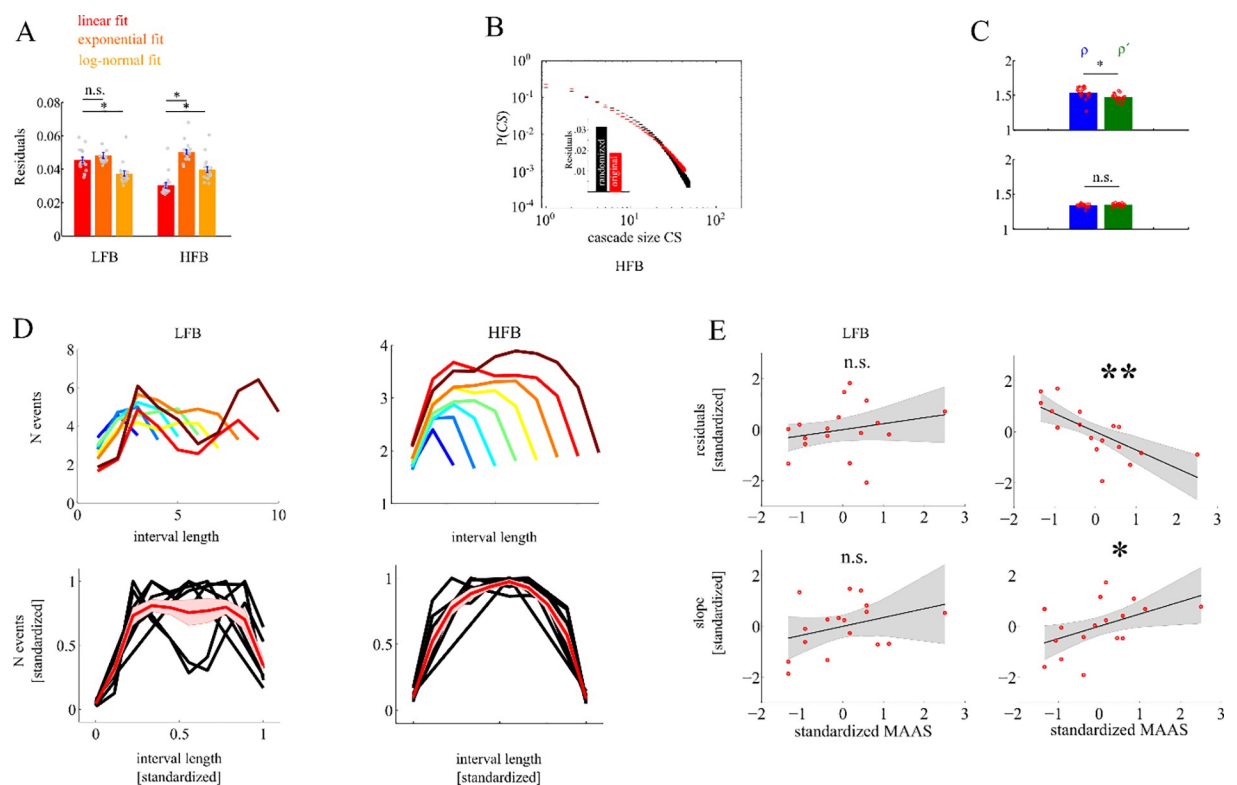
Fig 3. Depiction of cascade size distribution across frequencies. *A* We found better linear fits in the HFB compared to exponential and log-normal fits but no such pattern in the LFB. *B* We found high residuals of the linear fit to the CS taken from randomized data (black) as compared to empirical data (red). *C* ratio of CS and CD slopes were not different from correlation slopes between CS and CD indicating criticality in HFB but not in the LFB. *D* shows cascade evolution (shape) as a function of cascade length for both LFB and HFB. Note that only HFB shows comparable cascade shapes for different cascade sizes. *E* in the HFB higher MAAS score predicted a better linear fit as indicated by smaller residuals and were also correlated with the slope of the linear regression.

https://doi.org/10.1371/journal.pone.0233589.g003

Scaling of cascades can be directly assessed by analyzing the cascade shapes, i.e. its momentary size as a function of cascade duration (**Fig 3D**). In the HFB all cascades have the shape of a parabola. With different cascade sizes this shape is scaled by a power-law reflecting the underlying scale-free avalanche dynamics. Indeed, in the HFB, all shapes collapse when scaled individually to unit length. This is again not the case for the LFB. Here, cascade shapes are much more variable, and are not simply scaled versions of each other.

To assess the behavioral relevance of our findings, we correlated both the residuals of individual power-law fits as indicators of scale-freeness, and the corresponding exponents as an indicator of criticality with individual MAAS scores of mindfulness across subjects (**Fig 3E**). In the HFB a significant negative correlation was found for the residuals (r = -.71; p = .0015) demonstrating a better goodness of scale-free power-law fits with increasing MAAS score. In parallel, a significant positive correlation was found between individual linear exponents and the MAAS score (r = .48; p = .049). No significant correlations were found for the LFB, neither for the residuals (r = .23; p = .36), nor the exponents (r = .34; p = .17). Altogether, a dynamics showing scale-free, near critical dynamics could be only verified for the HFB.

Differences between mindful focused attention and rest

The previous analysis of criticality was carried out on background MEG pooled across all conditions. We then analyzed the dependence of criticality on our experimental conditions by reconstructing cascade size distributions separately for groups and block conditions in the HFB. **Fig 4A** shows the goodness of power-law quantified by the coefficient of determination for the resting blocks and the MFA blocks in group 1, and for the resting blocks and the MW blocks in group 2. In all conditions coefficients of determination were high ($R^2 > 0.93$). Between MFA and rest R^2 showed a significant difference ($t_{16} = 6.6$, p < .0001) while there was no such difference between MW and rest ($t_9 = 1.2$, p = .25). Nevertheless, our results show that cascade size distributions were scale-free in all conditions. However, as can be seen in **Fig 4B**, the exponent of the power-law was significantly more negative during MW and rest than during MFA ($t_{16} = 3.7$; p = .002). No difference was found between exponents of the rest and MW condition (t = .65; p = .53). Therefore, with an equally high goodness of power-law fit, power-law exponents were closer to the critical value of $\alpha = -1.5$ during MFA. Apparently, MFA shifted the dynamics from a supercritical closer to a critical state. Notably, even for the individual experimental blocks in group 1 (**Fig 4C**) we found significantly more negative exponents
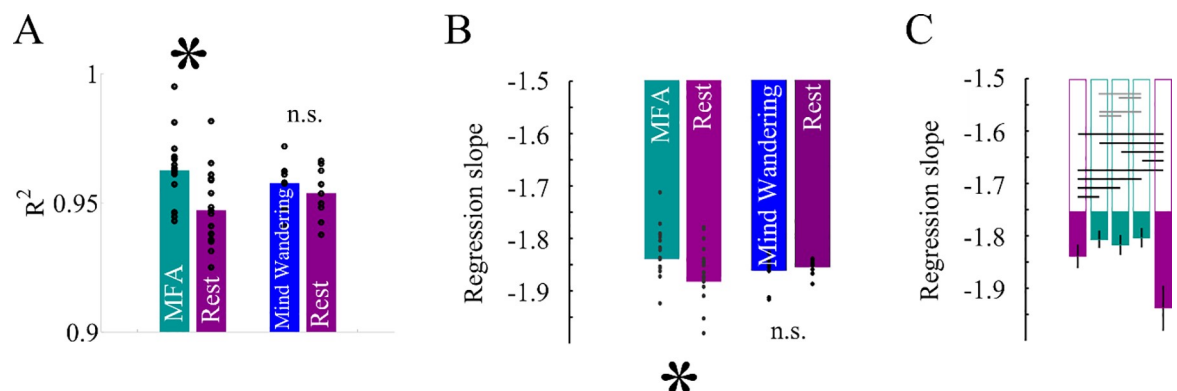
Fig 4. A shows that the linear fit explained almost perfectly variance in the cascade size distributions of both conditions in both groups. **B** shows that only the HFB showed a significant difference between blocks in group 1 with CS more closely to $\alpha = -1.5$ during MFA but not for the control group. **C** shows regression slope α for each of the 5 blocks. All black lines indicate statistically significant pairwise differences. The gray lines indicate pairwise comparisons which did not show significant differences.
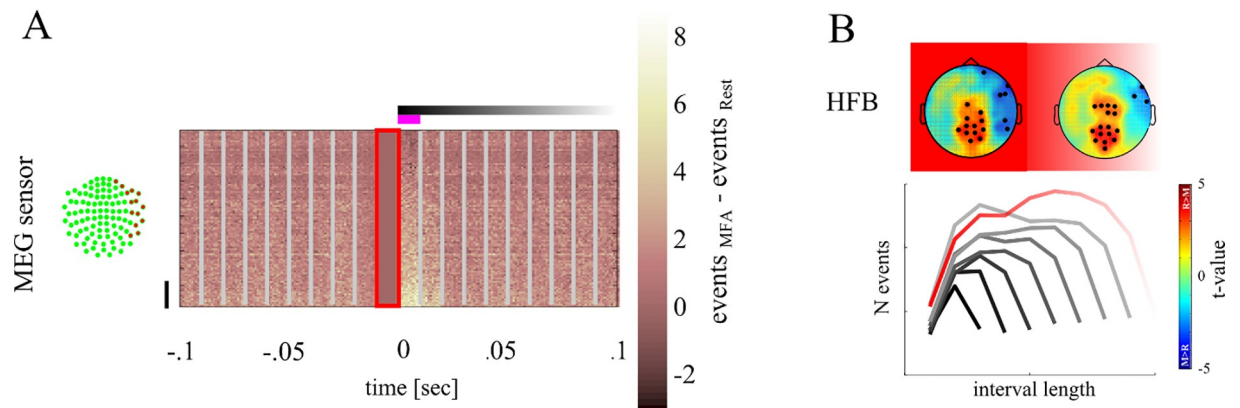
Fig 5. Depiction of topographical distribution differences between conditions. *A* shows events centred on start of the cascade as marked by 0 for each magnetometer (y-axis). The red framed area denotes the time bin in which no event was found. In each MEG magnetometer we summed all events found at each sample point both for rest and MFA. Here we depict the difference in the number of events. Light areas indicate that more events were found in the MFA condition while darker areas indicate that more events were found in the Rest condition. The upper panel shows the events found in the HFB. Vertical lines show the temporal bins of 10 msec. MEG magnetometers were sorted according to the number of events found in the first time bin. MEG magnetometers marked by the black vertical line are those showing the strongest difference between rest and MFA and are located over the right hemisphere. This difference is stronger in the HFB than in the LFB. *B* shows the topographical distribution of the likelihood of MEG magnetometers to be involved in HFB cascades (left in the first time bin and right across all time bins). Blue areas show regions of MEG magnetometers in which the likelihood is higher during MFA than during rest. Red areas show regions of MEG magnetometers in which the likelihood is higher during rest than meditation. MEG magnetometers at which we observed a significant difference are marked with a black dot.

https://doi.org/10.1371/journal.pone.0233589.g005

below -1.5 in the HFB of the resting blocks compared to the 2nd (p = .005), 3rd (p = .02) and 4th MFA block (p = .02), while there was no difference in the exponent across the MFA blocks (all $p > .13$). In contrast, the exponent in the last (5th) resting block of group 1 was much more negative than in any other block, including the first resting block (*p*s < .001), and the 2nd (p = .0003), 3rd (p = .0003) and 4th (p = .0008) MFA blocks. No changes were observed across blocks of MFA that could be attributed simply to the passing of time. In contrast, the exponent in the HFB during the last resting block was more negative consistent with a more supercritical regime than in all other blocks, which might indicate fatigue in the course of experiment. This might also explain the slightly reduced goodness of fit in the resting condition particularly of group 1. All this confirms that meditation shifted the scale-free brain dynamics closer to the critical point.

Topographic distribution of avalanches

Fig 5A shows the distribution of cascade events as function of time and magnetometer channels relative to avalanche onset. From these spatiotemporal distributions we assessed whether cascades started and/or spread across the same cortical regions during the different experimental conditions. For each magnetometer we determined the likelihood of being member of a cascade either at its start, or during the entire time of its spread. We then compared the regions from which cascades were triggered, or that were traversed by cascades more often in the MFA vs rest condition, respectively. The rationale is that when MEG magnetometer are more often involved at the start or during a cascades at rest compared to MFA, then cascades branch across different regions under these conditions.

Fig 5B shows topographical distributions of t-values of the likelihood of magnetometers contributing to rest vs. MFA at the start *(left)* or throughout the entire cascade *(right)* for the HFB, i.e. whether cascades more often started at or spread over a magnetometer during rest (red areas, positive t-values) compared to MFA (blue areas, negative t-values), respectively.

Magnetometers with statistically significant t-values compared against the surrogate distribution (t_{crit} = 2.5) are marked by black circles.

MEG magnetometers covering the right fronto-temporal-parietal region triggered HFB cascades more often during MFA (t_{16} = -2.8; p = .003). A similar pattern was found in the HFB across the entire cascade duration. MEG magnetometers covering the mid-central regions were more often involved in cascades during rest (t_{16} = 2.9; p = .003), whereas right fronto-temporal-parietal regions were traversed by HFB cascades more often during MFA than during rest (t_{16} = -2.6; p = .006). In summary, we found that cascades spread differently across cortical regions during rest and MFA. Note, that this does not necessarily mean that cascades were confined to these regions.

Discussion

Previous analyses on criticality have been carried out on broad-band filtered signals. However, filtering the MEG signal in a broad-band does not necessarily imply that criticality itself is a broad-band phenomenon. In a true broad-band phenomenon, all frequency should similarly contribute to power-law scaling. Our study however shows that peaks and troughs in the broad-band MEG commonly used to reconstruct neural avalanches are phase locked to oscillations in the low (<50Hz) and high (>100Hz), but not in the mid-frequency range. Thus, peaks and troughs are part of spatiotemporally extended oscillatory structures in these two bands. In parallel, power-law fitting yielded low residuals and near-critical exponents in a low (LFB: 9–37 Hz) and a high frequency band (HFB: 170–275 Hz). Thereby troughs showed a significantly better fit in a low and a high frequency band overlapping with LFB and HFB, respectively. Clear evidence for criticality, also, was only found for troughs from MEG signals filtered in the HFB: only in the HFB the goodness of fit to power-law scaling was significantly better than for alternative exponential and log-normal distributions, and also better than for randomly permuted surrogate data. Also the exponent relationship of cascade size and duration distribution proposed by [28] as a genuine sign of criticality, only held for the HFB, but not for the LFB. Furthermore, temporal profiles of avalanches of different size were power-law scaled versions of the same parabolic shape, and could be collapsed onto each other after rescaling. This is regarded as an indicator of criticality, which, however, was only found for the HFB, but not for the LFB. Moreover, only in the HFB, the MAAS score of mindfulness was positively correlated both with the goodness of the power-law fit, and with the exponent of the linear fit across subjects. Our study therefore demonstrates, that criticality in the MEG during MFA is associated with brain oscillations in the high frequency (>100 Hz) range of the MEG.

The frequency dependence of criticality, and the significantly better power-law fit of troughs indicates that peaks and troughs might at least stem partially from different phases of an oscillatory generator, or even from different generators contributing differently to the critical dynamics of the system. In any case, including both, peaks and troughs in the analysis can bias the avalanche size distributions towards larger cascade sizes. By counting peaks and troughs, the contribution of a single dipole, or a single oscillatory generator to an avalanche would be counted twice, and in case of different, superimposed oscillatory generators, avalanches including peaks and troughs would represent a stronger mixture of physiologically different events than peaks or troughs alone. In order to reduce this bias, the analysis of critical brain dynamics on a macroscopic level should take into account the polarity and the frequency of the brain signals. Temporal filtering and selection of troughs thereby can separate the contribution of different generators, and improve the specificity of avalanche reconstruction.

As has been shown, high frequency (>80 Hz) activity in field potentials reflects the feedforward propagation of action potentials more directly than other bands [30]. Thus, high

frequency activity would be an ideal carrier of neural avalanches that can spread over the brain revealing the dynamic state of the brain underlying the transmission process.

Importantly, during MFA neural avalanche dynamics reconstructed from the HFB was closer to the critical point compared to MW and rest. While all conditions yielded a similar goodness of fit to a scale free power-law, exponents were closer to the critical value of -1.5 during MFA, and more negative during MW and rest, indicating a shift towards a supercritical dynamics. The largest negative deviation from the critical exponent -1.5 was found in the final resting block most likely due to fatigue.

In our experiment we instructed subjects to breathe normally. However, drawing attention to the breathing cycle as during MFA, breathing might have been altered which could in turn lead to spectral changes. In a recent study, evidence has been found that the breathing rate correlates with slow cortical potentials characterized by oscillations below 1 Hz [31], which is however outside the MEG-bandwidth we investigated and evidence for breathing to alter criticality is lacking. Also, there were no other low frequency changes in the MEG-spectrum of our data that would point towards an altered breathing pattern. The main spectral power effect we found was in a high frequency band (>40 Hz), which could in principle be due to muscle artifacts. As reported in a review by [32], muscle artifacts in the MEG are characterized by broadband high-frequency activity in the range of 20–300 Hz but with the largest power at the lower end of this range. Therefore, changes in muscle activity should have altered lower beta/gamma-power, as well, which was not the case in our data. Furthermore, a significant correlation between high-frequency power reduction and MAAS score was found only unilateral at a right fronto-temporal site. With respect to the initiation and overall contribution to cascades, largest differences between conditions were found at mid-occipital and again at right fronto-temporal sensors. Such topographic distributions would be hard to explain by MFA related changes in muscle activation. Given the additional fact that we rejected muscle-contaminated MEG signals without noting differences between experimental conditions, a mere muscle effect on criticality is unlikely. Notably, the critical dynamics we observed especially in the high frequency band corresponds to a lower signal power in this band. Hence, we would conclude that at least critical dynamics was not driven by muscle artifacts. If any, reconstruction of avalanche dynamics could have been affected by muscle artifacts during resting state conditions. In this case, MFA would have facilitated the detection of critical brain dynamics by reduction of muscle activity.

However, given the fact that both the goodness of fit of the power-law and the power-law exponent were correlated with the MAAS score rather suggests that the shift of the exponent towards criticality during MFA was truly related to a change in brain dynamics. We used the MAAS score as independent measure of the subject's tendency toward mindfulness, a trait of the subject that is not related to the actual performance during the experiment. Notably, subjects did not differ as to their trait level of mindfulness between the MFA and the MW group, which shows that group differences in critical dynamics was related to the instruction, and not to differences in the subject's meditative capabilities. To our knowledge, there are no well-established psychophysiological or behavioral markers that specifically quantify such a state without being confounded by unspecific effects like vigilance. We therefore thoroughly instructed our subjects to perform meditation without changing breathing, and explicitly used naïve subjects to show the differences between rest and mediation. To control for vigilance effects, our experimental design used blocks of rest in the beginning and at the end. Under the assumption of drowsiness we would have expected that brain dynamics alters progressively across the entire experiment. Indeed, a vigilance effect was found in the meditation group. Between the first and the second resting state at the end of the experiment, the cascade size exponent became more negative than -1.5 indicating a shift towards supercritical behavior.

This might be an effect of drowsiness. But this was only found in the resting state blocks, whereas no significant change occurred across meditation blocks. Also, we did not find differences in alpha band power indicating a vigilance effect, and our experiment was relatively short (~30 min in total) reducing the influence of vigilance decrements.

A few other studies have also analyzed the relationship between meditation and criticality. Irrmischer et al. [16] showed a reduction of long range temporal correlations (LRTCs) during MFA. They hypothesized that attention is balanced at a critical point of instability between order and disorder allowing for both, transient focus and swift change of attentional resources. They argue that the focus of attention reduces information propagation by shifting the system towards a subcritical regime, which seems to be in contrast to our findings. However, consistent with our study, the authors did not find effects of MFA on critical brain dynamics in novices at frequencies < 45 Hz. Also, in our study, the power-law exponent changed from values more negative than -1.5 to values close to -1.5, i.e. in a similar direction from a supercritical to a critical dynamics. Furthermore, differences between our study and Irrmischer et al. [16] might arise from difference in measurement (MEG vs. EEG) and analysis (various avalanche based indices of criticality vs. detrended fluctuation analysis, DFA). Thereby, it is not straight forward to relate DFA to the power-law distributions and criticality indices used in our analysis. Most importantly, their study did not include higher frequencies from 170 to 270 Hz as our study and their effects were only found in trained subjects. Fagerholm et al. [10] found that in the resting state broad-band cascades were associated with an approximate critical power-law form, while the focused task state was associated with a subcritical dynamics. This parallels our study insofar as critical dynamics were found when subjects are instructed to focus on their internal milieu and refrain from the external world. Our study adds an important point to the knowledge of criticality since we showed that critical dynamics are driven by high frequency activity which was not assessed in previous EEG studies. Notably, Fagerholm et al. [10] focused on stimulus-driven attention rather than on self-regulated modulation of top-down attention as in MFA. Also, subjects had to respond as fast and accurately as possible, which necessarily confounds brain dynamics underlying attention with stimulus-evoked responses, visual information processing, decision processes, and movement-related activation. Hence, subcritical dynamics could not be ascribed exclusively to attentional modulation. In general, motor tasks that require decisions under focused attention are not the best candidates to contrast with rest, especially since fluctuation between stability and instability as the identifying feature of criticality is suspended during motor tasks, leading to increased stability [33]. Hence, studies on deviation from or convergence to criticality during attention must control for motor activity, visual input and decision processes. Finally, while Fagerholm et al. [10] proposed that the distribution of cascades changes with different cognitive states rather than where their origin, we found that cascades during MFA were triggered more often in the right hemisphere. Our finding thereby is consistent with several studies showing that during top-down attention right-hemispheric regions play a prominent role [34,35]. Unlike in our study, Lutz et al., while recording EEGs in long-term Buddhist meditation practitioners, observed in the gamma-band high amplitude oscillations and phase synchrony between fronto-parietal electrodes at frequencies from 25 Hz to 42 Hz, i.e. at lower frequencies than the high-frequency effects in our study [36]. The differences between Lutz et al. and our findings may be due to different styles of meditation, since Lutz et al. aimed at a state of non-referential compassion meditation, for which a focused attention on a particular object, was not required.

In our study, we asked the subjects to rest in the first and last block and to perform MFA in the intermittent blocks. The instruction to rest allows the mind to wander [37]. Mind wandering is characterized by a lower level of alertness [38], and reduced external information processing, which could also explain the larger distance from a critical state, as is the case under

rest, particularly if the subjects get tired. Moreover, during mind wandering attention is assumed to be decoupled from the environment [38]. By contrast, MFA requires the detection and inhibition of mind-wandering, and the refocusing of breath, which involves constant monitoring and executive control, particularly in novices. Clearly, self-regulated top-down modulation of attention as required during MFA is not well described by a fixed filter with a narrow aperture. This process is better characterized by a balance of noise and stability, of integration and segregation, of excitation and inhibitions, as might be implemented by brain states close to an instable critical point at the border between order and disorder. The observed decrease in power of the high-frequency activity during MFA in our study might thereby reflect a lower rate of neuronal spiking in right fronto-parietal regions during MFA, and thus a reduced destabilizing drive, "distracting" the brain from its balanced critical state during mind-wandering.

It is usually assumed that during rest the Default Mode Network (DMN) is activated, whereas studies of focused concentrative mediation have reported fronto-parietal executive network activity during meditation [39]. Particularly, as shown by functional magnetic resonance imaging (fMRI), MFA is correlated with activation of prefrontal cortex, premotor cortex, and dorsal anterior cingulate cortex that have been also shown to be involved in self-regulation of attention [40], as well as a reduced activation of posterior cingulate cortex, and the posterior parietal lobule of the DMN that have been related to mind-wandering, before [39,41].

In conclusion, we have shown that criticality as obtained from avalanches in MEG recordings was only observed at high frequencies > 100 Hz, and that during mindful focused attention avalanche dynamics was closer to a critical point than during states of rest. Together with the finding that mindfulness meditation leads to topographic changes in the avalanches relative to rest, our results show that self-regulated attention as required during meditation tunes brain dynamics to criticality providing a functional link between criticality and cognition.

Supporting information

S1 Data. Anleitung meditation.
(DOCX)

Author Contributions

Conceptualization: Stefan Dürschmid, Giulio Tononi, Matthias Deliano.

Data curation: Stefan Dürschmid, Nike Walter.

Formal analysis: Stefan Dürschmid, Christoph Reichert.

Methodology: Stefan Dürschmid, Matthias Deliano.

Project administration: Stefan Dürschmid, Matthias Deliano.

Supervision: Stefan Dürschmid.

Validation: Stefan Dürschmid.

Visualization: Stefan Dürschmid.

Writing – original draft: Stefan Dürschmid, Christoph Reichert, Nike Walter, Hans-Jochen Heinze, Frank W. Ohl, Giulio Tononi, Matthias Deliano.

Writing – review & editing: Stefan Dürschmid, Christoph Reichert, Nike Walter, Hermann Hinrichs, Hans-Jochen Heinze, Frank W. Ohl, Giulio Tononi, Matthias Deliano.

References

1. Bak P. How Nature Works. 2nd ed. copernicus; 1996.

2. Cocchi L, Gollo LL, Zalesky A, Breakspear M. Criticality in the brain: A synthesis of neurobiology, models and cognition. Prog Neurobiol. 2017; 158:132–52. https://doi.org/10.1016/j.pneurobio.2017.07.002 PMID: 28734836

3. Beggs JM, Plenz D. Neuronal Avalanches in Neocortical Circuits. J Neurosci. 2003; 23(35):11167–77. https://doi.org/10.1523/JNEUROSCI.23-35-11167.2003 PMID: 14657176

4. Shew WL, Yang H. Neuronal Avalanches Imply Maximum Dynamic Range in Cortical Networks at Criticality. 2009;(September 2014).

5. Shew WL. Neuroscientist The Functional Benefits of Criticality in the Cortex. 2012;(May 2012).

6. Arcangelis L De, Herrmann HJ. Learning as a phenomenon occurring in a critical state. 2010;(February 2010).

7. Beggs JM, Timme N. Being critical of criticality in the brain. Front Physiol. 2012; 3 JUN(June):1–14. https://doi.org/10.3389/fphys.2012.00001 PMID: 22275902

8. Linkenkaer-hansen K, Nikouline V V, Palva JM, Ilmoniemi RJ. Long-Range Temporal Correlations and Scaling Behavior in Human Brain Oscillations. 2001; 21(4):1370–7.

9. Shriki O, Alstott J, Carver F, Holroyd T, Henson RNA, Smith ML, et al. Neuronal avalanches in the resting MEG of the human brain. J Neurosci. 2013; 33(16):7079–90. https://doi.org/10.1523/JNEUROSCI.4286-12.2013 PMID: 23595765

10. Fagerholm ED, Lorenz R, Scott G, Dinov M, Hellyer XPJ, Mirzaei N, et al. Cascades and Cognitive State: Focused Attention Incurs Subcritical Dynamics. 2015; 35(11):4626–34.

11. Dam NT Van, Vugt MK Van, Vago DR. Mind the Hype: A Critical Evaluation and Prescriptive Agenda for Research on Mindfulness and Meditation. 2017;(October).

12. Kerr CE, Jones SR, Wan Q, Pritchett DL, Wasserman RH, Wexler A, et al. Effects of mindfulness meditation training on anticipatory alpha modulation in primary somatosensory cortex. Brain Res Bull [Internet]. 2011; 85(3–4):96–103. Available from: https://doi.org/10.1016/j.brainresbull.2011.03.026 PMID: 21501665

13. Moore A, Gruber T, Derose J, Malinowski P. Regular, brief mindfulness meditation practice improves electrophysiological markers of attentional control. 2012;(March 2014). https://doi.org/10.3389/fnhum.2012.00018 PMID: 22363278

14. van Leeuwen S, Singer W, Melloni L. Meditation increases the depth of information processing and improves the allocation of attention in space. Front Hum Neurosci. 2012; 6(MAY 2012):1–16. https://doi.org/10.3389/fnhum.2012.00001 PMID: 22279433

15. Brewer JA, Worhunsky PD, Gray JR, Tang Y, Weber J, Kober H. Meditation experience is associated with differences in default mode network activity and connectivity. 2011; 108(50).

16. Irrmischer M, Houtman SJ, Mansvelder HD, Tremmel M, Ott U. Controlling the Temporal Structure of Brain Oscillations by Focused Attention Meditation. 2018;(January):1825–38.

17. Cahn BR, Polich J. Meditation (Vipassana) and the P3a event-related brain potential. Int J Psychophysiol [Internet]. 2009; 72(1):51–60. Available from: https://doi.org/10.1016/j.ijpsycho.2008.03.013 PMID: 18845193

18. Lazar SW, Kerr CE, Wasserman RH, Gray JR, Greve DN, Treadway MT, et al. Meditation experience is associated with increased cortical thickness. Neuroreport. 2005; 16(17):1893–7. https://doi.org/10.1097/01.wnr.0000186598.66243.19 PMID: 16272874

19. Pagnoni G, Cekic M. Age effects on gray matter volume and attentional performance in Zen meditation. Neurobiol Aging. 2007; 28(10):1623–7. https://doi.org/10.1016/j.neurobiolaging.2007.06.008 PMID: 17655980

20. Slagter HA, Lutz A, Greischar LL, Francis AD, Nieuwenhuis S, Davis JM, et al. Mental training affects distribution of limited brain resources. PLoS Biol. 2007; 5(6):1228–35.

21. Mittner M, Boekel W, Tucker AM, Turner BM, Heathcote A, Forstmann BU. When the Brain Takes a Break: A Model-Based Analysis of Mind Wandering. J Neurosci. 2014; 34(49):16286–95. https://doi.org/10.1523/JNEUROSCI.2062-14.2014 PMID: 25471568

22. Kucyi A, Salomons T V., Davis KD. Mind wandering away from pain dynamically engages antinociceptive and default mode brain networks. Proc Natl Acad Sci. 2013; 110(46):18692–7. https://doi.org/10.1073/pnas.1312902110 PMID: 24167282

23. Zhou X, Lei X. Wandering Minds with Wandering Brain Networks. Neurosci Bull [Internet]. 2018; 34(6):1017–28. Available from: https://doi.org/10.1007/s12264-018-0278-7 PMID: 30136075

24. Kakumanu RJ, Nair AK, Venugopal R, Sasidharan A, Ghosh PK, John JP, et al. Dissociating meditation proficiency and experience dependent EEG changes during traditional Vipassana meditation practice. Biol Psychol. 2018; 135:65–75. https://doi.org/10.1016/j.biopsycho.2018.03.004 PMID: 29526764

25. Brown KW. Mindful Attention Awareness Scale (MAAS), trait version. J Pers Soc Psychol. 2003; 84 (58):822–48.

26. Welch PD. The Use of Fast Fourier Transform for the Estimation of Power Spectra: A Method Based on Time Aver. aging Over Short, Modified Periodograms. IEEE Trans Audio Electroacoust. 1967; 15 (2):70–3.

27. Groppe DM. Mass univariate analysis of event-related brain potentials/fields I: A critical tutorial review. 2011; 48(12):1711–25.

28. Friedman N, Ito S, Brinkman BAW, Shimono M, Deville REL, Dahmen KA, et al. Universal critical dynamics in high resolution neuronal avalanche data. Phys Rev Lett. 2012; 108(20).

29. Marshall N, Timme NM, Bennett N, Ripp M, Lautzenhiser E, Beggs JM. Analysis of Power Laws, Shape Collapses, and Neural Complexity: New Techniques and MATLAB Support via the NCC Toolbox. 2016; 7(June):1–18.

30. Buzsáki G, Anastassiou C a., Koch C. The origin of extracellular fields and currents—EEG, ECoG, LFP and spikes. Nat Rev Neurosci [Internet]. 2012; 13(June):407–20. Available from: http://dx.doi.org/10.1038/nrn3241

31. Hinterberger T, Walter N, Doliwa C, Loew T. The brain's resonance with breathing—decelerated breathing synchronizes heart rate and slow cortical potentials. J Breath Res. 2019; 13(4).

32. Muthukumaraswamy SD. High-frequency brain activity and muscle artifacts in MEG/EEG: A review and recommendations. Front Hum Neurosci. 2013; 7(MAR):1–11. https://doi.org/10.3389/fnhum.2013.00001 PMID: 23355817

33. Solovey G, Miller KJ, Ojemann JG, Magnasco MO, Cecchi GA. Self-regulated dynamical criticality in human ECoG. Front Integr Neurosci. 2012; 6(July):1–9.

34. Corbetta M, Shulman GL. Control of Goal-directed and Stimulus-driven Attention in the Brain. 2002; 3 (March).

35. Corbetta M, Kincade JM, Ollinger JM, Mcavoy MP, Gordon L. Voluntary orienting is dissociated from target detection in human posterior parietal cortex. 2000; 3(3).

36. Lutz A, Greischar LL, Rawlings NB, Ricard M, Davidson RJ. Gamma Synchrony During Mental Practice. Proc Natl Acad Sci. 2004; 101(46):16369–73. https://doi.org/10.1073/pnas.0407401101 PMID: 15534199

37. Ward AF, Wegner DM, Norton M, Business H. Mind-blanking when the mind goes away. 2013; 4(September):1–15.

38. Oken B, Health O. Vigilance, alertness, or sustained attention: physiological basis and measurement. Clin Neurophysiol. 2006;(October).

39. Hasenkamp W, Wilson-Mendenhall CD, Duncan E, Barsalou LW. Mind wandering and attention during focused meditation: A fine-grained temporal analysis of fluctuating cognitive states. Neuroimage. 2012; 59(1):750–60. https://doi.org/10.1016/j.neuroimage.2011.07.008 PMID: 21782031

40. Fox KCR, Dixon ML, Nijeboer S, Girn M, Floman JL, Lifshitz M, et al. Functional neuroanatomy of meditation: A review and meta-analysis of 78 functional neuroimaging investigations. Neurosci Biobehav Rev [Internet]. 2016; 65:208–28. Available from: https://doi.org/10.1016/j.neubiorev.2016.03.021 PMID: 27032724

41. Buckner RL. The brain's default network: Origins and implications for the study of psychosis. Dialogues Clin Neurosci. 2008; 15(3):351–8.

Behavioral/Cognitive

Frontotemporal Regulation of Subjective Value to Suppress Impulsivity in Intertemporal Choices

Stefan Dürschmid,[1,2*] Andre Maric,[2*] Marcel S. Kehl,[3] Robert T. Knight,[4] Hermann Hinrichs,[1,2,5,6,7] and Hans-Jochen Heinze[1,2,5,6,7]

[1]Department of Behavioral Neurology, Leibniz Institute for Neurobiology, Magdeburg, 39120, Germany, [2]Department of Neurology, Otto-von-Guericke University, Magdeburg, 39120, Germany, [3]Department of Epileptology, University Hospital Bonn, Bonn, 53127, Germany, [4]Helen Wills Neuroscience Institute and Department of Psychology, University of California, Berkeley, California 94720, [5]German Center for Neurodegenerative Diseases, Magdeburg, 39120, Germany, [6]Forschungscampus STIMULATE, Otto-von-Guericke University, Magdeburg, 39106, Germany, and [7]Center of Behavioral Brain Sciences, Otto-von-Guericke University, Magdeburg, 39106, Germany

Impulsive decisions arise from preferring smaller but sooner rewards compared with larger but later rewards. How neural activity and attention to choice alternatives contribute to reward decisions during temporal discounting is not clear. Here we probed (1) attention to and (2) neural representation of delay and reward information in humans (both sexes) engaged in choices. We studied behavioral and frequency-specific dynamics supporting impulsive decisions on a fine-grained temporal scale using eye tracking and MEG recordings. In one condition, participants had to decide for themselves but pretended to decide for their best friend in a second prosocial condition, which required perspective taking. Hence, conditions varied in the value for themselves versus that pretending to choose for another person. Stronger impulsivity was reliably found across three independent groups for prosocial decisions. Eye tracking revealed a systematic shift of attention from the delay to the reward information and differences in eye tracking between conditions predicted differences in discounting. High-frequency activity (175-250 Hz) distributed over right frontotemporal sensors correlated with delay and reward information in consecutive temporal intervals for high value decisions for oneself but not the friend. Collectively, the results imply that the high-frequency activity recorded over frontotemporal MEG sensors plays a critical role in choice option integration.

Key words: delay discounting; eye tracking; frontal cortex; high-frequency activity; impulsivity; MEG

Significance Statement

Humans face decisions between sooner smaller rewards and larger later rewards daily. An objective benefit of losing weight over a longer time might be devalued in face of ice cream because they prefer currently available options because of insufficiently considering long-term alternatives. The degree of contribution of neural representation and attention to choice alternatives is not clear. We investigated correlates of such decisions in participants deciding for themselves or pretending to choose for a friend. Behaviorally participants discounted less in self-choices compared with the prosocial condition. Eye movement and MEG recordings revealed how participants represent choice options most evident for options with high subjective value. These results advance our understanding of neural mechanisms underlying decision-making in humans.

Introduction

Reward value decreases as a function of time: the longer we have to wait, the less a reward is typically valued. Hence,

delayed delivery of a larger reward converts an objective value into a perceived lesser value. This results in choosing a smaller but sooner (SS) rather than a larger but later reward (LL), a phenomenon known as delay discounting (DD). Impulsive decisions might be because of the tendency to prefer SS rewards compared with LL rewards. Previous fMRI studies focused on neuroanatomical correlates of subjective valuation, and observed interactions of multiple independent valuation systems in the ventromedial PFC (vmPFC) and the dorsolateral PFC (dlPFC) (McClure et al., 2004, 2007) where goal values correlate with vmPFC activity and the amount of self-control with dlPFC activity (Hare et al., 2009). Impulsivity might also result from insufficiently considered objective alternatives (Ainslie, 1975; Myerson et al.,
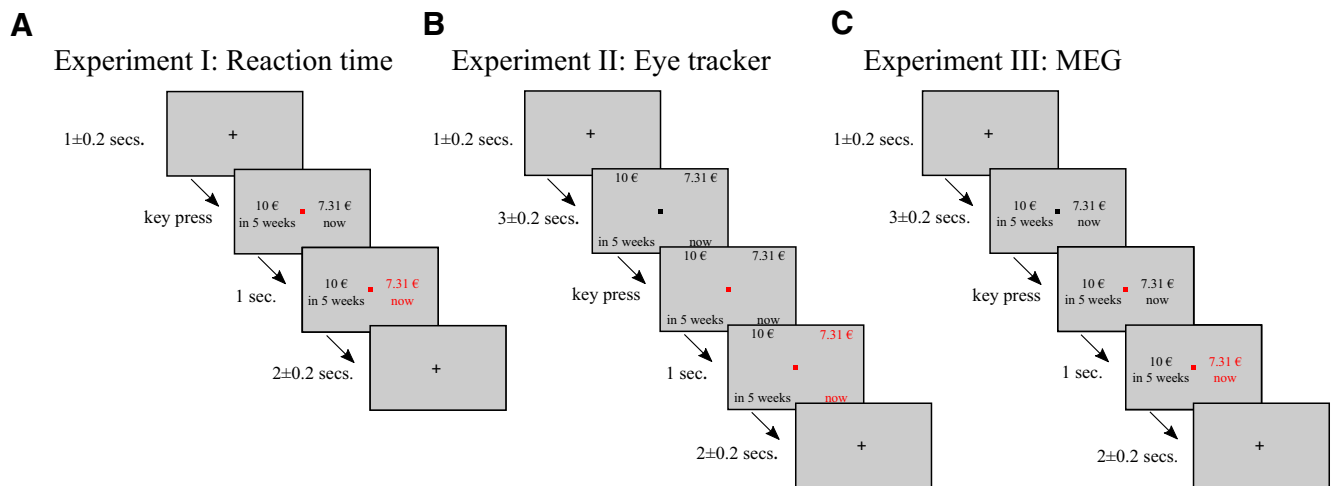
Figure 1. Depiction of choice options presentation. ***A***, Reaction time experiment. ***B***, Eye tracking. ***C***, MEG experiment. In the first experiment, we tested for differences in decision times; hence, participants were asked to respond as fast as possible (***A***). ***B***, ***C***, Both in the eye tracking and MEG experiment, participants were presented with the choice options and instructed to withhold decision until fixation points turned red. ***B***, During eye movement recording, choice options were presented further apart.

2003; Olson et al., 2007), which have to be translated into subjective values (Mazur, 1987; Green and Myerson, 2004). This view suggests that poor attention to objective values might lead to stronger DD.

Differences in discounting between participants could also be because of insufficient representation of choice options in working memory (Fuster, 1990; Baddeley, 1992; Goldman-Rakic, 1992) before an option is selected. Importantly, self-awareness counteracts this difference in discounting (Peters and Büchel, 2010). This observation suggests that choices neglecting self-awareness should lead to steeper discounting, but two contributions to these effects are still debated. First, how attentional mechanisms and the degree of neural representation contribute to decisions in intertemporal choices remains uncertain. Specifically, the time course and neuroanatomical basis of integration of choice options (delay and reward) for subjective valuation are not defined. Second, whether and how these mechanisms are modulated qualitatively by subjective awareness are not clear. We propose that attentional selection and neural representation require more effort when deciding for oneself, which is reduced in prosocial decisions (Lockwood et al., 2017). In accordance with previous studies (Lockwood et al., 2017), we tested how taking perspective of another person alters the effort to attentional select and represent choice options. The experimental contrast relies on taking perspective of the best friend (pretending to decide for the best friend), which is a prerequisite for prosocial acts and by definition reduces self-awareness.

Using eye tracking and temporal resolution of MEG recordings, we compared patterns of attentional evaluation and representation of objective values in a DD paradigm in two conditions. In one condition, participants decided on their own reward; whereas in a second anonymous prosocial condition, they pretended to decide for an imagined best friend. Hence, the conditions differed only in the subjective awareness of reward for the participants. We tested the hypothesis that participants decide more impulsively in prosocial decisions, even if this decision is completely anonymous since participants only visualize their best friend (Lockwood et al., 2017). We further hypothesized that objective choice alternatives are less considered and consequently less represented when decisions are made for others. Eye movements are a

sensitive proxy of attentional shifts, and we assessed the time course of the attentional focus using eye movement recordings and predicted less attention in choices made for others. Using MEG in an initial approach, we first evaluated whether frequency specific activity integrates choices options and second, whether differences in choice options (reward and delay in SELF vs OTHER) within the attentional focus yielded differences in neural activation.

Materials and Methods
General paradigm
In all experiments, participants were asked to choose between an LL amount of 10€ at a variable delay *D* (1, 2, 5, 11, 24, or 52 weeks; presented in pseudorandom order such that all delays were evenly distributed across the entire experiment) and SS reward. Participants made 10 choices for each delay while SS was adjusted according to the previous response to reach the individual indifference point with equivalent LL and SS option. SS was calculated as follows:

$$SS = \frac{LL}{(1 + k \cdot D)}$$

with *k* denoting the discount parameter (van den Bos et al., 2014). In the first trial, the discount parameter *k* was set to 0.02 in all participants and both conditions (van den Bos et al., 2014; Wang et al., 2016). Choosing SS instead of LL means that the subjective value of LL was lower than SS. Consequently, SS was decreased by increasing *k*. If LL was chosen, *k* was decreased for a higher SS. To allow a fast change toward the individual discount parameter in the beginning in the first 20 trials *k* was increased/decreased by 10% of *k* in the previous trial ($k_{t+1} = k_t \pm k_t \cdot 0.1$; *t* denoting the trial number). To allow a fine-grained variation in following trials, *k* was adjusted by 5% of *k* in the previous trial ($k_{t+1} = k_t \pm k_t \cdot 0.05$). Each trial started with a fixation point (3 s ± 200 ms) before the LL and SS choice options were presented simultaneously either on the left or right side of the screen, respectively, in pseudorandom order. The monetary reward was always presented above fixation and the delay below fixation (see Fig. 1). Participants were instructed to evaluate choice options closely before responding and to indicate their choice by pressing a left or right button with their left or right index finger in two conditions. In one condition, participants were instructed to evaluate choices and decide which amount has a higher value for themselves (self condition – SELF). In the second prosocial but anonymous condition, participants were instructed to evaluate choices regarding the presumable higher value for their best friend (other condition – OTHER)
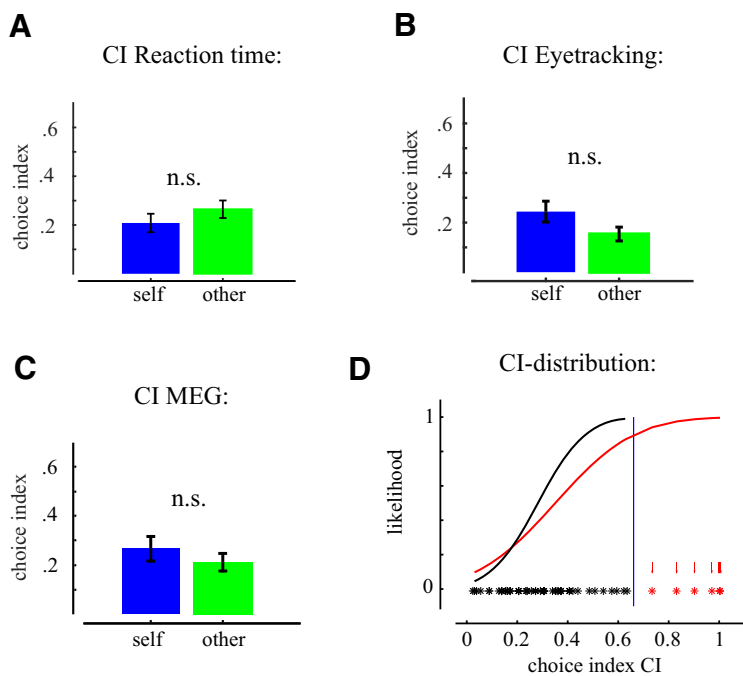
Figure 2. CI distribution. ***A–C***, Participants chose LL and SS options equally often and did not differ between conditions. Error bars indicate SEM. ***D***, Distribution of choice indices over all experiments with our cutoff at CI ≥ 0.66.

([Lockwood et al., 2017]). All participants made their decisions in both conditions in separate blocks in counterbalanced order. Before blocks started, participants were instructed whether they have to make their decisions for themselves (SELF) or whether they had to pretend to decide for their best friend (OTHER). Participants were instructed before the experiment that, on completion of the experiment, one trial is randomly chosen from all presented choices (SELF and OTHER) and the respective monetary reward will be paid at the respective delay to avoid the belief that outcomes were only hypothetical. Participants were informed that this trial will be chosen randomly from both the SELF and OTHER condition to avoid biasing decisions to one of the two conditions. Prosocial behavior is commonly assessed as the willingness to benefit others. Altruism adds that this benefit has to be at their own costs. Most, if not all, theories of reciprocity, altruism, or prosocial behavior start from the assumption that perspective taking is the starting point of each social act. Our critical experimental condition is the instruction to assume the perspective of their best friend and to pretend to perform an act that (hypothetically) benefits others.

General analysis
This paradigm only allows a limited number of trials before participants arrive at their indifference point. In accord with previous studies, we used 60 trials. In addition, especially in MEG recordings, trials have to be rejected often because of artifacts. In participants with a strong trend to choose only one option across trials, this reduction would affect the option with fewer trials disproportionately stronger. As a result, averaged MEG responses could be largely determined by a prepotent motor response but not signals related to decision, especially in the OTHER condition in which we assumed that objective choice alternatives are less considered. To compare results across groups, we applied the criterion to all participants in all experiments. To identify participants with a strong trend to choose only one option across trials, we calculated a choice index (*CI*) as follows:

$$CI = \left| \frac{N_{SS} - N_{LL}}{N_{SS} + N_{LL}} \right|$$

With N_{SS} denoting the number of SS choices and N_{LL} denoting the number of LL choices. Participants with $CI \geq 0.66$, that is, one option

was chosen almost 5 times as often as the other option, were excluded (see [Fig. 2]) in both conditions. We used the average across the last 10 updated $\ln(k)$ parameters separately as proxy for individual indifference point in SELF and OTHER decisions. A higher k value indicates steeper discounting of delayed rewards and thus more impulsive choices. As the distribution of discount rates is highly right-skewed, we used log-transformed k ($\ln k$) in all statistical analyses.

Statistical analysis. To correct statistical significance for multiple comparisons, we compared each statistical parameter against a surrogate distribution, which was constructed by randomly yoking labels of the trials and repeating the ANOVA, t tests, or Pearson's correlation coefficient. Consequently, reported p values represent the statistical significance relatively to the constructed surrogate distribution. All permutations (see detailed information for each test below) were conducted with MATLAB, and each surrogate distribution was constructed by running 1000 label permutations yielding 1000 surrogate values against which the observed statistical parameters were compared. Significance criterion in all these tests was statistical parameters corresponding with $p < 0.025$. These critical values represent the 97.5% confidence and are denoted as F_{crit}, T_{crit}, or r_{crit}. This approach counters the possibility that MEG and/or eye tracking data might be differently distributed. In general, bootstrap methods have the advantage of accounting for the dependence structure of p values. Bootstrapping offers a way to deal with situations in which the test statistic may not follow the distribution assumed by large sample theory.

Power of correlation analysis. We conducted individual correlation analyses (e.g., gaze stability in eye tracking vs discount parameter or MEG activity vs discount parameter) where the number of participants has to be high to avoid false positives. Too few participants might not correctly reflect a small correlation leading to the false assumption that there is no correlation despite a *de facto* but low (e.g., $\rho = 0.3$) correlation at the population level. Hence, a high number of subjects is needed for low correlation strength, but fewer participants can correctly reveal higher correlations at the population level (e.g., $\rho = 0.6$). Increasing the number of participants without changing mean and SD decreases the p value and hence increases the likelihood of exaggerating small effects. The number of participants used in our study are a trade-off between both approaches: a well-powered individual differences analysis without inflating mean effects. We determined the power of the maximal correlation coefficient r using G*Power 3.1 ([Erdfelder et al., 2009]). The power values are given as β separately for each analysis.

Reaction time experiment
Choice options were presented on the computer screen spanning a visual field with a horizontal visual angle of 9.5° and vertical visual angle of 1.4°. Participants were instructed to closely evaluate the choice options and press one of two buttons indicating their choice when they had the feeling that they made their decision. If they did not respond following 10 s, the next trial started (see [Fig. 1A]). We compared mean decision time and $\ln(k)$ parameters across participants between conditions using separate paired t tests (see [Fig. 3A,B]).

Eye tracking experiment
Participants were instructed to withhold decision until the fixation point turned red (3 s ± 200 ms following presentation of choice options; sufficiently long to exceed mean decision time in the first experiment) to eliminate any impact of button presses (see [Fig. 1B]). Choice options were presented further away from each other spanning an area of 41 × 15.5 cm (horizontal visual angle of 32° and vertical visual angle of 12°) to clearly distinguish gaze direction to the delay and reward. We used for eye movement recording the Eyelink 1000 system operated on Windows 7 and a desktop-mounted Eyelink CL camera with a TV lens (35 mm 1:1.6). All participants used a chin and forehead rest with 71.5 cm

distance to the monitor and 59 cm to the camera. Visual stimuli were presented on a Samsung Syncmaster 2233 (22 inch) with a resolution of 1680 × 1050. In each participant, we tracked the pupil diameter and corneal reflex of the left eye with a sampling rate of 2000 Hz. Before each trial block, we performed a calibration session with the built-in 9-point grid method.

Data preprocessing. The resulting eye tracking data (time series of vertical eye movements to the reward presented above and delay below fixation cross) were used to characterize temporal dynamics of evaluation of delay and monetary reward. First, we identified trials (−1 to 4 s around stimulus onset) with low fixation in the baseline period (−1 s to stimulus onset). That is, we calculated for each trial the mean y coordinate (vertical eye movements between reward and delay). Trials with a mean y value >2 SDs (indicating low fixation) of all trials were excluded from analyses. Since delay and reward were always presented below and above fixation, respectively (LL and SS options were presented pseudorandomly to the left and right), we focused on analyzing y coordinates across time. We baseline-corrected by subtracting from each data point (y coordinate) the mean y coordinate within the −1 s preceding the stimulus onset in each trial. To define gaze direction as a function of time across trials, we then calculated at each time point a histogram of all y coordinates (see Fig. 4B) separately for each participant. This results in high probability values for fixation before stimulus onset and high probability values for delay and reward following stimulus onset. These can be identified as colored bands in front of an otherwise dark blue background (locations on the screen where participants did not look at consistently) in Figure 4B. From these probability maps, we extracted three time series defined by gaze to delay D_t, to fixation F_t, and monetary reward R_t, representing time varying probability to look at delay, fixation, and reward, respectively. Since participants did not look exactly at one location, we defined a spatial margin around each of the three spatial regions based on the real eye movements. To this end, individual probability maps were averaged across participants and conditions and across time, leading to three probability maxima, which correspond with spatial location of delay, fixation, and reward (see Fig. 4B, right, dashed lines). The margin around these maxima is defined by the inflection points (solid lines). Probability values around the three maxima corresponding with spatial location on the screen (see Fig. 4B) were averaged at each time point, leading to three time series for each participant and condition. Figure 4B (bottom) shows the time series for delay and reward.

Data analysis. Discounting differences. First, we compared $ln (k)$ parameters across participants to test whether participants discounted differently between conditions (see Fig. 4A) with a paired t test.

Intervals of option evaluation. To test for difference of gaze direction, we conducted a t test at each time point between D_t and R_t time series across participants, leading to T_{DR} time series. This time series shows when participants inspected on average more the delay or the reward. The level of significance of T_{DR} was corrected for multiple comparisons by comparing each T_{DR} value against a surrogate distribution. This surrogate distribution was constructed by randomly reassigning the labels (delay vs reward) to the single participants in 1000 permutations. This leads to 1000 surrogate T_{DR} value time series. Significance criterion was a T_{DR} value with $p < 0.025$ within the surrogate distribution of all T values (see Fig. 4B).

Differences in option evaluation. We tested whether participants evaluated choice options differently in both conditions. To test for difference of gaze direction between conditions, we conducted a t test at each time point for F_t, D_t, and R_t across participants, leading to three t value time series (T_F, T_D, and T_R) capturing the differences between conditions. The level of significance of each of the three t value time series was corrected for multiple comparisons by comparing each t value time series against a surrogate distribution as above but swapping labels (SELF vs OTHER). Significance criterion was a t value with $p < 0.025$ within the surrogate distribution of all surrogate t values (see Fig. 4C).

Correlation of gaze entropy and decision. We hypothesized that differences in decision-making result from differences in choice evaluation. D_t
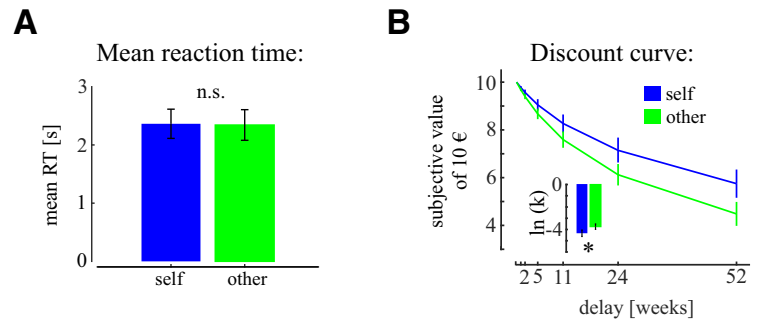
Figure 3. Reaction time experiment. *A*, Participants did not show differences in decision times between conditions that were made within 3 s. *B*, Discount curves for both conditions. The discount parameters (small inset) were significantly different with stronger discounting in the prosocial condition. Error bars indicate SEM.

and R_t time series representing the probability to look at the delay and the reward were used to estimate the entropy, which gives the average of information of all events (here gaze at delay and reward) and reflects the predictability or stability of gaze direction. If gaze entropy is high, it is hard to predict whether participants look at the delay or the reward; but if gaze entropy is low, then gaze direction is stable and prediction is high. In both conditions, entropy was calculated at each time point t as follows:

$$H_t = \sum_{i}^{m} -p_{i,t} \cdot log_2 p_{i,t}$$

With i denoting the reward and delay, p as the likelihood to direct gaze at one of the two events. The resulting entropy time series H_{OTHER} was subtracted from H_{SELF}, leading to an H_Δ time series for each participant. Individual differences in discount parameters were correlated with H_Δ values at each time point, leading to a new Pearson's correlation r time series. The level of significance of r was corrected for multiple comparisons by comparing each r against a surrogate distribution. This surrogate distribution was constructed in the following way. For each iteration, we randomly assigned the individual entropy values H_Δ across participants. We then correlated these randomly assigned values with the individual discount values of our participant in 1000 permutations. This leads to 1000 surrogate r value time series. Significance criterion was a r value with $p < 0.025$ within the surrogate distribution of all r values (see Fig. 4D).

MEG recordings

Data acquisition. In a third group, participants ($N = 24$; 7 female; mean age: 26.17; SD = 5.16) were seated in a magnetically shielded room in which mMEG activity was recorded while participants performed the experiment. To record vertical and horizontal eye movements, electrooculographic activity was obtained. Electrode impedance was kept <10 kΩ. For the data acquisition, a whole-head, 102-channel magnetometer array (Elekta Neuromag TRIUX) with internal helium recycler has been used. The MEG system contains 102 sensor fields, each equipped with one magnetometer measuring the normal field component and two orthogonally oriented planar gradiometers for measuring the gradient components. The participants sat in an upright position underneath the MEG "helmet." MEG data were sampled at 2000 Hz with a bandpass filter from DC to 660 Hz.

First, we tested whether participants discount more in the OTHER condition compared with the SELF condition comparing log-transformed discount parameters between conditions. Participants were instructed to withhold decision until the fixation point turned red (3 s ± 200 ms following presentation of choice options; sufficiently long to exceed mean reaction time in the first experiment) to eliminate the impact of button presses (see Fig. 1C). In the eye tracking experiment, we forced participants to shift gaze and hence their attentional focus. Here, to suppress eye movements, choice options were presented on the screen spanning an area of 3 × 12 cm (horizontal visual angle of 6.8° and vertical visual angle of
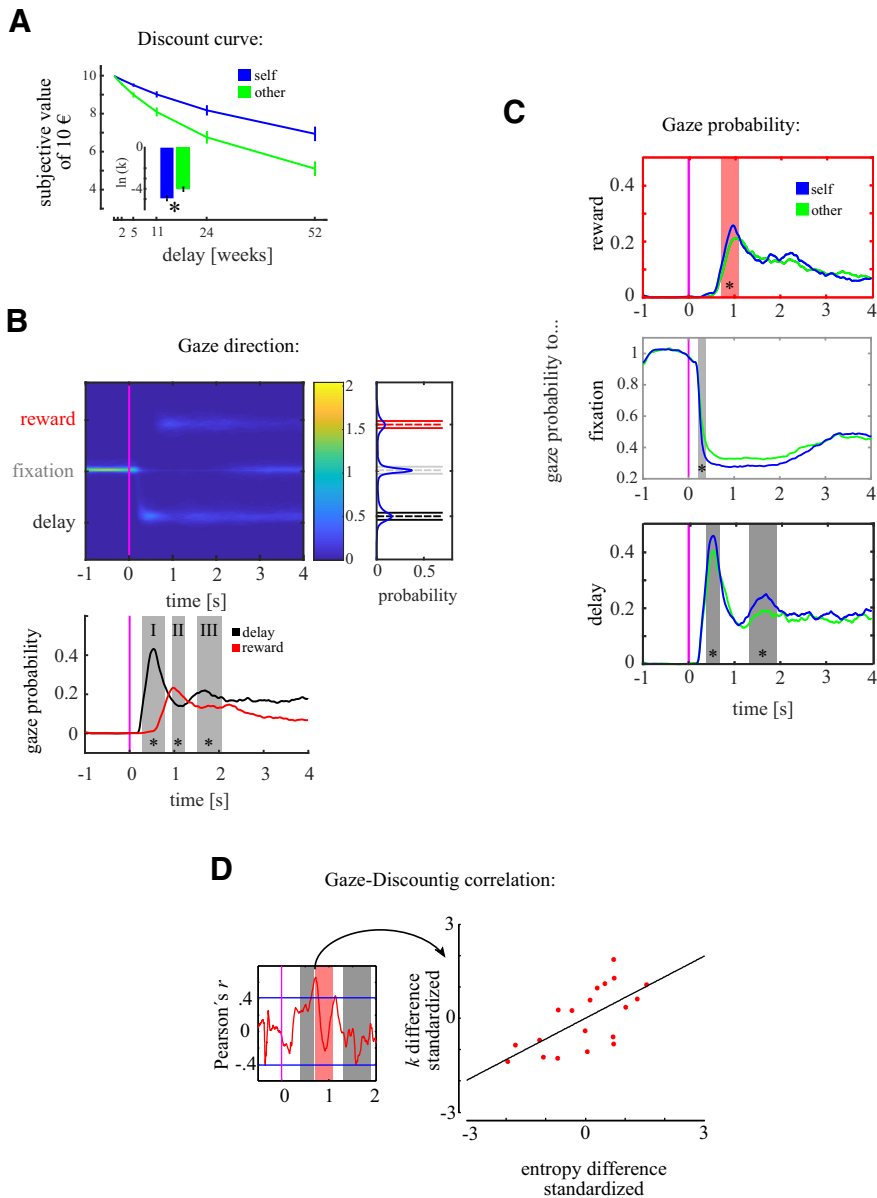
Figure 4. Eye tracking results. **A**, Stronger discounting in the OTHER condition as indicated by differences in discount parameters (small inset). Error bars indicate SEM. **B**, Color-coded gaze probability as a function of time to choice option onset (x axis) averaged across all participants and conditions. y axis indicates the location of reward, fixation, and delay presented on the screen. Yellow band before stimulus onset (magenta vertical line) indicates that participants looked at the fixation cross. Following stimulus onset, participants directed gaze to delay and reward as indicated by light green and light yellow streaks across time. Right, Average across time. Peaks (dashed lines) correspond to exact locations on the screen of reward, fixation, and delay. Bell-shaped averaged probability values indicate that participants inspected reward and delay with spatial variability. Probability values within inflection points (solid lines) were averaged, leading to time series representing gaze probability to delay, reward, and fixation. Bottom, A consistent chronology of first delay and then reward inspection. Black and red lines indicate probability to direct gaze to delay and reward, respectively, averaged across participants. First gray shaded area represents the interval in which participants gazed to delay more than to reward as indicated by a significant t value; the second gray shaded area, vice versa. **C**, Time-varying probability to direct gaze to fixation in both conditions averaged across participants. Gray shaded area represents the temporal interval, with significant difference between SELF (blue) and OTHER (green) condition indicating that participants disengaged slower from fixation in the OTHER condition. Bottom, Gaze direction to the delay (black frame) separately for both conditions. Top, Gaze direction to reward (red frame) separately for both conditions. Gray shaded areas represent intervals of significant differences between conditions, indicating that both delay and reward were inspected more closely in the SELF compared with the OTHER condition. **D**, Correlation of differences of gaze entropy and difference of discount parameter between conditions at the time point shown in the left small diagram. Greater differences in gaze entropy are correlated with greater differences in discounting.

1.79°). This allows us to assess potential intervals when delay and reward are within the attentional focus, ruling out the possibility that differences in MEG activity result from eye movements. Furthermore, all trials with activity >2 SDs of all electro-oculographic trials were rejected.

Preprocessing. We used MATLAB 2013b (The MathWorks) for all offline data processing. All filtering (see below) was done using zero phase-shift IIR filters. First, we used an absolute threshold of 300 fT to discard signal epochs of excessive, non-physiological amplitude. We then visually inspected all data, excluded epochs exhibiting excessive muscle activity, as well as time intervals containing artifactual signal distortions, such as signal steps or pulses. We refrained from applying artifact reduction procedures that affect the dimensionality and/or complexity of the data (e.g., independent component analysis). The raw signal of all remaining epochs was filtered between 1 and 275 Hz. A notch filter was applied to remove line noise (± 2 Hz around the first 5 harmonics) before filtering in specific frequency bands (see below).

Data analysis. Discounting differences. First, we compared $ln(k)$ parameters across participants to test whether participants discounted differently between conditions (see Fig. 5A).

Choice options related to amplitude modulation. Next, we tested whether brain activity shows significant amplitude modulation to presentation of choice options. For each trial (-2 s to 6 s around stimulus onset – sufficiently long to prevent any edge effects during filtering), we bandpass filtered each electrode's time series at 37 frequency bands (log-spaced between 1 and 330 Hz) with a bandwidth of 15% of the center frequency. We obtained the analytic amplitude $A_f(t)$ of each frequency f by Hilbert-transforming the filtered time series. We smoothed the time series such that the amplitude value at each time point n is the mean of 10 ms around each time point n. We then baseline-corrected the brain activity by subtracting the mean activity from the -1 to 0 s preceding the stimulus onset in each trial of each magnetometer.

We then identified stimulus-responsive frequency bands showing a significant amplitude modulation in each frequency band following the onset of choice display. We first averaged A_f across all trials, magnetometers, and participants, resulting in one amplitude time series for each frequency. We then calculated the average baseline activity $\overline{B}_f$ across the 500 ms preceding the stimulus onset. For each frequency band activity, we subtracted $\overline{B}_f$ from the activity modulation $\overline{A}_f$ averaged across the 3 s following the stimulus onset. To control the significance threshold for multiple comparisons, the difference between $\overline{B}$ and $\overline{A}$ was compared against an empirical distribution derived from randomly shifted time series ($N_{permutations} = 1000$). In each iteration, time series of each channel (circular shift of the entire trial time series) separately and new (surrogate) trial averages ($\overline{B}$ and $-A$) were calculated from the shifted trials. Frequency bands exceeding the 97.5th or below the 2.5th percentile of the frequency specific surrogate $\overline{B}_f\overline{A}_f$ distribution (see Fig. 5B, dashed

gray lines) were classified as showing a significant amplitude modulation following presentation of choice options.

The previous analysis informed us which frequency band showed a significant modulation to presentation of choice options. Next, we tested which channels contributed significantly to the stimulus response modulation in frequency bands with significant amplitude modulation. Hence, we filtered raw time series in the broader frequency bands showing significant amplitude modulation found in the previous analysis. We first averaged A_f across all trials and participants and repeated the analysis as outlined above. Magnetometer's signals exceeding the two-sided 95th percentile of the surrogate $\overline{B_f A_f}$ distribution were classified as showing a significant amplitude modulation following presentation of choice options (see Fig. 5B).

Amplitude modulation with delay. In the next step, we tested whether these frequency bands code objective values and hence showed amplitude modulation as a function of delay and/or reward. First, we grouped trial activity recorded at magnetometers with significant amplitude modulation according to the six different delays and averaged across all participants. This was done since the six different delays were the same in all participants. This leads to six new time series for each magnetometer, each representing the mean activity modulation to one of the six delays. At each time point, we linearized amplitude differences between these 6 time series by assigning a rank value to each of the 6 amplitude values (1 being the lowest amplitude and 6 representing the highest amplitude). Integer ranks can help to stabilize effects, which can be obscured because of these fluctuations. This was used to identify temporal intervals. To corroborate our hypothesis, statistical tests were conducted using the real data. Next, we tested whether these ranks as a proxy for the amplitude values correspond with the delays. A rank order matching the number of delay (1 [shortest delay] to 6 [longest delay]) would indicate that a given frequency band responds with a gradually increasing amplitude modulation to a gradually increasing delay. To test this, we used a linear least square fit to the rank values at each time point. This results in a new slope time series with positively/negatively highest slopes when amplitude modulation varies with delay and slopes at ~0 when amplitude is not modulated by the delay. The level of significance was corrected for multiple comparisons by comparing each slope value against a surrogate distribution. This surrogate distribution was constructed by randomly reassigning the labels (delay 1-6) to the six time series in 1000 permutations for each channel. This leads to 1000 surrogate slope values. Frequency bands exceeding the two-sided 95th percentile of the surrogate distribution were classified as showing a significant correlation of amplitude and delay. To assess differences between frequency bands, we used a time point-by-time point one-way ANOVA to test for differences of slope values across magnetometers. We determined the empirical significance threshold for *F* values by randomly reassigning the frequency band labels in 1000 permutations of the same time point-by-time point ANOVA. Last, in the temporal interval of significant amplitude-by-delay covariation, we used a one-way ANOVA to test for differences of amplitude values between
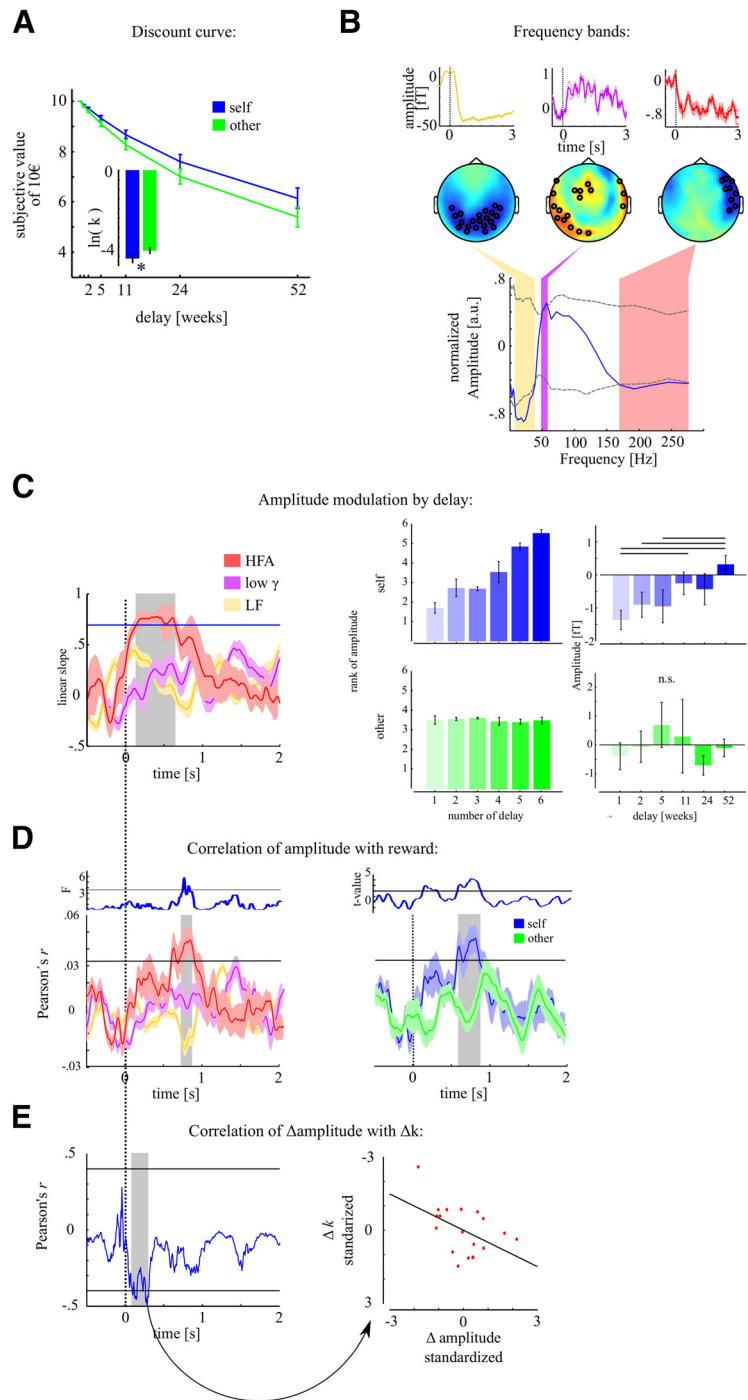
Figure 5. MEG results. *A*, Behavioral results. *B*, Amplitude modulation in three different frequency bands with topographical distributions. Two gray dashed lines indicate the upper and lower confidence interval (obtained from a permutation test) and hence distinguishes the frequency bands with significant amplitude decrease (below the lower gray line) from frequency band with significant amplitude increase (above the upper gray line). In each frequency band, we determined MEG sensors with significant amplitude modulation over baseline based on a permutation procedure. *C*, Only HFA shows correlation with delay. Differences in amplitude modulation as a function of delay was only found in the SELF but not in the OTHER condition. Error bars indicate SEM. *D*, In a temporal interval following the coding of the delay, we found significant correlation with reward information only in the high frequency band and exclusively in the SELF condition. *E*: Differences in amplitude modulation between conditions were correlated with differences of discounting between conditions.

6 delays across participants. The same analysis was conducted in the OTHER condition (see Fig. 5C).

Correlation with reward. To test whether amplitude modulation varied as a function of the reward, we correlated the trial-to-trial variation of reward with the trial-to-trial variation of amplitude averaged across

Table 1. Participants characteristics and exclusion criteria

	n (total participants)	Age (mean $\pm$ SD)	Gender (m/f)	MEG artifacts $>$ 30%	CI $\geq$ 0.66	n (final sample size)
Reaction time	22	24.10 $\pm$ 5.16	9/13	—	6	16
Eye tracking	20	22.58 $\pm$ 2.06	10/10	—	1	19
MEG	24	26.17 $\pm$ 5.16	17/7	5	0	19

MEG sensors showing significant amplitude modulation at each time point. This analysis was done in each participant since monetary reward values depended on individual decisions and consequently differed across participants. This results in a Pearson's r time series for each participant. The level of significance was corrected for multiple comparisons by comparing each r value against a surrogate distribution. This surrogate distribution was constructed by randomly reassigning the amplitude values of one participant to the discount values of another participant in 1000 permutations. This leads to 1000 surrogate r value time series. Significance criterion was an r value with $p < 0.025$ within the surrogate distribution of all r values (see Fig. 5D).

Correlation of MEG response and discount differences. Finally, we assessed whether differences in amplitude modulation could explain differences of discounting behavior between conditions. We averaged in frequency bands showing significant amplitude modulation across MEG sensors representing objective choice options in both conditions and calculated the difference time series ($\Delta_{amplitude}$) for each participant. At each time point, we calculated Pearson's r between $\Delta_{amplitude}$ and Δ_k denoting the difference in discount parameter in each participant. The level of significance was corrected for multiple comparisons by comparing each r value against a surrogate distribution. This surrogate distribution was constructed by randomly reassigning the amplitude values of one participant to the discount values of another participant in 1000 permutations. This leads to 1000 surrogate r value time series. Significance criterion was an r value with $p < 0.025$ within the surrogate distribution of all r values (see Fig. 5E).

Results

In all experiments, participants were asked to choose between a LL amount of 10€ at a variable delay D (1, 2, 5, 11, 24, or 52 weeks; presented in pseudorandom order) and SS (now) reward (for a detailed description of the paradigm, see Materials and Methods; Fig. 1). Participants made 10 choices for each delay in pseudorandom order, while SS was adjusted according to the previous response to reach equivalent LL and SS options (see Materials and Methods; Table 1).

Decision time experiment
In the first experiment, we tested 22 participants (13 female; mean age 24.1 years; SD = 5.16; all righthanded with normal or corrected-to-normal vision) (1) for differences in decision time and (2) whether they discounted differently between both conditions (analysis steps are explained in more detail in Materials and Methods). We calculated a CI, which parameterizes how evenly participants chose both options. Six participants strongly preferred one choice option (see Materials and Methods; $CI \geq 0.66$), which means that one option was chosen 5 times as often as the other one and were excluded. The remaining participants did not differ on average in their CI ($CI_{SELF} = 0.21$, SD = 0.15; $CI_{OTHER} = 0.26$, SD = 0.14; $t_{(15)} = 1.5$; $p = 0.15$; Fig. 2A) and in their decision time ($RT_{SELF} = 2.36$ s, $RT_{OTHER} = 2.34$; $t_{(15)} = 0.16$; $p = 0.8$; Fig. 3A). However, they discounted stronger in the OTHER condition ($t_{(15)} = 2.3$; $p = 0.03$) as indicated by higher discount parameters (mean $ln(k_{OTHER}) = -3.7$; SD = 0.23; mean $ln(k_{SELF}) = -4.3$; SD = 0.29; Fig. 3B).

Eye tracking experiment
To further assess OTHER condition discounting effects, we compared the discounting parameters ln(k) (the natural logarithm of

the k parameter adjusted throughout the experiment) in a second group ($N = 20$, 10 female; mean age 22.58 years; SD = 2.06). Eye tracking data (time series of vertical eye movements between reward presented above and delay below fixation cross) were used to characterize temporal dynamics of evaluation of delay and monetary reward. Analysis steps are explained in more detail in Materials and Methods. In general, we tested for differences in discounting behavior (see Discounting differences), whether participants showed on average a consistent chronology of delay and reward evaluation (see Intervals of option evaluation), whether participants evaluated choice options differently in both conditions (see Differences in option evaluation). These analyses test for stability choice option evaluation (gaze entropy; reflects the predictability or stability of gaze direction). In the final step, we tested whether discounting differences can be explained by differences in choice evaluation (see Correlation of gaze entropy and decision).

Discounting differences
One participant was excluded because of his strong bias toward one option ($CI \geq 0.66$). The remaining participants showed on average no difference in CI ($CI_{SELF} = 0.24$, SD = 0.17; $CI_{OTHER} = 0.15$, SD = 0.11; $t_{(18)} = 1.7$; $p = 0.11$; Fig. 2B). Replicating Experiment 1, participants discounted stronger in the OTHER condition ($t_{(18)} = 3.5$; $p = 0.0025$; Fig. 4A) as indicated by higher discount parameters (mean $ln(k_{OTHER}) = -3.9$; SD = 0.84; mean $ln(k_{SELF}) = -4.8$; SD = 0.62; Fig. 4A).

Intervals of option evaluation
We tested the chronological order of the inspection of delay and reward. Participants tended to inspect delay first (Fig. 4B, I; significant difference to reward between 182 ms and 816 ms; $t_{crit} = \pm 2.05$; $t_{max} = 12.35$ at 536 ms; $p < 0.000001$). Participants then inspected the reward (Fig. 4B, II) between 998 and 1201 ms indicated by higher probability for gaze at reward compared with delay ($t_{max} = 2.45$ at 1102 ms; $p = 0.01$). Third, they returned to the delay (Fig. 4B, III) between 1447 and 2110 ms ($t_{max} = 3.68$ at 1628 ms; $p = 0.002$) with higher probability for gaze at delay compared with reward.

Differences in option evaluation
Here we tested for temporal differences of inspection as a function of our experimental conditions. We found that participants more closely inspected the delay (I) in the SELF condition (Fig. 4C, bottom) in the temporal interval from 367 to 626 ms ($t_{crit} = \pm 2.075$; $t_{max} = 2.8$ at 416 ms; $p = 0.0038$). Second, we found that participants more closely inspected the reward (II) in the SELF condition (Fig. 4C, top) in the temporal interval from 686 to 1032 ms ($t_{max} = 2.95$ at 925 ms; $p = 0.0026$). Third, when participants returned to the delay information, they also more closely inspected the delay (III) in the SELF condition between 1434 and 1634 ms ($t_{max} = 2.36$ at 1686 ms; $p = 0.012$).

Correlation of gaze entropy and decision
In the last step, we tested whether differences in gaze entropy (how stable participants looked at choice options) between conditions correlate with differences in discount parameter between

conditions. We found a significant correlation (critical r value was ± 0.41) between differences in discount parameter and differences in gaze entropy between 628 and 778 ms ($r_{max} = 0.66$ at 722 ms, $\beta = 89\%$; $p = 0.0025$; Fig. 4D).

MEG experiment

In a third group of participants ($N = 24$; 7 female; mean age: 26.17 years; SD = 5.16 years), we assessed discounting behavior (see Discounting differences) using MEG activity across specific frequency bands (see Choice options-related amplitude modulation). We then tested whether these specific frequency bands represent the delay (see Amplitude modulation with delay), and/or the reward (see Correlation with reward) and whether differences of MEG activity between conditions correlate with differences in discounting behavior (see Correlation of MEG response and discount differences). Analysis steps are explained in more detail in Materials and Methods.

Discounting differences
Five participants were excluded since >30% of trials had to be rejected because of artifacts (we recorded only 60 trials in each condition). None of the remaining participants had to be rejected because of a strong bias toward one option ($CI \geq 0.66$). The remaining participants did not differ with respect to CI ($t_{(18)} = 1.34$, $p = 0.2$) but show differences in discounting ($t_{(18)} = 2.85$, $p = 0.01$) consistently with the other two groups (Fig. 5A).

Choice options-related amplitude modulation
We found a low-frequency band (LF: 6-35 Hz) and high-frequency band (HF: 150-275 Hz) with significant amplitude decrease compared with baseline bilaterally located over occipital cortex and over right frontotemporal cortex, respectively (Fig. 5B). Additionally, we found γ frequency (50-70 Hz) increase over baseline following stimulus onset in a central and occipital ROI (Fig. 5B).

Amplitude modulation with delay
Only HF amplitude varied with the delay information (critical slope value: 0.69) between 138 and 643 ms (slope$_{max}$ = 0.78 at 411 ms; $p = 0.03$; Fig. 5C). In the SELF condition, we found differences in amplitude modulation depending on the delay presented in this interval ($F_{(5,108)} = 2.4$; $p = 0.039$). *Post hoc* tests revealed a significant difference between 1 and 11 weeks ($p = 0.04$) and 1 and 52 weeks ($p = 0.0003$), 2 and 52 weeks ($p = 0.01$), and 5 and 52 weeks ($p = 0.03$). The OTHER condition exhibits no significant differences ($F_{(5,108)} = 0.5$). In addition, we found a highly significant interaction between the OTHER and SELF condition ($F_{(5,216)} = 9.06$; $p < 0.00001$).

Correlation with reward
The HF amplitude was correlated with reward between 576 and 876 ms ($r_{max} = 0.05$; $p = 0.0009$ at 816 ms; Fig. 5D), which is also corroborated by a significant difference between frequency bands between 741 and 826 ms ($F_{crit} = 3.6$; $F_{max} = 5.8$ at 756 ms; $p < 0.00001$). Importantly, in the OTHER condition, HF amplitude was not correlated with the monetary reward. Next, we compared directly the correlation values between both conditions at each time point. Figure 5D shows the resulting t value time series. We found that correlation values differed between conditions (561 and 861 ms; $t_{max} = 4.3$ at 741 ms; $p < 0.000001$). This analysis revealed that the significant reward correlation in the SELF condition is not only significant but also larger than in the OTHER condition.
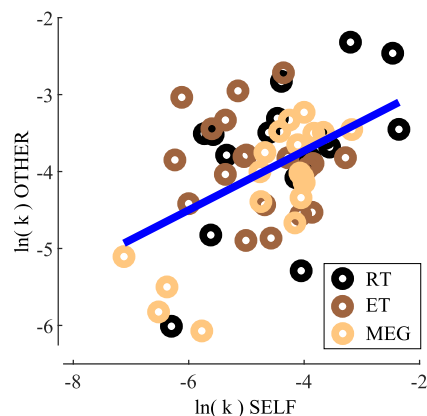
Figure 6. Follow-up analysis. Correlation of discount parameters between conditions across all three experiments: reaction time (RT), eye tracking (ET), and MEG.

Correlation of MEG response and decision
We found that the differences of the HFA predicted differences in discounting behavior between 96 and 310 ms ($r_{min} = -0.5$ at 286 ms; $p = 0.01$, $\beta = 0.64$; Fig. 5E). Although significant, the power of this analysis is relatively low compared with the correlation analysis in the eye tracking paradigm and the follow-up analysis (see below). Moreover, the individual differences analysis was conducted in a time-resolved manner. Hence, there is considerable variation over time and only for a specific temporal interval we can reliably define a correlation. We hypothesize that future studies, designed to specifically test for an intermediate correlation strength using more participants, might be able to delineate the temporal evolution of individual differences between MEG responses and decisions with higher accuracy.

Follow-up analysis

We tested whether discounting behavior in the SELF condition was correlated with the OTHER condition across the three different groups. Differences in discounting parameters accompanied by a significant correlation indicate a similar baseline mechanism for decision-making, which utilizes a different level of objective information. We found, across all experiments, ln (k) parameters correlated between both conditions ($r = 0.48$; $p = 0.0003$, $\beta > 0.95$; Fig. 6).

Discussion

Studies on DD have focused on the representation of subjective value signals by contrasting differential activation associated with smaller and sooner versus larger and longer choices (McClure et al., 2004; He et al., 2012; Kim et al., 2012; Cooper et al., 2013; Peper et al., 2013; van den Bos and McClure, 2013; van den Bos et al., 2014, 2015). Impulsivity, the choice of SS, is associated with preferring sooner rewards compared with later rewards or to insufficiently considering objective alternatives (Ainslie, 1975; Myerson et al., 2003; Olson et al., 2007).

We tested whether subjective value (by contrasting self-referential decisions with prosocial decisions) counteracts impulsivity. There is considerable debate whether humans are truly prosocial. In intertemporal choices, it is unclear whether either a higher reward or an earlier gratification is prosocial. Previous studies showed that participants put in more effort when acts benefited themselves (Lockwood et al., 2017). In our experimental settings across different groups, participants showed impulsive decisions

(discounted less in self-referential compared with prosocial decisions) but did not show condition decision time differences seen in impulsive actions (Cho et al., 2010; Wang et al., 2016; Yates et al., 2016). Hence, we hypothesized that differences in discounting result from differences in depth of evaluation of choice options. Therefore, prosocial decisions provide the opportunity to test how choice option integration in human participants is represented and whether information, which pertains to ourselves, is processed differently compared with prosocial decisions.

In order to elucidate the temporal evolution of the option integration process itself, we compared patterns of attentional reallocation (eye tracking) and choice option integration (MEG). In our eye tracking experiment, the increased spatial distance between choice options on the screen enhanced the effort to move the eyes, corroborating predictions of less effort in the prosocial condition (social apathy) (Lockwood et al., 2017). Patterns of choice option evaluation were similar explaining why decision times are not different but gaze stability differed between conditions, explaining interindividual differences in discounting behavior. We hypothesize that less attentional orientation limits representing and integrating choice options. MEG was recorded in a separate experiment with minimal spatial extent of choice option presentation on the screen, minimizing eye movement contamination of the temporal evolution of choice option integration allowing replication of behavioral results in two independent groups. To compare eye tracking with MEG results, we constructed time series representing the probability to look at a given spatial point as a function of time. We observed that intervals of attentional shift to the delay and reward in the eye tracking experiment were paralleled by intervals of representation of delay and reward in MEG in the HFA.

Intertemporal choices in DD experiments refer to the trade-off between benefits and costs, which can be either an increasing delay ("wait") or increasing effort ("work") to obtain the reward (Phung et al., 2019). Both can be dissociated by underlying neuronal circuits driving behavior toward reward maximization and effort minimization (Prévost et al., 2010; Massar et al., 2015; Klein-Flügge et al., 2016) accompanied by differences in discount curves with an inverted sigmoid function and hyperbolic function in effort and DD, respectively. We did not see an initial concave shape in the prosocial condition typical for effort discounting arguing against the notion that both conditions recruit different neuronal networks. Instead, we propose that differences in discounting result from differences in choice option evaluation. This provides evidence that evaluating gaze stability is a proxy of attentional direction to choice options, and predicts DD.

The MEG study showed that only high-frequency activity (HFA; 175-250 Hz) was modulated by choice options exclusively in the self-referential condition, providing evidence that activity distributed in MEG sensors over frontotemporal regions reflects integration of delay and the reward in humans. HFA is assumed to reflect nonrhythmic synaptic activity (Buzsáki et al., 2012) and is a key marker of cortical activation (Edwards et al., 2005; Ray et al., 2008). Intracranial recordings of HFA response dynamics in humans have enhanced our understanding of cortical information integration in attention, language, memory, emotion, decision-making, and motor control (Johnson et al., 2020). These studies imply that HFA acts as an index of local cortical computation (Buzsáki et al., 2012; Rich and Wallis, 2017). HFA bridges a long-standing gap to fMRI studies on DD. Power modulation in higher frequencies has been shown to explain BOLD

responses better than activity in lower frequencies, which are instead thought to reflect activity in broadly distributed networks (Nir et al., 2007; Mukamel et al., 2014). The temporal precision of MEG adds to the spatial resolution of fMRI and is able to delineate mechanisms of choice option integration in time, which is in line with previous studies on humans and nonhuman primates showing that HFA captured reward-related information (Hunt et al., 2015). HFA has been regarded as a good measure of neuronal spiking (Liu and Newsome, 2006; Berens et al., 2008), consistent with the idea that HFA reflects aggregate local neuronal output (Buzsáki et al., 2012) because of high correlations between HFA and multiunit activity. Both can distinctively be localized in granular/infragranular and supragranular layers, respectively, in V1 and A1 in monkeys and PFC in humans. Supragranular HFA contributes significantly more to the surface field potential than deeper layers, and it is argued that HFA may contain a substantial representation of input from cortical feedback pathways (Leszczyński et al., 2020). Recent single-neuron studies in monkeys provide insight into the neural mechanism for the estimation of interval time (Brody et al., 2003). Single-unit activity is modulated by the amount of an expected reward (Leon and Shadlen, 1999; Wallis and Miller, 2003) and encodes the relative reward value (Tremblay and Schultz, 1999; Cai et al., 2011). Furthermore, single-neuron recordings in pigeons showed that neural delay activity was modulated by increasing delay length and additionally covaried with expected reward amount (Kalenscher et al., 2005).

The right dlPFC, associated with executive and control functions, potentially represents choice options (Bickel et al., 2009; Achterberg et al., 2016) and response selection among the most advantageous (Ho et al., 2016). Our results indicate that self-referential decisions are characterized by a response selection suppression mitigating impulsive decisions. Activity in the medial and right dlPFC is also positively correlated with self-risk (Hu et al., 2017) and cathodal transcranial direct current stimulation (tDCS), associated with inhibition, reduces impulsivity and risky behavior in Parkinson patients (Benussi et al., 2017). Thus, lower levels of activity are associated with less impulsivity, which is in line with a relative HFA reduction during SELF compared with OTHER decisions in our study. Importantly, we did not evaluate the activity level of impulsive versus patient decisions but the neural activity accompanying choice option presentation preceding these decisions. The disruption of right dlPFC with low-frequency repetitive transcranial magnetic stimulation reduces emotional weight during decision-making in social contexts (Tassy et al., 2012), indicating that the dlPFC actually integrates objective choice options. These findings are controversial since the impact of tDCS on the right dlPFC is complex (low risk aversion in gain frames after tDCS but high-risk aversion in loss frames after stimulation) (Ye et al., 2016). Other studies showed that the right dlPFC mediates action value comparisons in value-based decision-making (Morris et al., 2014) and plays a causal role in the computation of values of choices (Camus et al., 2009).

Mapping of sources to sensors is ill-posed in noninvasive recordings. Hence, a multitude of different source combinations could generate the field pattern. Only direct intracranial recordings can reliably distinguish anatomic localizations. Furthermore, we operationalized prosocial acts by taking perspective of the best friend. It could be argued that participants did not perform genuine prosocial acts since they did not directly benefit others because of the hypothetical outcomes. How real rewards, directly paid to others, influence prosocial

decisions in intertemporal choices should remain to be determined. Moreover, future studies can test for an intermediate correlation strength using more participants to delineate with higher accuracy the temporal evolution of correlation between MEG responses and decisions.

Intertemporal behavior has emphasized trait-like variance (Luo et al., 2014). We found correlation between the discount parameter in the SELF and OTHER condition arguing in favor of an individual disposition to discount delayed values. In sum, we argue that impulsivity does not result from oversensitivity to one option but a lack of attentional allocation to choice options. The HFA measured over the right frontotemporal cortex shows broadband amplitude modulation only when decisions have a high value for the self but not during anonymous prosocial decisions. Intervals of delay and reward representation match intervals of gaze toward delay and reward. In sum, our results highlight a unique role of high frequency band activity recorded over the right frontotemporal cortex representing objective values important to suppressing impulsivity.

References

Achterberg M, Peper JS, van Duijvenvoorde AC, Mandl RC, Crone EA (2016) Frontostriatal white matter integrity predicts development of delay of gratification: a longitudinal study. J Neurosci 36:1954–1961.

Ainslie G (1975) Specious reward: a behavioral theory of impulsiveness and impulse control. Psychol Bull 82:463–496.

Baddeley A (1992) Working memory: the interface between memory and cognition. J Cogn Neurosci 4:281–288.

Benussi A, Alberici A, Cantoni V, Manenti R, Brambilla M, Dell'Era V, Gazzina S, Manes M, Cristillo V, Padovani A, Cotelli M, Borroni B (2017) Modulating risky decision-making in Parkinson's disease by transcranial direct current stimulation. Eur J Neurol 24:751–754.

Berens P, Keliris GA, Ecker AS, Logothetis NK, Tolias AS (2008) Feature selectivity of the gamma-band of the local field potential in primate primary visual cortex. Front Neurosci 2:199–207.

Bickel WK, Pitcock JA, Yi R, Angtuaco EJ (2009) Congruence of BOLD response across intertemporal choice conditions: fictive and real money gains and losses. J Neurosci 29:8839–8846.

Brody CD, Hernández A, Zainos A, Romo R (2003) Timing and neural encoding of somatosensory parametric working memory in macaque prefrontal cortex. Cereb Cortex 13:1196–1207.

Buzsáki G, Anastassiou CA, Koch C (2012) The origin of extracellular fields and currents: EEG, ECoG, LFP and spikes. Nat Rev Neurosci 13:407–420.

Cai X, Kim S, Lee D (2011) Heterogeneous coding of temporally discounted values in the dorsal and ventral striatum during intertemporal choice. Neuron 69:170–182.

Camus M, Halelamien N, Plassmann H, Shimojo S, O'Doherty J, Camerer C, Rangel A (2009) Repetitive transcranial magnetic stimulation over the right dorsolateral prefrontal cortex decreases valuations during food choices. Eur J Neurosci 30:1980–1988.

Cho SS, Ko JH, Pellecchia G, Van Eimeren T, Cilia R, Strafella AP (2010) Continuous theta burst stimulation of right dorsolateral prefrontal cortex induces changes in impulsivity level. Brain Stimul 3:170–176.

Cooper N, Kable JW, Kim BK, Zauberman G (2013) Brain activity in valuation regions while thinking about the future predicts individual discount rates. J Neurosci 33:13150–13156.

Edwards E, Soltani M, Deouell LY, Berger MS, Knight RT (2005) High gamma activity in response to deviant auditory stimuli recorded directly from human cortex. J Neurophysiol 94:4269–4280.

Erdfelder E, Faul F, Buchner A, Lang AG (2009) Statistical power analyses using G∗Power 3.1: tests for correlation and regression analyses. Behav Res Methods 41:1149–1160.

Fuster JM (1990) Behavioral electrophysiology of the prefrontal cortex of the primate. Prog Brain Res 85:313–314.

Goldman-Rakic PS (1992) Working memory and the mind. Sci Am 267:110–117.

Green L, Myerson J (2004) A discounting framework for choice with delayed and probabilistic rewards. Psychol Bull 130:769–792.

Hare TA, Camerer CF, Rangel A (2009) Self-control in decision-making involves modulation of the vmPFC valuation system. Science 324:646–648.

He JM, Huang XT, Yuan H, Chen YG (2012) Neural activity in relation to temporal distance: differences in past and future temporal discounting. Conscious Cogn 21:1662–1672.

Ho BC, Koeppel JA, Barry AB (2016) Cerebral white matter correlates of delay discounting in adolescents. Behav Brain Res 305:108–114.

Hu J, Li Y, Yin Y, Blue PR, Yu H, Zhou X (2017) How do self-interest and other-need interact in the brain to determine altruistic behavior? Neuroimage 157:598–611.

Hunt LT, Behrens TE, Hosokawa T, Wallis JD, Kennerley SW (2015) Capturing the temporal evolution of choice across prefrontal cortex. Elife 4:e11945.

Johnson EL, Kam JW, Tzovara A, Knight RT (2020) Insights into human cognition from intracranial EEG: a review of audition, memory, internal cognition, and causality. J Neural Eng 17:051001.

Kalenscher T, Windmann S, Diekamp B, Rose J, Güntürkün O, Colombo M (2005) Single units in the pigeon brain integrate reward amount and time-to-reward in an impulsive choice task. Curr Biol 15:594–602.

Kim B, Sung YS, McClure SM (2012) The neural basis of cultural differences in delay discounting. Philos Trans R Soc Lond B Biol Sci 367:650–656.

Klein-Flügge MC, Kennerley SW, Friston K, Bestmann S (2016) Neural signatures of value comparison in human cingulate cortex during decisions requiring an effort-reward trade-off. J Neurosci 36:10002–10015.

Leon MI, Shadlen MN (1999) Effect of expected reward magnitude on the response of neurons in the dorsolateral prefrontal cortex of the macaque. Neuron 24:415–425.

Leszczyński M, Barczak A, Kajikawa Y, Ulbert I, Falchier AY (2020) Dissociation of broadband high-frequency activity and neuronal firing in the neocortex. Sci Adv 6:eabb0977.

Liu J, Newsome WT (2006) Local field potential in cortical area MT: stimulus tuning and behavioral correlations. J Neurosci 26:7779–7790.

Lockwood PL, Hamonet M, Zhang SH, Ratnavel A, Salmony FU, Husain M, Apps MA (2017) Prosocial apathy for helping others when effort is required. Nat Hum Behav 1:0131.

Luo S, Ainslie G, Monterosso J (2014) The behavioral and neural effect of emotional primes on intertemporal decisions. Soc Cogn Affect Neurosci 9:283–291.

Massar SA, Libedinsky C, Weiyan C, Huettel SA, Chee MW (2015) Separate and overlapping brain areas encode subjective value during delay and effort discounting. Neuroimage 120:104–113.

Mazur JE (1987) An adjusting procedure for studying delayed reinforcement. Hillsdale, NJ: Erlbaum.

McClure SM, Laibson DI, Loewenstein G, Cohen JD (2004) Separate neural systems value immediate and delayed monetary rewards. Science 306:503–507.

McClure SM, Ericson KM, Laibson DI, Loewenstein G, Cohen JD (2007) Time discounting for primary rewards. J Neurosci 27:5796–5804.

Morris RW, Dezfouli A, Griffiths KR, Balleine BW (2014) Action value comparisons in the dorsolateral prefrontal cortex control choice between goal-directed actions. Nat Commun 5:1–10.

Mukamel R, Fried I, Malach R (2014) Coupling between neuronal firing, field potentials, and fMRI in human auditory cortex. Science 309:951–954.

Myerson J, Green L, Hanson J, Scott Holt DD, Estle SJ (2003) Discounting delayed and probabilistic rewards: processes and traits. J Econ Psychol 24:619–635.

Nir Y, Fisch L, Mukamel R, Gelbard-Sagiv H, Arieli A, Fried I, Malach R (2007) Coupling between neuronal firing rate, gamma LFP, and BOLD fMRI is related to interneuronal correlations. Curr Biol 17:1275–1285.

Olson EA, Hooper CJ, Collins P, Luciana M (2007) Adolescents' performance on delay and probability discounting tasks: contributions of age, intelligence, executive functioning, and self-reported externalizing behavior. Pers Individ Dif 43:1886–1897.

Peper JS, Mandl RC, Braams BR, de Water E, Heijboer AC, Koolschijn PC, Crone EA (2013) Delay discounting and frontostriatal fiber tracts: a combined DTI and MTR study on impulsive choices in healthy young adults. Cereb Cortex 23:1695–1702.

Peters J, Büchel C (2010) Episodic future thinking reduces reward delay discounting through an enhancement of prefrontal-mediotemporal interactions. Neuron 66:138–148.

Phung QH, Snider SE, Tegge AN, Bickel WK (2019) Willing to work but not to wait: individuals with greater alcohol use disorder show increased delay discounting across commodities and less effort discounting for alcohol. Alcohol Clin Exp Res 43:927–936.

Prévost C, Pessiglione M, Météreau E, Cléry-Melin ML, Dreher JC (2010) Separate valuation subsystems for delay and effort decision costs. J Neurosci 30:14080–14090.

Ray S, Niebur E, Hsiao SS, Sinai A, Crone NE (2008) High-frequency gamma activity (80-150 Hz) is increased in human cortex during selective attention. Clin Neurophysiol 119:116–133.

Rich EL, Wallis JD (2017) Spatiotemporal dynamics of information encoding revealed in orbitofrontal high-gamma. Nat Commun 8:1139.

Tassy S, Oullier O, Duclos Y, Coulon O, Mancini J, Deruelle C, Attarian S, Felician O, Wicker B (2012) Disrupting the right prefrontal cortex alters moral judgement. Soc Cogn Affect Neurosci 7:282–288.

Tremblay L, Schultz W (1999) Relative reward preference in primate orbitofrontal cortex. Nature 398:704–708.

van den Bos W, McClure SM (2013) Towards a general model of temporal discounting. J Exp Anal Behav 99:58–73.

van den Bos W, Rodriguez CA, Schweitzer JB, McClure SM (2014) Connectivity strength of dissociable striatal tracts predict individual differences in temporal discounting. J Neurosci 34:10298–10310.

van den Bos W, Rodriguez CA, Schweitzer JB, McClure SM (2015) Adolescent impatience decreases with increased frontostriatal connectivity. Proc Natl Acad Sci USA 112:E3765–E3774.

Wallis JD, Miller EK (2003) Neuronal activity in primate dorsolateral and orbital prefrontal cortex during performance of a reward preference task. Eur J Neurosci 18:2069–2081.

Wang Q, Chen C, Cai Y, Li S, Zhao X, Zheng L, Zhang H, Liu J, Chen C, Xue G (2016) Dissociated neural substrates underlying impulsive choice and impulsive action. Neuroimage 134:540–549.

Yates JR, Darna M, Beckmann JS, Dwoskin LP, Bardo MT (2016) Individual differences in impulsive action and dopamine transporter function in rat orbitofrontal cortex. Neuroscience 313:122–129.

Ye H, Huang D, Wang S, Zheng H, Luo J, Chen S (2016) Activation of the prefrontal cortex by unilateral transcranial direct current stimulation leads to an asymmetrical effect on risk preference in frames of gain and loss. Brain Res 1648:325–332.

OXFORD

ORIGINAL ARTICLE

Sensory Deviancy Detection Measured Directly Within the Human Nucleus Accumbens

Stefan Dürschmid[1,3,4], Tino Zaehle[3,4,5], Hermann Hinrichs[3,4,6,7], Hans-Jochen Heinze[3,4,6,7], Jürgen Voges[5,6], Marta I. Garrido[8,9,10], Raymond J. Dolan[11,12,13], and Robert T. Knight[1,2]

[1]Helen Wills Neuroscience Institute, [2]Department of Psychology, University of California, Berkeley, CA, USA, [3]Department of Behavioral Neurology, Leibniz Institute of Neurobiology, Magdeburg, Germany, [4]Department of Neurology, [5]Department of Stereotactic Neurosurgery, Otto-von-Guericke University, Magdeburg, Germany, [6]German Center for Neurodegenerative Diseases (DZNE), Magdeburg, Germany, [7]Forschungscampus STIMULATE, [8]Queensland Brain Institute, [9]Centre for Advanced Imaging, [10]Australian Research Council Centre of Excellence for Integrative Brain Function, The University of Queensland, Brisbane St Lucia, QLD 4072, Australia, [11]Wellcome Trust Centre for Neuroimaging, UCL, London, UK, [12]Visiting Einstein Fellow, Humboldt University Berlin, Berlin, Germany, and [13]Max Planck UCL Centre for Computational Psychiatry and Ageing Research, London, UK

Address correspondence to Stefan Dürschmid. Email: stefan.duerschmid@googlemail.com

Abstract

Rapid changes in the environment evoke a comparison between expectancy and actual outcome to inform optimal subsequent behavior. The nucleus accumbens (NAcc), a key interface between the hippocampus and neocortical regions, is a candidate region for mediating this comparison. Here, we report event-related potentials obtained from the NAcc using direct intracranial recordings in 5 human participants while they listened to trains of auditory stimuli differing in their degree of deviation from repetitive background stimuli. NAcc recordings revealed an early mismatch signal (50–220 ms) in response to all deviants. NAcc activity in this time window was also sensitive to the statistics of stimulus deviancy, with larger amplitudes as a function of the level of deviancy. Importantly, this NAcc mismatch signal also predicted generation of longer latency scalp potentials (300–400 ms). The results provide direct human evidence that the NAcc is a key component of a network engaged in encoding statistics of the sensory environmental.

Key words: auditory mismatch, P3, prediction error, predictive coding, nucleus accumbens, saliency

Introduction

The ability to detect unexpected environmental events is a fundamental property of organized mammalian behavior (Kane et al. 1993, 1996). This capacity depends on a comparison of the actual state of our sensory world with predictions based on immediate and long-term contextual knowledge. Predictive coding theory, first articulated within the visual domain, postulates that neural networks learn statistical regularities of the natural world,

signaling deviations from these regularities to higher centers in order to guide behavior (Rao and Ballard 1999). This allows predictable components of an input signal to be removed and redundancy reduced. At a neurophysiological level, it has been suggested that backward connection strength is increased, and forward connections decreased, with temporal regularities (Kumar et al. 2011) so as to establish stable sensory memory representations when no prediction error (PE) signals occur.

One subcortical region implicated in the expression of PEs is the nucleus accumbens (NAcc), a region implicated in goal-directed behavior (Goto and Grace 2008) and known to be sensitive to novelty (Wood et al. 2004), contextual deviance (Axmacher et al. 2010), aversive stimuli (Becerra et al. 2001; Baliki et al. 2010), and reward PEs in humans (Abler et al. 2006; Spicer et al. 2007). These findings indicate that the NAcc may serve as a critical hub in deviancy detection. However, the neural underpinnings engaged in the human NAcc during deviancy detection and generation of sensory PEs are unknown.

We recorded directly from the NAcc in 5 human subjects participating in an experiment (Garrido et al. 2008), permitting detailed analysis of gradual strengths of sensory mismatch and expectancy. We predicted that the NAcc would weight how new information fits into an ongoing sensory context and convey information about this deviation to regions in the cortical hierarchy. This led us to hypothesize that (1) the NAcc would generate a sensory-evoked mismatch signal, (2) that this mismatch signal should vary as a function of deviance strength, and (3) that a NAcc mismatch response would contribute to the later onset of cortical mismatch components involved in behavioral adjustments. Here, we provide intracranial and simultaneous scalp electroencephalographic (EEG) data that show NAcc signals the strength of a PE during perception of auditory regularities and this PE predicts later cortical activity.

Methods

Five patients (mean ± SD age: 40 ± 9.02 years; 3 males/4 females, all right-handed) with a history of intractable epilepsy participated in this study. We recorded intracranially from bilateral NAcc (Fig. 1A) and bilateral anterior thalamus (ANT). We also recorded from electrodes positioned at midline scalp sites. For details on surgery, deep brain stimulation approach, and placement of surface electrodes see Zaehle et al. (2013).

Paradigm

We employed a paradigm requiring passive listening to a sequence of sine wave sounds (tone pips) with an interstimulus interval of 0.5 s and constant loudness (Fig. 1B; Garrido et al. 2008). The frequency of sounds varied across 7 different levels between 500 and 800 Hz with increments of 50 Hz. Sounds of the same frequency formed a train and train length was defined by the number of repetitions of the initial sound. The number of repetitions ranged between 0 and 10 (Fig. 1). The first sound with a frequency other than the previous train was defined as a deviant sound. This sound along with its next N repetitions formed the next train. To prevent an onset clicking sound for the stimuli, a 10-ms sigmoid ramp was applied to the on- and offset of each sound. Each sound was presented for 70 ms. Participants were presented with either 1800 (Pat01/Pat02: 15 min) or 1200 trials (Pat03/Pat04/Pat05: 10 min).

Stimulus Repetition

The number of repetitions (N_{rep}) varied between 0 and 10. In the case of 0 repetitions, a deviant stimulus was followed by another deviant stimulus. In the case of 10 repetitions, the deviant stimulus was followed by 10 standards (resulting in 11 sounds of the same tone pitch in a train; Fig. 1C). The probability of $N_{rep} \geq 5$ was 87.5% compared with $N_{rep} < 5 = 12.5\%$ to assure that deviant stimuli were perceived as rare events (Fig. 1C). To compare deviant trials as a function of the train length, we chose the same probability of trains with $N_{rep} \geq 5$ to equate the number of deviant trials. Sequences of N_{rep} were randomly presented throughout the experiment independent of the frequency of the sounds. This means that a 500-Hz sound could be repeated by 0 – 10 500 Hz sounds as well as an 800-Hz sound or all other sounds of the 7 pitch levels. Hence, sound pitch and N_{rep} of the following sound were unpredictable. The probability of a deviant stimulus was approximately 15%.

Deviation Strength

The absolute deviation strength (DS) varied with 6 levels of DS. The strongest deviation was 300 Hz (i.e., 500–800 or 800–500 Hz), and the weakest deviation was defined as a 50-Hz change (i.e., 500–550 or 700–650 Hz; Fig. 1B).

Data Collection

Intracranial recordings were obtained using a Walter Graphtek (Walter Graphtek GmbH, Lübeck, Germany) system, with a sampling rate of 256 Hz and analog bandwidth of 200 Hz. In the left and right NAcc and ANT, adjacent electrodes were referenced to the neighboring contact (i.e., 1–2, 2–3, 3–4, with "1"
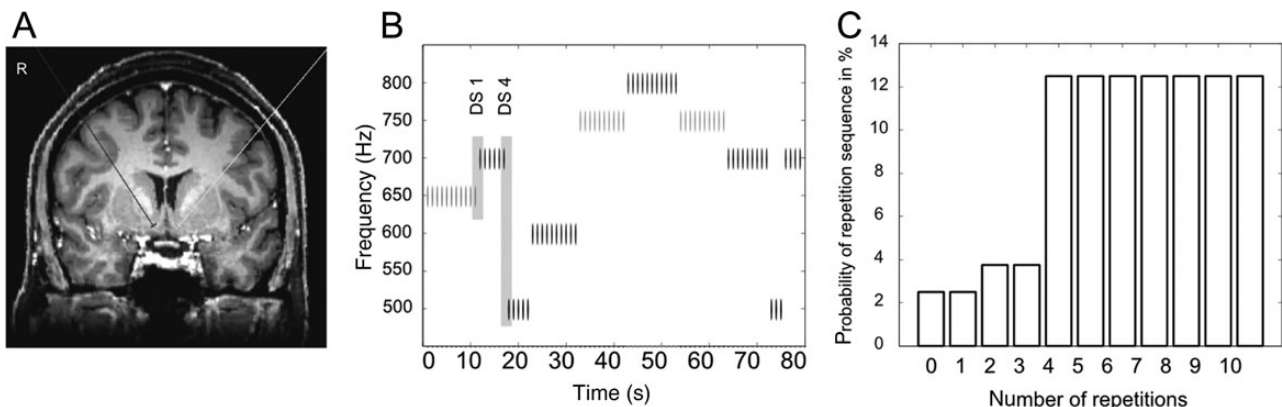
Figure 1. Depiction of the roving paradigm. (A) Anatomical location of bilateral NAcc depth electrodes. (B) Seven different sound levels were defined differing only with respect to their frequency (500–800 Hz). Each sound as indicated by the grayscale vertical lines was presented with a random number of repetitions, which were independent of the frequency of the sound. The difference in tone pitch between the standards and the deviant sound defined the DS. (C) The number of repetitions varied between 0 and 10.

representing the most ventral and "4" representing the most dorsal electrode contact). This resulted in a bipolar montage with each NAcc/ANT monitored by 3 electrode positions. This montage was used to enhance the spatial resolution of the intracranial recordings and to ensure that the recorded activity was not due to far-field activity from nearby non-NAcc structures.

General Data Analysis

We used Matlab 2009b (Mathworks, Natick, MA, USA) for all off-line data processing. The resulting time series for the electrodes located in the NAcc were segmented in epochs of −1 to 2 s relative to the event (stimulus onset). We filtered the resulting epochs applying a bandpass filter between 0.1 and 20 Hz. All filtering was done using a fourth-order Butterworth filter (IIR-filters). To exclude trials affected by artifacts, we defined a threshold for the exclusion of trials in each analysis. In each trial t, we calculated the variance of the bandpass filtered activity across the epoch. All trials exceeding 2 SD above the mean variance were excluded from analysis.

We tested the hypotheses that a response in the NAcc (1) differentiates between standard and deviant stimuli and (2) represents the strength of deviation. In addition, we hypothesized (3) that the NAcc capacity to signal deviation depends on the strength of recent memory so that small deviations are better signaled if a memory trace is well established. Finally, the most prominent component of novelty is the fronto-parietal P300 response dependent on frontal–hippocampal regions in humans (Knight 1996; Knight and Scabini 1998; Boly et al. 2011). Thus, (4) we also predicted that a NAcc computation of a PE would drive a scalp P300 response. In each analysis, we compared the statistical parameters with an empirical distribution derived from a permutation procedure. In that procedure, all baseline-corrected epochs comprising the trial duration (0–500 ms) were randomly shifted in time. All epochs both of each trial and of each subject were shifted independently. In temporal intervals exceeding the 95% confidence interval (CI), we also report the minimal P-value within the empirical distribution.

Coding of the PE

The mismatch signal is defined as the difference in the event-related activity between standard and deviant stimulus-related potentials. To measure this we calculated the event-related potential for both standard and deviant stimuli for each subject. For both stimulus types, we averaged across all intracranial recording sites and trials. The evoked responses of the 4th to the last (10th) standard in a train were assigned to the set of standard trials to equate for the number of trials for standards and deviants. For each epoch, we subtracted the baseline activity (−500 to 0 ms before the stimulus onset) and calculated the t-value using a paired t-test for each time point. The resulting t-value time series represents the strength of difference between standard and deviant stimuli across participants as a function of time. The statistical significance of each t-value was assessed by comparing the t-values with an empirical distribution derived from a permutation procedure (Blair and Karniski 1993). All epochs were randomly shifted in time, and the shifted epochs were averaged and the t-values between standard and deviant stimuli were calculated for each time point exactly as for the observed time series. This permutation procedure was repeated 500 times. For each time point, the CIs (2.5% and 97.5%) of a normal distribution were determined. All P-values reported show the probability of the observed t-value within the distribution derived from the permutation procedure.

PE Depending on Deviation Strength

Throughout the experiment, we randomly varied the DS and the number of standards. We directly tested the gradual deviancy variation with a linear regression and grouped trials associated with deviant stimuli according to the absolute strength of deviation to assess a gradual variation in the DS. Here, the strength of deviation is defined as the difference in frequency between each deviant sound and the preceding standard sound. We used deviant sounds following trains of 5–11 sounds, meaning deviants following the 4th to the 10th standard (corresponding to the same set of trains as in the section "Coding of the PE"). Six different groups of DS were classified ranging from DS = 50 Hz (e.g., 500–550 or 700–650 Hz) to DS = 300 Hz (500–800 or 800–500 Hz). We averaged across trials within each deviation group. This results in 6 time series per subject each 1 trial long. Using linear regression, we tested the hypothesis that differences in DS predict differences in recorded amplitude. For each point in time, we estimated the linear equation

$$\hat{y} = a \times x + b$$

with the vector x as the 6 amplitude values, $\hat{y}$ as the predicted DS, a as the slope parameter, and b as the intercept. The individual slope parameters were averaged across participants and the averaged slope parameters were used to determine the temporal intervals in which differences in amplitude predict differences in DS. The slope parameter is positively/negatively high if a stronger deviation elicits greater amplitude values in a given temporal interval. To assess significance, we performed a permutation procedure with 500 runs in which the same linear regression analysis was conducted with randomly shifted time series. All epochs were shifted in time separately. The shifted epochs were averaged and the slope values were calculated for each time point exactly as for the observed time series. For each time point, the CIs (2.5% and 97.5%) of a normal distribution were determined. Time points with the slope parameter a exceeding the CI were considered significant. Reported P-values show the probability of the observed slope value within the distribution derived from the permutation procedure.

PE Depending on Auditory Regularity

We hypothesized that sensitivity to deviant stimuli with only a small DS varies as a function of the number of preceding standard sounds (Haenschel et al. 2005). We tested whether a mismatch of small DS following a long train elicits an enhanced mismatch signal compared with the mismatch signal following a short train. This would indicate that a longer and regular train facilitates discrimination of small deviations. We also assessed whether sensitivity to a small DS varies as a function of the number of preceding standard sounds with the linear regression approach. We used trials associated with a deviant stimulus and grouped the trials according to the number of preceding standard sounds. We initially used the 3 levels of lowest DS (≤150 Hz) out of the 6 levels of deviations. We used small deviations for 2 reasons. First, finding no amplitude variation could derive from the fact that amplitude variations to large deviations might show a ceiling effect obscuring the gradient as a function of train length. Secondly, if all DSs were collapsed one could argue that small deviations do not have the same impact as large deviations. To prevent this, we tested the influence on small deviations. Note that the same analysis with all 6 levels of DS yielded a comparable result (see Supplementary Results). As outlined in the section "Coding of the PE", the evoked

responses of the fourth to the last repetition in a train were designated to the set of standard trials. This results in 7 time series for each subject. Time series were averaged across all recording channels. The individual slope parameters were averaged across participants and the averaged slope parameters were used to determine the temporal intervals in which differences in amplitude predict differences in the number of preceding standards.

NAcc–Cortex Interaction

We tested whether the mismatch signal on the level of the NAcc predicts cortical activity by determining trial-by-trial cross-correlation between the NAcc and cortical time series in 2 cortical regions of interest (ROIs). The frontal ROI encompassed Fpz, Fz, and FCz, and the centro-parietal ROI encompassed Pz and Cz. In each trial, the time series were averaged separately across intracranial and surface recording channels leading to 2 time series per trial (intracranial and surface activity). Pearson's correlation r coefficients were used to quantify the coupling between responses in NAcc and the cortical ROIs. Cross-correlation means that the activity at each time point across trials in the NAcc was correlated with the activity at each time point across trials on the cortical recordings. This provides information about both the strength of correlation and the temporal relation of the correlation. Here, the set of trials designated to the deviant stimuli was used and the same analysis with the set of standard trials revealed no significant interaction between the NAcc and scalp recording sites. We calculated r values at each sample point ($N_{comparisons} = 129 \times 129$) and averaged the resulting r-values across participants. Since r is not a metric measure before averaging across participants, we transformed r-values using the inverse hyperbolic tangent in the following equation:

$$\text{atanh}(r) := \frac{1}{2}\ln\left(\frac{1+r}{1-r}\right) \text{ for } |r| < 1.$$

This correlation approach requires statistically independent observations. Statistical significance was assessed by a permutation procedure, which encompasses 500 runs of the same analysis with the same time series but randomly shifted in time and results in CIs for each r-value. We Bonferroni-corrected for multiple comparisons by dividing the significance threshold by the number of comparisons as follows:

$$P_{corr} = \frac{0.05}{N_{comparisons}}.$$

The Bonferroni-corrected P-value within the empirical distributions was used as the threshold for statistical significance.

Results

Deviancy Detection in the NAcc

The NAcc Mismatch Signal

We found that between 20 and 130 ms ($t_4 = -2.9$; $P = 0.001$) and between 290 and 410 ms ($t_4 = 4.1$; $P < 0.0001$), the time series for deviant stimuli generated a mismatch signal (Fig. 2A), indicating that the NAcc differentiated between standard and new (deviant) stimuli at these time-epochs. These differences in amplitude were confined to low frequencies (see Supplementary Material and Supplementary Fig. 1), being maximal for 11 Hz (range 4–18 Hz) around 240 ms ($t_4 = 4.866$; $P = 0.004$; uncorrected, see Supplementary Material for differences between temporal intervals in both analyses). In contrast to the NAcc, the ANT does not
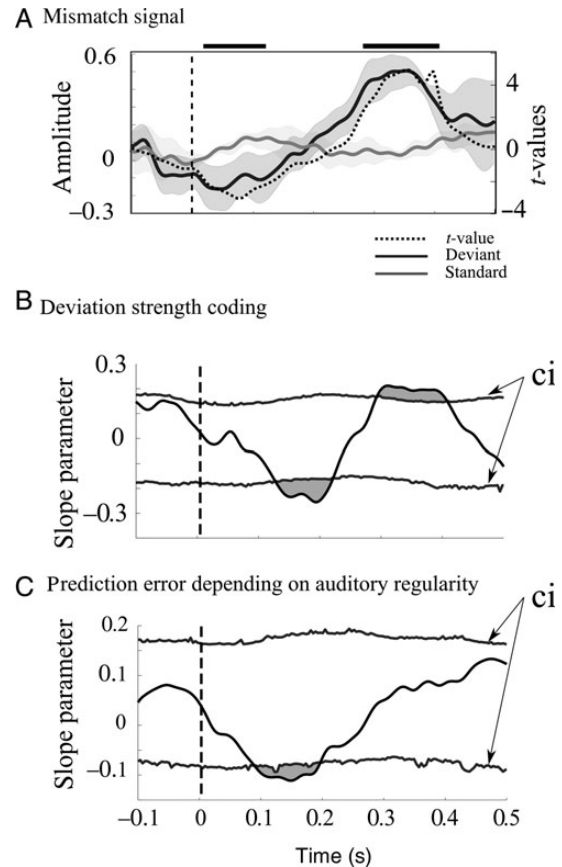
Figure 2. In each plot, the vertical dashed line marks the stimulus onset. (A) The NAcc shows a mismatch signal (difference between deviant and standard stimuli) following the presentation of a deviant stimulus. The bold black line gives the mean amplitude for deviant stimuli across participants and the shaded area show the standard error (SE) across participants. The bold gray line shows the mean amplitude for standard trials across participants. The shaded area provides the SE across participants. The left y-axis shows the amplitude values for standard and deviant event-related components. The right y-axis gives the t-values for the difference between standard and deviant stimuli. The dashed line shows the t-values as a function of time. The horizontal black bars show the temporal intervals of corrected significant differences. (B) The strength of the deviation (difference in tone pitch between previous standard and the deviant sound) is coded in the NAcc. The amplitude following a deviant stimulus decreases as a function of DS in an early temporal interval and increases gradually later. The black line shows the slope parameter derived from a linear regression at each time point. The curves show the 97.5% and 2.5% CIs derived from a permutation procedure. The gray-shaded areas mark those temporal intervals in which the observed slope parameter underwent or exceeded the empirical distribution. (C) The results presented in B imply that small deviations yield a smaller mismatch signal compared with stronger deviations. We tested whether the amplitude of the mismatch signal to a small DS is modulated by the number of preceding standard trials and hence, auditory regularity. The black line shows the slope parameters as a function of time together with the CIs derived from a permutation procedure. The negative slopes imply that the mismatch signal increases with a negative polarity with an increasing number of preceding standards around 100 ms (gray-shaded area). We tested whether this can be in part due to a repetition suppression within a long train of standards.

differentiate by differences in amplitude between standard and deviant stimuli (see Supplementary Fig. 2).

Activity in the NAcc Represents the Deviation Strength

We then examined whether the NAcc codes for different levels of DS (difference in frequency between the deviant stimulus and

the preceding standard sound). We used all levels of DS ranging from 50 to 300 Hz and predicted the DS from the amplitude value at each time point using linear regression. The observed slope parameters derived from the linear regressions were compared with CIs derived from the permutation procedure. In the time range between 138 and 224 ms ($P = 0.002$) and 302 and 408 ms ($P = 0.008$), the observed slope parameters were significant (Fig. 2B). This indicates that the first significant mismatch signal with a negative polarity linearly codes the DS with a stronger negative amplitude for stronger deviations. The second positive polarity mismatch signal linearly codes the DS with a stronger positive amplitude for stronger deviations.

The NAcc Mismatch Signal Depends on the Number of Preceding Standards

To address whether human NAcc responsivity is dependent on the recent past, we evaluated the dependency between the number of prior standard auditory stimuli and the responsivity to a deviant. We hypothesized that sensitivity to deviant stimuli would vary as a function of the number of preceding standard sounds, where the latter can be thought of in terms of an evolving belief or prior. We tested whether a small DS results in an enhanced amplitude of response as a function of increasing length of a preceding train of standard stimuli. To formally test this, we compared trials with a low DS (≤ 150 Hz) but differing numbers of preceding standard tones. In the time range between 95 and 196 ms ($P = 0.007$), the mismatch elicited a more prominent amplitude following long trains of standards (Fig. 2C). We found a comparable result even when all deviant trials of all levels of DS were subjected to this analysis (see Supplementary Results). This effect might be explained by repetition suppression (see Supplementary Material) with an increasing length of preceding trains, but this is unlikely since our test for repetition suppression was not significant (see Supplementary Fig. 3).

Relation of NAcc Activity to the Cortical Response

A cross-correlation revealed that the NAcc trial-to-trial amplitude variation is linked ($P < P_{corr}$) to the trial-to-trial amplitude variation recorded at centro-parietal, but not frontal, leads. Figure 3 shows that early activity in the NAcc (80–180 ms)
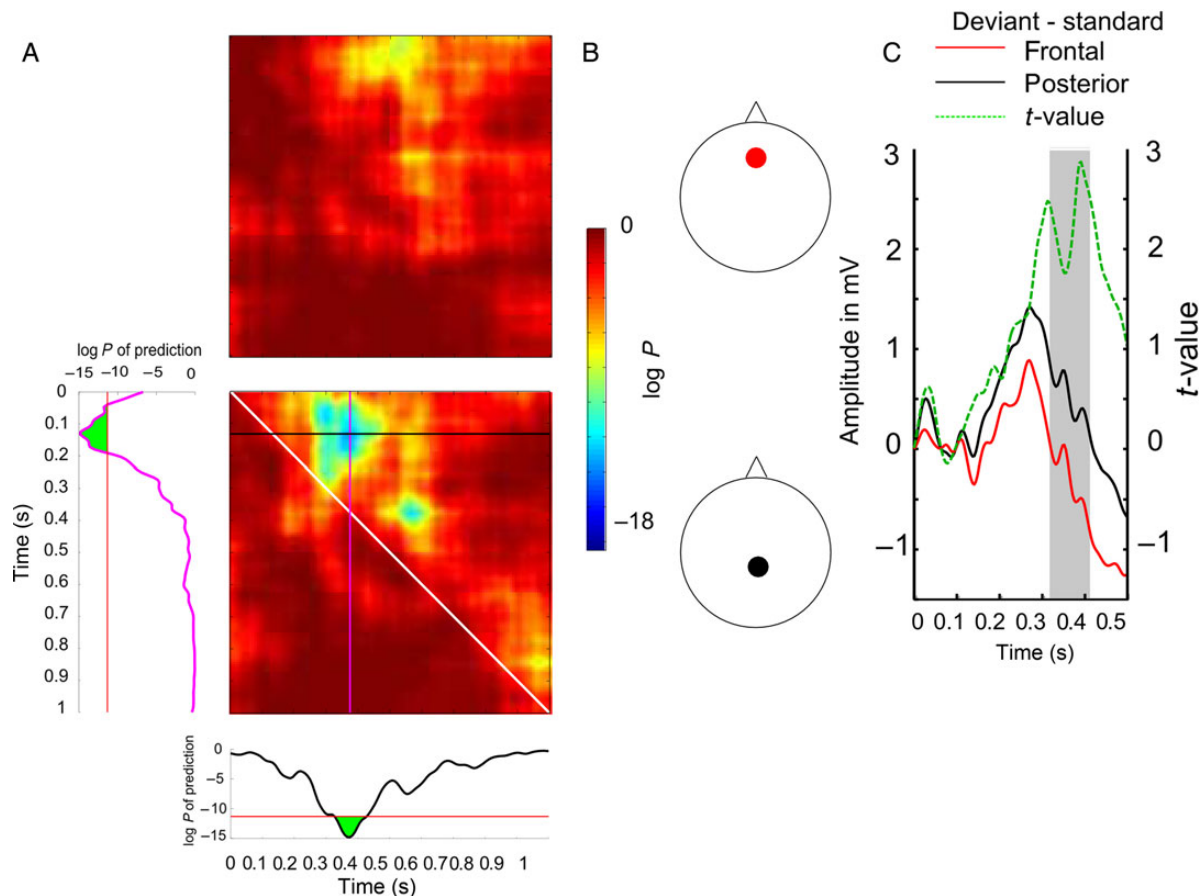
Figure 3. Depiction of the cross-correlation analysis. (A) Each point in the upper and lower square matrix shows the correlation strength between the NAcc and the frontal (upper) and the centro-parietal (lower) ROI by means of the probability. The white diagonal separates the direction of temporal relation. All values in the upper triangle show activity in the NAcc preceding surface activity. The lower triangle shows the correlation for surface activity preceding NAcc activity. P-values were derived from a permutation procedure. The strongest correlation as indicated by the smallest P-values is observed between NAcc activity around 120 ms and surface activity around 350 ms. The magenta line shows the correlation of surface activity at around 350 ms with the NAcc at all time points. The black line shows the correlation of NAcc activity at around 120 ms with surface activity at all time points. The red line shows the Bonferroni-corrected significance level. The vertical and horizontal dashed with lines mark the beginning of the next trial. (B) The red and black dots show the frontal and centro-parietal ROIs, respectively. (C) Depiction of the difference waves between standard and deviant stimuli within the frontal ROI (red line) and the centro-parietal ROI (black line). Only in the frontal ROI, there is a slight mismatch negativity following 100 ms, which appears to be absent in the centro-parietal potential. The green line gives the t-value for the differences between both ROIs for each time point. In the time range of significant posterior P3 prediction, the frontal and centro-parietal P3 differ significantly.

correlates with activity between 330 and 410 ms at centro-parietal recording sites (maximal $r = -0.22$). Note that the negative correlation coefficient reflects a positive relationship between the amplitude variation at both recording sites. Specifically, the negative correlation results from a correlation between the amplitude of negative deflection in the NAcc and the amplitude of the positive deflection of the P3.

The second positive mismatch signal in the NAcc linearly codes the DS with a stronger positive amplitude for greater deviations. We were unable to establish a scalp correlate of this later NAcc activity. The enhanced early latency NAcc–cortical event related potential correlation was observed for deviation trials, but not for standard trials (see Supplementary Fig. 4). Note that the frontal P3 was reduced in this time interval relative to the centro-parietal response as is typically observed in paradigms with relatively low stimulus novelty and multiple deviancy repetitions (Polich 1989a, 1989b; Polich and McIsaac 1994; Fig. 3C). Within the temporal interval of significant prediction, that is NAcc–cortex interaction, the centro-parietal P3 differed significantly from the frontal P3 ($t_{(4)} = 2.37$, $P = 0.038$). Based on these results, we tested for a specific dependency of the posterior P3 amplitude on DS and the number of preceding standards. We conducted the same analysis as described for the NAcc. We found that the posterior, but not the frontal, potential showed a linear dependency on the DS in the time range between 320 and 370 ms ($P = 0.0065$) matching the temporal interval of significant interaction with the NAcc amplitude variation (Fig. 4A). We also observed that the posterior, but not the frontal scalp, potential showed a linear dependency on the number of preceding standard trials as revealed by statistically significant slope parameters in the time range between 310 and 350 ms ($P = 0.0031$; Fig. 4B). Moreover, the centro-parietal scalp potential was best predicted by channels located in the central region of the NAcc (see Supplementary Fig. 5).

Discussion

We recorded intracranially from the human NAcc using an auditory deviancy paradigm to assess the processing of sensory deviations, allowing us to test whether NAcc contributes to the computation of statistics in local auditory irregularities. We also determined whether NAcc activity generated to deviant events was linked to a modulation of cortical activity. We observed that human NAcc activity reliably tracks the statistics of the local auditory scene and predicts later cortical activity.

We found that the strength of deviation coded in the NAcc displayed larger responses if they occurred following longer trains of standards. We employed a bipolar montage to insure that the recorded NAcc activity was not due to far-field activity from nearby non-NAcc structures. As a further subcortical control, the anterior thalamic recordings did not signal deviancy from expectancy nor amplitude variation as a function of DS. Thus, the amplitude variation in the NAcc indicates that this activity is dependent on information regarding temporal succession, an effect possibly originating in the hippocampal formation. Indeed, the strong anatomical and functional connection with the hippocampus (HC; Finch 1996; Goto and Grace 2008) makes the NAcc an ideal structure to track representations of the recent past stored in the HC (Lisman and Grace 2005), an idea supported by Strange et al. (2005) and Axmacher et al. (2010). Lisman and Grace (2005) proposed a model of novelty detection and memory formation consisting in a functional loop between HC–ventral tegmental area (VTA). This model assumes feedforward and feedback connections. Our NAcc and scalp data in deviation trials provide support for such a functional loop. In contrast, activity evoked by standard stimuli does not influence the late cortical response, suggesting that information about a correct prediction as in the case of a standard trial does not activate the HC–VTA loop.

One question is whether the HC sends information about the quality of deviation or a general signal of deviancy (Strange et al. 2005). Dolan and Fletcher (1997) showed a functional dissociation between medial temporal and dorsolateral prefrontal (dlPFC) areas during encoding auditory–verbal stimuli, with a medial temporal area more responsive to general novelty and dlPFC responsive to associations between category and exemplars. The present findings support the idea that the NAcc might receive a general novelty signal from the HC. This HC signal might indicate that a PE was committed but not the quality in terms of DS. Support for this interpretation emerges from Strange et al. (2005) who
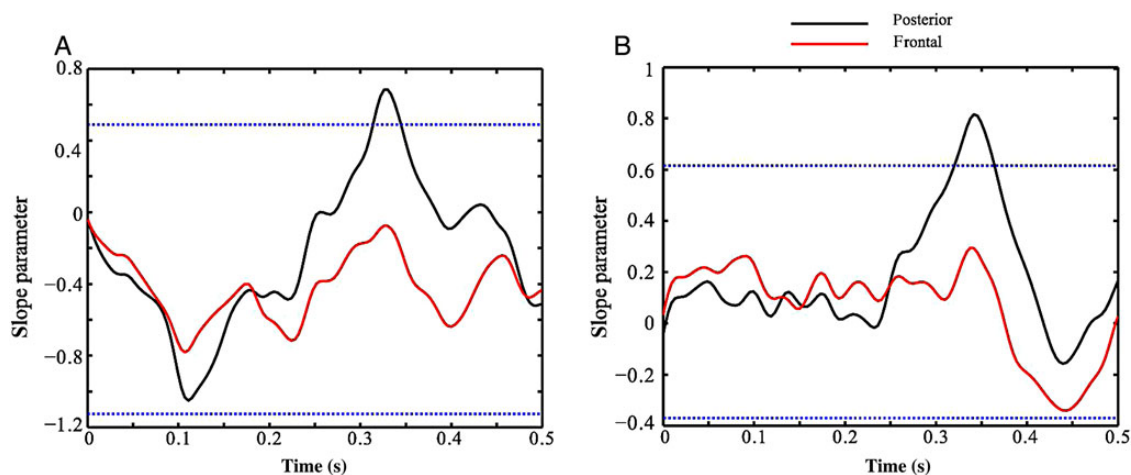
Figure 4. (A) The strength of the deviation (difference in tone pitch between previous standard and the deviant sound) is coded in the posterior P3. The amplitude following a deviant stimulus increases as a function of DS in the temporal interval of the P3. The black line shows the slope parameter derived from a linear regression at each time point for the posterior P3, and the gray-dashed line for the frontal P3. The horizontal lines show the 97.5% and 2.5% CIs derived from a permutation procedure. (B) We tested whether the amplitude of the scalp potential modulated by the number of preceding standard trials and hence, auditory regularity. The black line shows the slope parameter derived from a linear regression at each time point for the posterior P3, and the gray-dashed line for the frontal P3. The horizontal lines show the 97.5% and 2.5% CIs derived from a permutation procedure.

showed that the HC response is modulated by entropy. This quantifies expected information rather than the information itself and their study showed that unpredictable stimulus streams led to greater activity in the anterior HC.

We observed the NAcc discriminates deviant events at an earlier latency than previously reported (Axmacher et al. 2010). This might be explained by the simplicity of the stimuli used in our study, and the differences in modality since visual stimuli elicit mismatch-related components with a prolonged latency compared with auditory oddball stimulation (Comerchero and Polich 1999). We speculate that the processing of the visual stimuli called for a cognitive evaluation reducing any automatic early components as observed in the current study. The passive listening in our current study underscores the rapid pre-attentive and automatic process represented in the NAcc signal.

The NAcc is proposed to play a prominent role in goal-directed behavior by integrating inputs from other limbic structures and the prefrontal cortex (Goto and Grace 2008). Since our task design did not require behavioral responses, the influence of detecting local auditory irregularities for directing subsequent behavior cannot be inferred directly. However, the fact that the early mismatch signal in the NAcc selectively correlates with the central–parietal P300 underscores the notion that the NAcc is central to behavioral adjustments. The scalp P300 component is linked to memory storage and detecting behavioral-relevant targets (Knight 1996, 1998; Polich and Criado 2006; Polich 2007). Our study used weak deviants that typically activate only the centro-parietal P300 response to deviant events. This might suggest that contextual deviancy detection occurs in a hippocampal–NAcc network, and this information is used to trigger the activation of a broader attentional network manifested in a scalp P300 potential.

A role for NAcc activity in goal-directed behavior is further supported by differences in the P300 prediction as a function of the subregions of the NAcc assessed in our study. P300 scalp prediction is maximal in central NAcc sites pointing to differences in functional significance of subregions of the human NAcc. In rats, lesions to the NAcc core decreased habituation to a novel environment due to failure in the detection of perturbations (Cardinal et al. 2001). Furthermore, studies in rats show that the core region is involved in inhibitory control of goal-directed behavior (Pothuizen et al. 2005) and is especially necessary for processing of stimuli deviating from expectancy.

Patient intracranial studies carry a possibility of impacting critical processes relevant to mismatch detection and other cognitive functions. All 5 patients were awake, attentive, and responsive during the recording session. Hence, we consider the likelihood of an impact on this automatic process to be relatively small. Furthermore, despite the small number of participants, the effect is strong enough to reliably detect a mismatch signal across subjects.

Taken together, our findings demonstrate that, within an ongoing stream of information, the NAcc contributes to coding the statistics of the auditory environment manifested by a gradual variation of amplitude of the local field potential in the NAcc. This NAcc gradient predicts generation of a subsequent scalp P300 dependent on cortical–hippocampal circuits. These findings emphasize the importance of the NAcc in the automatic integration of sensory information. Furthermore, the relationship between NAcc and the P300 provides evidence for a role of NAcc activity in mnemonic functions possibly by binding neural activity that is shared between medial temporal lobe and dopaminergic midbrain structures.

Supplementary Material

Supplementary material can be found at: http://www.cercor.oxfordjournals.org/.

Funding

Notes

Conflict of Interest: None declared.

References

Abler B, Walter H, Erk S, Kammerer H, Spitzer M. 2006. Prediction error as a linear function of reward probability is coded in human nucleus accumbens. Neuroimage. 31:790–795.

Axmacher N, Cohen MX, Fell J, Haupt S, Dümpelmann M, Elger CE, Schlaepfer TE, Lenartz D, Sturm V, Ranganath C. 2010. Intracranial EEG correlates of expectancy and memory formation in the human hippocampus and nucleus accumbens. Neuron. 65:541–549.

Baliki MN, Geha PY, Fields HL, Apkarian AV. 2010. Predicting value of pain and analgesia: nucleus accumbens response to noxious stimuli changes in the presence of chronic pain. Neuron. 66:149–160.

Becerra L, Breiter HC, Wise R, Gonzalez RG, Borsook D. 2001. Reward circuitry activation by noxious thermal stimuli. Neuron. 32:927–946.

Blair RC, Karniski W. 1993. An alternative method for significance testing of waveform difference potentials. Psychophysiology. 30:518–524.

Boly M, Garrido MI, Gosseries O, Bruno MA, Boveroux P, Schnakers C, Massimini M, Litvak V, Laureys S, Friston K. 2011. Preserved feedforward but impaired top-down processes in the vegetative state. Science. 332:858–862.

Cardinal RN, Pennicott DR, Sugathapala CL, Robbins TW, Everitt BJ. 2001. Impulsive choice induced in rats by lesions of the nucleus accumbens core. Science. 292:2499–2501.

Comerchero MD, Polich J. 1999. P3a and p3b from typical auditory and visual stimuli. Clin Neurophysiol. 110:24–30.

Dolan RJ, Fletcher PC. 1997. Dissociating prefrontal and hippocampal function in episodic memory encoding. Nature. 388:582–585.

Finch DM. 1996. Neurophysiology of converging synaptic inputs from the rat prefrontal cortex, amygdala, midline thalamus, and hippocampal formation onto single neurons of the caudate/putamen and nucleus accumbens. Hippocampus. 6:495–512.

Garrido MI, Friston KJ, Kiebel SJ, Stephan KE, Baldeweg T, Kilner JM. 2008. The functional anatomy of the MMN: a DCM study of the roving paradigm. Neuroimage. 42:936–944.

Goto Y, Grace AA. 2008. Limbic and cortical information processing in the nucleus accumbens. Trends Neurosci. 31:552–558.

Haenschel C, Vernon DJ, Dwivedi P, Gruzelier JH, Baldeweg T. 2005. Event-related brain potential correlates of human auditory sensory memory-trace formation. J Neurosci. 25:10494–10501.

Kane NM, Curry SH, Butler SR, Cummins BH. 1993. Electrophysiological indicator of awakening from coma. Lancet. 341:688.

Kane NM, Curry SH, Rowlands CA, Manara AR, Lewis T, Moss T, Cummins BH, Butler SR. 1996. Event-related potentials–neurophysiological tools for predicting emergence and early outcome from traumatic coma. Intensive Care Med. 22:39–46.

Knight R. 1996. Contribution of human hippocampal region to novelty detection. Nature. 383:256–259.

Knight RT. 1998. Electrophysiology and behavior converge in human extrastriate cortex. Nat Neurosci. 1:546–547.

Knight RT, Scabini D. 1998. Anatomic bases of event-related potentials and their relationship to novelty detection in humans. J Clin Neurophysiol. 15:3–13.

Kumar S, Sedley W, Nourski KV, Kawasaki H, Oya H, Patterson RD, Howard MA III, Friston KJ, Griffiths TD. 2011. Predictive coding and pitch processing in the auditory cortex. J Cogn Neurosci. 23:3084–3094.

Lisman JE, Grace AA. 2005. The hippocampal-VTA loop: controlling the entry of information into long-term memory. Neuron. 46:703–713.

Polich J. 1989a. Frequency, intensity, and duration as determinants of p300 from auditory stimuli. J Clin Neurophysiol. 6:277–286.

Polich J. 1989b. P300 from a passive auditory paradigm. Electroencephalogr Clin Neurophysiol. 74:312–320.

Polich J. 2007. Updating p300: an integrative theory of p3a and p3b. Clin Neurophysiol. 118:2128–2148.

Polich J, Criado JR. 2006. Neuropsychology and neuropharmacology of p3a and p3b. Int J Psychophysiol. 60:172–185.

Polich J, McIsaac HK. 1994. Comparison of auditory p300 habituation from active and passive conditions. Int J Psychophysiol. 17:25–34.

Pothuizen HHJ, Jongen-Rêlo AL, Feldon J, Yee BK. 2005. Double dissociation of the effects of selective nucleus accumbens core and shell lesions on impulsive-choice behaviour and salience learning in rats. Eur J Neurosci. 22:2605–2616.

Rao RP, Ballard DH. 1999. Predictive coding in the visual cortex: a functional interpretation of some extra-classical receptive-field effects. Nat Neurosci. 2:79–87.

Spicer J, Galvan A, Hare TA, Voss H, Glover G, Casey B. 2007. Sensitivity of the nucleus accumbens to violations in expectation of reward. Neuroimage. 34:455–461.

Strange BA, Duggins A, Penny W, Dolan RJ, Friston KJ. 2005. Information theory, novelty and hippocampal responses: unpredicted or unpredictable? Neural Netw. 18:225–230.

Wood DA, Kosobud AEK, Rebec GV. 2004. Nucleus accumbens single-unit activity in freely behaving male rats during approach to novel and non-novel estrus. Neurosci Lett. 368:29–32.

Zaehle T, Bauch EM, Hinrichs H, Schmitt FC, Voges J, Heinze HJ, Bunzeck N. 2013. Nucleus accumbens activity dissociates different forms of salience: evidence from human intracranial recordings. J Neurosci. 33:8764–8771.

Deep brain stimulation of the nucleus basalis of Meynert attenuates early EEG components associated with defective sensory gating in patients with Alzheimer disease – a two-case study

Stefan Dürschmid,[1,2] (iD) Christoph Reichert,[1] Jens Kuhn,[3,4] Hans-Joachim Freund, Hermann Hinrichs[1,2,5,6,7] and Hans-Jochen Heinze[1,2,5,6,7]

[1]Department of Behavioral Neurology, Leibniz Institute for Neurobiology, Brenneckestr. 6, 39120 Magdeburg, Germany
[2]Department of Neurology, Otto-von-Guericke University, Magdeburg, Germany
[3]Department of Psychiatry and Psychotherapy, Medical Faculty, University of Cologne, Cologne, Germany
[4]Johanniter Hospital Oberhausen, EVKLN, Oberhausen, Germany
[5]Stereotactic Neurosurgery, Otto-von-Guericke University, Magdeburg, Germany
[6]German Center for Neurodegenerative Diseases (DZNE), Magdeburg, Germany
[7]CBBS – center of behavioral brain sciences, Otto-von-Guericke University, Magdeburg, Germany

Abstract

Alzheimer′s disease (AD) is associated with deterioration of memory and cognitive function and a degeneration of neurons of the nucleus basalis of Meynert (NBM). The NBM is the major input source of acetylcholine (ACh) to the cortex. The decreasing cholinergic innervation of the cortex due to degeneration of the NBM might be the cause of loss of memory function. NBM-Deep brain stimulation (NBM-DBS) is considered to serve as a potential therapeutic option for patients with AD by supporting residual cholinergic transmission to stabilize oscillatory activity in memory-relevant circuits. However, whether DBS could improve sensory memory functions in patients with AD is not clear. Here, in a passive auditory oddball paradigm, patients with AD ($N = 2$) listened to repetitive background tones (standard tones) randomly interrupted by frequency deviants in two blocks with NBM-DBS OFF and then NBM-DBS ON, while age-matched healthy controls ($N = 6$) repeated the experiment twice. The mismatch negativity in NBM-DBS OFF significantly differed from controls in both blocks, but not under NBM-DBS, which was likely due to a pronounced P50 increase overlapping with the N1 in NBM-DBS OFF. This early complex of EEG components recovered under stimulation to a normal level as defined by responses in controls. In this temporal interval, we found in patients with NBM-DBS ON (but not with NBM-DBS OFF) and in controls a strong repetition suppression effect to standard tones – with more attenuated responses to frequently repeated standard tones. This highlights the role of NBM-DBS for sensory gating of familiar auditory information into sensory memory.

Introduction

Alzheimer′s disease (AD) is associated with progressive deterioration of memory and cognitive function and is the most common cause of dementia in middle and late life as a result of organic brain disease (Terry & Davies, 1980)]. Previous studies have shown that in patients with AD, neurons of the nucleus basalis of Meynert (NBM) undergo massive degeneration (Whitehouse *et al.*, 1982). The NBM is densely connected with a variety of cortical and subcortical structures. In the primate brain, the NBM receives its major input from the ventral tegmental area, substantia nigra pars compacta, retrorubral field, raphe nuclei and the locus coeruleus, serotonergic projections from the dorsal raphe nucleus and ventral tegmentum, and cholinergic projections from pedunculopontine and laterodorsal tegmental nuclei. The human NBM provides the major source of cholinergic innervation to the neocortex (Mesulam *et al.*, 1983), with projections to the frontal, parietal, cingulate cortex, amygdala, anterior auditory cortex and the temporal pole (Gratwicke *et al.*, 2013).

Acetylcholine (ACh) is one important neuromodulator released in the cortex. It is presumed that the neuromodulatory impact of ACh encompasses the enhancement of cortical plasticity (Rasmusson, 2000) and is involved in many cognitive functions including attention (Voytko *et al.*, 1994; McGaughy *et al.*,1996; Sarter & Bruno, 2000; Furey *et al.*, 2008; Herrero *et al.*, 2008) and memory encoding/learning (Miasnikov *et al.*, 2001, 2008; Thiel *et al.*, 2002; Warburton *et al.*, 2003; Weinberger, 2003; Froemke *et al.*, 2007). The cholinergic receptor blocker scopolamine results in a specific learning impairment, possibly through the limitation of the acquisition of new information and the storage of new memories (Aggelopoulos *et al.*, 2011). Pharmacological increase in cerebral ACh concentration (via an acetylcholinesterase inhibitor) has been employed in the treatment of brain injury and advanced dementia. Inhibition of acetylcholinesterase leads to an increase in cerebral ACh concentration and has been reported to have a neuroprotective effect on rats with cerebral infarcts or mild traumatic brain injury (TBI) (Fujiki *et al.*, 2005, 2008). Other acetylcholinesterase inhibitors have also been used for the treatment of Alzheimer's disease (Howes & Perry, 2011).

Hence, in patients with AD, a decreasing cholinergic innervation of the cortex due to the degeneration of the NBM might be the cause of progressive loss of memory function. At present, among pharmacological approaches to increase the cholinergic level in patients with AD, the deep brain stimulation of the NBM (NBM-DBS) is considered to be a potential therapeutical option. The rationale of NBM-DBS is to support residual cholinergic transmission by stabilizing oscillatory activity in memory-relevant circuits and improves cognitive functions (Kuhn *et al.*, 2015a,b; Hardenacke *et al.*, 2016). NBM-DBS is an experimental, in selected cases therapeutically effective, non-lesional treatment method delivering current rectangular pulses into dysfunctional brain structures via chronically implanted stimulation electrodes. NBM-DBS is a recognized method applied in movement disorders and is increasingly evaluated as a possible therapeutic option for psychiatric diseases such as refractory obsessive-compulsive disorders, Gilles de la Tourette syndrome, major depression and substance-related addiction (Kuhn *et al.*, 2010; Hardenacke *et al.*, 2013). However, whether DBS has the potential to improve sensory memory functions in patients with AD is not clear.

In humans, sensory memory can be evaluated with auditory oddball paradigms in which a sensory memory to frequently presented standard tones is established and violated by randomly interspersing deviant tones differing in tone frequency. In EEG recordings, the amplitude difference between standard tones and rare and randomly presented deviant tones can be measured in the form of an ERP component called the mismatch negativity (MMN). The MMN is considered a correlate of the automatic detection of changes in the acoustic environment (Lindín *et al.*, 2013) and is regarded as the classical prediction error signal elicited during passive listening (Näätänen *et al.*, 1978). The MMN is defined as difference wave with the amplitude modulation to frequent standard tones subtracted from the enhanced amplitude modulation to infrequent deviant tones. Previous scalp MMN studies reported response differences between standard and deviant tones peaking between 100 and 250 ms (reviewed in ref. (Näätänen *et al.*, 2007), which overlaps largely with the timing of the P50, and N1, and even the later P300 response.

Converging evidence suggests that the MMN has interacting generators in the secondary auditory cortex on the superior temporal plane and superior temporal gyrus as well as in the prefrontal cortex (Deouell, 2007; Shalgi & Deouell, 2007), but the distinct contribution of each part of this network is not clear as subcortical regions

also generate mismatch signals that interact with cortically measured mismatch components (Dürschmid *et al.*, 2016). To detect a change, it is necessary to have an overview of the recent past or to make a comparison between an incoming stimulus and a short-lived sensory memory trace. As such, the MMN is considered to reflect storage of information in sensory memory (Gaeta *et al.*, 1999; Pekkonen *et al.*, 2001) and speed of acoustic sensory discrimination (Engeland *et al.*, 2002). In patients with AD, the MMN amplitude decrease as a function of the interstimulus interval is more strongly pronounced than in healthy controls. This suggests that the memory trace decays faster in the patients with AD than in age-matched healthy controls (Pekkonen *et al.*, 1994). Together with behavioural changes, the MMN seems to be largely affected in patients with AD. For example, Cheng *et al.* (2012) and Hsiao *et al.* (2014) reported larger source amplitudes and shorter peak latencies in the right temporal magnetic mismatch responses of young controls compared to elderly controls and patients with AD. Also, Lindín *et al.* (2013) found a reduced MMN in patients with amnestic mild cognitive impairment, but not in controls. However, the MMN seems to be preserved under ignore condition (Kazmerski *et al.*, 1997), when attention to the stimuli was not required. Engeland *et al.* (2002) found that nicotine, a cholinergic agonist, enhancing a number of cognitive processes, shortened the MMN latency, and hence enhances pre-attentive temporal processing. Scopolamine, a centrally acting cholinergic antagonist, reduced the MMN amplitude (Pekkonen *et al.*, 2001). Previous studies also showed that the amplitude of the P50 component is elevated in patients with mild cognitive impairment or early AD, as compared to healthy controls (Polich *et al.*, 1990; Golob & Starr, 2000; Golob *et al.*, 2007, Cheng *et al.*, 2012). A stronger P50 in patients with AD could explain the observed differences in the MMN. The larger amplitude may indicate an impairment of pre-attentive inhibition of repetitive auditory inputs (Cheng *et al.*, 2012). It is unclear whether amplitude modulation of patients with AD or mild cognitive impairment (MCI) reflects a pathology of cortical neurons or is instead a functional consequence of the pathology of remote structures such as the NBM.

In this study, we investigated brain responses to repetitive stimuli in an oddball paradigm in patients with AD treated with NBM-DBS and compared them with responses in age-matched healthy controls to test two hypotheses. The first hypothesis was that patients would show different mismatch responses with or without NBM-DBS, and that such differences cannot be ascribed to a repeated auditory stimulation, as in our control group. Second, we hypothesized that the response to standard tones in particular would be altered in patients with AD without NBM-DBS, possibly due to an amplitude modulation in the P50/N1 complex.

Methods

Participants

Patients

The youngest two patients with AD (P1: 63 years.; P2: 61 years) from the former MEYND-DBS (Kuhn *et al.*, 2015a,b; Hardenacke *et al.*, 2016) cohort participated in the experiment after providing their written informed consent. Recordings took place at the University of Cologne and were approved by the local ethics committee (Otto von Guericke University Magdeburg). A low-frequency NBM-DBS (20 Hz, 1V) was implemented. Details of implantation of the low-frequency stimulation are described in Kuhn *et al.* (2015a,b). The initial MEYND-DBS study started 6 years before the study

described here. Unfortunately, the remaining six patients were not able to participate due to their progressively deteriorated dementia.

Controls

Six controls (mean age 59 years; std 1.2) were recruited from a pool of healthy normal subjects at the Otto-von-Guericke University of Magdeburg and participated in the experiment after providing their written informed consent.

Paradigm

Participants listened to stimuli consisting of 180 ms long (10 ms rise and fall time) harmonic sounds with a fundamental frequency (F0) of 500 or 550 Hz and the three first harmonics with descending amplitudes (-6, -9, -12 dB relative to the fundamental), with a stimulus onset asynchrony of 600 ms (see Fig. 1). The stimuli were generated using MATLAB software (The MathWorks, Natick, MA). The stimuli were presented using the loudspeakers of the notebook. The participants were asked to ignore auditory stimuli and watched an engaging visual slide show on the screen of the notebook. Sequences consisted of 600 trials with 100 deviant tones randomly embedded in standard tones. The trains of standard tones had a minimum length of three and a maximum length of seven standard tones in a row and each of the five different train lengths had the same probability (20%).

NBM-DBS OFF vs. NBM-DBS ON

Twenty minutes before running the experiment, the NBM-DBS was switched off and participants were familiarized with the experiment. Then, the auditory stimulation was started while the stimulation remained off (NBM-DBS OFF condition). Twenty minutes before the next presentation, the NBM-DBS stimulation was switched on (NBM-DBS ON condition). We ran the same experiment in the controls two times with a break of 20 min. We reasoned that if we do not observe differences in controls across blocks but that the patients' EEG components converged to a normal amplitude modulation as defined by controls, then differences in patients between NBM-DBS OFF and NBM-DBS ON can be ascribed to the stimulation but not to the temporal order. However, fatigue may affect the patients with AD differently. Hence, we directly tested the impact of fatigue on EEG components. We reasoned that if fatigue may influence amplitude modulation, then changes in EEG components can be explained by the frequent repetition during stimulation and hence within the first block.

EEG recording

During presentation of the oddball paradigm, we recorded EEG activity from 21 channels according to the 10–20 setting with a sampling rate of 256 Hz. At both the University in Cologne and Magdeburg, the same portable EEG system set-up by the same personnel was used. Scalp impedances were kept below 5 kΩ. Data were referenced against left and right mastoid (channels 22 and 23) during recording. The resulting raw data were segmented in epochs ranging from -1 to 2 s around the stimulus onset. Epochs with amplitudes > 40 μV were rejected. Data of both patients and controls were notch-filtered offline around 20 Hz ($\pm$ 2 Hz) and its three harmonics to remove artifacts due to NBM-DBS stimulation in the ON condition and 50 Hz ($\pm$ 2 Hz) and its three harmonics to remove line noise. This notch filter was applied to both patients and controls to make EEG activity comparable across blocks and groups. We then bandpass filtered the data between 1 and 40 Hz. All epochs were baseline corrected by subtracting mean activity in the 100 ms preceding stimulus onset.

Data analysis

In general, we reasoned that if we do not observe differences in controls across blocks but patients' EEG components converged under stimulation to normal amplitude modulation, as defined by controls, then differences in patients between NBM-DBS OFF and NBM-DBS ON could be attributed to the stimulation but not to the temporal order. We estimated the effect due the NBM-DBS in the following way. We first selected channels showing a stimulus-responsive activity modulation in either standard or deviant tones (I – Stimulus-responsive activity modulation). In the next step, we verified that both patients did not differ in their response across blocks and stimulus types (II – Response Similarity between Patients). Then, we quantified the mismatch response and tested for differences between patients and controls across blocks (III – Mismatch signal). Next, we tested for effects of NBM-DBS on responses to standard and deviant tones separately (IV – Response differences to deviant and standard tones between groups and blocks). In the last step, we analyzed the evolution of sensory gating by means of repetition suppression (V – Repetition Suppression).

I – Stimulus-responsive activity modulation

We first identified stimulus-responsive channels showing a significant (compared to an empirical distribution, see below) amplitude modulation to auditory stimulation. For each EEG channel, we averaged across patients and controls and calculated the average baseline activity B across the 100 ms preceding the stimulus onset. We then averaged the absolute stimulus response across the 200 ms following the stimulus onset encompassing largely the P50 and N1 components (see Fig. 2). The resulting average stimulus-response A was subtracted from B. The difference between A and B was compared against an empirical distribution derived from randomly shifted time series (1000 permutations). We compared the empirical values against the surrogate distribution to correct for the multiple tests
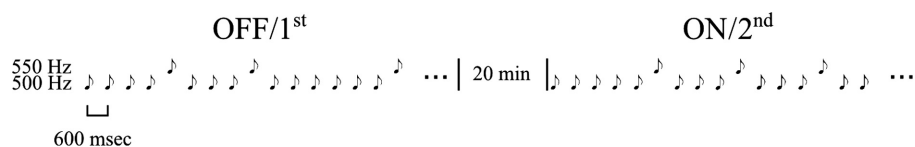
FIG. 1. Depiction of the experimental paradigm. Patients and controls listened to stimuli consisting of 180-ms-long (10 ms rise and fall time) sounds. High-probability standard tones (500 Hz) mixed with low-probability deviants [550 Hz; stimulus onset asynchrony (SOA) = 600 ms] were presented unpredictably (pseudorandom sequence: minimum three consecutive standard tones in two blocks. Patients started with NBM-DBS OFF followed with NBM-DBS ON after a 20 min break.
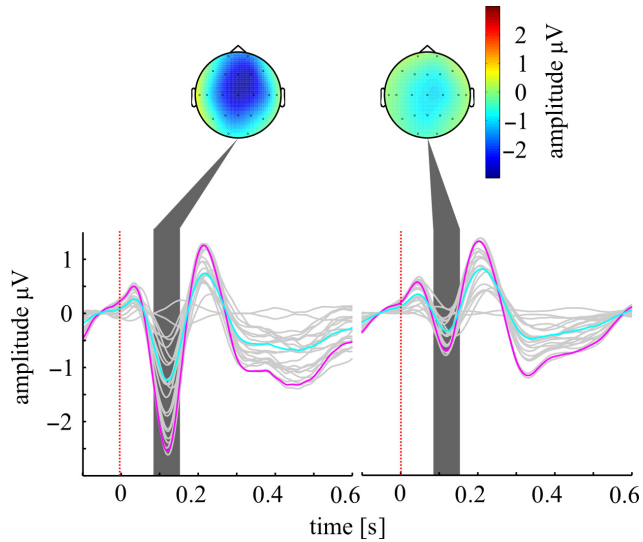
FIG. 2. Depiction of responses to deviant (left) and standard tones (right) collapsed across both groups (patients and controls) and both blocks (OFF/1st and ON/2nd). The upper row shows the topographical distribution of the N1 response between 90 and 150 ms (grey shaded area). Fz, Cz, C3 and C4 showed significant amplitude modulation compared with baseline activity (-100 ms preceding stimulus onset) with a pronounced negative-going deflection as indicated by blue areas. The lower row shows the responses of all channels (grey lines) to deviant and standard tones. The dashed red line marks the stimulus onset. The light blue time series shows the mean response across all channels, and the purple time series shows the mean response across all significant channels.

applied. In each permutation, the time series of each channel and each trial were shifted (circular shift of the entire trial time series between -0.1 and 0.6 s) separately, and new (surrogate) trial averages were calculated from the shifted trials. We then calculated the difference between $A_{surrogate}$ and $B_{surrogate}$ leading to 1000 difference values. Channels exceeding the 97.5th percentile of the channel-specific surrogate distribution were classified as showing a significant stimulus response.

II – Response similarity between patients

Due to the small number of patients, we could not compare patients with controls across subjects. Hence, our random variable in each test was trials. This provides a sufficiently high number of data points (500 standard tone trials for each subject in each block and 100 deviant tone trials for each subject in each block) for the use of inference statistical tests like t- and F-tests. A prerequisite for each test was that patients did not differ in their response to the stimulation in either the first or in the second block, to exclude the possibility that differences between blocks can be ascribed to only one patient. Within the mean activity averaged across the responsive channels, we carried out a two-way ANOVA with factor stimulus type (standard vs. deviant tones) and patient (patient 1 vs. patient 2) at each time point, separately for the NBM-DBS OFF and ON (with single trials as random variable). This yielded a time series of F-values representing the interaction effect of stimulus type and patient between -100 and 600 ms. The $F_{interaction}$ value parameterizes the difference between patients in their response to the two different stimulus types. To set a threshold for significant $F_{interaction}$ values, an empirical distribution of the interaction effect was constructed by randomly reassigning the labels (standard vs. deviant tones and patient 1 vs. 2) to the single trials in 1000 permutations. To rule out

fatigue as a potential influencing variable, we compared the first third of trials against the last third of trials in the patient group. We carried out a time point by time point t-test in order test each EEG component separately. A high t-value would indicate a robust change in a given EEG component due to the frequent repetition in the first block. The resulting t-values time series was compared against a surrogate distribution derived from a randomly shifted time series (1000 permutations).

III – Mismatch signal

To determine the strength of the mismatch response, we carried out a t-test comparing standard and deviant tones at each time point (random variable is trials) separately for patients and controls, both in the 1st/OFF block and the 2nd/ON block. This yielded four time series representing the mismatch response (see Fig. 3). The area encompassed by these time series is typically interpreted as a differential response to deviants compared to standard tones, due to a prediction error. We asked whether patients' mismatch response differs from controls both in the 1st/OFF block or the 2nd/ON block. A significant difference in the NBM-DBS OFF from controls but not in the NBM-DBS ON condition would indicate a normalized auditory processing under stimulation. Therefore, we converted the area encompassed by each time series within the 250 ms following stimulus onset into a frequency distribution of amplitude values. Figure 3 shows a red and blue area under the t-value time series for 1st block of controls and NBM-DBS OFF block of patients, respectively. We used receiver operation curve (ROC) analysis to evaluate the overlap of each pair of frequency distributions. We estimated the area under the ROC (AUC) for the frequency distributions. Each AUC was compared against a surrogate distribution. In 1000 runs, we randomly reassigned labels (group, block, stimulus type) and calculated the 1000 $AUC_{surrogate}$ values.
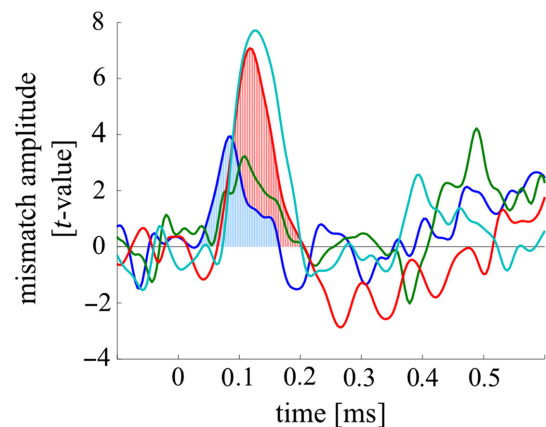
FIG. 3. Depiction of Mismatch responses. For each group (patients and controls) in each block (OFF/1st and ON/2nd), we quantified the mismatch response by calculating the t-values as the difference between responses to standard and deviant tones for each time point. Here, we tested whether controls showed a difference in their mismatch response across blocks and whether patients differed from the response of the controls. To estimate the difference, we estimated the overlap of the integral under the t-value time series. For example, the blue line shows the mismatch response in patients without stimulation (OFF). The red line shows the mismatch response in controls in the 1st block. The amount of overlap between both integrals was assessed by receiver operating curve. While the response of patients in the OFF block was significantly different from controls the response of patients in the ON block was not.

IV – Response differences to deviant and standard tones between groups and blocks

We tested whether the difference in MMN can be attributed to the response to deviant or to standard tones separately. Specifically, we asked whether responses to either of the stimuli evolved differentially between the groups across blocks. We expected a difference in the response to one of the stimuli in the patient group as compared to the control group. At each time point, we calculated a two-way ANOVA with the factors group (patients vs. controls) and block ('OFF'/1st vs. 'ON'/2nd). A significant interaction would indicate that patients and controls evolve differently in their response across blocks. Specifically, we expected a stronger variation in the patient group than in the control group. We reasoned that effects in the patient group across blocks, which were not paralleled by differences in the control group across blocks, could be attributed to the stimulation but not to repetition of the same experiment itself. The observed F-values were compared against a surrogate distribution, which was constructed by randomly reassigning the labels (group and block) in 1000 runs. In addition to the ANOVA, we compared both the patient and control group regarding their effect size. Again, our rationale was that if there is a difference between the blocks in the patient group but not in the control group, then most likely differences in EEG components are due to NBM-DBS. We estimated the effect size at each time point as the difference between the mean across trials and subjects in the first block (NBM-DBS ON in patients) and the mean across trials and subjects in the second block (NBM-DBS OFF in patients), divided by the common standard deviation. The effect size is a statistical measure, reflecting how much two standardized means are different between two populations. The larger the effect size is, the more the two populations are distinct in a studied parameter.

V – Repetition suppression

Next, we assessed whether patients and controls show different patterns of adaptation to standard tones. Within the temporal interval of the significant interaction, we grouped standard tones according to the number of repetitions (1–7). The averaged absolute amplitude modulation to standard tones was correlated with the number of repetitions separately for each group (patients vs. controls) and separately for each block. Again, we assessed the difference in the patient group across blocks with the difference in the control group across both blocks. To assess significance of the difference of Pearson's correlation coefficient in the patient group in the 'OFF' vs. 'ON' block, we compared the difference value against a surrogate distribution. In 1000 runs, we first reassigned the labels (number of repetitions) randomly to the trials. Then, we regrouped trials according to the newly assigned labels and correlated them with the number of repetition separately for each block. Then, we calculated the difference between all combinations of the resulting 1000 r values between both blocks. The difference values Δr of the patient group between NBM-DBS OFF and NBM-DBS ON were compared against resulting $\Delta r_{\mathrm{surrogate}}$ values.

Results

I – Stimulus-responsive activity modulation

We first identified channels showing a significant amplitude modulation to the auditory stimulation. EEG channels Fz, Cz, C3 and C4 showed significant modulation to both standard and deviants tones

compared to baseline (Bonferroni corrected for multiple comparisons).

II – Response similarity between patients

The threshold $F_{\mathrm{interaction}}$ value derived from the surrogate distribution was 5.5. The empirical $F_{\mathrm{interaction}}$ values did not reach significance, indicating no differences between patients with respect to their response to standard and deviants tones. The maximal $F_{\mathrm{interaction}}$ values observed in NBM-DBS OFF were 2.2 and 4.2 in NBM-DBS ON. The $F_{\mathrm{interaction}}$ value of 4.1 of the three-way interaction (stimulus type × patient × block) did not reach significance either (all P-values > 0.1).

III – Mismatch signal

Figure 3 shows the mismatch responses of patients under NBM-DBS OFF (blue), NBM-DBS ON (green), and in controls in the 1st block (red) and in the 2nd block (light blue). We quantified the mismatch response as the integral under the t-values time series and compared these areas using receiver operating curve (ROC) statistics. We found the mismatch response in the patient group under NBM-DBS OFF was significantly earlier than the mismatch response under NBM-DBS ON, and also earlier than the mismatch response of controls both in the 1st and 2nd block (see Table 1 for a complete list of AUC values and P-values within the surrogate distribution). The mismatch response of patients under NBM-DBS ON did not differ from the controls either in the 1st or in the 2nd block. As the mismatch response depends both on the response to deviant and standard tones, we assessed both separately in the next step.

IV – Response differences to deviants and standard tones between groups and blocks

We assessed whether patients and controls evolved differently in their responses to the stimulus types across blocks. We found a significant interaction between the factors of group (patients vs. controls) and block (OFF 1st vs. ON 2nd), in response to frequent standard tones but not to deviant tones ranging from 75 to 140 ms (see Fig. 4). The peak $F_{\mathrm{interaction}}$ value was 7.75 at 124 ms ($P < 0.00001$), indicating an altered response to standard tones under NBM-DBS OFF compared to NBM-DBS ON and controls in both blocks. The response to standard tones recovers under stimulation to a normal level comparable to the response in controls. For *post hoc* tests, we averaged the response in the time range from 75 to 140 ms in each trial and compared patients and controls in both blocks. We found a significant difference between NBM-DBS OFF and NBM-DBS ON [$t_{3721} = 4.8$; $P < 0.0001$], between patients OFF and controls in the 2nd block [$t_{3762} = 5.3$; $P < 0.0001$], and between patients OFF and controls in the first block [$t_{1874} = 5.3$; $P = 0.01$; significant at an uncorrected level]. However, there were no

TABLE 1. Provides a summary of differences in MMN between groups and blocks as the area under the receiver operating curve

Comparison	PG OFF vs. PG ON	PG OFF vs. CG 1st	PG OFF vs. CG 2nd	PG ON vs. CG 1st	PG ON vs. CG 2nd	CG 1st vs. CG 2nd
AUC	0.74	0.8	0.85	0.55	0.64	0.59
P	0.003	0.0003	0.00002	0.25	0.06	0.13

differences between patients ON and controls (both *P*-values > 0.1) and between both blocks of controls (*P* = 0.1). The maximal effect size *d* in the temporal interval of the P50-N1 of the patient group was *d* = 0.2 (*P* < 0.00001; CI$_{99\%}$ −0.09 to 0.09) at 28 ms. The maximal effect size in the control group was *d* = 0.06 at 128 ms and hence fell below the significance threshold. This effect cannot be ascribed to fatigue as in the temporal interval of the P50-N1, we did not find a significant change over the first block (see Fig. 4).

V – Repetition suppression

In the temporal interval lasting from 75 to 140 ms, we observed a significant effect of interaction between the factors of group and block, indicating a significant reduction in the N1 response to the standard tones in the patient group without stimulation. In this temporal interval, we observed a negative correlation of amplitude with the number of repetitions in the control group, both in the 1st and the 2nd block. We did not observe a significant difference between both blocks (Δr_{CG} = 0.08; *P* = 0.6; see Fig. 5). We observed a positive correlation in the OFF block in the patients. In contrast, we observed a negative correlation resembling the pattern in controls in the ON block. The correlation in patients in the OFF block was significantly different from the correlation in patients in ON block (Δr = −1.1; *P* = 0.0005) and from correlation in the controls in the 1st (Δr = −0.92; *P* = 0.003) and the 2nd block (Δr = −0.84; *P* = 0.006). The correlation in patients in the ON block was not significantly different from correlation in controls in the 1st (Δr = 0.17; *P* = 0.7) and the 2nd block (Δr = 0.25; *P* = 0.77).

Discussion

We assessed neural responses of AD patients with and without NBM-DBS stimulation to standard and deviant tones in a passive oddball paradigm to study the effect of electrical stimulation on auditory processing. We used a group of age-matched healthy controls to quantify the effect of a repeated auditory stimulation with the same paradigm. We reasoned that changes in the patient group between

OFF and ON NBM-DBS, which are not paralleled by the repeated auditory stimulation in the control group, can be attributed to the DBS and not to the repetition of the same paradigm itself. We found that the mismatch response occurred significantly earlier without NBM-DBS compared to the NBM-DBS ON condition and compared to controls in the 1st and 2nd block. This earlier MMN is most likely due to the altered response to the standard tones in the NBM-DBS OFF condition. Indeed, we found a different response to the standard tones in the patient group when the NBM-DBS was switched off. Here, we observed a stronger positive-going deflection in the P50 interval overlapping with a therefore markedly reduced N1 component. Under NBM-DBS stimulation, this response resembled the response in age-matched healthy controls. In contrast, we did not find such a pattern in the response to the deviant tones.

The mismatch negativity is a prominent EEG component most likely signalling prediction errors and originates in the frontal and temporal cortex. Other AD studies have indeed found changes in MMN, too (Cheng *et al.*, 2012, Hsiao *et al.*, 2014; Lindín *et al.*, 2013), but MMN responses were rather delayed in these studies. The differences in response delays can be explained by task differences. For example, Cheng *et al.* (2012) used 1000 Hz sine wave tones both for standard and deviant tones but with a shorter stimulus presentation time (50 ms) for deviant tones compared to standard tones (100 ms). The earlier MMN in our study is a direct result of the altered response to standard tones when the stimulation is switched off.

Our early positive deflection in the time range of the P50 matches the results found in previous studies in which the P50 is altered in MCI and AD. The enhanced P50 response is well described in patients with AD and MCI (Green *et al.*, 2015). Another study compared amnestic MCI patients treated with cholinesterase inhibitors to untreated patients and found larger P50 amplitudes in untreated patients with MCI (Irimajiri *et al.*, 2007). Another interesting study compared the brain responses of healthy subjects with and without AD relatives (Boutros *et al.*, 1995a). The authors found significantly higher P50 and P300 responses to frequent stimuli in subjects whose relatives had AD as compared with subjects who had no relatives suffering from AD. Additionally, P50 amplitudes have been shown
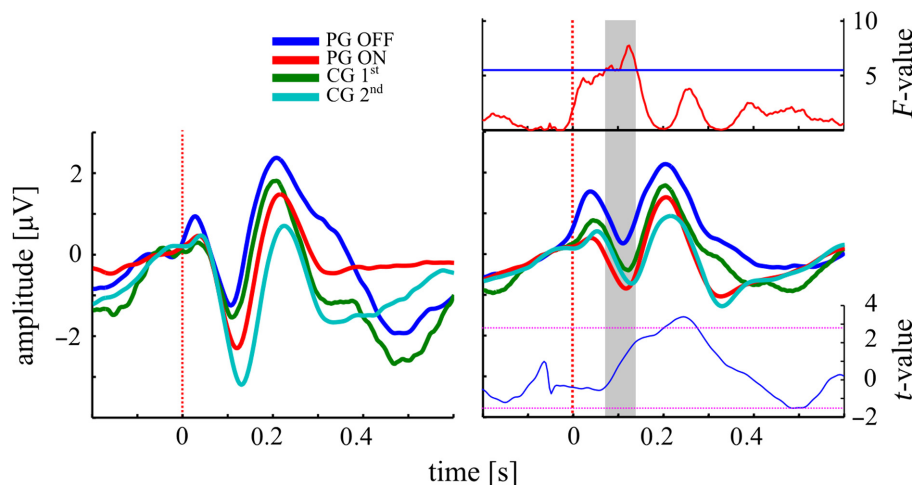
FIG. 4. Depiction of response stimuli separately for each group and block. We compared responses to both stimulus types separately across blocks and patients at each time point. The upper right plot shows the $F_{interaction}$-value time series (red line). The blue line shows the significance threshold (CI$_{99\%}$ = 5.5). We found a significant effect of interaction to standard tones between patients and controls indicating a significant difference between blocks in patients compared to controls. This indicates that under NBM-DBS response to standard tones in patients normalizes while in controls response remains stable across blocks. This effect cannot be ascribed to the influence of fatigue in the patients group on EEG components. We compared the 1st with the last third of trials in the patients group with a time point by time point *t*-test (thin blue line in the lower inset). The dashed magenta lines give the 99.9% confidence interval. Only the amplitude in the temporal interval of the P300 decreases across the NBM-OFF block. Within the P50-N1 interval, we did not find differences which can be ascribed to fatigue.
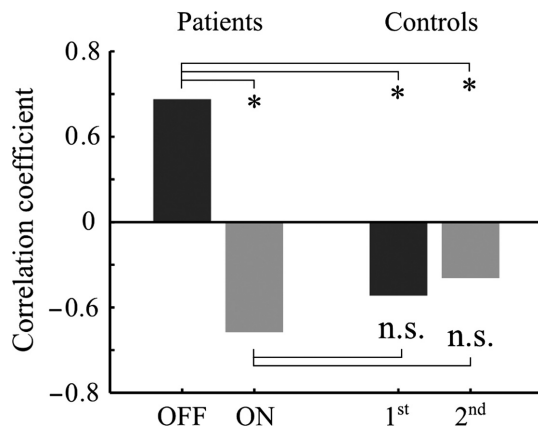
FIG. 5. Depiction of repetition adaptation effects. We evaluated whether N1 responses to standard tones adapted with the number of repetitions. We grouped trials according to their number of repetitions. In the time range of significant interaction (see Fig. 3), we correlated the amplitude with the number of repetitions. Controls showed a negative correlation in this time range which was not significantly different from repetition effect in patients under NBM-DBS. Patients showed a positive correlation without NBM-DBS most likely due to the reduction in N1 and overlap with the P50. This correlation was significantly different from patients under NBM-DBS and controls in both blocks. Asterisks denote a statistically significant difference.

to be even higher to frequent stimuli compared to deviant stimuli in healthy subjects (Boutros *et al.*, 1995b). The authors argue that this increase in P50 amplitude reflects the system's recognition of novel stimuli or gating of sensory input. The MEG homologue (the M50) also showed a larger amplitude in the elderly subjects (Cheng *et al.*, 2012). In this study, as was also the case in our study, the subjects were also asked to ignore the auditory stimulation. The elevated M50 response indicates an impairment of pre-attentive inhibition of repetitive auditory inputs. Furthermore, this pre-attentive P50 increase has been shown to be age dependent (Azumi *et al.*, 1995; Amenedo & Diaz, 1998). This age-dependent pattern first has been observed in attentive oddball paradigm in which the amplitude of the P50 was higher in elderly compared with young subjects (Golob *et al.*, 2007). Another study tested whether the P50 deficit is due to a primary deficit in P50 generation in patients with AD, and the authors did not find differences in patients with AD compared to elderly controls with very long inter-stimulus intervals. The authors argued that if there is a P50 deficit in patients with AD, it is the result of the accumulative effect of repetitive stimulation rather than a primary deficit in P50 generation (Fein *et al.*, 1994). Our specific difference in amplitude between the patient group and control group across blocks manifests rather later, specifically in the temporal interval of the N1. However, we sought to estimate the time course of the interaction effect and did not chose peak amplitude values in a predefined interval. The P50 is often defined by its peak in a narrow temporal interval around 50 ms following stimulus onset (see Irimajiri *et al.* (2007) for an example). Our parameter of differences between groups across blocks (i.e. the interaction effect) already increases in the temporal interval of the P50. However, we compared differences against a rather conservative significance threshold derived from the surrogate distribution. Taken together with the vanishing N1 response, as indicated by the peak interaction of groups and blocks, we hypothesize that the P50 superimposes on the N1. This pattern may explain why especially the N1 latency in other studies discriminated demented Parkinsonian patients from demented patients with AD (Goodin & Aminoff, 1987). In sum, the increase in the P50 indicates a deficit filtering out known information.

Another pattern associated with recognition of familiar information is the reduction in the neuronal response to stimulus repetition, which is known as repetition suppression effect. It is assumed that rapid and precise processing of environmental sounds contributes to communication functions. This repetition effect is associated with decreased reaction times (Murray *et al.*, 2008). Here, we found a decrease in amplitude with an increasing number of standard tones in a row in controls and patients under NBM-DBS but not when NBM-DBS was switched off, indicating that DBS indeed improves sensory gating. It is well established that evoked responses recorded from sensory cortex show decreases with stimulus repetition that do not generalize to novel or different stimuli (Eliades *et al.*, 2014) and hence it is assumed that repetition suppression may improve auditory perception in complex listening environments. It is assumed that repetition suppression is a prerequisite to generate predictions of the incoming stimulus (Costa-Faidella *et al.*, 2011) and can be found as early as the N1, where the repetition effect occurs regardless of attention. In contrast, repetition effects on later components like the P2 are more dependent on attention (Hsu *et al.*, 2014). This repetition effect most likely originates in the temporal cortex (Murray *et al.*, 2008). FMRI studies have found activity in the anterior MTL during repeated stimuli inversely related to performance in a recognition task. The failure of response suppression to familiar information may be a sensitive marker of memory impairment in ageing and prodromal AD (Pihlajamäki *et al.*, 2011). Also, MTL activity increased in patients with AD as compared to normal controls in fMRI recordings(Pihlajamäki *et al.*, 2008), suggesting that the typical episodic memory impairment seen in mild AD may manifest as a failure of normal repetition suppression.

The primary goal of our study was to assess a potential beneficial impact of NBM-DBS on sensory gating, which is, despite the limited generalizability due to the small number of patients, an important opportunity in light of the small number of publications on NBM-DBS in AD. However, in this very rare occasion to record from AD patients with NBM-DBS, we found consistent responses across patients and statistics across trials gave a robust difference between groups when compared across blocks. Furthermore, a direct comparison of DBS and cholinesterase inhibitors could help to clarify what is the most helpful tool to treat these patients.

Our consistent results lead to the critical conclusion that NBM-DBS has a beneficial effect on the recognition of familiar stimuli. This result highlights the role of NBM-DBS in the treatment of patients with AD and its role in the clinical context should be investigated more in the future. In sum, our results support the hypothesis that NBM-DBS has a positive impact on sensory gating into memory.

Acknowledgements

Conflict of interest

No Conflict of interest.

Author contribution

S.D. designed research, J.K., H.J.F. provided clinical information S.D. analyzed the data, S.D. interpreted the data S.D., C.R., H.H., H.J.H., J.K. wrote the manuscript.

Data accessibility

Data are available on request by the authors.

References

Aggelopoulos, N., Liebe, S., Logothetis, N. & Rainer, G. (2011) Cholinergic control of visual categorization in macaques. *Front. Behav. Neurosci.*, **5**, 73.

Amenedo, E. & Diaz, F. (1998) Effects of aging on middle-latency auditory evoked potentials: a cross-sectional study. *Biol. Psychiat.*, **43**, 210–219.

Azumi, T., Nakashima, K. & Takahashi, K. (1995) Aging effects on auditory middle latency responses. *Electromyogr. Clin. Neurophysiol.*, **35**, 397–401.

Boutros, N., Torello, M., Burns, E., Wu, S. & Nasrallah, H. (1995a) Evoked potentials in subjects at risk for alzheimer's disease. *Psychiatry Res.*, **57**, 57–63.

Boutros, N., Torello, M., Barker, B., Tueting, P. & Wu, S.C. (1995b) The p50 evoked potential component and mismatch detection in normal volunteers: implications for the study of sensory gating. *Psychiatry Res.*, **57**, 83–88.

Cheng, C., Wang, P., Hsu, W. & Lin, Y. (2012) Inadequate inhibition of redundant auditory inputs in alzheimer's disease: an meg study. *Biol. Psychol.*, **89**, 365–373.

Costa-Faidella, J., Grimm, S., Slabu, L., Díaz-Santaella, F. & Escera, C. (2011) Multiple time scales of adaptation in the auditory system as revealed by human evoked potentials. *Psychophysiology*, **48**, 774–783.

Deouell, L. (2007) The frontal generator of the mismatch negativity revisited. *J. Psychophysiol.*, **21**, 188–203.

Dürschmid, S., Zaehle, T., Hinrichs, H., Heinze, H., Voges, J., Garrido, M., Dolan, R. & Knight, R. (2016) Sensory deviancy detection measured directly within the human nucleus accumbens. *Cereb. Cortex*, **26**, 1168–1175.

Eliades, S., Crone, N., Anderson, W., Ramadoss, D., Lenz, F. & Boatman-Reich, D. (2014) Adaptation of high-gamma responses in human auditory association cortex. *J. Neurophysiol.*, **112**, 2147–2163.

Engeland, C., Mahoney, C., Mohr, E., Ilivitsky, V. & Knott, V. (2002) Nicotine and sensory memory in alzheimer's disease: an event-related potential study. *Brain Cogn.*, **49**, 232–234.

Fein, G., Biggins, C. & van Dyke, C. (1994) The auditory p50 response is normal in alzheimer's disease when measured via a paired click paradigm. *Electroencephalogr. Clin. Neurophysiol.*, **92**, 536–545.

Froemke, R., Merzenich, M. & Schreiner, C. (2007) A synaptic memory trace for cortical receptive field plasticity. *Nature*, **450**, 425–429.

Fujiki, M., Kobayashi, H., Uchida, S., Inoue, R. & Ishii, K. (2005) Neuroprotective effect of donepezil, a nicotinic acetylcholine-receptor activator, on cerebral infarction in rats. *Brain Res.*, **1043**, 236–241.

Fujiki, M., Kubo, T., Kamida, T., Sugita, K., Hikawa, T., Abe, T., Ishii, K. & Kobayashi, H. (2008) Neuroprotective and antiamnesic effect of donepezil, a nicotinic acetylcholine-receptor activator, on rats with concussive mild traumatic brain injury. *J. Clin. Neurosci.*, **15**, 791–796.

Furey, M., Pietrini, P., Haxby, J. & Drevet, W. (2008) Selective effects of cholinergic modulation on task performance during selective attention. *Neuropsychopharmacology*, **33**, 913–923.

Gaeta, H., Friedman, D., Ritter, W. & Cheng, J. (1999) Changes in sensitivity to stimulus deviance in alzheimer's disease: an erp perspective. *NeuroReport*, **10**, 281–287.

Golob, E. & Starr, A. (2000) Effects of stimulus sequence on event-related potentials and reaction time during target detection in alzheimer's disease. *Clin. Neurophysiol.*, **111**, 1438–1449.

Golob, E., Irimajiri, R. & Starr, A. (2007) Auditory cortical activity in amnestic mild cognitive impairment: relationship to subtype and conversion to dementia. *Brain*, **130**, 740–752.

Goodin, D. & Aminoff, M. (1987) Electrophysiological differences between demented and nondemented patients with parkinson's disease. *Ann. Neurol.*, **21**, 90–94.

Gratwicke, J., Kahan, J., Zrinzo, L., Hariz, M., Limousin, P., Foltynie, T. & Jahanshahi, M. (2013) The nucleus basalis of meynert: a new target for deep brain stimulation in dementia? *Neurosci. Biobehav. Rev.*, **37**, 2676–2688.

Green, D., Payne, L., Wolk, D. & Kounios, J. (2015) P50: a candidate erp biomarker of prodromal alzheimer's disease. *Brain Res.*, **1624**, 390–397.

Hardenacke, K., Shubina, E., Bührle, C., Zapf, A., Lenartz, D., Klosterkötter, J., Visser-Vandewalle, V. & Kuhn, J. (2013) Deep brain stimulation as a tool for improving cognitive functioning in alzheimer's dementia: a systematic review. *Front. Psychiat.*, **4**, 159.

Hardenacke, K., Hashemiyoon, R., Visser-Vandewalle, V., Zapf, A., Freund, H., Sturm, V., Hellmich, M. & Kuhn, J. (2016) Deep brain stimulation of the nucleus basalis of meynert in alzheimer's dementia: potential predictors

of cognitive change and results of a long-term follow-up in eight patients. *Brain Stimul.*, **9**, 799–800.

Herrero, J., Roberts, M., Delicato, L., Gieselmann, M., Dayan, P. & Thiele, A. (2008) Acetylcholine contributes through muscarinic receptors to attentional modulation in v1. *Nature*, **454**, 1110–1114.

Howes, M. & Perry, E. (2011) The role of phytochemicals in the treatment and prevention of dementia. *Drugs Aging*, **28**, 439–468.

Hsiao, F., Chen, W., Wang, P., Cheng, C. & Lin, Y. (2014) Temporo-frontal functional connectivity during auditory change detection is altered in alzheimer's disease. *Hum. Brain Mapp.*, **35**, 5565–5577.

Hsu, Y., Hämäläinen, J. & Waszak, F. (2014) Repetition suppression comprises both attention-independent and attention-dependent processes. *NeuroImage*, **98**, 168–175.

Irimajiri, R., Michalewski, H., Golob, E. & Starr, A. (2007) Cholinesterase inhibitors affect brain potentials in amnestic mild cognitive impairment. *Brain Res.*, **1145**, 108–116.

Kazmerski, V., Friedman, D. & Ritter, W. (1997) Mismatch negativity during attend and ignore conditions in alzheimer's disease. *Biol. Psychiat.*, **42**, 382–402.

Kuhn, J., Gründler, T.J., Lenartz, D., Klosterkötter, J., Sturm, V. & Huff, W. (2010) Deep brain stimulation for psychiatric disorders. *Dtsch Arztebl Int.*, **107**, 105–113.

Kuhn, J., Hardenacke, K., Lenartz, D., Gruendler, T., Ullsperger, M., Bartsch, C., Mai, J.K., Zilles, K. *et al.* (2015a) Deep brain stimulation of the nucleus basalis meynert in alzheimer's dementia: results from a phase i study (meynd-dbs). *Mol. Psych.*, **20**, 353–360.

Kuhn, J., Hardenacke, K., Shubina, E., Lenartz, D., Visser-Vandewalle, V., Zilles, K., Sturm, V. & Freund, H.J. (2015b) Deep brain stimulation of the nucleus basalis of meynert in early stage of alzheimer's dementia. *Brain Stimul.*, **8**, 838–839.

Lindín, M., Correa, K., Zurrón, M. & Díaz, F. (2013) Mismatch negativity (mmn) amplitude as a biomarker of sensory memory deficit in amnestic mild cognitive impairment. *Front. Aging Neurosci.*, **5**, 79.

McGaughy, J., Kaiser, T. & Sarter, M. (1996) Behavioral vigilance following infusions of 192 igg-saporin into the basal forebrain: selectivity of the behavioral impairment and relation to cortical ache-positive fiber density. *Behav. Neurosci.*, **110**, 247–265.

Mesulam, M., Mufson, E., Levey, A. & Wainer, B. (1983) Cholinergic innervation of cortex by the basal forebrain: cytochemistry and cortical connections of the septal area, diagonal band nuclei, nucleus basalis (substantia innominata), and hypothalamus in the rhesus monkey. *J. Comp. Neurol.*, **214**, 170–197.

Miasnikov, A., McLin, D. & Weinberger, N. (2001) Muscarinic dependence of nucleus basalis induced conditioned receptive field plasticity. *NeuroReport*, **12**, 1537–1542.

Miasnikov, A., Chen, J. & Weinberger, N. (2008) Specific auditory memory induced by nucleus basalis stimulation depends on intrinsic acetylcholine. *Neurobiol. Learn. Mem.*, **90**, 443–454.

Murray, M., Camen, C., Spierer, L. & Clarke, S. (2008) Plasticity in representations of environmental sounds revealed by electrical neuroimaging. *NeuroImage*, **39**, 847–856.

Näätänen, R., Gaillard, A. & Mäntysalo, S. (1978) Early selective-attention effect on evoked potential reinterpreted. *Acta Physiol. (Oxf)*, **42**, 313–329.

Näätänen, R., Paavilainen, P., Rinne, T., Alho KNäätänen, R., Paavilainen, P., Rinne, T. & Alho, K. (2007) The mismatch negativity (mmn) in basic research of central auditory processing: a review. *Clin. Neurophysiol.*, **12**, 2544–2590.

Pekkonen, E., Jousmäki, V., Könönen, M., Reinikainen, K. & Partanen, J. (1994) Auditory sensory memory impairment in alzheimer's disease: an event-related potential study. *NeuroReport*, **5**, 2537–2540.

Pekkonen, E., Hirvonen, J., Jääskeläinen, I., Kaakkola, S. & Huttunen, J. (2001) Auditory sensory memory and the cholinergic system: implications for alzheimer's disease. *NeuroImage*, **14**, 376–382.

Pihlajamäki, M., DePeau, K.M., Blacker, D. & Sperling, R.A. (2008) Impaired medial temporal repetition suppression is related to failure of parietal deactivation in alzheimer disease. *Am. J. Geriat. Psychiat.*, **16**, 283–292.

Pihlajamäki, M., DePeau, K.M., Blacker, D. & Sperling, R.A. (2011) Failure of repetition suppression and memory encoding in aging and alzheimer's disease. *Brain Imaging Behav.*, **5**, 36–44.

Polich, J., Ladish, C. & Bloom, F. (1990) P300 assessment of early alzheimer's disease. *Electroencephalogr. Clin. Neurophysiol.*, **77**, 179–189.

Rasmusson, D. (2000) The role of acetylcholine in cortical synaptic plasticity. *Behav. Brain Res.*, **115**, 205–218.

Sarter, M. & Bruno, J. (2000) Cortical cholinergic inputs mediating arousal, attentional processing and dreaming: differential afferent regulation of the basal forebrain by telencephalic and brainstem afferents. *Neuroscience*, **95**, 933–952.

Shalgi, S. & Deouell, L. (2007) Direct evidence for differential roles of temporal and frontal components of auditory change detection. *Neuropsychologia*, **45**, 1878–1888.

Terry, R. & Davies, P. (1980) Dementia of the alzheimer type. *Annu. Rev. Neurosci.*, **3**, 77–95.

Thiel, C., Bentley, P. & Dolan, R. (2002) Effects of cholinergic enhancement on conditioning-related responses in human auditory cortex. *Eur. J. Neuorsci.*, **16**, 2199–2206.

Voytko, M., Olton, D., Richardson, R., Gorman, L., Tobin, J. & Price, D. (1994) Basal forebrain lesions in monkeys disrupt attention but not learning and memory. *J. Neurosci.*, **14**, 167–186.

Warburton, E., Koder, T., Cho, K., Massey, P., Duguid, G., Barker, G., Aggleton, J., Bashir, Z. *et al.* (2003) Cholinergic neurotransmission is essential for perirhinal cortical plasticity and recognition memory. *Neuron*, **38**, 987–996.

Weinberger, N. (2003) The nucleus basalis and memory codes: auditory cortical plasticity and the induction of specific, associative behavioral memory. *Neurobiol. Learn. Mem.*, **80**, 268–284.

Whitehouse, P., Price, D., Struble, R., Clark, A., Coyle, J. & Delon, M. (1982) Alzheimer's disease and senile dementia: loss of neurons in the basal forebrain. *Science*, **215**, 1237–1239.

Hierarchy of prediction errors for auditory events in human temporal and frontal cortex

Stefan Dürschmid[a,b,c,1], Erik Edwards[d], Christoph Reichert[a,e], Callum Dewar[c], Hermann Hinrichs[a,b,e,f,g], Hans-Jochen Heinze[a,b,e,f,g], Heidi E. Kirsch[d], Sarang S. Dalal[h], Leon Y. Deouell[i,j], and Robert T. Knight[c]

[a]Department of Behavioral Neurology, Leibniz Institute for Neurobiology, 39120 Magdeburg, Germany; [b]Department of Neurology, Otto von Guericke University, 39120 Magdeburg, Germany; [c]Helen Wills Neuroscience Institute and Department of Psychology, University of California, Berkeley, CA 94720; [d]Department of Neurology, University of California, San Francisco, CA 94143; [e]Forschungscampus Stimulate, Otto von Guericke University, 39106 Magdeburg, Germany; [f]German Center for Neurodegenerative Diseases, 39120 Magdeburg, Germany; [g]Center of Behavioral Brain Sciences, Otto von Guericke University, 39106 Magdeburg, Germany; [h]Zukunftskolleg and Department of Psychology, University of Konstanz, 78457 Konstanz, Germany; [i]Department of Psychology, The Hebrew University of Jerusalem, Jerusalem 91905, Israel; and [j]Edmond and Lily Safra Center for Brain Sciences, The Hebrew University of Jerusalem, Jerusalem 91904, Israel

Predictive coding theories posit that neural networks learn statistical regularities in the environment for comparison with actual outcomes, signaling a prediction error (PE) when sensory deviation occurs. PE studies in audition have capitalized on low-frequency event-related potentials (LF-ERPs), such as the mismatch negativity. However, local cortical activity is well-indexed by higher-frequency bands [high-γ band (Hγ): 80–150 Hz]. We compared patterns of human Hγ and LF-ERPs in deviance detection using electrocorticographic recordings from subdural electrodes over frontal and temporal cortices. Patients listened to trains of task-irrelevant tones in two conditions differing in the predictability of a deviation from repetitive background stimuli (fully predictable vs. unpredictable deviants). We found deviance-related responses in both frequency bands over lateral temporal and inferior frontal cortex, with an earlier latency for Hγ than for LF-ERPs. Critically, frontal Hγ activity but not LF-ERPs discriminated between fully predictable and unpredictable changes, with frontal cortex sensitive to unpredictable events. The results highlight the role of frontal cortex and Hγ activity in deviance detection and PE generation.

predictive coding | prediction error | mismatch negativity | frontal cortex | high γ-activity

The ability to detect unexpected environmental events results from a comparison of the actual state of our sensory world with predictions based on immediate and long-term contextual knowledge. Predictive coding theory, first articulated within the visual domain, postulates that distributed neural networks learn statistical regularities of the natural world, generating a prediction error (PE) signal as deviations from these predictions occur (1). Because of the difficulty of recording high-frequency activity in scalp EEG recordings, studies on PE in audition have focused on low-frequency event-related potentials (LF-ERPs). The mismatch negativity (MMN) is considered the classic PE signal elicited during passive listening to deviant sounds interrupting the context provided by a sequence of repeated standard stimuli (2). Converging evidence suggests that the MMN has interacting generators in the secondary auditory cortex on the superior temporal plane and superior temporal gyrus (STG) as well as in the prefrontal cortex (3, 4), but the distinct contribution of each part of this network, especially the prefrontal part, is not clear. Evidence from neuropsychological event-related potentials and neuroimaging studies supports a key role of the prefrontal cortex in contextual processing (5, 6), suggesting a crucial role of this brain region in predictive coding.

Importantly, low-frequency scalp-recorded responses, like the MMN, do not reveal the full spectrum of the neuronal response to prediction violation. Whereas recording high frequencies with scalp EEG has major methodological issues related to low signal to noise (7, 8), numerous studies using electrocorticography (ECoG; recorded on the cortical surface) have shown high γ-band (Hγ) response to be a localized index for functionally selective activity (9, 10). It is not clear whether cortical neuronal activity responsible for deviance detection is best indexed by low- or higher-frequency bands. This differentiation is critical, because the Hγ has distinct response properties compared with LF-ERPs (11). Using intracranial recordings, involvement of low frequency-evoked activity and Hγ-induced activity in auditory PE signals were found in temporal regions (12, 13), where Hγ amplitude was shown to increase earlier than lower-frequency bands (12). In inferior frontal regions, previous ECoG studies (12, 14) did not find evidence for Hγ frontal activity in response to local deviations [as opposed to global ones; discussed in the work by El-Karoui et al. (14)], although low-frequency effects were reported in some (15, 16) but not all (17) studies.

Using the high temporal and spectral resolution of direct cortical recordings from subdural ECoG electrodes, we compared frontal and temporal cortical patterns of LF-ERPs and Hγs in five patients listening to trains of task-irrelevant auditory stimuli in two conditions. The conditions differed in the predictability of deviation from repetitive background stimuli (fully predictable: four standards always followed by a deviant vs. unpredictable: deviants randomly embedded in trains of standard stimuli). Subjects were instructed to ignore the sounds and watch a visual slideshow. We focused on the amplitude and latency variation of both LF-ERPs and Hγs as metrics of the PE (mismatch signal). Based on previous findings, we hypothesized that Hγ activity signals the mismatch earlier than LF-ERPs and that the temporal (auditory) cortices

---

Significance

To survive, organisms must constantly form predictions of the future based on past regularities. When predictions are violated, action may be needed. Different scales of environmental regularity need to encompass both subsecond repetitions and complex structures spanning longer timescales. How different parts of the brain monitor these temporal regularities and produce prediction error signals is unclear. Utilizing subdural electrocorticographic electrodes with an auditory paradigm involving local and global regularities, we show that frontal cortex is sensitive to the big picture, responding with high γ-band activity exclusively to globally unpredictable changes, whereas the temporal cortex equally responds to any change in the immediate history. These results reveal a hierarchy of predictive coding recorded directly from the human brain.

NEUROSCIENCE

would be sensitive to local probabilities and not affected by the predictable vs. unpredictable manipulation. In contrast, the frontal cortex, assumed to be sensitive to higher-order regularities, would be differently affected by periodic vs. nonperiodic deviations. This differential frontal response could be either a stronger response to predictable than unpredictable deviants, signaling a mechanism of suppression of orienting response toward the expected repeating deviant, or a stronger response to unpredictable deviants compared with predictable deviants, signaling the PE.

Results

Participants ($n = 5$) (*Methods*) listened to sound trains of high-probability standards ($P = 0.8$; $F_0 = 500$ Hz) mixed with low-probability deviants ($P = 0.2$; $F_1 = 550$ Hz) in blocks of 400 sounds, with a stimulus onset asynchrony (SOA) of 600 ms. The order of the sounds was either pseudorandom, with a minimum of three standard tones before a deviant, or regular, such that exactly every fifth sound was a deviant (Fig. 1*A*). Thus, in the regular condition, deviants were fully predictable, whereas in the irregular condition, exact prediction was not possible. In both conditions, the participants were instructed to ignore the sounds and watch a slideshow of a variety of visual images changing at an unpredictable slow pace (~3 s per picture; unsynchronized with the auditory stimuli). The pictures were displayed on a liquid crystal display (LCD) monitor positioned over the patient's bed. Channel time series were used for the following analysis steps that are explained in more detail in *Methods*. We first selected channels showing stimulus-responsive activity modulation in the Hγ and the LF-ERP band (*Methods, I: Stimulus-responsive activity modulation* and Fig. 1). In each of these channels, we calculated a time point by time point ANOVA on stimulus type (standard or deviant) and determined the $F_{stimulus\ type}$ value time series (*Methods, II: Mismatch signal*). We used a principal component analysis (PCA) and found the course of $F_{stimulus\ type}$ across time accounting for the highest variance within the set of stimulus-responsive channels (*Methods, III: PCA*). We selected channels loading highly on the principal component (*Methods, IV: Data reduction*). We then compared time points of onset and peak (maximal) F values across channels (*Methods, V: Comparison of mismatch signal timing*) and verified the results on a group level (within subject) [*Methods, VI: Group (within-subject) analysis*]. We verified that differences in onset and peak latency between frequency bands are independent of anatomical locations [region of interest (ROI)] (*Methods, VII: ROI-specific analysis*). Finally, we tested in which anatomical location a predictability effect is represented (*Methods, VIII: Predictability effect*). In *Methods*, we provide detailed descriptions of each of these steps. The steps were taken separately for the LF-ERPs and Hγ signals. We studied 287 channels across all subjects. Stimulus-related activity was found for the Hγ ($n = 40$ channels; 13%) and the LF-ERP ($n = 116$ channels; 40%) (Table 1 shows numbers of stimulus-responsive channels per subject) bands across multiple frontal and temporal recording sites (Fig. 1*B*). The $F_{stimulus\ type}$ values in highly loading LF-ERP channels ($n = 14$) passed the empirical threshold around 143 ms (SD across channels = 44.9 ms) and peaked around 221 ms on average (SD = 8.8 ms) (Fig. 1*C*); the small SD is because of the fact that these are the channels loading highly on a single temporal PCA component. That is, these channels should necessarily have high resemblance in their temporal structure. F values in stimulus-responsive Hγ channels loading highly on the first Hγ principal component ($n = 7$) passed the empirical threshold around 72 ms (SD = 34 ms) and peaked around 141 ms on average (SD = 9 ms). The temporal differences between LF-ERP and Hγ for onset latency ($t_{20} = 3.8$; $P = 0.0011$) as well as for peak F values ($t_{20} = 13.92$; $P < 0.0001$) (Fig. 1*C*) across channels were significant. These differences were replicated in a within-subject group analysis (Hγ: 100.8 ms; SD = 70.4 ms; LF-ERP: 286.1 ms; SD = 140.2 ms; Wilcoxon rank sum test for onset $P = 0.024$; peak latency difference: Hγ: 139.3 ms; SD = 90.3 ms; LF-ERP: 343.5 ms; SD = 168.1 ms; Wilcoxon rank sum test for peak $P = 0.039$) (Fig. 1*D*).
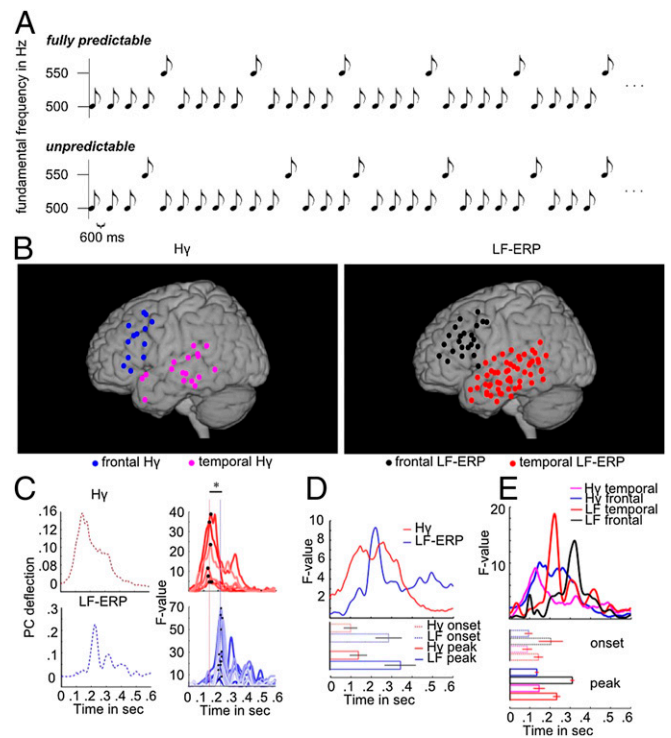
Fig. 1. Temporal profile of mismatch signal of Hγ and LF-ERP bands. (*A*) Participants listened to stimuli consisting of 180-ms-long (10 ms rise and fall time) sounds. High-probability standards (500 Hz) mixed with low-probability deviants [550 Hz; stimulus onset asynchrony (SOA) = 600 ms] were presented either unpredictably (pseudorandom sequence: minimum three consecutive standards) or fully predictable (regular: exactly every fifth sound was a deviant). (*B*) Stimulus-responsive regions in the Hγ and low-frequency (LF) band for all subjects. *C, Left* shows the principal components (PCs) of F-value time series of all task active channels for (*Upper*) the Hγ and (*Lower*) the LF bands. *C, Right* shows channels of $F_{stimulus\ type}$ time series of highly loading channels. Differences in color were chosen to better distinguish the F time course of different channels. The time course of the PC reveals a statistically significant difference (asterisk) in latency with an earlier maximum of the peak F values (black dots) in the Hγ band than in the LF-ERP band. (*D, Upper*) Averaged subject-specific F-value time course for the Hγ (red) and event-related potential (blue). (*D, Lower*) Onset and peak latency of PCs. Onset and peak latencies differ significantly across subjects between Hγs and LF-ERPs. Error bars indicate the SE across subjects. *E, Upper* shows $F_{stimulus\ type}$ time series separately averaged across highly loading frontal Hγ (magenta), temporal Hγ (blue), temporal LF (black), and frontal LF channels (red). (*E, Lower*) Mean onset and peak latencies of F values for each frequency band and anatomical ROI (Table 2 shows mean onset and peak latency). Error bars show SE across channels.

ROI Analysis. We tested for the differential effect of the mismatch signal over frequency bands, comparing electrodes placed over the lateral temporal lobe and electrodes placed over the lateral frontal cortex. Fig. 2 shows the $F_{stimulus\ type}$ variation across time averaged across highly loading channels separately for the frontal and temporal Hγ and LF-ERP bands. We found a significant effect of frequency band ($F_{onset} = 6.53$; $P = 0.02$ and $F_{peak} = 27.5$; $P < 0.0001$; df = 1, 28) (Fig. 2 and Table 2 show average onset and peak latencies of Hγ and LF-ERP band differences between ROIs) but no main effect of ROI or effect of interaction ($P > 0.1$). Hence, Hγ activity shows an earlier discrimination between deviants and standards than LF-ERP in both lateral temporal and frontal cortex.

Predictability Effects. Fig. 2 shows the amplitude variation (averaged across highly loading channels) in response to standard and deviant trials for the LF-ERP and the Hγ band in the frontal and temporal ROIs together with the time point by time point F statistic for the

Dürschmid et al.

Table 1. Number of stimulus-responsive LF-ERPs and Hγ channels per subject

Patient	Stimulus-responsive LF-ERP channels (temporal/frontal/parietal)	Stimulus-responsive Hγ channels (temporal/frontal/parietal)	Total no. of electrodes*
I	31 (14/12/5)	18 (6/7/5)	60
II	25 (12/1/12)	6 (4/1/1)	59
III	19 (10/5/4)	9 (4/3/2)	52
IV	10 (4/3/3)	2 (1/1/0)	56
V	31 (17/2/12)	5 (2/1/2)	60
$\sum$	116	40	287

*Excluding electrodes rejected for epileptic activity or excessive artifacts.

main effects of stimulus type, predictability, and their interaction across highly loading channels. Because the channels were selected to show a stimulus type effect in the first stages of the analysis, significance values of the main effect of stimulus type in this analysis may be inflated. However, the focus here is on the critical effects of predictability on neural responses. Table 3 summarizes maximal F values and corresponding P values for each ROI and frequency band. The threshold F value derived from the empirical distribution center is around 4.4 for all tests. LF-ERPs differentiate between standards and deviants starting around 200 ms but do not show amplitude variation as a function of predictability (Fig. 2) or an interaction between stimulus type and predictability. In contrast, the frontal Hγ channels show an effect of interaction between stimulus types (standards vs. deviants) and predictability (Fig. 2) driven by the stronger response to deviants than standards when the deviants were unpredictable than when they were predictable. The corresponding within-subject analysis also revealed a significant interaction in frontal but not the temporal sites for Hγ activity (Fig. S1) as indicated by a strong Hγ mismatch response (MMR) to unpredictable deviants but nearly no MMR for predictable deviations in frontal electrodes. Furthermore, only frontal Hγ showed sustained activity (*Methods* and Fig. S2). These results indicate that frontal Hγ discriminates between predicted and unpredicted deviants, with a selective response to unpredicted deviations.

Discussion

We examined the role of frontal and temporal cortices in generation of a PE signal for auditory deviants operationalized as the difference between the response to deviant and standard stimuli. Deviations from auditory background stimuli modulated the response to the sounds in both the lower frequencies event-related potentials, typically associated with the scalp-recorded MMN, and the power of the Hγ band recorded directly from the cortex. The PE signal emerged earlier in the Hγ amplitude than in the LF-ERPs and was evident at both temporal and frontal channel locations. However, only the frontal cortex Hγ differentiated between fully predictable and unpredictable deviations, emphasizing the key role of frontal cortex in PE.

The effect that we found with ECoG started at ~140 ms and peaked at 230 ms. Previous scalp MMN studies reported response differences between standard and deviant stimuli onsetting and peaking between 100 and 250 ms (reviewed in ref. 18). The LF-ERPs effects observed in our study are at the longer latency range of these scalp findings, which may reflect the difference between scalp and epicortical recordings. For example, most studies of MMN have not dissociated N1 refractoriness effects from the memory-based MMN (19, 20). When measures are taken to isolate the MMN from N1 refractoriness effects, the MMR has a longer latency than when the traditional MMN (deviant–standard) derivation is used (20–23). We used the traditional contrast of deviant–standard. However, our ECoG electrodes, located on the lateral surface of the brain, are less sensitive to refractoriness-sensitive N1 or earlier (24) sources located on the supratemporal plane within the sylvian fissure (25, 26) than at frontal/central scalp electrodes, where the scalp MMN is typically measured. Hence, whereas ECoG allows high

accuracy in spatial localization of effects, scalp recordings may provide a more global picture of the evolution of deviance related activity in time at the cost of spatial uncertainty. In addition, we cannot rule out the possibility that the special conditions of ECoG intensive care unit recordings might have slowed neural responses relative to laboratory conditions typical of EEG.

Studies using the mismatch paradigm with scalp EEG or magnetoencephalography (MEG) support the presence of separate temporal and frontal generators of the MMR (3, 27, 28).
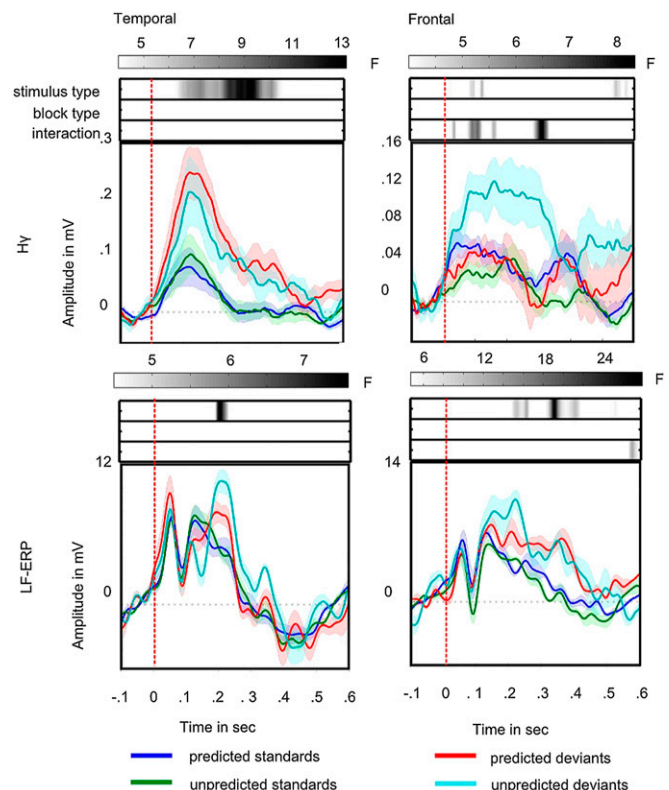
Fig. 2. Predictability effect. Frontal and temporal Hγ and LF-ERP activities differ with respect to effect of predictability. Colored lines show the evoked response to stimuli separately for frontal and temporal Hγs and LF-ERPs. Zero marks the auditory stimulus presentation. Blue lines show response to fully predictable standards, green lines show response to unpredictable standards, red lines show response to fully predictable deviants, and cyan lines show response to unpredictable deviants. Shaded areas denote the SE across highly loading channels. Corresponding *F*-value time series for the ANOVA across channels are set above, depicting the strength of statistical significance of the main effect for stimulus type (first row), the main effect for predictability (second row), and the effect of interaction (third row) in gray scale. Darker shades denote higher *F* values; time windows with *F* values smaller than the corresponding statistical significance threshold are shown in white.

NEUROSCIENCE

Table 2. Onset and peak F values

Amplitude	Hγ frontal	Hγ temporal	LF-ERP frontal	LF-ERP temporal
Onset	92	85	202	141
Onset SD	31	65	102	68
Peak	132	143	306	229
Peak SD	15	85	20	59

Summary of mean latency and SD of peak *F*-value latency across channels per ROI and frequency band in milliseconds.

However, because of the ill-posed inverse problem, EEG and MEG are not well-suited for localizing brain sources with certainty or spatially resolving adjacent sources. Moreover, recording high-frequency activity from the scalp is limited by low signal to noise ratio in this band (7, 8). Functional MRI data using similar paradigms support the presence of both temporal and prefrontal activity, but whether they have distinct response profiles could not be clearly discerned, partly because of the lack of temporal resolution of functional MRI (3, 29).

The use of intracranial recording directly from the surface or depth of the cortex allows simultaneously high spatial and temporal resolution of local neural activity in the human cortex. Previous intracranial findings using a mismatch paradigm have converged on showing responses to deviants over the STG (30, 31). In contrast, although some studies reported MMRs over inferior frontal cortex, others did not find such evidence (3), perhaps because of the sparse and variable spatial sampling of ECoG, and in some cases, the reported frontal responses could have been caused by volume conduction from temporal sources (15). Most of these previous studies have only examined low-frequency event-related responses. However, Edwards et al. (12) have also shown that broadband temporal Hγ responses to deviants are stronger than for standards. Eliades et al. (31) suggested that this effect is a result of adaptation to the repeating standard. Our results, showing clear deviant-related responses over both the temporal and frontal cortex for both frequency bands, support a frontal cortex contribution to the MMR. Moreover, the dissociation between the pattern of response to the predictable and unpredictable stimuli across the two regions provides evidence for distinct processing in these two regions.

Indeed, the major finding of our study is that predictability affected the PE response of the frontal cortex as measured by the Hγ activity, whereas no such modulation was found in temporal electrodes. Although the response measured over temporal cortex revealed a mismatch signal, regardless of the global structure of the sequence (i.e., its predictive value), the frontal PE was seen almost exclusively in response to unpredictable deviants.

The lack of predictability effects at the level of the auditory cortex is in line with previous scalp EEG studies using a similar task design. Volosin and Horváth (32) found the P3 response to be sensitive to periodicity, whereas early components, such as the N1 and the MMN, which are generated by sources in the auditory cortex, are unaffected, especially when participants were instructed to ignore the auditory stimulation (33, 34). Effects of predictability at the MMN time window also depend on the interstimulus interval (ISI). Sussman et al. (35) found that the scalp MMN was suppressed when the sequence in the fully predictable condition had very short ISIs (100 ms), such that repeating sequences of stimuli could be integrated and perceived as united auditory objects. In contrast, longer ISIs, in the range used here, yielded similar MMN amplitudes in response to both fully predictable and unpredictable deviants. One explanation for the dissociation between predictable and unpredictable deviants that we found at the frontal sites could be that the frontal cortex integrates over longer timescales than the auditory cortex. Under this premise, although for the auditory cortex, with the ISIs used, the unit of processing would be the individual tone and the deviant tone would be an oddball in both predictable and unpredictable sequences, for the frontal cortex, the predictable

sequence would be seen as repeating identical units, each composed of four low tones and one high tone.

A recent intracranial study using depth electrodes also examined local and global deviations. El-Karoui et al. (14) used a design in which local and global deviations were embedded in the same sequence. Trials were composed of a rapid sequence (SOA = 150 ms) of either five identical tones (SSSSS) or four identical tones followed by one deviant tone (SSSSD). In some blocks, SSSSS trials were frequent (80%), and SSSSD trials were rare (20%), whereas in the other blocks, this probability was reversed. The final D tone compared with a final S tone represents local deviation in either block. It was also a global deviant when the SSSSD trials were rare. The final S tone is always a local standard, but it represents a global deviant when SSSSS trials are rare and a global standard when SSSSS trials are frequent, arguably allowing for a pure measurement of a global effect. For local deviations, both LF-ERP responses and broadband Hγ responses were restricted to mainly superior temporal lobe contacts, with the exception of one frontal electrode that showed Hγ response. In contrast, global deviations elicited more widespread and protracted responses, including low-frequency effects and Hγ augmentation in temporal and left frontal contacts and a frontotemporoparietal depression in the β-band.

In our study, all deviants may be considered local deviants, but only in the nonpredictive block are they also global deviants. Consistent with the work by El-Karoui et al. (14), in our study, both local and global deviations elicited a response in both the LF-ERP and Hγ bands in lateral temporal contacts. Furthermore, in both studies, global deviations included a significant frontal cortex response. However, unlike in the work by El-Karoui et al. (14), we observed an LF-ERP frequency response to local deviation (predictable or not) in frontal electrodes, as did others (15, 16, 36). There are two limitations that preclude direct comparisons between our study and the work by El-Karoui et al. (14). First, our study compared responses to predictable and unpredictable tones that were both irrelevant to the task and in an unattended modality. This scenario probed the automatic response to the environment to enable orienting attention to critical or unexpected events. The global deviation in the study by El-Karoui et al. (14) was the target, and subjects had to count and memorize the total number of global deviations. Consequently, their global effect is a target-related response and not an automatic response. Second, although the design of the study by El-Karoui et al. (14) was a 2 × 2 design, they only examined the main effects of local and global deviation and did not examine the interaction that would be important if local deviants elicit stronger responses in blocks when they are also global deviants.

The findings of earlier responses in the γ-band than in the lower frequencies are consistent with the findings in the work by Crone et al. (11), which found that the functional response properties of Hγ

Table 3. F values per ROI and frequency band

Effect type	Temporal	Frontal
Hγ		
ME$_{st}$	$F_{(1,32)} = 13.9$; $P < 0.00001$*	$F_{(1,20)} = 5.07$; $P = 0.004$*
ME$_{bt}$	n.s.	n.s.
IE$_{st-x-bt}$	n.s.	$F_{(1,20)} = 8.2$; $P < 0.00001$*
LF-ERP		
ME$_{st}$	$F_{(1,24)} = 7.56$; $P = 0.011$*	$F_{(1,8)} = 27.86$; $P < 0.00001$*
ME$_{bt}$	n.s.	n.s.
IE$_{st-x-bt}$	n.s.	n.s.

Summary of maximal *F* values per ROI and frequency band and corresponding *P* values. Only significant *F* values are reported. Differences in df are because of the different numbers of significant electrodes selected per ROI and frequency band. IE$_{st-x-bt}$, effect of interaction between stimulus type and block type; ME$_{bt}$, main effect of block type; ME$_{st}$, main effect of stimulus type; n.s., not significant.
*Statistically significant.

activity are distinct from lower-frequency modulations in timing and spatial location. Specifically, lower frequencies, such as α-activity, reach peak amplitude later than Hγ. The fact that Hγ activity signals the PE earlier than LF-ERPs in our data could be because of enhanced signal to noise ratio in the higher band. However, the distinct effect of predictability, found only in the Hγ signals, suggests that the two frequency bands reflect different neuronal mechanisms.

Limitations and Future Research. We did not find sensitivity to periodic structure in auditory cortex contacts, such as it was shown for the rat or macaque auditory cortex (37, 38). Yaron et al. (37) found neurons responding differently to fully predictable and unpredictable standards and deviants. However, the largest fraction of neurons in the rat auditory cortex responded similarly in the fully unpredictable condition. The registered cortical signal in ECoG recordings is determined by population activity. Hence, the activity patterns of a minority of neurons may be missed by ECoG macroelectrodes. Nevertheless, even if a periodicity effect in the human temporal cortex is present at a finer neuronal level, this effect is more prominent in the human frontal cortex.

The predictability in our study results from periodicity–every fifth sound was a deviant. However, context effects on the MMN or adaptation can be experimentally studied by manipulating different sources of expectation, which may depend on dissociable neural mechanisms. For example, Todd et al. (39, 40) found that, when the identities of the standard and deviants were switched during the experiment, the MMN for the initial order was larger than for the subsequent order, especially when longer sequences were played before the switch. This "primacy effect" suggests a long-term memory of the initial standard. Other studies found that, for fast, isochronous sequences (SOA = 150 ms), two MMNs occur for a pair of deviants only when some deviants also occur alone (41, 42), suggesting that, when the second deviant is highly expected, MMN is attenuated. This expectancy suppression seems to be dissociable from pure repetition suppression (43). Another source of expectancy may depend on the variance of the standards (44).

Our critical conclusion is that frontal and temporal cortices have different functions in signaling the deviation or PE. Frontal Hγ selectively signals unpredictable deviants with sustained Hγ activation, whereas temporal Hγ shows responses to both unpredictable and fully predictable deviants. This result highlights a selective role of frontal structures in computing a PE. A feature-based adaptation mechanism, as seen in the auditory cortex (13, 31, 45), is expected to produce a response independent of the degree of periodicity of occurrence of deviants. Because on average, the probability of stimuli in the predictable and unpredictable sequences was identical, a purely adaptation-based model (31) would not predict the differential activity that we found in frontal electrodes. Thus, the frontal cortex Hγ provides evidence of a selective PE to unpredictable events. The selective Hγ amplitude modulation to unpredictable deviants might also reflect a switch of attention (4). However, both functional explanations (selective response to unpredictable events or a switch of attention) indicate that frontal Hγ activity reflects a mechanism that tracks the expected input and generates a response when predictions are violated.

In sum, our findings support the notion that Hγ activity in the frontal cortex signals detection of unpredictable deviations from the auditory background.

Methods

Patients. Five epilepsy patients (mean age = 33 y old; SD = 9.23) undergoing presurgical monitoring with subdural electrodes participated in the experiment after providing their written informed consent. Experimental and clinical recordings were taken in parallel. Recordings took place at the University of California, San Francisco and approved by the local ethics committees (Committee for the Protection of Human Subjects at the University of California, Berkeley).

Stimuli. Participants listened to stimuli consisting of 180-ms-long (10 ms rise and fall time) harmonic sounds with a fundamental frequency (F_0) of 500 or 550 Hz and the three first harmonics with descending amplitudes (−6, −9, and −12 dB relative to the fundamental). The stimuli were generated using Cool Edit 2000 software (Syntrillium). The stimuli were presented from loudspeakers positioned at the foot of the subject's bed at a comfortable loudness. High-probability standards ($P = 0.8$; $F_0 = 500$ Hz) were mixed with low-probability deviants ($P = 0.2$; $F_1 = 550$ Hz) in blocks of 400 sounds, with an SOA of 600 ms (Fig. 1A). The order of the sounds was either pseudo-random, with a minimum of three standard tones before a deviant, or regular, such that exactly every fifth sound was a deviant. Thus, in the regular condition, deviants were fully predictable, whereas in the irregular condition, exact prediction was not possible. In both conditions, the participants were instructed to ignore the sounds and watch a slideshow of a variety of visual images changing at an unpredictable slow pace (~3 s per picture; unsynchronized with the auditory stimuli). The pictures were displayed on an LCD monitor positioned over the patient's bed.

Data Processing. Details of data recording and data preprocessing are in *SI Methods*. The resulting time series were used to characterize brain dynamics over the time course of auditory mismatch detection in terms of the LF-ERPs and Hγ activity. For each trial (−1–2 s around stimulus onset—sufficiently long to prevent any edge effects during filtering), we band pass filtered each electrode's time series at two frequency bands: a low-frequency band (LF-ERP; the "LF-ERP range" traditionally used for scalp MMN studies) and a high-frequency band (Hγ range: 80–150 Hz) (selection of frequency bands is discussed below and in *Fig. S3 A and B*). We obtained the Hγ analytic amplitude $A_{HG}(t)$ by Hilbert transforming the Hγ filtered time series. We smoothed both the LF-ERP and the Hγ band time series, such that amplitude value at each time point n is the mean of 10 ms around each time point n. We then baseline corrected the trial activity by subtracting the mean activity from the 100 ms preceding the stimulus onset in each trial of each channel.

I: Stimulus-responsive activity modulation. We first identified stimulus-responsive channels showing a significant (compared with an empirical distribution; see below) amplitude modulation in either the Hγ or LF-ERP band or both after the onset of standard stimuli, deviant stimuli, or both. Standard and deviant trials were averaged separately. For each type of stimulus, we first calculated the average baseline activity $\overline{B}_{H\gamma}$ and $\overline{B}_{LF}$ across 100 ms preceding the stimulus onset. For the Hγ activity, we subtracted $\overline{B}_{H\gamma}$ from the activity modulation $\overline{A}_{H\gamma}$ averaged across 250 ms after the stimulus onset (Fig. S3C). For the LF-ERP band, we subtracted $\overline{B}_{LF}$ from the activity modulation $\overline{A}_{LF}$ in three different intervals centered on the main peaks of the mean response (I, 0–60 ms; II, 60–120 ms; and III, 120–250 ms in Fig. S3C). This early time window allowed us to select fast-responding channels in both frequency ranges (confirmation that the selected length of stimulus response intervals had no effect on the selection stimulus-responsive channels is in *SI Methods* and *Fig. S4*). The difference between $\overline{B}$ and $\overline{A}$ was compared against an empirical distribution (*SI Methods*).

II: Mismatch signal. Within each stimulus-responsive channel and separately for Hγs and LF-ERPs, we carried out a one-way ANOVA with factor stimulus type (standard vs. deviant) at each time point, with single trials as random variable. This analysis yielded a time series of F values for each channel representing the main effect of stimulus type between −100 and 600 ms. In both conditions, we left out the first two trains, because the periodicity can only be detected after a repeated completion of whole trains of stimuli. The F value of the main effect "stimulus type" parameterizes the mismatch signal with high F values, indicating a large difference in amplitude between the standard and deviant stimuli. To set a threshold for significant difference, an empirical distribution of the main effect was constructed by randomly reassigning the labels (standard or deviant) to the single trials in 1,000 permutations.

III: PCA. Using a PCA, we identified consistent temporal patterns of Hγ/LF-ERP activity among the entire set of stimulus-responsive channels pooled across patients. The PCA was used to find the course of the mismatch signal ($F_{stimulus\ type}$) across time, accounting for the highest variance within the set of stimulus-responsive channels.

IV: Data reduction. Channel time series strongly resembling the mismatch signal determined in III (highly loading on the first principal component of the PCA) are those that exhibit large differences between standard and deviant stimuli in terms of amplitude. The degree of resemblance with the mismatch signal is given as Pearson's r. We chose Pearson's r exceeding the 75th percentile of all positive r values as the cutoff criterion for highly loading channels. We set this level as a tradeoff, because setting the criterion too high would exclude too many channels and reduce generalization across the cortex, whereas setting it too low would include channels with minor effects.

NEUROSCIENCE

V: Comparison of mismatch signal timing. In each highly loading channel (exceeding the cutoff criterion), we tested which frequency band (LF-ERP vs. Hγ) showed a mismatch signal first by determining the onset and peak latency of significant F values. The onset latency of the mismatch signal was determined as the first point in which the F value exceeded the confidence interval of the empirical distribution. Both latency of maximal F values in the Hγ and LF-ERP band and the onset of significant F values were used to quantify temporal differences of the PE between the frequency bands. Onsets and peak latencies were compared in a two-sample (because of different numbers of channels per frequency band) t test comparing the two frequency bands.

VI: Group (within-subject) analysis. To verify that the results presented are valid at a group level and not driven by single subjects, a PCA was used in each subject to find the course of the mismatch signal across time, accounting for the highest variance for both the LF-ERP and the Hγ bands. The onset and peak latencies of the LF-ERP and Hγ principal components were compared in a within-subject analysis using a Wilcoxon rank sum test.

VII: ROI-specific analysis. In the next step, we tested whether differences regarding the onset and maximum of deviance detection between frequencies depend on anatomical locations. An interaction between the frequency band and the ROI effects would indicate such dependence. The pool of all LF-ERP and Hγ stimulus-responsive channels were grouped according to a frontal and temporal ROI to analyze ROI-specific patterns of PE. Steps III and IV were then performed separately

for each ROI. We determined the peak and onset latencies of the mismatch signals for each channel and frequency band as described in step V and conducted a two-way ANOVA across channels with the factors frequency band (Hγ vs. LF-ERP) and ROI (temporal vs. frontal).

VIII: Predictability effect. Finally, to test the effect of the predictability of deviance, we used a time point by time point ANOVA to look for an interaction of the block type (predictable and unpredictable) with the effect of stimulus type across channels separately for each ROI and frequency band limited to the channels that loaded highly on the first principal component (from step IV). Because the channels were selected to show a stimulus type effect in the first stages of the analysis, significance values of the main effect of stimulus type in this analysis may be inflated ("double dipping" effect). However, the critical effects of predictability and the interaction are not. The significance values were assessed using bootstrap procedures as outlined above.

1. Rao RP, Ballard DH (1999) Predictive coding in the visual cortex: A functional interpretation of some extra-classical receptive-field effects. *Nat Neurosci* 2(1):79–87.
2. Näätänen R, Gaillard AW, Mäntysalo S (1978) Early selective-attention effect on evoked potential reinterpreted. *Acta Psychol (Amst)* 42(4):313–329.
3. Deouell LY (2007) The frontal generator of the mismatch negativity revisited. *J Psychophysiol* 21(3-4):188–203.
4. Shalgi S, Deouell LY (2007) Direct evidence for differential roles of temporal and frontal components of auditory change detection. *Neuropsychologia* 45(8):1878–1888.
5. MacDonald AW, 3rd, Cohen JD, Stenger VA, Carter CS (2000) Dissociating the role of the dorsolateral prefrontal and anterior cingulate cortex in cognitive control. *Science* 288(5472):1835–1838.
6. Fogelson N, Shah M, Scabini D, Knight RT (2009) Prefrontal cortex is critical for contextual processing: Evidence from brain lesions. *Brain* 132(Pt 11):3002–3010.
7. Muthukumaraswamy SD (2013) High-frequency brain activity and muscle artifacts in MEG/EEG: A review and recommendations. *Front Hum Neurosci* 7:138.
8. Yuval-Greenberg S, Tomer O, Keren AS, Nelken I, Deouell LY (2008) Transient induced gamma-band response in EEG as a manifestation of miniature saccades. *Neuron* 58(3):429–441.
9. Crone NE, Miglioretti DL, Gordon B, Lesser RP (1998) Functional mapping of human sensorimotor cortex with electrocorticographic spectral analysis. II. Event-related synchronization in the gamma band. *Brain* 121(Pt 12):2301–2315.
10. Miller KJ, et al. (2007) Spectral changes in cortical surface potentials during motor movement. *J Neurosci* 27(9):2424–2432.
11. Crone NE, Sinai A, Korzeniewska A (2006) High-frequency gamma oscillations and human brain mapping with electrocorticography. *Prog Brain Res* 159:275–295.
12. Edwards E, Soltani M, Deouell LY, Berger MS, Knight RT (2005) High gamma activity in response to deviant auditory stimuli recorded directly from human cortex. *J Neurophysiol* 94(6):4269–4280.
13. Fishman YI, Steinschneider M (2012) Searching for the mismatch negativity in primary auditory cortex of the awake monkey: Deviance detection or stimulus specific adaptation? *J Neurosci* 32(45):15747–15758.
14. El Karoui I, et al. (2015) Event-related potential, time-frequency, and functional connectivity facets of local and global auditory novelty processing: An intracranial study in humans. *Cereb Cortex* 25(11):4203–4212.
15. Rosburg T, et al. (2005) Subdural recordings of the mismatch negativity (MMN) in patients with focal epilepsy. *Brain* 128(Pt 4):819–828.
16. Liasis A, Towell A, Alho K, Boyd S (2001) Intracranial identification of an electric frontal-cortex response to auditory stimulus change: A case study. *Brain Res Cogn Brain Res* 11(2):227–233.
17. Baudena P, Halgren E, Heit G, Clarke JM (1995) Intracerebral potentials to rare target and distractor auditory and visual stimuli. III. Frontal cortex. *Electroencephalogr Clin Neurophysiol* 94(4):251–264.
18. Näätänen R, Paavilainen P, Rinne T, Alho K (2007) The mismatch negativity (MMN) in basic research of central auditory processing: A review. *Clin Neurophysiol* 118(12):2544–2590.
19. Schröger E, Wolff C (1996) Mismatch response of the human brain to changes in sound location. *Neuroreport* 7(18):3005–3008.
20. Jacobsen T, Schröger E (2001) Is there pre-attentive memory-based comparison of pitch? *Psychophysiology* 38(4):723–727.
21. Ruhnau P, Herrmann B, Schröger E (2012) Finding the right control: The mismatch negativity under investigation. *Clin Neurophysiol* 123(3):507–512.
22. Jacobsen T, Schröger E, Horenkamp T, Winkler I (2003) Mismatch negativity to pitch change: Varied stimulus proportions in controlling effects of neural refractoriness on human auditory event-related brain potentials. *Neurosci Lett* 344(2):79–82.
23. Hsu WY, et al. (2010) Memory-based mismatch response to changes in duration of auditory stimuli: An MEG study. *Clin Neurophysiol* 121(10):1744–1750.
24. Grimm S, Escera C (2012) Auditory deviance detection revisited: Evidence for a hierarchical novelty system. *Int J Psychophysiol* 85(1):88–92.
25. Alho K (1995) Cerebral generators of mismatch negativity (MMN) and its magnetic counterpart (MMNm) elicited by sound changes. *Ear Hear* 16(1):38–51.
26. Huotilainen M, et al. (1998) Combined mapping of human auditory EEG and MEG responses. *Electroencephalogr Clin Neurophysiol* 108(4):370–379.
27. Giard MH, Perrin F, Pernier J, Bouchet P (1990) Brain generators implicated in the processing of auditory stimulus deviance: A topographic event-related potential study. *Psychophysiology* 27(6):627–640.
28. Deouell LY, Bentin S, Giard MH (1998) Mismatch negativity in dichotic listening: Evidence for interhemispheric differences and multiple generators. *Psychophysiology* 35(4):355–365.
29. Opitz B, Rinne T, Mecklinger A, von Cramon DY, Schröger E (2002) Differential contribution of frontal and temporal cortices to auditory change detection: fMRI and ERP results. *Neuroimage* 15(1):167–174.
30. Deouell LY, Deutsch D, Scabini D, Soroker N, Knight RT (2008) No disillusions in auditory extinction: Perceiving a melody comprised of unperceived notes. *Front Hum Neurosci* 1:15.
31. Eliades SJ, et al. (2014) Adaptation of high-gamma responses in human auditory association cortex. *J Neurophysiol* 112(9):2147–2163.
32. Volosin M, Horváth J (2014) Knowledge of sequence structure prevents auditory distraction: An ERP study. *Int J Psychophysiol* 92(3):93–98.
33. Sussman E, Winkler I, Huotilainen M, Ritter W, Näätänen R (2002) Top-down effects can modify the initially stimulus-driven auditory organization. *Brain Res Cogn Brain Res* 13(3):393–405.
34. Scherg M, Vajsar J, Picton TW (1989) A source analysis of the late human auditory evoked potentials. *J Cogn Neurosci* 1(4):336–355.
35. Sussman E, Ritter W, Vaughan HG, Jr (1998) Predictability of stimulus deviance and the mismatch negativity. *Neuroreport* 9(18):4167–4170.
36. Bekinschtein TA, et al. (2009) Neural signature of the conscious processing of auditory regularities. *Proc Natl Acad Sci USA* 106(5):1672–1677.
37. Yaron A, Hershenhoren I, Nelken I (2012) Sensitivity to complex statistical regularities in rat auditory cortex. *Neuron* 76(3):603–615.
38. Selezneva E, et al. (2013) Rhythm sensitivity in macaque monkeys. *Front Syst Neurosci* 7:49.
39. Todd J, Provost A, Cooper G (2011) Lasting first impressions: A conservative bias in automatic filters of the acoustic environment. *Neuropsychologia* 49(12):3399–3405.
40. Todd J, et al. (2014) What controls gain in gain control? Mismatch negativity (MMN), priors and system biases. *Brain Topogr* 27(4):578–589.
41. Sussman E, Winkler I (2001) Dynamic sensory updating in the auditory system. *Brain Res Cogn Brain Res* 12(3):431–439.
42. Tavano A, Widmann A, Bendixen A, Trujillo-Barreto N, Schröger E (2014) Temporal regularity facilitates higher-order sensory predictions in fast auditory sequences. *Eur J Neurosci* 39(2):308–318.
43. Todorovic A, de Lange FP (2012) Repetition suppression and expectation suppression are dissociable in time in early auditory evoked fields. *J Neurosci* 32(39):13389–13395.
44. Garrido MI, Sahani M, Dolan RJ (2013) Outlier responses reflect sensitivity to statistical structure in the human brain. *PLOS Comput Biol* 9(3):e1002999.
45. Ulanovsky N, Las L, Farkas D, Nelken I (2004) Multiple time scales of adaptation in auditory cortex neurons. *J Neurosci* 24(46):10440–10453.

Dürschmid et al.

Supporting Information

Dürschmid et al. 10.1073/pnas.1525030113

SI Methods

Data Recording. The ECoG was recorded at the University of California, San Francisco using 64 platinum–iridium–electrode grids arranged in an 8 × 8 array with 10-mm center to center spacing (Ad-Tech Medical Instrument Corporation) (grid location is shown in Fig. 1). Exposed electrode diameter was 2.3 mm. The data were recorded continuously throughout the task at a sampling rate of 2,003 Hz.

Data Preprocessing. We used Matlab 2013b (Mathworks) for all offline data processing. All filtering was done using zero-shift infinite impulse response (IIR) filters [Butterworth filter of order 4: filtfilt() function in Matlab]. We excluded channels exhibiting ictal activity or excessive noise from additional analysis. In the remaining "good" channels (Table 1), we then excluded time intervals containing artefactual signal distortions, such as signal steps or pulses, by visual inspection. Finally, we rereferenced the remaining electrode time series by subtracting the common average reference

$$x_{CAR}(t) = \frac{1}{n} \sum_{c=1}^{n} x_c(t)$$

calculated from each channel time series x_c.

Empirical Distribution of Stimulus-Responsive Activity Modulation. The difference between $\overline{B}$ and $\overline{A}$ was compared against an empirical distribution derived from randomly shifted time series (1,000 permutations). In each iteration, time series of each channel and each trial were shifted (circular shift of the entire trial time series between −0.1 and 0.6 s) separately, and new (surrogate) trial averages ($\overline{B}$ and $\overline{A}$) were calculated from the shifted trials. Channels exceeding the 97.5th percentile of the channel-specific surrogate $\overline{B}_{H\gamma} - \overline{A}_{H\gamma}$ distribution were classified as showing a significant Hγ modulation after the standard or deviant stimuli or both. Note that, in contrast to the analytic amplitude of the Hγ band, which is always equal or larger than zero, the LF-ERP band is a time series of activity and comprises both positive and negative going deflections (e.g., like P1-N1). Hence, channels with an LF-ERP amplitude modulation in interval I or III greater than the 97.5th percentile (significantly elevated amplitude over baseline) and channels with an LF-ERP amplitude modulation in interval II smaller than the 2.5th percentile were classified as showing a significant LF-ERP modulation after the standard or deviant stimuli or both. Extending the critical windows up to 300, 400, 500, or 600 ms did not affect the selection of channels or the principal components.

Selection of Frequency Bands. To test which frequency band was the most informative in signaling the PE, we filtered all time series of each channel in each trial in 39 bands between 2 and 180 Hz (log spaced), each with a bandwidth of 10% of the center frequency. We applied the same pipeline as in the main analysis up to stage V, except that all channels were included in this analysis (skipping stage I). On average, 8.15 channels were chosen in each frequency band (SD = 1.2) based on their high loading on the first principal component within each band. The profile of the response shows that the PE is concentrated in the low-frequency (∼1–20 Hz) and Hγ (∼80–150 Hz) range, whereas the response between 20 and 80 Hz is lower (Fig. S3). Thus, for the main analysis, a low (1–20 Hz) band and a high band (80–150 Hz) were tested (*Methods*).

Sustained Activity. Fig. 2 suggests that, in contrast to temporal activity, frontal Hγ activity to unpredictable deviants plateaus, indicating sustained activity. We tested posthoc whether frontal Hγ activity to unpredictable deviants persists longer than temporal Hγ (Fig. S4). Hence, we compared the length (time in milliseconds) of Hγ activity over baseline between the frontal and temporal ROIs across channels. We standardized frontal and temporal activity between zero and one.

With

$$Y_{roi} = X_{roi} - \min(X_{roi}),$$

we set Y_{roi}—denoting all time series of ECoG channels in a given ROI—above zero. The next step,

$$Z_{roi} = Y_{roi} \times \frac{1}{\max(Y_{roi})},$$

compresses all values of Y_{roi}, such that the resulting matrix Z_{roi} ranges between zero and one. This standardization preserves the typical time course but enables a joint baseline distribution (100 ms preceding stimulus presentation). We estimated the upper confidence interval (CI; $CI_{97.5\%}$) from the baseline distribution across all channels in both ROIs. For each channel, we determined the duration of activity over baseline (greater than $CI_{97.5\%}$) in milliseconds. The durations were compared in a t test between ROIs across channels. On average, Hγ activity measured in frontal electrodes persists longer over baseline ($M = 337$ ms; SD = 176 ms) than temporal Hγ ($M = 148$ ms; SD = 102 ms; $t_{15} = 2.85$; $P = 0.012$).

Fig. S1. Frontal and temporal Hγ differ with respect to effect of predictability on a group level. (*Middle*) Colored lines show the evoked response to stimuli separately for frontal and temporal Hγ. Zero marks the auditory stimulus presentation. Blue lines show response to fully predictable standards, green lines show response to unpredictable standards, red lines show response to fully predictable deviants, and cyan lines show response to unpredictable deviants. Shaded areas denote the SE across subjects. (*Top*) Corresponding *F*-value time series for the ANOVA across subjects were set, depicting the strength of statistical significance of the main effect for stimulus type (first row), the main effect for predictability (second row), and the effect of interaction (third row) in gray scale. *F* values smaller than the *F* value corresponding with the statistical significance threshold are shown in white. *Bottom* shows evoked Hγ responses of a representative subject (S03). Colored lines show the average across channel.

Fig. S2. Comparison of amplitude modulation time over baseline. (*Left*) Depiction of standardized amplitude modulation to unpredictable deviants of the Hγ (HG) band in the frontal (green) and temporal (blue) ROIs. We standardized the amplitude to (*i*) correct for differences in modulation and (*ii*) estimate the CI of a joint baseline distribution (red lines). (*Right*) Frontal Hγ amplitude was longer activated over baseline (>97.5%) than temporal Hγ amplitude.

Fig. S3. (*A*) Depiction of differences of mismatch signal as a function of frequency. Each line shows the average of highly loading channels on the frequency-specific principal component accounting for the highest variance across time. Note that the profile of the response (maximal *F*) displayed in *B* shows that the PE is concentrated at low frequency (LF; ~1–20 Hz) and Hγ (~80–150 Hz), whereas the response between 20 and 80 Hz is lower. (*C*) Depiction of grand averages of Hγ and LF amplitude modulation. In each frequency band, the amplitude modulation to the onset of auditory stimulation was averaged across trials and then, across all channels pooled across all subjects. In each frequency band, we compared the first 250 ms with 100 ms baseline preceding the onset of standard and deviant tones. We obtained the Hγ analytic amplitude $A_{HG}(t)$ by Hilbert transforming the Hγ filtered time series. Note that, in contrast to the analytic amplitude of the Hγ band, which is always equal to or larger than zero, the LF band is a time series of activity and has both positive and negative going deflections (e.g., like P1-N1). Hence, channels with an LF amplitude modulation in interval I or III greater than the 97.5th percentile (significantly elevated amplitude over baseline) and channels with an LF amplitude modulation in interval II smaller than the 2.5th percentile were classified as showing a significant LF-ERP modulation after the standard or deviant stimuli or both.

Fig. S4. Depiction of *F*-value time series averaged across stimulus-responsive channels as a function of length of activation period. Amplitude modulation of Hγ and low-frequency (LF) activity of 300–500 ms after stimulus onset was compared with baseline activity (−100–0 ms). Selected principal components estimated within the set of stimulus-responsive channels in each interval are similar.

ORIGINAL ARTICLE

Direct Evidence for Prediction Signals in Frontal Cortex Independent of Prediction Error

Stefan Dürschmid[1,2], Christoph Reichert[1,6], Hermann Hinrichs[1,2,3,4,5,6], Hans-Jochen Heinze[1,2,3,4,5,6], Heidi E. Kirsch[7], Robert T. Knight[8] and Leon Y. Deouell[9]

[1]Department of Behavioral Neurology, Leibniz Institute for Neurobiology, Brenneckestr. 6, 39120 Magdeburg, Germany, [2]Department of Neurology, Otto-von-Guericke University, Leipziger Str. 44, 39120 Magdeburg, Germany, [3]Stereotactic Neurosurgery, Otto-von-Guericke University, Leipziger Str. 44, 39120 Magdeburg, Germany, [4]German Center for Neurodegenerative Diseases (DZNE), Leipziger Str. 44, 39120 Magdeburg, Germany, [5]Forschungscampus STIMULATE, Otto-von-Guericke University, Universitätsplatz 2, 39106 Magdeburg, Germany, [6]CBBS—Center of Behavioral Brain Sciences, Otto-von-Guericke University, Universitätsplatz 2, 39106 Magdeburg, Germany, [7]Department of Neurology, University of California, 400 Parnassus Avenue, San Francisco, CA 94122, USA, [8]Helen Wills Neuroscience Institute and Department of Psychology, University of California, Berkeley, CA 94720, USA and [9]Edmond and Lily Safra Center for Brain Sciences and Department of Psychology, The Hebrew University of Jerusalem, Mount Scopus, Jerusalem 91904, Israel

Address correspondence to Stefan Dürschmid, Department of Behavioral Neurology, Leibniz Institute for Neurobiology, Brenneckestr. 6, 39120 Magdeburg, Germany. Email: stefan.duerschmid@googlemail.com and Leon Deouell, Edmond and Lily Safra Center for Brain Research and Department of Psychology, The Hebrew University of Jerusalem, Jerusalem 91904, Israel. Email: leon.deouell@mail.huji.ac.il

Abstract

Predictive coding (PC) has been suggested as one of the main mechanisms used by brains to interact with complex environments. PC theories posit top-down prediction signals, which are compared with actual outcomes, yielding in turn prediction error (PE) signals, which are used, bottom-up, to modify the ensuing predictions. However, disentangling prediction from PE signals has been challenging. Critically, while many studies found indirect evidence for PC in the form of PE signals, direct evidence for the prediction signal is mostly lacking. Here, we provide clear evidence, obtained from intracranial cortical recordings in human surgical patients, that the human lateral prefrontal cortex evinces prediction signals while anticipating an event. Patients listened to task-irrelevant sequences of repetitive tones including infrequent predictable or unpredictable pitch deviants. The broadband high-frequency amplitude (HFA) was decreased prior to the onset of expected relative to unexpected deviants in the frontal cortex only, and its amplitude was sensitive to the increasing likelihood of deviants following longer trains of standards in the unpredictable condition. Single-trial HFA predicted deviations and correlated with poststimulus response to deviations. These results provide direct evidence for frontal cortex prediction signals independent of PE signals.

Key words: frontal cortex, high gamma activity, predictive coding, prestimulus activity, temporal cortex

"Prediction is very difficult, especially if it's about the future"

Niels Bohr

Introduction

Making predictions about upcoming events is a crucial brain function. Predictive coding (PC) theories postulate that the brain iteratively optimizes an internal model of the environment based on sensory inputs (Rao and Ballard 1999; Bastos et al. 2012; Lee and Noppeney 2014; Heilbron and Chait 2018) and generates prediction error (PE) signals if predictions are violated (Winkler and Schröger 2015), to improve the future interaction with the environment. Most PC schemes suggest separate prediction and PE signals/neurons, but separating the 2 in practice has proved challenging (for a comprehensive introduction and review, see Heilbron and Chait (2018)). One important reason is that most evidence for an anticipatory pre-event prediction comes from the ultimate PE signals, elicited after the (un)predicted event has occurred. Hence, recording predictive signals prior to the onset of the stimuli would be strong evidence for prospective, active predictions.

A critical question is also whether predictions are formed automatically (by default) even when the stimuli are not attended. Here, we utilized the high-temporal and -spectral resolution of direct cortical recordings from subdural ECoG electrodes to compare frontal and temporal prediction signals in 5 patients exposed with trains of task-irrelevant and meaningless auditory stimuli in 2 conditions, while attending a visual slide show. The conditions differed in the predictability of deviation from repetitive background stimuli. In "regular" sequences, every deviant followed exactly 4 standards, whereas in "irregular" sequences, deviants were randomly embedded in trains of standard stimuli.

In a previous report, we concentrated on poststimulus activity variations as a response to fully predictable and unpredictable deviants (i.e., on the PE) using the same data set (Dürschmid et al. 2016). Here, we show that in frontal cortex modulation of prestimulus broadband high-frequency amplitude (HFA) heralds ensuing deviants and correlates with the poststimulus PE signal. In contrast, and commensurate with poststimulus activity, prestimulus activity in temporal cortex is insensitive to sequence statistics but reflects only the immediate history.

Methods

Patients

Five epilepsy patients (mean age 33, SD = 9.23) undergoing pre-surgical monitoring with subdural electrodes participated in the experiment after providing their written informed consent. Experimental and clinical recordings were taken in parallel. Recordings took place at the University of California, San Francisco (UCSF) and were approved by the local ethics committees ("Committee for the Protection of Human Subjects at UC Berkeley"). The analysis of the poststimulus effects from these patients with the same data set was previously reported by Dürschmid et al. (2016).

Stimuli

Participants listened to stimuli consisting of 180 ms long (10 ms rise and fall time) harmonic sounds with a fundamental frequency of 500 or 550 Hz and the 3 first harmonics with descending amplitudes (−6, −9, −12 dB relative to the fundamental). The stimuli were generated using Cool Edit 2000 software (Syntrillium). The stimuli were presented from loudspeakers positioned at the foot of the subject's bed at a comfortable loudness.

Procedure

While reclined in their hospital bed, participants watched an engaging slide show while sound trains were played in the background. Sound trains included high-probability standards (P = 0.8; f_0 = 500 Hz) mixed with low-probability deviants (P = 0.2; f_0 = 550 Hz) in blocks of 400 sounds, with a stimulus onset asynchrony (SOA) of 600 ms. In different blocks, the order of the sounds was either pseudorandom, with a minimum of 3 standard tones before a deviant (irregular condition), or regular, such that exactly every fifth sound was a deviant (Fig. 1A). Thus, under the regular condition, standards and deviants were fully predictable, whereas under the irregular condition, exact prediction was not possible.

Data Recording

The electrocorticogram (ECoG) was recorded at UCSF using 64 platinum–iridium electrode grids arranged in an 8 × 8 array with 10 mm center-to-center spacing (Ad-Tech Medical Instrument Corporation; see Fig. 2 for grid location). Grids were positioned based solely on clinical needs. Exposed electrode diameter was 2.3 mm. The data were recorded continuously throughout the task at a sampling rate of 2003 Hz.

Preprocessing

We used Matlab 2013b (The Mathworks) for all offline data processing. All filtering were done using zero phase-shift IIR filters. We excluded channels exhibiting ictal activity or excessive noise from further analysis. In the remaining "good" channels, we then excluded time intervals containing artifactual signal distortions such as signal steps of pulses by visual inspection. Finally, we rereferenced the remaining electrode time series by subtracting the common average reference

$$x_{CAR}(t) = \frac{1}{n} \sum_{c=1}^{n} x_c(t)$$

calculated over the n good channels c from each channel time series x_c. The resulting time series were used to characterize brain dynamics over the time course of auditory stimulus prediction. For each trial (−1 to 2 s around stimulus onset—sufficiently long to prevent any edge effects during filtering) we band-pass filtered each electrode's time series in the broadband high frequency range (80–150 Hz; see Supplementary Material). We obtained the analytic amplitude $A_f(t)$ of this band by Hilbert-transforming the filtered time series (HFA). We smoothed the HFA time series such that amplitude value at each time point t is the mean of 10 ms around each time point t. We then baseline-corrected by subtracting from each data point the mean activity of the −700 to −600 ms preceding the stimulus onset (i.e., 100 ms prior to trial $N − 1$) in each trial and each channel.

Prestimulus time series of HFA were used for the following analysis steps (explained in detail in the following). We first parameterized the prediction of upcoming stimuli as the interaction of Stimulus type (standard, deviant) and Block type (regular, irregular) using a time-resolved ANOVA ("I—Estimation of Prediction"). Next, we assessed the involvement of frontal or temporal cortices in this prediction effect ("II—Comparison
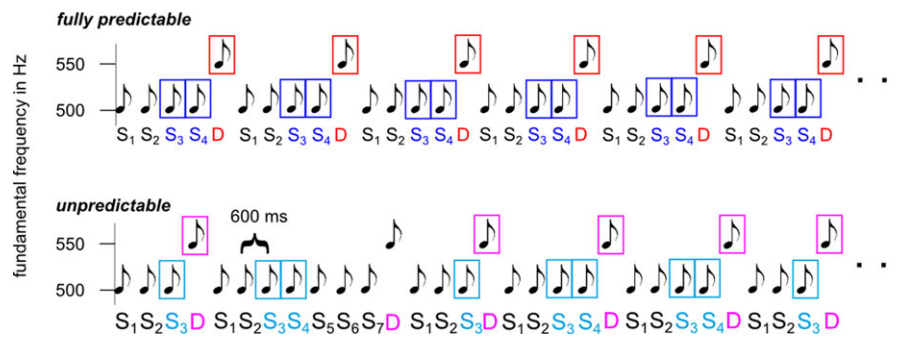
Figure 1. Paradigm. Participants watched a slide show while hearing passively sequences of sounds. High-probability standards mixed with low-probability deviants were presented either unpredictably or were fully predictable (exactly every fifth sound was a deviant). Standards (S_{1-n}) are numbered based on their position relative to the previous deviant. Only standards following at least 2 standards were used for analysis (marked by rectangles)

Between Temporal and Frontal Cortices"). Finally, we tested for an increasing predictability of deviants under the irregular condition following longer trains of standards ("III—Increase in Predictability as a Function of Train Length").

I—Estimation of Prediction

Given the fixed repetition of 4 standards followed by a deviant under the regular condition, the occurrence of both standards and deviants should be predictable. We assumed that in areas with predictive activity, the activity P prior to (expected) deviants should be different from the brain activity prior to frequent standards:

$$P_{standard} \neq P_{deviant}$$

Conversely, since under the irregular condition the system does not know a priori which stimulus will be heard the most frequent class (*standard tone*) is predicted, and, as a result, the activity P prior to the standards and deviants is equal:

$$P_{standard} \approx P_{deviant}$$

Statistically, the difference between conditions can be expressed as an effect of interaction using a 2-way ANOVA with the factors stimulus type (upcoming standard vs. upcoming deviant) and block type (regular vs. irregular), with the stimulus type effect expected to be larger in the regular than irregular condition. We ran this 2-way ANOVA for each electrode (with trials as random variable), at every time point, with HFA as the dependent variable. This leads to 3 F-value time series (2 main effects and one interaction: $F_{stimulus\ type}$, $F_{block\ type}$, $F_{interaction}$) for each channel with the $F_{interaction}$ capturing the prediction effect. The level of significance was corrected for multiple comparisons as described below.

Only deviants following the third and the fourth standard in a row (S_3 and S_4, respectively; see Supplementary Material for a full list of trials subjected to analysis) under the irregular condition were included in the analysis. All deviants following $S_5,...,S_N$ were excluded (see Fig. 1 and Supplementary Material). This results in a pool of deviant trials which consist of regular deviants which always occurred after S_4 and irregular deviants following S_3 and S_4. Note that due to the design of the quasi-random sequence under the irregular condition, with the constraint of at least 3 standards before a deviant, the probability of deviants occurring after S_3 and S_4 was nearly identical (0.17 and 0.2 respectively; see discussion of the hazard function in the following).

The pool of standard trials included only S_3 and S_4 trials under both the regular and irregular conditions. We did not include the first and second standards after a deviant, since during the prestimulus interval of S_1 a deviant is presented and the prestimulus interval of S_2 might still be influenced by the preceding deviant due to the short ISI. We excluded $S_5,...,S_N$ trials under the irregular condition since we hypothesized that the occurrence of deviants would be increasingly expected due to the "hazard function." That is, we hypothesized that while longer trains of standards under the irregular condition increase the local probability of the standard, the occurrence of deviants also becomes more likely: since a deviant has not occurred for an extended sequence of events, its likelihood increases. By not including irregular deviant following $S_5,...,S_N$ we also made the conditions more comparable for analysis, as under the regular conditions deviants never appeared after 5 or more standards. We focused on high-frequency broadband HFA, which in our previous study showed earlier poststimulus deviation signals than low-frequency ERPs (Dürschmid et al., 2016) and differentiated between fully predictable and unpredictable deviation in frontal and temporal cortices (for prediction signal in other bands of the time–frequency spectrum see *Supplementary Material*).

II—Comparison Between Temporal and Frontal Cortices

Principal component analysis

As noted in step I, the $F_{interaction}$ captures the prediction effect. We tested whether the $F_{interaction}$ effect is localized to the temporal or the frontal cortex in the following way. The $F_{interaction}$ time series were calculated in all channels separately over frontal and temporal regions of interest (ROIs). A principal component analysis (PCA) was used to find the course of a common $F_{interaction}$ across time, accounting for the highest variance, separately within the set of frontal and temporal channels. Channels loading highly on the first principal component are those that exhibit the strongest variation in terms of interaction amplitude across time.

Data reduction

We chose the channels for which the Pearson correlation r with the principal component exceeded the 75th percentile of all positive r-values. We set this level as a trade-off between a higher statistical power of a smaller number of channels and a stronger generalization across the cortex with a higher number of channels. We averaged the $F_{interaction}$-values in these channels and checked whether the averaged $F_{interaction}$-values in each region exceeded the empirically determined threshold derived from a surrogate distribution. This surrogate distribution
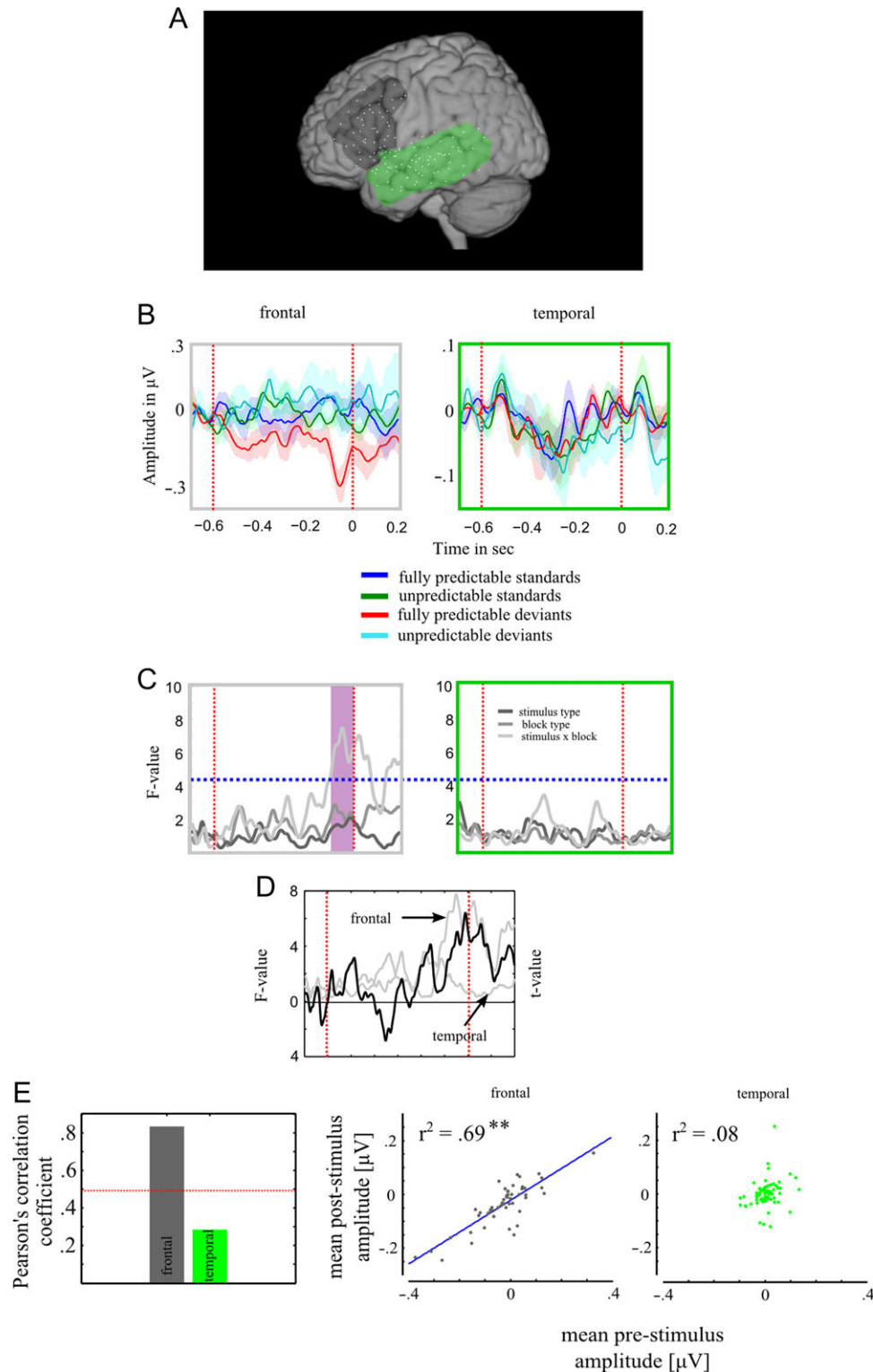
Figure 2. Time-resolved analysis of variance. (A) Frontal (gray) and temporal (green) regions of interest (ROIs). (B) Baseline-corrected HFA modulation prior to both stimulus types under both conditions (shaded areas denote the standard error across channels). (C) Mean F (ME—main effects, IE—Interaction effects) time series of channels loading highly on the frontal (gray frame) and temporal (green frame) $F_{interaction}$ first principal components. The horizontal dashed blue line indicates the critical $F_{interaction}$ value based on permutation. The shaded area in the left panel indicates the temporal interval of significant interaction. (D) $F_{interaction}$ time series for frontal and temporal electrodes (indicated by arrows) together with the t-values (black line) of the difference between the 2 ROIs in the degree of Type X Block interaction. Frontal cortex shows stronger interaction before stimulus onset. (E) Correlation between prestimulus and poststimulus HFA across channels over the frontal and temporal cortices. Left: Pearson's correlation values for each of the 2 ROIs. The dashed line gives the 99% confidence interval of the surrogate distribution. Middle: covariation of prestimulus and poststimulus amplitude of electrodes over the frontal ROI. Each dot represents one electrode. The blue line shows the linear fit to the data. Right: covariation of prestimulus and poststimulus amplitude of electrodes over the temporal ROI. Only in the frontal ROI pre and poststimulus amplitude are significantly correlated.

of the interaction effect was constructed by randomly reassigning the labels (standard, deviant, regular, irregular) to the single trials in 1000 permutations for each channel. This leads to 1000 surrogate $F_{interaction}$ time series. Significance criterion was an $F_{interaction}$-value with $P < 0.01$ within the surrogate distribution of all $F_{interaction}$ values. We next compared $F_{interaction}$ effects between frontal and temporal electrodes with an unpaired t-test at each time point between the 2 groups of electrodes (frontal vs. temporal). To determine significance, in 1000 runs we randomly reassigned the labels (temporal vs. frontal) and applied the unpaired t-test.

Group (within-subject) analysis

In the first analysis, we have chosen channels loading highly on the first principal component which are those that exhibit the strongest variation in terms of interaction amplitude across time, regardless of which subject they were taken from. As statistical significance in the analysis across electrodes might be driven by single subjects, we verify that the results presented are valid at a group level. To that end, we repeated the above stages at the single-subject level, using a 2-step procedure (common in fMRI studies). At the first level, we ran the above ANOVA in each subject separately, across trials. Then, as done in the previous section, we ran a PCA on the $F_{interation}$ time series for each subject within region, maintained the channels with the highest loading on the first PC, and averaged their $F_{interaction}$ time series. This led to 2 time series for each subject, one for the temporal channels and one for the frontal. Then, we ran a second level analysis to determine, at each time point and for each region, whether the $F_{interaction}$ exceeded the significance level, at the group level (i.e., with subjects as random variable). Significance was determined relative to a permutation-derived surrogate distribution of the interaction effect. The distribution was constructed by randomly reassigning the labels (standard, deviant, regular, irregular) to the single trials in 1000 permutations for each channel. This leads to 1000 surrogate $F_{interaction}$ time series. Significance criterion was an $F_{interaction}$-value with $P < 0.01$ within the surrogate distribution of all $F_{interaction}$ values.

III—Increase in Predictability as a Function of Train Length

Throughout the experiment, we pseudorandomly varied the train length of standards under the irregular condition. This resulted in standard trains of 3–8 standards before deviants. We directly tested whether predictability varies as a function of train length under the irregular condition, congruent with a hazard function (the probability of a deviant increases from 0 after 1 and 2 standards, to 0.17 (1/6) after 3 consecutive standards, and gradually increases to 1 after 8 consecutive standards have occurred in a row). We hypothesized that if HFA modulation correlates with predictability of the next stimulus, then longer standard trains would result in stronger modulation of HFA before the occurrence of deviants. Specifically, we correlated the HFA preceding deviants with the length of the standard train before deviant under the irregular condition. While in the previous analysis, we only used deviants following S_3 and S_4, here all deviants entered the analysis. To assess significance, Pearson's correlation coefficient of each channel was compared against a surrogate distribution. This surrogate distribution was constructed by randomly reassigning the actual train lengths of single-trial predeviant HFA values in 1000 runs.

For each channel, the confidence intervals (CI; 99.5%) of a normal distribution were determined.

Results

Comparison Between Temporal and Frontal Cortices

We studied 287 channels across all subjects, of which 120 were centered over frontal and temporal cortices. HFA was subject to a Stimulus Type (predeviant, prestandard) × Block Type (regular, irregular) ANOVA at every time point from −700 to +200 ms and we evaluated the interaction term ($F_{interaction}$) as a signature of predictive activity, separately for all frontal ($N_{frontal} = 54$) and all temporal channels ($N_{temporal} = 66$; Fig. 2A). Within each region, we kept the channels loading highly on the first temporal principle component of the $F_{interaction}$, time series and compared their mean with the empirical surrogate distribution (Step I of data analysis in methods; Fig. 2C). Frontal HFA ($N_{elec} = 7$) activity showed significant $F_{interaction}$ values (maximal $F_{interaction} = 7.76$ $P < 0.00001$, at −51.4 ms) with neither a significant effect of stimulus type (maximal $F_{stimulus\ type} = 2.44$) nor of block type (maximal $F_{blocktype} = 3.36$) (left panel in Fig. 2C). Temporal activity ($N_{elec} = 10$) did not show significant F-values for any of the 3 effects (maximal $F_{stimulus\ type} = 3.37$; maximal $F_{block\ type} = 2.02$; maximal $F_{interaction} = 3.47$) (right panel in Fig. 2C). The high $F_{interaction}$-values in frontal cortex correspond in time with a decrease in HFA from −100 ms before and until the onset of deviants, compared with the onset of standards, in the regular blocks (where deviants and standards were predictable) but not in the irregular blocks (Fig. 2B, see Supplementary Material for parallel results at a single-trial level). $F_{interaction}$ effects were significantly larger in frontal than temporal sites ($t_{15} = 6.49$, permutation based $P < 0.00001$ at −11 ms; Fig. 2D). These results were confirmed at the group level (Supplementary Fig. 2): $F_{interaction}$-values in the frontal lobe exceeded the empirical significance threshold ($F_{crit} = 4.2$) between −0.099 and 0.02 s ($F_{max} = 6.8$) prior to the onset of the deviants. $F_{interaction}$ averaged across this interval were significantly different between frontal and temporal cortices ($P < 0.05$; signed-rank test (for paired samples)).

Correlation Between Prestimulus and Poststimulus Responses

Previously, we found that postdeviant HFA was reduced under the regular condition compared with the irregular condition in frontal electrodes (Dürschmid et al. 2016). Since we now found that predictable deviants under the regular condition are heralded by a prestimulus HFA decrease, we tested if the 2 phenomena are correlated. First, both in the frontal ($N_{electrodes} = 54$) and the temporal ROIs ($N_{electrodes} = 66$) we correlated HFA preceding stimulus onset (average across −100 to 0 ms) with the amplitude following stimulus onset (average across 0–300 ms) across channels. The 2 resulting Pearson's correlation values were tested against a surrogate distribution. This surrogate distribution was constructed by randomly assigning the prestimulus values of each channel with poststimulus values from another channel in 1000 iterations. Based on the distribution of r-values in this permutation analysis, the critical r-value denoting statistical significance was $r = 0.5$. Prestimulus amplitude correlated with poststimulus amplitude in frontal cortex ($r = 0.83$; $P = 0.000002$) but not in the temporal cortex ($r = 0.28$; see Fig. 2E). Next, we tested whether the prestimulus/poststimulus relation is also true at a single-trial level. Hence, we correlated within each electrode the average amplitude in the prestimulus and poststimulus interval across trials. Each individual Pearson's r was compared against a surrogate distribution and
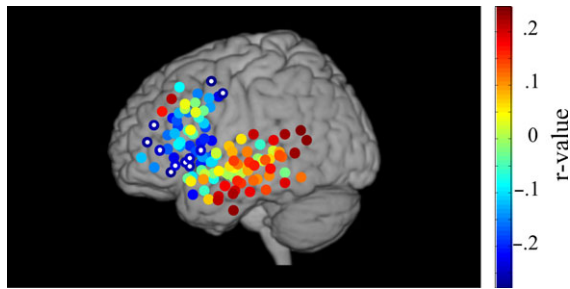
Figure 3. Prefrontal electrodes reflect the hazard function in irregular sequences. Each circle depicts channel positions with the color coding Pearson's correlation coefficient between train length and predevant HFA. Channels with a white dot show a statistically significant correlation. HFA significantly decreased after longer trains of standards in frontal cortex, while HFA tended to increase with longer trains of standards in temporal cortex.

excluded if smaller than the critical value ($r_{crit} = 0.1$). This surrogate distribution was constructed by randomly reassigning the prestimulus value of one trial to poststimulus value of another trial by randomly permuting the prestimulus values in 1000 iterations. On average, electrodes in the frontal cortex showed higher r-values than temporal ones (frontal: 0.39; temporal: 0.28; $t_{102} = 3.9$, $P = 0.0002$).

Increase in Predictability as a Function of Train Length

The train length of standards under the irregular condition varied pseudorandomly, allowing us to test whether prestimulus predictive activity varies gradually as a function of train length. We surmised that 2 effects could be operative. Temporally local effects suggest that the probability of a standard tone increases the more standard tones which are played in a row. In contrast, using a more global strategy, the so-called "hazard function" suggests that, given that deviations will happen eventually, expectation of a deviant increases the longer it is since the last deviation. To test whether and where such effects prevail, we correlated predevant HFA with train length of standards before deviants. Figure 3 shows that the direction of correlation between HFA and standard train length was different between temporal electrodes, showing mostly positive correlations, and frontal electrodes, showing mostly negative correlations. Individually, only the negative correlations in frontal channels reached the permutation critical r-values of $r_{crit} = \pm0.19$ (white dots in Fig. 3). Considering that the analysis of the regular versus irregular condition indicated that a decrease in HFA indicates proactive prediction of a deviant, these results suggest that frontal electrodes "apply" predictions even under the irregular condition based on the more global hazard function strategy.

Discussion

PC theories suggest that the brain continuously uses available information to predict forthcoming events and reduce sensory uncertainty (Arnal and Giraud 2012). However, the evidence supporting this notion comes mainly from postevent PE findings (Summerfield et al. 2008; Fogelson et al. 2009; Alink et al. 2010; den Ouden et al. 2010; Todorovic et al. 2011; Winkler and Czigler 2012; Sanmiguel et al. 2013; Bendixen et al. 2014, 2015; Dürschmid et al. 2016), providing only indirect evidence for prediction, since prediction-based neural activity should precede a predicted event. Here, we provide direct evidence for the

prediction of rare deviant events manifested by prestimulus HFA modulation, suggesting an automatic anticipation of the upcoming deviant.

Regular, and thus predictable, deviations were preceded by HFA decrease exclusively in the lateral frontal cortex, observed at both the group and single-trial levels. This complements our previous results, showing that lateral frontal (but not temporal) sites show reduced postevent PE signals to predictable compared with unpredictable stimuli (Dürschmid et al. 2016). Moreover, the predictive prestimulus power reduction correlated with the postdeviant HFA reduction, across both channels and trials, indicating a link between prestimulus HFA decrease and reduced response to predictable deviants (i.e., better prediction leading to less PE). Finally, we found evidence that the frontal but not the temporal cortex followed the statistics of the irregular sequence as well (the "hazard rate"). In sum, these results provide evidence for automatic generation of proactive, anticipatory processes in frontal cortex, which may provide the basis for reduced orienting response to predictable events in an unattended stream. More generally, the results corroborate a hierarchy of prediction in the human brain (Dürschmid et al. 2016). This hierarchy is in line with the notion that early stages of information processing is represented based on bottom-up signals, whereas in higher levels of cortical processing deviations from expectation are registered while predictable components are "filtered out" (Heilbron and Chait 2018).

The Frontal Cortex Follows Complex Statistics of the Input

The comparison between predictable versus irregular deviants pointed to HFA reduction as a signature for predicting a deviation. This observation allowed us to investigate whether anticipatory predictions are generated during irregular, random sequences as well. We found that in frontal cortex, prestimulus HFA decreased as the train of uninterrupted standards became longer. Considering our first conclusion that HFA reduction reflects increasing likelihood of a deviant, this pattern matches well the so-called "hazard function," in which an imminent event becomes more likely to occur the longer it has not occurred. This suggests that the frontal cortex predictive capacity is not limited to highly structured sequences, but rather, that it generates complex predictions based on sequence probabilities, even in a task-irrelevant irregular stream of events. This progressive increase in deviant prediction resembles the progressive increase in the contingent negative variation (CNV) as a function of distance from the last deviant reported by Chennu et al. (2013), although the CNV effect in Chennu et al. (2013) was only seen when subjects attended the stimuli (especially deviants), whereas in our case stimuli were task irrelevant. The temporal cortex in our study showed a trend toward an opposite effect with an increased prestimulus HFA activity the longer the standard train was. This is consistent with the notion that temporal cortex is based on recent history, such that with longer standard trains, "more of the same" (i.e., another standard) is expected.

Previous Attempts to Corroborate Proactive Prediction

Several studies approached the question of proactive prediction by investigating stimulus omissions (see Heilbron and Chait (2018) for an up-to-date review and discussion). Most omission-locked responses can be considered as violations of a general prediction for the occurrence of a stimulus at a given time

(a temporal prediction). Sanmiguel et al. (2013) had subjects generate environmental sounds by pressing a button. EEG responses to occasional sound omissions were found only when the same sound was repeatedly elicited by the button presses and was thus predictable due the subjects' intention which does not speak for nonintentional automatic prediction. In a passive task with visual distraction, Bendixen et al. (2015) presented sequential tone pairs in rapid succession. The intra-pair frequencies were identical, whereas the frequencies altered between pairs. Omission-locked responses were found when the identity of the omitted stimulus could be predicted (because it was the second sound in the pair), but not when only its timing could be predicted (because it was the first in the pair). However, subjects may have perceived each pair as an auditory object, and the omission of the second sound in the pair, which elicited the critical omission response, might be a post hoc response to a duration change rather than an anticipatory response.

Rather than looking at poststimulus or postomission responses, our results address the prestimulus time, a time window at which activity modulation has to be ascribed to prediction per se since no error could have been computed. Similarly, Kok et al. (2017) decoded from MEG recordings the orientation of visual grating stimuli, which could be predicted by a preceding auditory stimulus (valid visual stimulus) or not (invalid visual stimulus). Subtracting the signal of valid from invalidly cued gratings revealed differences before stimulus presentation, suggesting the pre-activation of an anticipated sensory template. Grisoni et al. (2017) found EEG evidence for prestimulus anticipatory motor preparation to specific action-verbs predicted by meaningful sentences, but the automatic nature of this prediction is not clear as subjects likely listened to the meaningful sentences. While these studies provide converging evidence for proactive prediction, using MEG or EEG data, the source and type of signal of this predictive activity remain unclear. Taking the advantage of the high signal-to-noise ratio, and the improved spatial resolution of the ECOG data, our findings show that predictable deviants are preceded by frontal cortex HFA decrease not seen in sensory cortex.

Implications for Models of the Poststimulus Mismatch Response

How is prestimulus modulation of the HFA signals related to accounts of the mismatch response elicited by the deviant? Two mechanisms differing with respect to the degree of memory involvement have been proposed by Fishman and Steinschneider (2012). Poststimulus effects like the mismatch negativity may involve different states of neural adaptation (stimulus-specific adaptation (Ulanovsky et al. 2003; Farley et al. 2010)) due to repeated presentation. This creates a model of the recent history, and under an assumption of stationarity, provides a reasonable prediction of future events (May and Tiitinen 2010). Other models (Näätänen et al. 2005) suggest that beyond adaptation, stimulus repetition increases the absolute excitability of neurons tuned to values not included in the repeated stimulus. By both accounts, new stimuli elicit a stronger response if not congruent with the current model, which generates a PE signal. However, our observation of predictive predeviant modulation of activity cannot be explained by either mechanism. First, we compared the response with deviants following a similar number of standards in the random and predictable conditions, and overall deviants and standards had the same probability under both conditions. Thus, either adaptation

or lateral excitation should have been similar across conditions. Second, since the effect occurred before the deviant, it cannot be due to activation of nonadapted/excited neurons sensitive to the pitch of the deviant or by a process of comparison. Instead, the results provide evidence of high-level prediction, modifying the poststimulus comparison between the actual input and the ongoing prediction.

Implications for Models of PC

Dynamic causal modeling (DCM) of EEG or MEG studies suggested a hierarchical feedforward-feedback cascade in which the inferior frontal cortex sits at the top, providing top-down predictions to (and receiving PE signals from) the superior temporal gyrus, which in turn provides top-down predictions to (and receives PE signals from) the early auditory cortex (Garrido et al. 2009). Recently, Phillips et al. (2015) and Phillips et al. (2016) validated the models, originally tested on EEG/MEG data, with ECoG data from 2 patients. However, Phillips et al.'s models suggested that the prediction signal affecting the IFG is limited to temporal deviations (duration deviations and gaps in their study), but not pitch, intensity, or location deviations, whereas our findings showed clear effects of predictability in the ventral frontal cortex when the deviation was in pitch.

Our prestimulus predictive effects were not limited to temporal predictions. In fact, suppression of HFA indexed both the identity (standard or deviant) of the next stimulus in addition to its timing. Moreover, this was observed even though all stimuli were task-irrelevant, meaningless, did not require a response, and had no reward value. Previous findings of anticipatory response typically involved active preparation for an upcoming imperative stimulus, reflected in the CNV recorded on the scalp (Trillenberg et al. 2000; Janssen and Shadlen 2005), listening to meaningful verbal material (Grisoni et al. 2017) or reward-prediction signals of different types (Fiorillo et al. 2003). The current finding provides evidence for ongoing, task-independent, anticipatory predictive signals, operative even before the stimulus occurred.

Previous studies argued that predictions and PE signals are compartmentalized across cortical layers and segregated by spectral content. They suggested that predictions are generated and fed-back by deep (infragranular) layers of the cortex at relatively lower frequencies of alpha/beta, whereas PE are fed forward from superficial (supragranular) layers at high (gamma) frequencies (Bastos et al. 2012, 2015). The fact that our proactive prediction signal was found in the HFA modulation may seem at odds with this model. However, for several reasons we remain agnostic about how the HFA modulation relates to the more detailed, laminar models of PC. First, the HFA signal should not be mistaken for any narrowband power modulation. Multiple studies using intracranial signals, as well as computational modeling, suggested that the high-frequency broadband signal is a good correlate of population neural firing rate (Mukamel et al. 2005; Liu and Newsome 2006; Manning et al. 2009; Miller, Sorensen et al. 2009; Ray and Maunsell 2011), making HFA modulation the preferred proxy for asynchronous (nonperiodic) areal activation in ECOG studies (Miller, Sorensen et al. 2009; Privman et al. 2013; Miller et al. 2014; Coon and Schalk 2016; Kupers et al. 2018). That is, although we parameterize this signal using frequency decomposition, no oscillation (i.e., narrowband periodic activity) is implied. In fact, as argued by Miller and colleagues, the measured HFA may reflect a frequency nonspecific power increase across the spectrum, while changes in the lower frequencies are masked by stronger

oscillatory activity in the lower ranges (Miller et al. 2007; Miller, Zanos et al. 2009). Second, our knowledge about the relationship between activity at specific laminae and how they are reflected in the mesoscopic measurement of the surface electrode is highly limited. Third, whereas the columnar model of PC suggested by Bastos et al. (2012, 2015) specifies some of the components (feedback predictions, feedforward PEs) in frequency content terms, it does not provide that detail about the dynamics of the interlaminar connections (e.g., projection of "expectation neurons" in supragranular layers to deep layers forming the predictions). In fact, the columnar organization vis a vis components of the PC model is still debated (Spratling 2010; Heilbron and Chait 2018). Fourth, it is not clear whether the prestimulus HFA modulation reflects the same prediction signal specified in PC models, or the outcome of this predictive signal (e.g., inhibition of firing rate in anticipation of a deviant). Specifically, current PC models do not account for long-term prospective predictions across hundreds of milliseconds as we see here. Thus, we believe that any speculations from our data to these models would be premature.

Maintaining Parallel and Inconsistent Predictions

Under the PC framework, prediction signals should be transmitted to lower nodes of the network, and PE signals should be carried forward to higher nodes in the network, to allow modification of the current model and influence the next prediction. However, our findings challenge this simple information flow, which must address multiple levels of possibly conflicting predictions (Pieszek et al. 2013). For instance, just prior to a deviant in the regular condition, and also after a long train of standards under the irregular condition, processes based on local effects predict another standard, whereas predictions based on the global statistics predict a deviant. In this situation, it seems efficient to prevent PE signals elicited at the temporal (auditory) cortex from propagating up the hierarchy and modifying a veridical model of the environment. Similarly, it seems that the prediction of an upcoming deviant based on global statistics, present at the frontal cortex, does not propagate down the network to mitigate the PE signal invoked by the expected deviant in the temporal cortex (Schröger et al. 2015). Our results therefore suggest that the flow of information up and down the hierarchy of the network is not as simple as gleaned from typical DCM diagrams (Garrido et al. 2009; Phillips et al. 2015, 2016). We speculate on the functional advantage of maintaining segregated predictions. Specifically, maintaining predictions that account for global regularities allows the prefrontal cortex to efficiently direct attention only to unexpected events (Sussman et al. 2003), whereas for the auditory cortex, detecting all local changes is advantageous for parsing the auditory input into meaningful chunks (e.g., in speech perception)

Relationship Between the Predictive Prestimulus Activity and Attention

Previous selective attention studies have shown prestimulus activation (increased firing rate or BOLD response) prior to task relevant stimuli (Colby et al. 1996; Beck and Kastner 2009) and deactivation prior to task-irrelevant stimuli (Langner et al. 2011; Rodgers and DeWeese 2014). Our study did not use a classic selective attention task but could be considered as involving a competition between the primary task of viewing a slide show, and the potential distraction caused by the auditory stream, especially by deviant events. Thus, the HFA decrease

observed prior to an expected deviant could reflect the same filtering mechanism previously observed during selective attention. Under this premise, the current results suggest that this inhibitory anticipation can be generated selectively, and in predictive manner, in an unattended stream.

In sum, pre and poststimulus HFA responses reveal a unique role for prefrontal cortex in utilizing global regularity to control responses to deviant stimuli. Frontal HFA selectively signals upcoming regular deviants with a decreased amplitude prior to deviant onset. Subsequently, only unpredictable deviants elicit a strong HFA response, putatively related to triggering an orienting response to an environmental perturbation. At the same time, the sensory cortex continues to veridically respond to any change in the stream. Our results highlight a selective role of frontal structures in actively computing predictions to better navigate the environment.

Supplementary Material

Supplementary material is available at *Cerebral Cortex* online.

Notes

References

Alink A, Schwiedrzik CM, Kohler A, Singer W, Muckli L. 2010. Stimulus predictability reduces responses in primary visual cortex. J Neurosci. 30:2960–2966.

Arnal LH, Giraud AL. 2012. Cortical oscillations and sensory predictions. Trends Cogn Sci. 16:390–398.

Bastos AM, Usrey WM, Adams RA, Mangun GR, Fries P, Friston KJ. 2012. Canonical microcircuits for predictive coding. Neuron. 76:695–711.

Bastos AM, Vezoli J, Bosman CA, Schoffelen JM, Oostenveld R, Dowdall JR, De Weerd P, Kennedy H, Fries P. 2015. Visual areas exert feedforward and feedback influences through distinct frequency channels. Neuron. 85:390–401.

Beck DM, Kastner S. 2009. Top-down and bottom-up mechanisms in biasing competition in the human brain. Vision Res. 49:1154–1165.

Bendixen A, Scharinger M, Strauß A, Obleser J. 2014. Prediction in the service of comprehension: modulated early brain responses to omitted speech segments. Cortex. 53:9–26.

Bendixen A, Schwartze M, Kotz SA. 2015. Temporal dynamics of contingency extraction from tonal and verbal auditory sequences. Brain Lang. 148:64–73.

Chennu S, Noreika V, Gueorguiev D, Blenkmann A, Kochen S, Ibáñez A, Owen AM, Bekinschtein TA. 2013. Expectation and attention in hierarchical auditory prediction. J Neurosci. 33: 11194–11205.

Colby CL, Duhamel JR, Goldberg ME. 1996. Visual, presaccadic, and cognitive activation of single neurons in monkey lateral intraparietal area. J Neurophysiol. 76:2841–2852.

Coon WG, Schalk G. 2016. A method to establish the spatiotemporal evolution of task-related cortical activity from electrocorticographic signals in single trials. J Neurosci Methods. 271:76–85.

den Ouden HEM, Daunizeau J, Roiser J, Friston KJ, Stephan KE. 2010. Striatal prediction error modulates cortical coupling. J Neurosci. 30:3210–3219.

Dürschmid S, Edwards E, Reichert C, Dewar C, Hinrichs H, Heinze HJ, Kirsch HE, Dalal SS, Deouell LY, Knight RT. 2016. Hierarchy of prediction errors for auditory events in human temporal and frontal cortex. Proc Natl Acad Sci USA. 113: 6755–6760.

Farley BJ, Quirk MC, Doherty JJ, Christian EP. 2010. Stimulus-specific adaptation in auditory cortex is an nmda-independent process distinct from the sensory novelty encoded by the mismatch negativity. J Neurosci. 30:16475–16484.

Fiorillo CD, Tobler PN, Schultz W. 2003. Discrete coding of reward probability and uncertainty by dopamine neurons. Science. 299:1898–1902.

Fishman YI, Steinschneider M. 2012. Searching for the mismatch negativity in primary auditory cortex of the awake monkey: deviance detection or stimulus specific adaptation? J Neurosci. 32:15747–15758.

Fogelson N, Wang X, Lewis JB, Kishiyama MM, Ding M, Knight RT. 2009. Multimodal effects of local context on target detection: evidence from p3b. J Cogn Neurosci. 21:1680–1692.

Garrido MI, Kilner JM, Kiebel SJ, Friston KJ. 2009. Dynamic causal modeling of the response to frequency deviants. J Neurophysiol. 101:2620–2631.

Grisoni L, Miller TM, Pulvermüller F. 2017. Neural correlates of semantic prediction and resolution in sentence processing. J Neurosci. 37(18):4848–4858.

Heilbron M, Chait M. 2018. Great expectations: is there evidence for predictive coding in auditory cortex? Neuroscience. 389:54–73.

Janssen P, Shadlen MN. 2005. A representation of the hazard rate of elapsed time in macaque area lip. Nat Neurosci. 8:234–241.

Kok P, Mostert P, de Lange FP. 2017. Prior expectations induce prestimulus sensory templates? Proc Natl Acad Sci USA 114: 10473–10478.

Kupers ER, Wang HX, Amano K, Kay KN, Heeger DJ, Winawer J. 2018. A non-invasive, quantitative study of broadband spectral responses in human visual cortex. PLoS One. 13:e0193107.

Langner R, Kellermann T, Boers F, Sturm W, Willmes K, Eickhoff SB. 2011. Modality-specific perceptual expectations selectively modulate baseline activity in auditory, somatosensory, and visual cortices. Cerebral cortex. 21:2850–2862.

Lee H, Noppeney U. 2014. Temporal prediction errors in visual and auditory cortices. Curr Biol. 24:R309–R310.

Liu J, Newsome WT. 2006. Local field potential in cortical area mt: stimulus tuning and behavioral correlations. J Neurosci. 26:7779–7790.

Manning JR, Jacobs J, Fried I, Kahana MJ. 2009. Broadband shifts in local field potential power spectra are correlated with single-neuron spiking in humans. J Neurosci. 29:13613–13620.

May PJC, Tiitinen H. 2010. Mismatch negativity (mmn), the deviance-elicited auditory deflection, explained. Psychophysiology. 47:66–122.

Miller KJ, Honey CJ, Hermes D, Rao RPN, denNijs M, Ojemann JG. 2014. Broadband changes in the cortical surface potential track activation of functionally diverse neuronal populations. Neuroimage. 85(Pt 2):711–720.

Miller KJ, Leuthardt EC, Schalk G, Rao RPN, Anderson NR, Moran DW, Miller JW, Ojemann JG. 2007. Spectral changes in cortical surface potentials during motor movement. J Neurosci. 27: 2424–2432.

Miller KJ, Sorensen LB, Ojemann JG, den Nijs M. 2009. Power-law scaling in the brain surface electric potential. PLoS Comput Biol. 5:e1000609.

Miller KJ, Zanos S, Fetz EE, den Nijs M, Ojemann JG. 2009. Decoupling the cortical power spectrum reveals real-time representation of individual finger movements in humans. J Neurosci. 29:3132–3137.

Mukamel R, Gelbard H, Arieli A, Hasson U, Fried I, Malach R. 2005. Coupling between neuronal firing, field potentials, and fmri in human auditory cortex. Science. 309:951–954.

Näätänen R, Jacobsen T, Winkler I. 2005. Memory-based or afferent processes in mismatch negativity (mmn): a review of the evidence. Psychophysiology. 42:25–32.

Phillips HN, Blenkmann A, Hughes LE, Bekinschtein TA, Rowe JB. 2015. Hierarchical organization of frontotemporal networks for the prediction of stimuli across multiple dimensions. J Neurosci. 35:9255–9264.

Phillips HN, Blenkmann A, Hughes LE, Kochen S, Bekinschtein TA, Cam-Can, Rowe JB. 2016. Convergent evidence for hierarchical prediction networks from human electrocorticography and magnetoencephalography. Cortex. 82:192–205.

Pieszek M, Widmann A, Gruber T, Schröger E. 2013. The human brain maintains contradictory and redundant auditory sensory predictions. PLoS One. 8(1):e53634.

Privman E, Malach R, Yeshurun Y. 2013. Modeling the electrical field created by mass neural activity. Neural Netw. 40:44–51.

Rao RP, Ballard DH. 1999. Predictive coding in the visual cortex: a functional interpretation of some extra-classical receptive-field effects. Nat Neurosci. 2:79–87.

Ray S, Maunsell JHR. 2011. Different origins of gamma rhythm and high-gamma activity in macaque visual cortex. PLoS Biol. 9:e1000610.

Rodgers CC, DeWeese MR. 2014. Neural correlates of task switching in prefrontal cortex and primary auditory cortex in a novel stimulus selection task for rodents. Neuron. 82: 1157–1170.

Sanmiguel I, Saupe K, Schröger E. 2013. I know what is missing here: electrophysiological prediction error signals elicited by omissions of predicted "what" but not "when". Front Hum Neurosci. 7:407.

Schröger E, Marzecová A, SanMiguel I. 2015. Attention and prediction in human audition: a lesson from cognitive psychophysiology. Eur J Neurosci. 41:641–664.

Spratling MW. 2010. Predictive coding as a model of response properties in cortical area v1. J Neurosci. 30:3531–3543.

Summerfield C, Trittschuh EH, Monti JM, Mesulam MM, Egner T. 2008. Neural repetition suppression reflects fulfilled perceptual expectations. Nat Neurosci. 11:1004–1006.

Sussman E, Winkler I, Schröger E. 2003. Top-down control over involuntary attention switching in the auditory modality. Psychon Bull Rev. 10(3):630–637.

Todorovic A, van Ede F, Maris E, de Lange FP. 2011. Prior expectation mediates neural adaptation to repeated sounds in the auditory cortex: an meg study. J Neurosci. 31:9118–9123.

Trillenberg P, Verleger R, Wascher E, Wauschkuhn B, Wessel K. 2000. Cnv and temporal uncertainty with 'ageing' and 'non-ageing' s1-s2 intervals. Clin Neurophysiol. 111:1216–1226.

Ulanovsky N, Las L, Nelken I. 2003. Processing of low-probability sounds by cortical neurons. Nat Neurosci. 6:391–398.

Winkler I, Czigler I. 2012. Evidence from auditory and visual event-related potential (erp) studies of deviance detection (mmn and vmmn) linking predictive coding theories and perceptual object representations. Intern J Psychophysiol. 83:132–143.

Winkler I, Schröger E. 2015. Auditory perceptual objects as generative models: setting the stage for communication by sound. Brain Lang. 148:1–22.

Supplementary Material

Assignment of trials to conditions

To reveal predictive signals prior to the onset of the stimulus, we evaluated the HFB amplitude modulation (HFA) in the pre-stimulus interval. The trials were grouped according to their identity in the post-stimulus interval (*Supplementary Table* 2). Column "Stimulus Type" and "Condition" give the group labels subjected to the 2 way within-channel ANOVA for stimulus type (deviant vs. standard) by condition (regular vs. irregular), respectively. The 2 way ANOVA was conducted at each time point in the **prestimulus interval** (-.7 to .2 sec). As indicated in the table, prestimulus interval always followed a standard (S_2, S_3, or S_4). The HBA time series in the prestimulus interval were corrected by subtracting the mean of the 100 ms preceding the prestimulus interval (**baseline interval**, from -.7 to -.6, which are the terminal .1 sec following S_1, S_2 or S_3 respectively). In this baseline interval we expect the prediction for the next stimulus to be for a standard in all cases. Note that in the irregular condition deviants may occasionally occur following a train of only 3 deviants. Hence, in the case a deviant could be predicted during the baseline interval of the prestimulus interval, even though S_4 actually follows. However, under the premise that all train lengths are evenly distributed, the likelihood of a deviant following S_3 is low. That is, it is much more likely (~ 6 times so) that a standard will occur after 3 standards even in the irregular condition. Note also that the response to the stimulus presented prior to the pre-stimulus interval (stimulus onset at -600 ms) should not be influenced by repetition suppression as we limited the analysis to the deviants following S_3 and S_4 and excluded deviants following S_5 to S_N.

1

Supplementary Table 2: Labels of trials used in statistical analyses. Intervals are labeled, by the last stimulus presented.

	Baseline interval	Prestimulus interval	Poststimulus interval	Stimulus type	Condition
Temporal interval in sec	-.7 to -.6	-.6 to 0	0 to .2		
Regular condition	S_3	S_4	$D_{4regular}$	1	1
	S_1	S_2	$S_{3regular}$	0	
	S_2	S_3	$S_{4regular}$		
Irregular condition	S_2	S_3	$D_{3irregular}$	1	0
	S_3	S_4	$D_{4irregular}$		
	S_1	S_2	$S_{3irregular}$	0	
	S_2	S_3	$S_{4irregular}$		

Specificity of predictive code in the High frequency activity

In this study we focus on HFA activity since HFA activity signaled prediction errors earlier and distinguished between fully and unpredictable deviants in the post-deviant interval in our previous study [**Fehler! Verweisquelle konnte nicht gefunden werden.**]. However, we additionally verified that a prediction signal operationalized as the $F_{interaction}$ value is represented mainly in the HFA range, in the following way. For each trial (-1 sec to 2 sec around stimulus onset – sufficiently long to prevent any edge effects during filtering) we band-pass filtered each electrode's time series at 42 frequency bands (log-spaced between 3 and 200 Hz) with a bandwidth of 10% of the center frequency. We obtained the analytic amplitude $A_f(t)$ of each frequency f by Hilbert-transforming the filtered time series. We smoothed the time series such that the amplitude value at each time point n is the mean of 10 ms around each time point n. We then baseline corrected the prestimulus trial (N-1) activity by subtracting the mean activity from the -700 to -600 ms preceding the stimulus onset in each trial of each channel (i.e., 100 ms prior trial N-1; as stated above this could be the last 100ms of S_1, S_2 or S_3). This prediction signal can

be equally high in different frequency bands but can be distributed across networks of different spatial extension and hence different sets of electrodes. Averaging across the whole set of all electrodes would favor frequency bands with a larger set of electrodes showing a high $F_{interaction}$ value. Hence, in each frequency we averaged the $F_{interaction}$-value across the prestimulus interval separately for each electrode. We then took the 5% of electrodes with the highest averaged $F_{interaction}$-value in this prestimulus interval and averaged the $F_{interaction}$-value time series across the selected channels. This results in one $F_{interaction}$-value time series for each frequency which were tested for significance against a surrogate distribution. This surrogate distribution of the interaction effect was constructed by randomly reassigning the labels (standard, deviant, regular, irregular) to the single trials in 1000 permutations for each channel. This leads to 1000 surrogate $F_{interaction}$ –value time series for each frequency. Significance criterion was a $F_{interaction}$-value with $p < .01$ within the surrogate distribution.

In the initial step of this analysis we chose a prestimulus interval ranging from -400 to 0 ms. The rationale was to separate any prediction signal (expected in the end of the prestimulus interval) from differences in response to the stimulus presented in the prestimulus interval. However, a shorter interval disadvantages low frequencies if one takes into account that at least 3 cycles of the underlying oscillation are necessary to evaluate an amplitude modulation. For example, the θ activity has a center frequency of 6 Hz and hence a cycle length of 166 ms. To fully cover 3 cycles an interval of at least 498 ms is necessary to evaluate amplitude modulation. In contrast, longer intervals decrease the possibility to detected transient fluctuations in higher frequencies. Therefore, we systematically varied the interval upon which we selected the 5% of best electrodes (-600/-500/-400/-300/-200 to 0 ms) in five different frequency bands (θ: 4-8Hz, α: 8-12Hz, β: 12-30 Hz, γ: 40-80 Hz, and HFA: 80-150Hz).
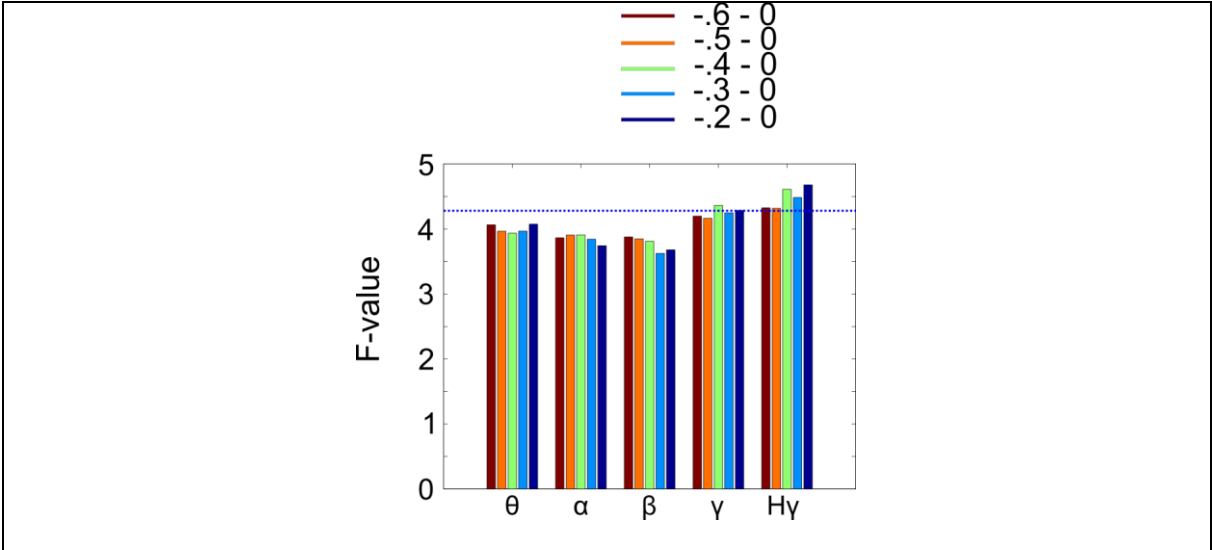
Supplementary Figure 1: $F_{interaction}$ values in 5 different prestimulus intervals across the best 5% of electrodes. Only high γ activity shows significant prediction signals in each of the five prestimulus intervals as indicated by the averaged $F_{interaction}$ values exceeding the confidence interval of the surrogate distribution derived from a permutation procedure in which trial labels (standard, deviant, regular, irregular) were randomly reassigned.

Group Analysis
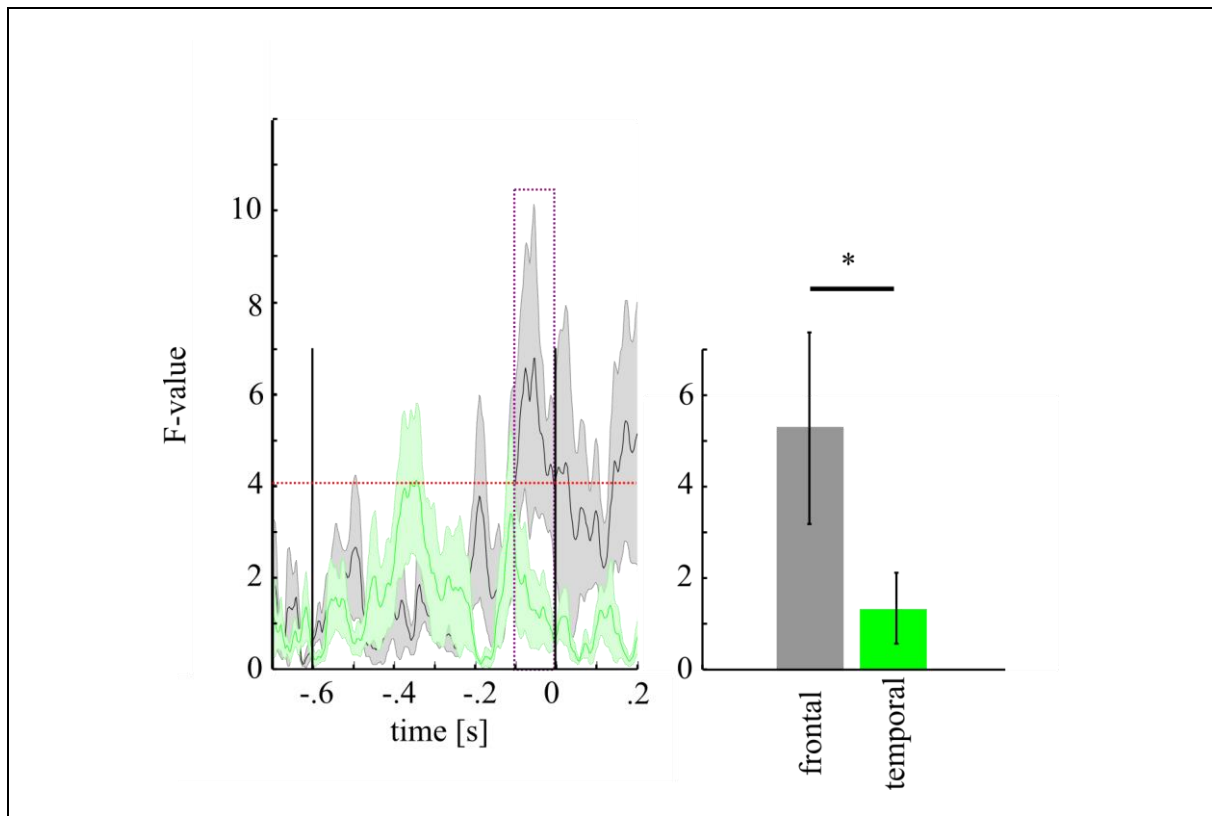
Supplementary Figure 2: Time resolved analysis of variance at the group level. Mean $F_{interaction}$ time series across subjects. For each subject, the channel loading highest on the frontal (gray frame) and temporal (green frame) $F_{interaction}$ 1st principal component was chosen. The horizontal dashed red line indicates the critical $F_{interaction}$ value based on permutation. The framed area in the left panel indicates the temporal interval of significant interaction. Shaded areas denote the standard error across subjects. Right: mean $F_{interaction}$ values (gray – frontal, green – temporal) averaged across the interval of significant interaction. Frontal cortex shows stronger interaction before stimulus onset. Error bars denote the standard error across subjects.

Single trial ROC analysis

We analyzed whether pre-stimulus amplitudes predicted the upcoming regular deviant at a single trial level. We computed the predictive index that approximates the probability with which an ideal observer can predict the upcoming stimulus (standard sound vs. deviant sound) from the pre-stimulus HFA on a single trial level, separately for the fully predictable and the unpredictable conditions.

We used Receiver Operating Characteristics (ROC) as a descriptive analysis to define whether and where pre-stimulus HFA predicted the upcoming stimulus at a single trial level. The **A**rea **U**nder the ROC **C**urve (AUC) value is a proxy for how strongly the distribution of HFA prior to standard and deviant trials overlap. This index was estimated at each time point for each channel , based on the

distributions of single trial amplitudes for all deviants and all standards, yielding an AUC time series for each channel. We next estimated whether AUC values varied as a function of anatomical location. AUC values where averaged across the 100 msec prior to onset of deviants and these values were correlated with both the relative x (posterior-anterior) - and y (ventro-dorsal) coordinates across all electrodes, separately for predictable and unpredictable sequences.

In the regular condition, the predictive power increased along the ventral to dorsal axis, as well as from posterior to anterior electrodes (Supplementary Figure 3A). AUC values are significantly correlated with anatomical location on both the x- and y-dimension in the fully predictable condition (r_y = -.3, p=.001; r_x = -.33, p=.0002) but not the unpredictable condition (r_y = -.07, p=.44; r_x = .22, p=.21; see *Supplementary Figure 3*).

Next, we defined the time course of AUC values for the frontal and temporal cortex. The AUC time series were subjected to PCA to find the course of AUC across time separately for the two regions of interest of the lateral cortex. In each region we determined channels loading highly on the respective first principal component and averaged the AUC time series across these channels, pooled across all subjects. We tested for significant deviations of the averaged AUC time series from predictive index at chance level (50%) using a permutation test. For this test, the empirical distribution of the main effect was constructed by randomly reassigning the labels (standard, deviant) to the single trials in 1000 permutations. We evaluated the statistical significance of the predictive index for each time point in each ROI in two ways. First, for each region and time point, to be considered as significant prediction, the averaged predictive index had to exceed the 95th percentile of the empirical distribution. Second, to assess the difference between regions, we used a time point-by-time point t-test to test for differences of AUC values between 2 regions separately in both conditions (regular vs. irregular) across channels. Again, we determined an empirical significance threshold for t values by randomly reassigning the two ROI labels in 1000 permutations of the same time point-by-time point ANOVA.

The above analysis pooled across subjects to achieve a higher power at the expense of generalization. However, we also tested statistical significance at a group level with subjects as random variable. For that aim, in each subject, in each of the two regions and in each condition, we chose the channels with

the maximal AUC value in the pre-stimulus interval (-600 to 0 ms) and compared their mean against a surrogate distribution.

Dorsal frontal channels exceeded the 99% significance threshold ($AUC_{ci99} = .595$) in the time range between -79 and -10 ms before the onset of the regular deviant (see *Supplementary Figure 3C*) but not the irregular deviants (*Supplementary Figure 3D*). A time-point-by-time-point t-test with AUC as dependent variable revealed a highly significant difference of AUC values between ROIs at the electrode level between -69 and -7 ms (max $t_6 = 5.6$; $p = 2.3^{-5}$ at -41 ms) and at the group level between -91 and 58 ms (max $t_4 = 11.3$; $p = 3.3^{-16}$ at -10 ms).
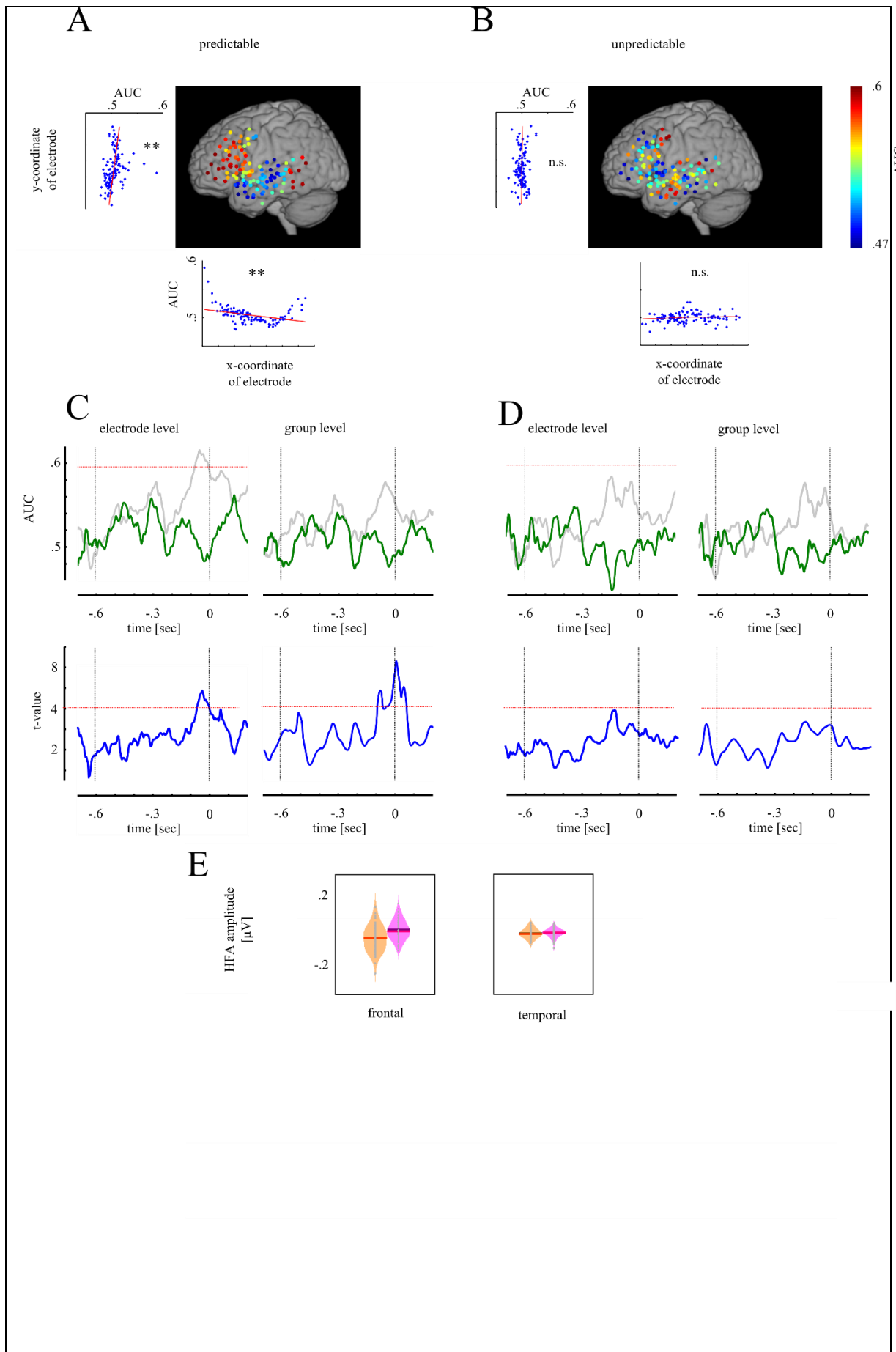
Supplementary Figure 3: *A* Correlation of AUC values prior to onset of deviants with y- and x-coordinates (left and below channel location, respectively) in the fully predictable condition. *B* shows the same for the unpredictable condition. AUC values are significantly correlated with anatomical location on both the x- and y-dimension in the fully predictable condition (denoted by the asterisks) but not the unpredictable condition. *C-D* Area under the curve (AUC) time series of the Receiver Operation Characteristics Curve (ROC) for predicting predictable (*C*) and unpredictable deviants (*D*) for channels loading highly on the 1st principal component. The left panel in both *C* and *D* show the analysis across channels and the right panel at the group level. Chance AUC is 0.5 and the dashed red horizontal line depicts the critical AUC for significance based on permutation analysis. The lower panel in *C* and *D* shows the t-value denoting the differences of AUC values between frontal and temporal ROI. Only frontal channels show a significant AUC value prior to predictable deviants. Furthermore, only in the predictable condition predictive signals are higher in the frontal cortex both at the level of channels and at the group level. *E* shows the distribution of HFA averaged across 100 msec prior to predictable (orange) and unpredictable (magenta) deviants for all channels and all trials separately for the frontal (left) and temporal (right) ROI. The red horizontal lines show the mean the black lines the median of the HFA single trial distributions.

Phase-amplitude cross-frequency coupling in the human nucleus accumbens tracks action monitoring during cognitive control

Stefan Dürschmid[1,2], Tino Zaehle[1,2], Klaus Kopitzki[1], Jürgen Voges[1], Friedhelm C. Schmitt[1], Hans-Jochen Heinze[1,2,3], Robert T. Knight[4,5] and Hermann Hinrichs[1,2,3]*

[1] Departments of Neurology and Stereotactic Neurosurgery, Otto-von-Guericke University, Magdeburg, Germany
[2] Department of Behavioural Neurology, Leibniz Institute for Neurobiology, Magdeburg, Germany
[3] German Center for Neurodegenerative Disease (DZNE), Magdeburg, Germany
[4] Department of Psychology, Helen Wills Neuroscience Institute, University of California, Berkeley, Berkeley, CA, USA
[5] Department of Psychology, University of California, Berkeley, Berkeley, CA, USA

The Nucleus Accumbens (NAcc) is an important structure for the transfer of information between cortical and subcortical structures, especially the prefrontal cortex and the hippocampus. However, the mechanism that allows the NAcc to achieve this integration is not well understood. Phase-amplitude cross-frequency coupling (PAC) of oscillations in different frequency bands has been proposed as an effective mechanism to form functional networks to optimize transfer and integration of information. Here we assess PAC between theta and high gamma oscillations as a potential mechanism that facilitates motor adaptation. To address this issue we recorded intracranial field potentials directly from the bilateral human NAcc in three patients while they performed a motor learning task that varied in the level of cognitive control needed to perform the task. As in rodents, PAC was observable in the human NAcc, transiently occurring contralateral to a movement following the motor response. Importantly, PAC correlated with the level of cognitive control needed to monitor the action performed. This functional relation indicates that the NAcc is engaged in action monitoring and supports the evaluation of motor programs during adaptive behavior by means of PAC.

Keywords: phase-amplitude coupling, nucleus accumbens, cognitive control, action monitoring, learning

1. INTRODUCTION

The nucleus accumbens (NAcc) is part of the ventral striatum and plays a pivotal role in integration of information (Goto et al., 2008) from the limbic system, particularly between the prefrontal cortex (PFC) and the hippocampus (HC). The NAcc is considered the interface by which the HC gates input from the prefrontal cortex (French et al., 2002). In rats the PFC and HC converge onto single NAcc-neurons (Finch et al., 1996; Goto et al., 2008) and the PFC-NAcc and HC-NAcc connections are mutually dependent. For instance, long term potentiation of the HC-NAcc association entails a long term depression of the PFC-NAcc association (Grace et al., 2007). It is assumed that this selective strengthening of the HC-NAcc connection is important for the rapid facilitation of goal-directed behaviors and for supporting automized actions (Goto et al., 2005; Belujon et al., 2008). Such automized actions are especially evident in motor learning tasks in which the NAcc integrates information for the planning of movements (Mogenson et al., 1980; Grace et al., 2000). Münte et al. (2007) speculated that the human NAcc evaluates the information used for the adjustment of response strategies. Accordingly, lesions in the NAcc limit the flexibility required for changes in behavior during learning (Grace et al., 2007). However, knowledge about the specific neural mechanisms utilized to integrate information from the PFC and the HC in the human brain is still limited.

Phase-amplitude cross-frequency coupling (PAC) of oscillations has been suggested as an effective mechanism for recruiting local networks to form functional global networks and to gate information (Buzsaki et al., 2004; Canolty et al., 2006, 2010; Cohen et al., 2009; Staudigl et al., 2012). PAC describes the dependency of the amplitude of a high frequency on the phase of a low frequency. In rats and mice there is a tight connection between the phase of the theta band (θ) of local field potentials (LFP) and single unit activity (SUA) (Chrobak et al., 1998; Sirota et al., 2003; Siapas et al., 2005) presumably allowing neurons to form a larger assembly of neurons by means of transient coupling (Chrobak et al., 1998). These studies suggest that the interaction between PFC and HC may occur via PAC. O'Donnell et al. (1995) showed that hippocampal hyper- and depolarization leads to hyper- and depolarization in the NAcc. In the state of depolarization neurons in the NAcc are more likely to fire action potentials in response to stimulation of the PFC (French et al., 2002; Goto et al., 2008) providing evidence for PAC with an enhancement of high frequency amplitudes during troughs in θ activity. Tort et al. (2008) showed transient θ phase—high gamma (γ) coupling in the rat's striatum during movement through a maze. Furthermore, Tort et al. (2009) demonstrated a function link between performance improvement and the strength of theta-gamma coupling during the course of learning. However, until now it has not been

established whether NAcc shows PAC between θ and high γ activity in a functionally specific manner in humans. This would indicate that integration of information within the NAcc could rely on transient coupling between frequencies.

We studied the NAcc activity in three human subjects directly by means of subcortical electrodes in a serial reaction time task (Nissen et al., 1987) in which the participants had to track and respond to a sequence of numeric stimuli in a fixed and a random order condition which modulated different cognitive control demands. From Tort et al. (2009) one can hypothesize that PAC transiently occurs in the NAcc and is modulated by the level of cognitive control. We tested the following hypotheses: PAC emerges in the NAcc. Second, PAC discriminates between phases of high and low cognitive control. Third, PAC varies systematically with behavioral performance measures across experimental conditions (high and low cognitive control—HCC and LCC) .

2. MATERIALS AND METHODS

2.1. PARTICIPANTS

3 patients (mean age 38.3 years ($SD = 12.34$), 2 female, all right handed) with a history of intractable epilepsy participated in this study. We directly recorded from the bilateral NAcc and the anterior Thalamus (ANT). For details on surgery and deep brain stimulation approach please see Appendix 6.1 and **Table A1** summarizing the clinical background of the patients.

2.2. PARADIGM

We carried out a serial reaction time task (see **Figure 1**) which required a single finger movement that was specified by a numeric stimulus presented on a monitor screen. Stimulus presentations were controlled by MATLAB. Patients were instructed to respond with their right thumb, index finger, middle finger, or little finger, which rested respectively on the spacebar, "j," "k," and ";" keys

FIGURE 1 | Subjects were presented with stimuli indicating which finger to move. Each block contained 60 trials (presentation of a single number). Colors denote the type of the sequence. Together, the subjects were presented with three blocks of a fixed sequence, two blocks of a random sequence, and one block in which they could choose a sequence on their own.

of a computer keyboard. Four different numbers (1, 2, 3, 5) were presented on the screen (height 2 cm, 0.15° visual angle). These numbers indicated the finger they had to use to press the key. Six blocks of 60 trials, each comprising the presented number and the corresponding finger movement, were conducted with each patient. The four numbers were presented in a fixed or random order depending on the block number, with 3 fixed order blocks followed by 2 random sequence blocks and a final block of self-paced finger movements. In the fixed order blocks a repetitive sequence of six numbers was presented in all three blocks. In sum, the participant performed 30 repetitions of the 6-number-sequence. In the random blocks the four numbers were presented randomly. In the self-paced block a fixation cross was presented instead of the numbers. The participants were not informed about the type of sequence. The interstimulus interval (ISI) was variable and depended on the reaction time of the participants, with a fixed time between response and next stimulus of 700 ms plus a jitter of ±110 ms. In this interval the stimulus remained presented. Thus, block and trial length depended on the participants reaction time (mean block length per participant: Pat01: 117 s (std: 18.4), Pat02: 93 s (std: 25.6), Pat03: 96 s (std: 26.03); mean trial length per participant: Pat01: 1.6 s (std: 0.52), Pat02: 1.01 s (std: 0.31), Pat03:1.03 s (std: 0.21). Blocks were separated by a 1 min rest. During this resting period an X was presented on the screen. A + presented for 5 s informed the participant about the beginning of a new block.

2.3. COGNITIVE CONTROL

These 3 types of sequences (fixed, random and self-paced) differed with respect to the need for ongoing monitoring of actions and performance outcomes and subsequently, adjustments of behavior and learning which we tagged cognitive control in accordance to MacDonald et al. (2000) and Ridderinkhof et al. (2004).

2.3.1. Fixed sequence

The fixed sequence allowed the participant to learn the sequence. During the early phase (cognitive phase Fitts et al., 1973) of learning, when the fixed sequence is unknown, a high level of cognitive control is necessary to establish a strategy to complete the task (Fitts et al., 1973) namely to associate the stimulus with the response. The longer the training the less necessary cognitive control is, since the stimulus-response association was learned and the participant knows which finger to move before the actual stimulus is presented on the screen.

2.3.2. Random sequence

The sudden onset of a novel or unpredictable event captures attention and disrupts ongoing performance (Barcelo et al., 2006). In our experiment switching from the fixed to the random sequence marks such onset of several unpredictable events. This interruption of stimulus predictability signals the need for a change in strategy from a learned and hence, automatic to an unlearned mode. The occurrence of errors makes cognitive control necessary which leads to post-error slowing in healthy participants and more careful responses after errors (Notebaert et al., 2009). Hence, less errors are expected during phases of high
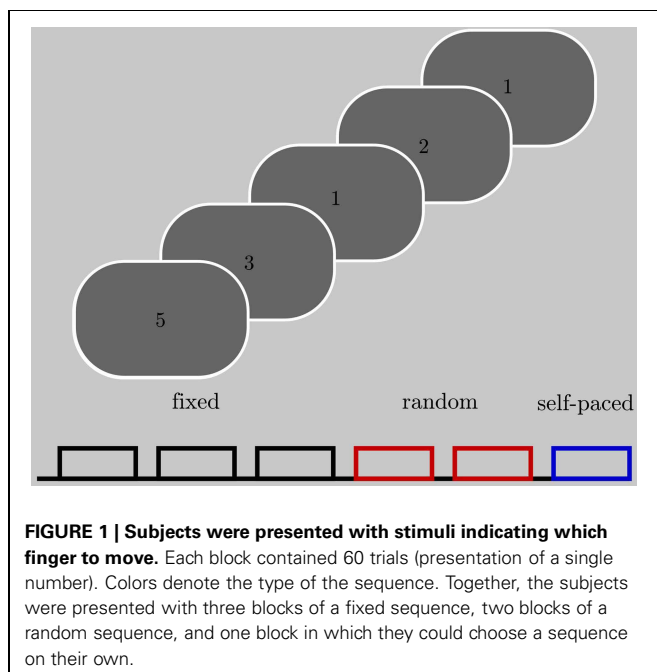
cognitive control. In healthy participants, differences in cognitive control are reflected by a reduction of initially long reaction times after the completion of several repitions of the 6-item sequence of the same fixed sequence (Nissen et al., 1987; Knopman et al., 1991). The presentation of random sequences after the fixed sequences will force the participant to abandon a learning strategy and elevate reaction times to a plateau value.

2.3.3. Self-paced sequence

During the last block, the participants could chose the sequence on their own with no obligation. Since the selected movement had not to be adjusted according to an external stimulus we expected short reaction times which would indicate less action monitoring or cognitive control. In sum, we classified trials of high cognitive control (HCC - initial tracking of the fixed sequence and tracking the random sequence) and low cognitive control (LCC - tracking the learned fixed sequence and during the self-paced sequence).

2.4. DATA COLLECTION

Intracranial recordings were obtained using a Walter Graphtek (Walter Graphtek GmbH, Lübeck, Germany) system, with a sampling rate of 512 Hz, a resolution of $0.25 \mu V$, and analog bandwidth of 200 Hz. We referenced online to the right earlobe. The ground electrode was placed at P8. During recording, a highpass filter of 0.19 Hz and a lowpass filter of 240 Hz was used. In the left and right NAcc and ANT (a total of 16 recording electrodes), adjacent electrodes were combined with each electrode referenced to the neighboring contact (i.e., 1–2, 2–3, 3–4, with "1" representing the most ventral and "4" representing the most dorsal electrode contact). This resulted in a bipolar montage with each NAcc/ANT monitored by three electrode positions. This montage was used to enhance the spatial resolution of the intracranial recordings and to ensure that the recorded activity originated from nearby tissue.

2.5. GENERAL DATA ANALYSIS

We used Matlab 2008a (Mathworks, Natick, USA) for all offline data processing. The resulting time series for the electrodes located in the NAcc were segmented in epochs of −1 to 2 s relative to the event (stimulus and response). In separate analyses these epochs were aligned to the motor response or onset of the instructive stimulus. These time series were used to characterize event-related brain dynamics in terms of PAC. We inspected the signal visually for artifacts and decided not to reject any epochs. Since we focused on single frequency bands we avoided signal drifts by applying bandpass filters for the frequency bands of interest (see below). All filtering was done using a 4th order butterworth filter (IIR-filter). All steps of data analysis were applied also to the recordings from the anterior thalamus.

2.6. BEHAVIORAL DATA

Two behavioral parameters—reaction times (RT) and error rate (p_e)—were assessed as indicators of cognitive control. The DBS procedure allows for the recording of only a limited pool of subjects (here $N = 3$). This limited number of subjects may influence strongly statistical test results so that effects can be missed even though potentially observable in a larger set of subjects. An ANOVA comparing RT differences across blocks—which may indicate differences in cognitive control—therefore, used RT of each trial in each subject as the random variable ($n = 180$) and blocks as factors ($p = 6$). Reaction times of each subject were z-scored across trials. Individual reaction times are summarized in **Table 1**. The summed number of errors in each participant was used to calculate p_e for each block except the self-paced block (errors cannot be made since the sequence was generated by the participant itself) we calculated

$$p_e = \frac{N_{\text{errors}}}{N_{\text{trials}}} \qquad (1)$$

Table 1B | Error rate.

Patient	Block # 1	Block # 2	Block # 3	Block # 4	Block # 5
1	4	6	7	5	1
2	1	1	2	4	1
3	3	2	1	0	2

Table shows the number of errors for each subject and block.

Table 1A | Reaction times in ms.

Patient	Block # 1	Block # 2	Block # 3	Block # 4	Block # 5	Block # 6
1	1027 (301)	1090 (261)	1077 (255)	1108 (284)	1057 (212)	645 (395)
z-score	0.079 (0.934)	0.268 (0.786)	0.229 (0.769)	0.323 (0.858)	0.170 (0.640)	−1.071 (1.191)
2	881 (214)	658 (106)	628 (146)	639 (122)	721 (180)	210 (182)
z-score	0.991 (0.823)	0.135 (0.407)	0.022 (0.562)	0.063 (0.469)	0.377 (0.692)	−1.588 (0.700)
3	814 (290)	642 (158)	604 (148)	655 (116)	680 (135)	510 (191)
z-score	0.804 (1.431)	−0.045 (0.782)	−0.230 (0.733)	0.022 (0.574)	0.143 (0.667)	−0.695 (0.943)

The table shows the mean reaction times and standard deviations of reaction times for each subject and block. Each value encompasses 60 trials. Since subjects differ in their reaction times (see Results) we z-scored the reaction times across all trials for each subject. This means that individual RTs were transferred into standard values by z-transformation individually for each subject. The second row of each patient shows the mean (std) of the z-scored reaction times. The subjects showed a different evolution of RTs across the experiment. But this concomitant in each group analysis—that individual subjects show only a trend which resembles the result of the group analysis or may slightly deviate from the trend in the group—does not challenge the statement resulting from the ANOVA for a group of participants. Even though we could only dispose of a very small group, the trend of behavioral changes in terms of RTs remains.

with N_{errors} designating the set of trials with false responses and N_{trials} as the total number of trials in a given block. A χ^2 test statistically compared the blockwise p_e. These values were related to PAC in a correlation analysis to test the specific hypothesis of a functional relationship between PAC and behavioral performance (see Section 2.7).

2.7. FREQUENCY ANALYSIS

In the first step we analysed whether oscillations show significant amplitude variations following the stimulus or the motor response. The rationale was to exclude the possibility that expected effects of PAC could be the result of the variation of only one frequency. We filtered the epochs in each trial in a broad range of frequencies ranging from 4 to 150 Hz (center frequencies) with a step of 2 Hz (band width of 4 Hz). By means of the absolute Hilbert transform we estimated the envelope of the oscillatory activity for each filtered time series in each trial. We then grouped the trials according to the HCC and LCC condition (see Section: Cognitive Control). In each frequency band and at each time point we compared the amplitude values across subjects and trials with a t-test. To assess statistical significance we corrected the significance threshold with a false discovery rate (FDR). Therefore, we fitted a cumulative normal distribution function to all p-values < the uncorrected significance threshold ($p < 0.05$; see **Figure 4**). All comparisons between HCC and LCC whose p-values < 0.05 in this new distribution were considered statistically significant. We furthermore asked, whether the amplitude in experimental conditions evolves differently with respect to their baseline. In each trial we calculated the differences between the baseline (average of 500 ms before motor response) and the averaged activity in the temporal interval of 500 ms following the motor response. We then tested by means of a t-test for differences between the experimental conditions (HCC-LCC).

2.8. PHASE-AMPLITUDE CROSS-FREQUENCY COUPLING (PAC)
2.8.1. Calculation of PAC

To define whether frequencies interact and whether this interaction shows a temporal pattern, we quantified the relationship between the phase of the θ frequency band and the amplitude of a high frequency band in a manner comparable to the approach of Tort et al. (2009). Specifically, for a given electrode e we used the temporal interval i around the button press in the fixed and random sequence trials ($N_{trials} = 300$) since in both the subject had to respond according to an external cue. In this interval i we separated the θ oscillation into 30 phase bins ($-\pi$ to π; $N_{bins} = 30$) and calculated the averaged high frequency amplitude within each phase bin (see **Figure 2A**). We filtered the raw signal in the θ (4–8 Hz (Axmacher et al., 2010)) band and a high frequency band covering the γ and high γ bands. The high frequency band was divided into narrow sub-bands with center frequencies ranging from 25 to 175 Hz, a bandwidth of 30 Hz and a step size of 2 Hz. We used the Hilbert transform to estimate the high frequency amplitude time series and the θ phase time series. From this the amplitude-phase-histograms were derived with the 2π-θ-cycle split into 30 phase bins of equal width (0.21 rad or 12°) in consecutive temporal intervals. We first calculated the cross-frequency spectrogram (amplitude variation of a high frequency

oscillations as a function of the phase of a low frequency oscillation) within each subject. This means that the θ-phase values over the temporal interval (166 ms) were sorted into 30 equally spaced phase bins. The window size of each temporal interval was set such that a full cycle of the center frequency (6 Hz) of the θ range (4–8 Hz) was covered (166 ms). Next, the high gamma amplitudes observed at the various time points were separately averaged for each phase bin. As the next step in each subject we fitted a cosine function to the resulting high gamma amplitude values over phase bins. To prove the dependency of the high gamma amplitude on a same θ phase across subjects we averaged the resulting fit functions (see **Figure 2**). As the final step in our analysis we statistically compared whether more variance is explained by the variance across subjects or more variance is explained by the averaged fit functions (see next paragraph). If the latter was the case then all subjects' high gamma amplitude depended on the same θ phase and the Modulation Index was high. For example, if coupling did not rely on the same θ phase then the variance across subjects would be higher compared to the variance across the θ cycle. In sum, first the subject specific electrophysiology was evaluated followed by the statistics within the entire group of subjects in which we tested whether despite averaging the fit function more variance is explained by the fit function than by the variability across subjects. The same analysis was also conducted with 2 underlying θ
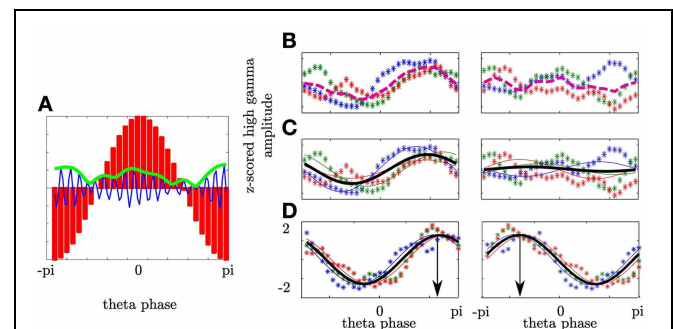
FIGURE 2 | Phase-amplitude cross-frequency coupling describes the dependency of high frequency amplitude on phase of low frequency oscillation. (A) θ oscillation was separated into 30 phase bins covering the entire cycle ($-\pi$ to π; red bars). In each bin the magnitude of the high γ analytic amplitude (green line) of the ongoing high γ band (blue line) was calculated. **(B)** Depiction of high γ amplitude as a function of θ phase for three subjects (colored asterisks) in one temporal interval. For each subject the mean high γ amplitude corresponding to each of the θ phase bins was calculated across trials. Afterwards, the variance across the mean over subjects (dashed line) was calculated. In the left plot (contralateral NAcc) the variance of the high frequency amplitude across the θ bins is greater as compared to the variance across subjects for a given bin resulting in an enhanced averaged variance as compared to the ipsilateral NAcc (right plot). **(C)** The variation of high γ amplitude as a function of θ phase was predicted by a cosine function assuming a unimodal dependency of high γ amplitude on the θ phase. A cosine function was fitted to individual high γ amplitudes (solid lines) and pooled across subjects (bold black line). In the left plot a high modulation index results from higher variation across the θ cycle than amplitude differences between subjects. **(D)** PAC defines the θ phase the high γ amplitude is coupled to. Both plots show the same coupling strength, however, with different coupling phases. In the left plot the high γ amplitude is coupled to the descending part of the θ cycle whereas in the right plot the coupling phase is the ascending part of the θ cycle.

cycles. These analyses yielded roughly the same results, but with a poorer temporal resolution. The window of analysis was shifted in time by 10 ms between −600 and 600 ms around both the stimulus and the motor responses. This led to 121 temporal intervals ($N_{interval}$). Subsequently, in each interval the phase-amplitude distribution (distribution of high gamma amplitude values across theta phase-bins) was averaged across the electrodes separately for each hemisphere (contra- and ipsilateral to the performing hand) and for stimulus and response alignment.

2.8.2. Quantification of PAC

To quantify PAC we used the variance σ^2_{PAC} of the mean high frequency amplitude and the Modulation Index (MI; see **Figures 2B,C**). σ^2_{PAC} is suited to be an exploratory measure since no specific model is assumed. In contrast the MI assumes a specific form of dependency of high frequency amplitude on the θ cycle and is defined by the strength of coupling and the phase to which the high frequency amplitude is coupled. In each temporal interval i we calculated the high γ amplitude distribution across the θ cycle per subject. We then averaged the high frequency amplitude across participants. This averaged high frequency amplitude is shown in **Figure 2B** as a dashed line. We calculated the variance σ^2 of the averaged high frequency amplitude as a function of the θ phase

$$\sigma^2_{(H\gamma/\theta)} = \frac{1}{N_{bins}} \sum_{i=1}^{N_{bins}} (a_i - \overline{a})^2 \qquad (2)$$

with a_i representing the mean high γ amplitude for a given phase bin across participants and $\overline{a}$ representing the averaged amplitude of a_i over θ phases. The larger σ^2 the larger are the differences of the high frequency amplitude at different θ phases. A high value of variance indicates a high concordance of PAC across participants. In **Figure 2B** we show this for two cases. The left plot shows a high variance of the averaged high frequency amplitude. The right plot shows that individual fluctuations of the high frequency amplitude are canceled out in the average. This leads to a small variance indicating a lack of coupling. To compare across different high frequency bands we normalized the amplitude values by z-scoring. We used the variance to compare the modulation of high frequencies by θ phase across all anatomical regions. Note that a high σ^2 only indicates that at different θ phases the high frequencies differ in amplitude: it does not explain whether the variance of the high frequency amplitudes is accounted for the θ cycle. Therefore, in each high frequency showing a significant variance level we determined the goodness of a cosine fit (F-value). The cosine function (representing the θ cycle) was fitted to the z-scored high frequency amplitude values in each subject. The best cosine fit function minimizes the sum of squares of errors. We termed the test statistic *modulation index* according to Tort et al. (2009). However, in our analysis the MI represents an ANOVA and hence, specifies whether more of the variance in the high frequency amplitude (MS_{cos} - explained by the θ cycle) is explained by the variation across the θ cycle or across the participants (MS_{error}—unexplained by the θ cycle). Therefore, we averaged the cosine fit functions across subjects and

assessed whether despite averaging more variance of the high frequency amplitude is explained by the θ cycle than the variance across subjects.

The variance between the θ phases is given as

$$MS_{cos} = \frac{SS_{cos}}{df_{cos}} \qquad (3)$$

with SS_{cos} as the sum of squares of high frequency amplitude between θ phases and df_{cos} as the degrees of freedom. The variance within the θ phases is given as

$$MS_{error} = \frac{SS_{error}}{df_{error}} \qquad (4)$$

with SS_{error} as the sum of squares of high frequency amplitude within θ phases and df_{error} as the degrees of freedom. MS_{error} takes the variability across subjects into account. The MI is given as the ratio between both as

$$MI = \frac{MS_{cos}}{MS_{error}} \qquad (5)$$

The larger the MI more of the variance in the high frequency amplitude is explained by the variation across the θ cycle than across the participants. In fact this MI is comparable to an ANOVA which directly compares an effect of a condition (here θ cycle) in relation to a random variable (here individual high γ amplitude values) in each factor of the condition (here each single phase bin of the θ cycle). If each subject would show coupling however, with a strong coupling phase angle shift this would result in a low MI. Also strong gamma bursts in one subject and hence not a smooth variation of the high gamma amplitude across the θ cycle would result in a low MI since the variation across subjects increases compared to the variation across the θ cycle.

Furthermore, PAC is defined not only by the coupling strength but also by the phase of the θ cycle at which the high gamma amplitude reaches its maximum. In **Figure 2D** we show differences in coupling phase with the same coupling strength. Here all subjects show strong coupling since the variation of high gamma amplitude values in each subject is accounted for the θ cycle. The bold line shows the average of the individual cosine fit functions. Despite averaging across subjects more variance is accounted for the θ cycle than for variance across subjects at each phase. In the left plot high gamma amplitude is coupled to the descending part of the θ cycle whereas in the right plot the high gamma amplitude is coupled to the ascending part of the cycle. The coupling phase was estimated by determining the θ phase where the averaged cosine fit function reaches its maximum.

2.8.3. Statistical test of PAC

To estimate the empirical distribution of σ^2 in each temporal interval we calculated the variance of original time series filtered in the high γ range but randomly shifted in time as a function of the original θ phase in 500 randomizations. The 97.5th percentile of this distribution was used as the critical value when appraising the significance of our results. To estimate the empirical distribution of MI in each temporal interval we calculated the

MI on the same set of randomizations as used for σ^2. The 97.5th percentile of this distribution was used as the critical value when appraising the significance of our results.

2.8.4. Functional relation between PAC and behavioral performance

We tested the specific hypothesis that a functional relationship between PAC and cognitive control exists. To this end we assessed the correlation between both RTs and p_e with PAC. In sliding windows of 50 consecutive trials with a step of 2 trials we calculated the grand average of reaction times (1. average of RT over trials, 2. average across subjects) and the p_e. In separate analyses we tested both behavioral measures p_e and RTs for possible correlations with MI and coupling phase.

2.9. PRECLUSION OF θ PHASE RESETTING

In each subject we investigated whether the coupling can be attributed to a resetting of the θ phase. At each time point across trials in each subject we calculated the phase concentration κ of circular data which is the reciprocal to the variance in a normal distribution to exclude the possibility that PAC results from phase realignment of the θ oscillation across trials. A high κ-value indicates a preferred θ phase across trials at a given time point. Statistical significance was assessed by a permutation procedure. In 500 runs the trial-wise time series were shifted in time separately. In each run κ was calculated. The confidence intervals for phase concentration κ were derived from the resulting 500 κ time series.

2.10. SPECIFICITY OF θ-HIGH γ COUPLING

We furthermore sought to preclude the possibility that the high frequency amplitude was coupled to the phase of frequencies other than θ. In the 200 ms following the motor response we calculated the variance of amplitude of all high frequency bands in the γ/high γ range (center frequencies: 55–165 Hz, bandwidth: 30 Hz, step size: 2 Hz) as a function of the phase of low frequencies ranging from 3 to 16 Hz (bandwidth: 4 Hz, step size: 1 Hz). Here, we first calculated the high frequency amplitude distribution across the cycle of each low frequency and then averaged across the subjects as shown in **Figure 2**. We then calculated the variance of the averaged high frequency amplitude distribution. The variance is high if all participants show a comparable distribution of the high frequency amplitude across the cycle of a given low frequency cycle. In contrast, the variance is low if participants did not show a comparable dependency of the high frequency amplitude on the low frequency cycle.

3. RESULTS

3.1. BEHAVIORAL RESULTS

First, we tested whether the participants performed differently throughout the task (see Materials and Methods) indicating differences in cognitive control. We assumed that tracking and responding to an unknown (i.e., block 1), a well-learned (i.e., block 2–3) or an unpredictable sequence (i.e., block 4–5) call for different cognitive control demands. Unknown and unpredictable sequences demand a high cognitive control since recent patterns cannot be extracted. Differences in reaction times across blocks (see **Table 1**) were confirmed with an ANOVA ($F_{(5, 1074)} = 87.11$,

$p < 0.0001$; see **Figure 3A**). **Figure 3C** shows the mean reaction times for each trial bin. *Post-hoc* paired t-tests confirmed changes in reaction time between blocks. These results were summarized in **Table 2**. The relative comparison between blocks shows that blocks 2 and 4 show more similar mean RTs than blocks 1 and 4. However, it is of note that blocks 1 and 2 are statistically different as well and even though not statistically significant there is a trend from block 2 to 3 and all the more important from 3 to 4. Therefore, the overall trend across the experiments suggests that there is a course from HCC to LCC during the second and third block to HCC in both random sequence blocks and again to LCC in the self-paced block in terms of reaction times. In sum, we interpret the results in an absolute way (global course across the experiment) given that we recorded behavioral data from (i) non-healthy subjects which participated in (ii) only one block due to the limited recording time. Furthermore, blocks differed with respect to the error rate p_e which was confirmed with a χ^2 test (mean p_e per block: 0.044, 0.050, 0.056, 0.050, 0.022, $p < 0.005$,

FIGURE 3 | Depiction of behavioral results. *x*-axis: sequence type. Numbers within the bars show the number of the block. HCC and LCC above the bars indicate the level of cognitive control necessary to perform the task (HCC—high cognitive control and LCC—low cognitive control) **(A)** Reaction times were pooled across subjects and trials. Each bar encompasses reaction times of 180 trials (1 block). Error bars represent the standard error across trials. The color of the bar indicates the sequence type as in **Figure 1**. Trialwise reaction times vary in accordance with sequence type. For more clarity *post-hoc* differences are summarized in **Table 2**. Participants show increasingly faster response with training the fixed sequence. Following the fixed sequence reaction times are slower during the random sequence. **(B)** Error rates per block pooled across subjects. Error rates are only shown for fixed and random blocks since no error can be calculated for self-paced blocks. **(C)** Depiction of the evolution of RT across the trial bins. The error bars in both plots denote the standard error of the mean. **(D)** Depiction of the evolution of error rate across the trial bins. The error bars in both plots denote the standard error of the mean

Table 2 | *Post-hoc* statistical *t*-tests.

Comparison	*t*-value	*p*-value
1–2	5.03	<0.0001
1–3	6.09	<0.0001
1–4	4.91	<0.0001
1–5	3.96	<0.0001
1–6	15.09	<0.0001
2–3	1.52	0.13
2–4	−.22	0.82
2–5	−1.54	0.12
2–6	13.41	<0.0001
3–4	−1.8	0.06
3–5	−3.05	0.002
3–6	12.04	<0.0001
4–5	−1.33	0.19
4–6	13.73	<0.0001
5–6	14.72	<0.0001

The left column shows which blocks were tested. The middle column gives the t-value for significance of mean differences and the right column the corresponding p-value.

please see **Table A2** for the pairwise comparisons). **Figure 3B** shows the continuous increase of p_e from block 1 (HCC) to block 3 (LCC) and a decrease of p_e from LCC to HCC in block 4 and 5. Note, in the self-paced block 6 no errors could be made and hence p_e could not be calculated. In **Figure 3D** we show the error rate for each trial bin.

3.2. AMPLITUDE VARIATION
To exclude the possibility that PAC results can solely result from significant amplitude variations in one frequency we compared amplitude variations in a broad range of frequencies ranging from θ to high γ, which neither for the amplitude variation at each time point nor the test for different evolution with respect to the baseline passed the significance threshold FDR-corrected for multiple comparisons (see **Figure 4**).

3.3. HIGH γ AMPLITUDE VARIES AS A FUNCTION OF θ PHASE IN THE CONTRALATERAL NAcc
Our general hypothesis was that the high γ amplitude varies as a function of θ phase in the NAcc. We tested the statistical significance of σ^2_{PAC} in the bilateral NAcc and the bilateral ANT associated both with the numeric stimulus and the response. We found an increase in σ^2_{PAC} shortly after the motor response solely in the contralateral NAcc (see **Figure 5**) but not in the ipsilateral NAcc nor in the ANT. **Figure 6** specifically shows σ^2_{PAC} and MI for the contralateral NAcc. The increase in the contralateral NAcc was statistically significant, exceeding the 97.5th percentile of our computed distribution of gamma variances σ^2_{PAC} (CI$_{97.5}$ = 0.57; **Figure 6A**). By calculating the MI we then tested whether the variance of the high frequency amplitude is accounted for the θ cycle (see **Figure 6A**). As for σ^2_{PAC} we found an increased MI following the motor response. The increase in the contralateral NAcc was statistically significant, exceeding the 97.5th percentile of our computed distribution of

MI$_{random}$ (CI$_{97.5}$ = 18, see **Figure 6A**). The increased σ^2_{PAC} of high gamma (100–140 Hz) amplitude in the contralateral NAcc could be accounted for the θ phase. This coupling was absent for the ipsilateral NAcc and following the stimulus, as well. We assumed that this is a result of different reaction times between subjects [$F_{(2, 1077)}$ = 136.54, $p < 0.0001$]. We furthermore verified that coupling was restricted to the θ-high γ interaction (see **Figure 12**) and that an increase of coupling could be found in each subject (see **Figure 13**). The individual coupling patterns all show a different temporal layout following the coupling on the population level. However, only in the temporal interval of coupling on the population level in all subjects the MI tends to increase.

3.4. COUPLING STRENGTH REFLECTS COGNITIVE CONTROL
Our second question was whether the MI changes as a function of cognitive control. We tested this for the MI between θ (4–8 Hz) and high gamma band (112–142 Hz) since both bands showed the strongest coupling increase collapsed across all trials. An initial comparison of the MI in HCC versus LCC trial bins (each containing 10 non-overlapping trials) revealed that MI is significantly greater in HCC trial bins (t_{16} = −2.54; p = 0.016, see **Figure 7**). In the next step we tested whether the MI shows a systematic variation as a function of the experimental condition (HCC: block 1, 4, and 5 and LCC: block 2, 3, and 6). Therefore, we calculated the MI for the contralateral NAcc for each temporal interval across trial bins. Trial bins contained 50 trials with a step size of 2. Thus, we calculated the MI first for the trials 1–50, then for trials 3–53, and continued until trial 300–349 (see **Figure 8A**). Between 0 and 200 ms we determined when the maximal MI occurred. In periods of high cognitive control (HCC) the MI exceeded the statistical significance threshold (see **Figure 8B**). Coupling decreased in the low cognitive control condition (late fixed trial bins and final self-paced movement block). Importantly, coupling peaks earlier during the LCC sequences (mean coupling time = 90 ms) compared to HCC sequences (mean coupling time = 140 ms, see **Figure 8C**; t_{99} = −8.27, $p < 0.1$–12). The point in time of maximal coupling and MI covaried significantly ($r = 0.7$; $p < 0.0001$ see **Figure 8D**). Note, that differences in MI cannot be explained by longer RTs since trials were aligned to the motor response.

3.5. FUNCTIONAL RELATION BETWEEN PAC AND BEHAVIOR
3.5.1. MI correlates with error rate
A further strong indication for functional relation between PAC and behavior would be provided by a covariation of MI with performance. It is assumed that the NAcc is engaged in action monitoring. We assume that high cognitive control allows for high action monitoring which should result in a low probability of making an error. In contrast, low cognitive control should result in a comparatively high probability of making an error. We therefore tested whether the PAC represented by the MI (coupling strength) or the coupling phase predicts the probability of making an error p_e or reaction times. To achieve a continuous measure in the consecutive trial bins containing 50 trials as described above we calculated p_e. Subjects showed on average a reduced p_e at the beginning of the experiment and while
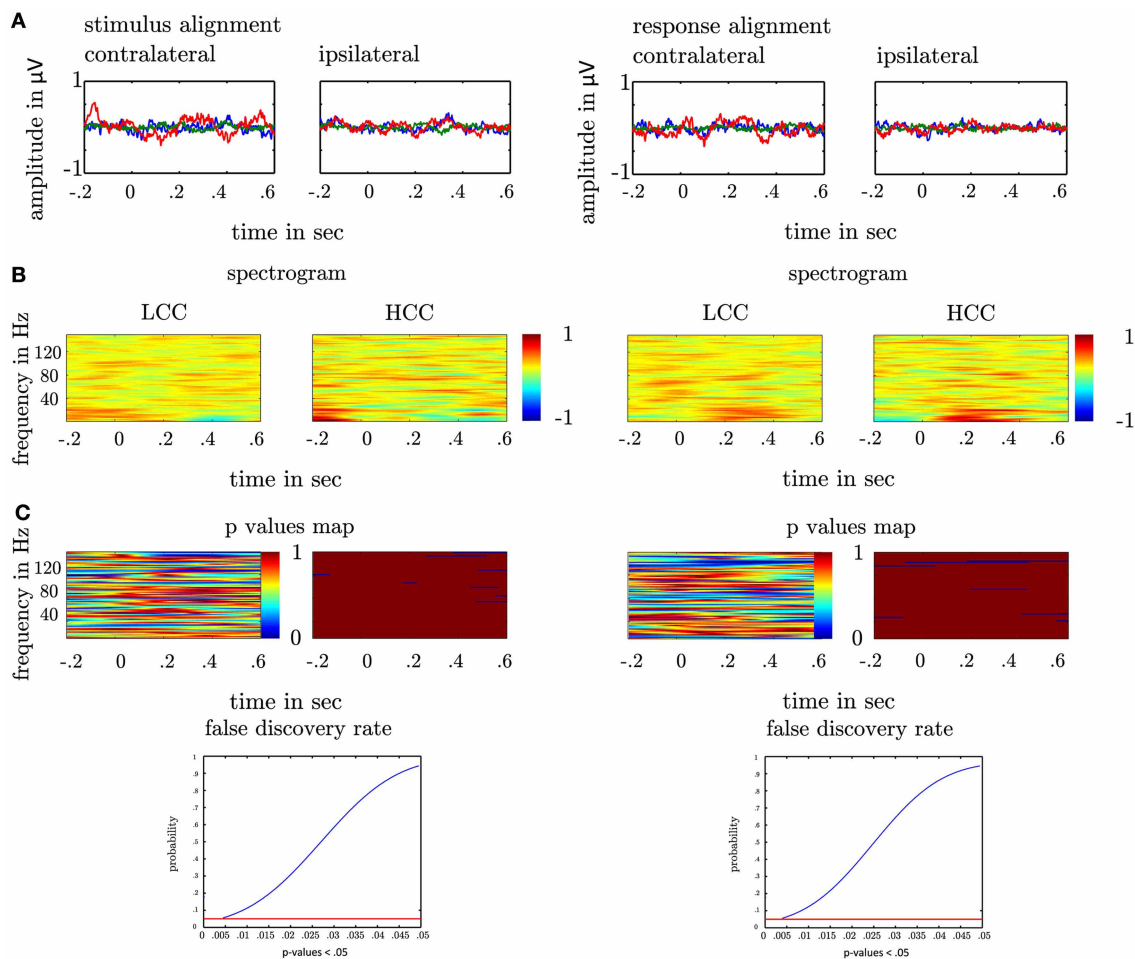
FIGURE 4 | (A) Depiction of local field potentials locked to the response and the stimulus presentation both for the contra- and ipsilateral recording sites. The LFP in each trial was filtered between 3 and 200 Hz. Each colored line represents one subject. **(B)** Depiction of spectrograms for the low cognitive control condition (left-LCC) and the high cognitive control condition (right-HCC). In each subject we estimated the spectrogram by means of the Hilbert transform. In each trial aligned to the motor response/stimulus, we calculated the envelope of the bandpass filtered time series (4–150 Hz, bandwidth: 4 Hz, step: 2 Hz). The upper plots show the average across subjects and trials both aligned to the response and the stimulus in the HCC and LCC. For a better comparison of the amplitude across frequencies the spectrogram was z-scored for

depiction only. All analysis were conducted on the non-standardized time series. The colorbar denotes the strength of amplitude in μV (z-score). **(C)** depicts the statistical evaluation by means of a t-test. At each time point in each frequency we calculated the p-value for the difference between LCC and HCC across subjects and trials (left plot). The right plot shows the time points and frequencies with a p-values < 0.05 (blue) on an uncorrected significance threshold. We corrected for multiple comparisons by taking the distribution of p-values < 0.05 into account. The 0.05% confidence interval of this new distribution (last row) served as a new significance threshold. Note that no p-value fell below this threshold indicating that between the HCC and the LCC condition no significant difference in amplitude modulation was found.

performing the random trials where the modulation index was high, which accords with the view that action monitoring is high when subjects first begin to track the fixed sequences and during the random sequences (HCC). The MI was significantly correlated with p_e ($r = -0.21$; $p < 0.05$). Additionally, since the trial bins were not statistically independent we determined the significance of Pearson's correlation coefficient r against the distribution of r values calculated from 500 shuffles of trials. We found that the observed r value could not have been derived from a chance distribution ($p = 0.01$). This indicates a statistical significance. In **Figure 9** we depict the p_e averaged across our three subjects (gray curve) together with the MI (blue curve). In contrast, MI did

not vary with reaction times in the same trial bins ($r = -0.15$; $p > 0.05$).

3.5.2. Coupling phase correlates with reaction times

Hasselmo et al. (2002) proposed a model of the functional relevance of the rat hippocampal θ rhythm in which the encoding and retrieval of memory information occur in different phases. He argues that this mechanism is important for the reversal of prior learning. Furthermore, we tested whether the coupling phase varies as a function of cognitive control. In each trial bin we determined the point in time of maximal MI, and evaluated the cosine function which served as the basis for the MI.
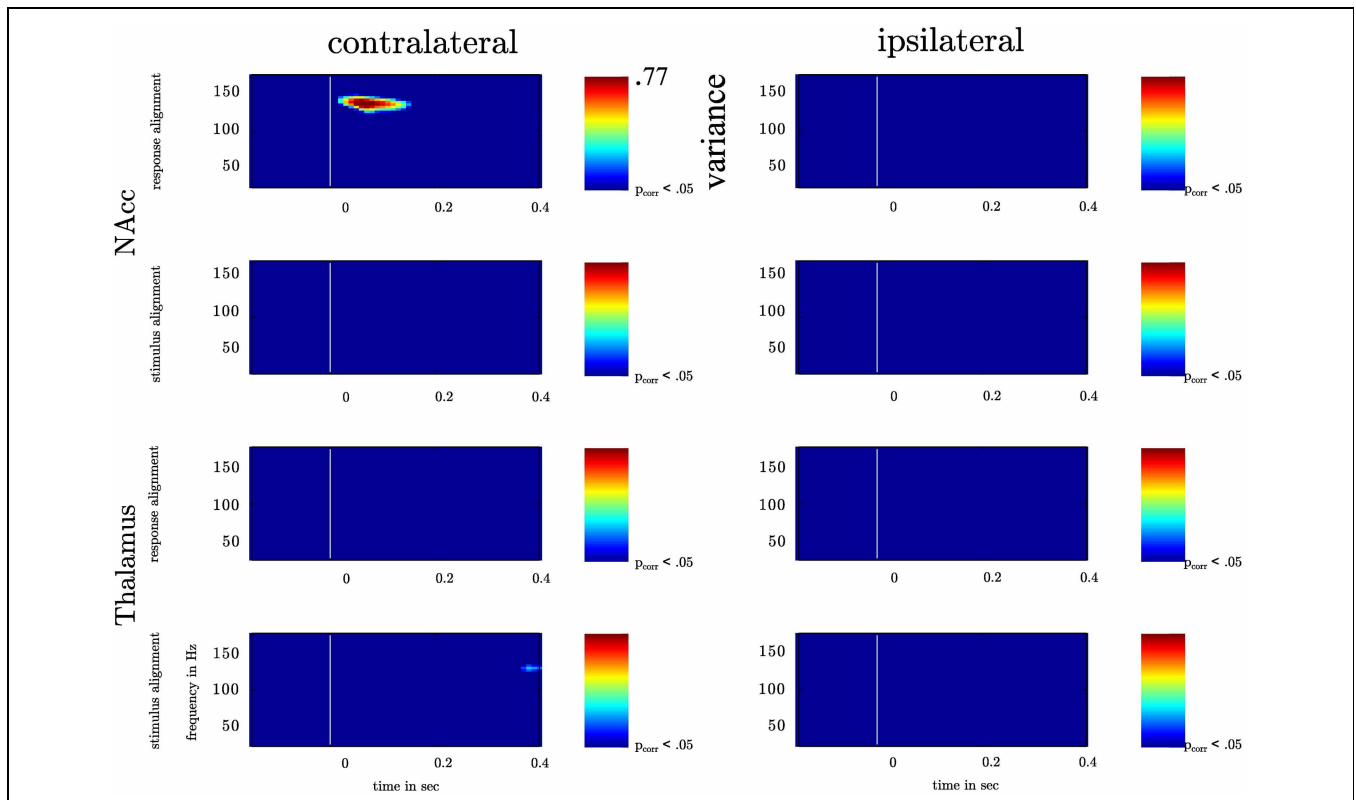
FIGURE 5 | Depiction of the variation of high γ amplitude across θ cycle for bilateral NAcc and bilateral anterior Thalamus. The recorded time series in the contra- and ipsilateral NAcc and Thalamus were aligned to the motor response or the instructive stimulus. In each frequency band ranging from 25 to 175 Hz (centerfrequencies) we calculated the variance of high

frequency amplitudes across the θ cycle (4–8 Hz) as a function of time. Variance increased significantly solely following the motor response in the contralateral NAcc (p-value corrected for the number of recording sites). Variance values corresponding with a p-value smaller than p_{corr} are depicted color-coded ranging from blue (small variance) to red (high variance).
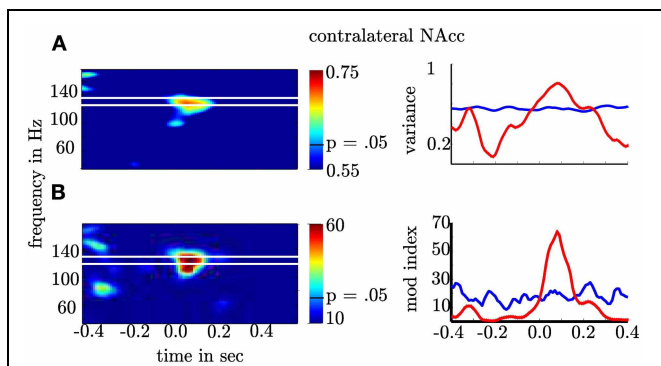
FIGURE 6 | Depiction of θ-high γ PAC for the contralateral NAcc. (A) The first row gives the $\sigma^2_{(H\gamma/\theta)}$ as a function of time (x-axis) and frequency (y-axis). **(B)** The second row shows the modulation index. The second column shows the frequency band (≈100–140 Hz; red line) with significant increase of $\sigma^2_{(H\gamma/\theta)}$ and PAC. The blue lines denote the 97.5th percentile used as confidence interval of the normal distribution for σ^2 and F-distribution for MI. Note that the variance and the Modulation index exceeded the significance threshold for more than 200 ms and each point is the result of a temporal interval of 166 ms. This means that coupling is present in non-overlapping temporal intervals and hence, extents across several cycles.
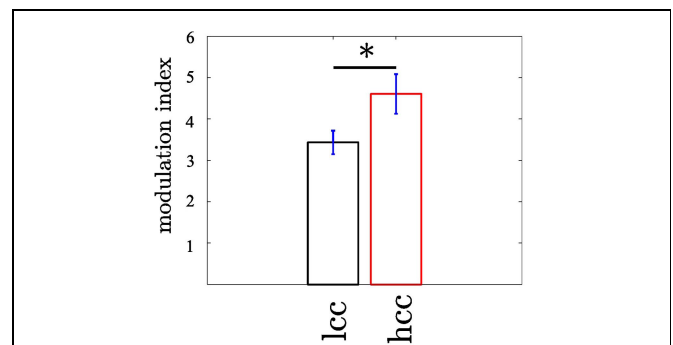
FIGURE 7 | The modulation of the high γ frequency by the θ phase differs between trials with low (LCC) vs. high (HCC) cognitive control (p < 0.05). The modulation index was calculated in non-overlapping trial bins of 10 trials. In trial bins containing only trials from the HCC condition the modulation was enhanced compared to trial bins of LCC trials. Error bars denote the standard error across trial bins. *p < 0.05.

The θ phase that corresponded with the maximal value of the cosine function representing the peak of the high γ amplitude was taken to be the coupling phase. We found the coupling phase discriminates between trial bins of HCC and LCC (see **Figure 10**).

FIGURE 8 | *Coupling strength varies with sequence type* (A) Variance of high γ as a function of θ phase (upper plot) and modulation of high γ by θ phase (lower plot). Both plots show the variance and the modulation as a function of time (*x*-axis) and trial bin (*y*-axis). Trial bins are arranged from top to bottom. Both show that across subjects coupling is elevated at the beginning of the fixed and during the random trials. For consecutive trialbins each containing 50 trials we calculated the modulation index. Following the motor response the MI varied with sequence type. The sequence type is indicated by the colored bar left to the magnification: black corresponds to fixed, red to random and blue to self paced trials. The alternating red-black bar denotes those trialbins containing both fixed and random trials. Note that including only a small proportion of random trials elevates the modulation index. Alternating blue-black bar denotes those trialbins containing both random and self-paced trials. **(B)** Depiction of points in time at which modulation peaks for trialbins. The right panel shows the dependency of maximal modulation index on trial bin in the 0–200 ms interval (see **Figure 5** right column) following the motor response. **(C)** In fixed trials coupling is earlier then in random trials. Only trial bins containing either fixed or random trials were used in this analysis. **(D)** Time of coupling between θ and high γ depends on coupling strength. **(E)** shows the individual summed square errors 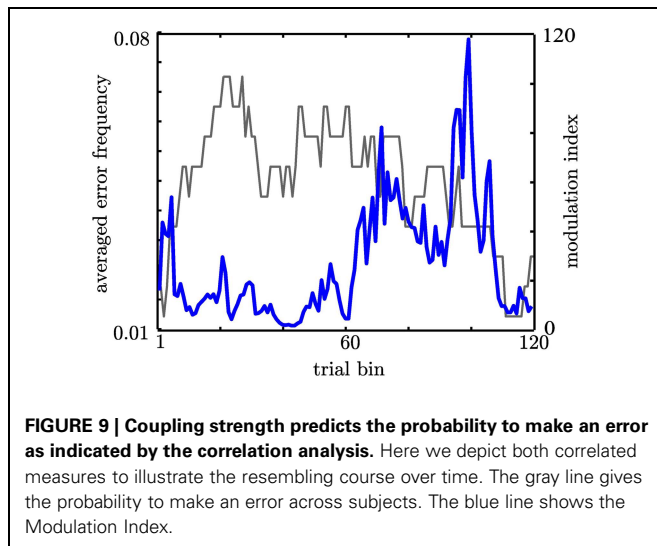of each subject from the mutual cosine fit function as a function of trial bin. The greater error of subject 1 does not mean that this subject does not exhibit a sine shaped dependency of the high gamma activity as shown in **Figure 2C**. As the blue line deviates more strongly from the black bold line compared to the red and green line the summed mean error is greater than for subjects 2 and 3. However, it shows a clear sine shaped dependency. This means that subject 1 either contributes less to the strength of the MI or probably attenuates the MI but this does not challenge the visual impression that the high gamma amplitude is coupled to a resembling phase as subject 2 and 3. ***$p < 0.001$.

In trial bins containing fixed trials the mean θ phase is 1.72, while for random trials it is 2.29. A Watson–Williams test for circular data confirmed the significance of this coupling phase difference ($F_{(1, 99)} = 23.6$; $p < 0.0001$). Again, since the phase scores of each trial bin are not statistically independent, we calculated the significance of phase differences against the distribution of F values calculated from 500 shuffles of trials. We found that the observed p value could not have been derived from a chance distribution ($p < 0.0001$). As for the MI we tested whether the change of phase as a function of cognitive control has a significance for the observed behavior. We used ρ as the correlation coefficient between one circular and one linear random variable. In contrast to the MI we found the coupling phase is significantly correlated with the reaction times ($ρ = 0.55$, $p < 0.001$; see **Figure 10A**). ρ could not have been found within the set of 500 trial shuffles ($p < 0.001$). However, the coupling phase did not predict pe ($ρ = 0.15$, $p > 0.05$).

Note that there is a slight phase angle shift between the subjects. However, as revealed by the MI, this phase shift does not influence that more variance is explained by the variation across the theta cycle than between subjects. This is explicitly considered in our MI measure. In trial bins (see paragraph on Functional

FIGURE 9 | Coupling strength predicts the probability to make an error as indicated by the correlation analysis. Here we depict both correlated measures to illustrate the resembling course over time. The gray line gives the probability to make an error across subjects. The blue line shows the Modulation Index.

FIGURE 10 | (A) Cognitive demands in different sequence types are reflected by difference in coupling phase. In each trialbin we determined the modulating phase of the θ cycle. Black dots denote the phase the high γ amplitude is coupled to for each trial bin. The sequence type is indicated by the colored line: black corresponds to fixed, red to random and blue to self paced trials. The alternating red-black line denotes those trial-bins containing both fixed and random trials. Alternating blue-black line denotes those trial-bins containing both random and self-paced trials. Phase differences were investigated comparing trial bins containing exclusively fixed and random trials, respectively (solid black and solid red intervals). Black arrows mark the mean θ phase. Coupling phases differ significantly between fixed and random trial bins. Please note that at the beginning of the entire experiment, when the sequence to be learned is unknown high gamma amplitude peaks at the same frequency as during the unpredictable random sequence. **(B)** During HCC high gamma amplitude is coupled to the θ trough across subjects while during LCC the coupling phase is different across subjects as indicated by the greater errorbars during trialbins of LCC. In each trial bin we grouped the high gamma amplitude according to the 30 θ bins for the temporal interval ranging from 0 to 200 ms. We fitted a cosine function to the resulting 30 high gamma amplitude values. The coupling phase of the θ oscillation was defined as the phase at which the high gamma amplitude was maximal. This leads to 3 coupling phases one per each subject in each trial bin. To better illustrate the in-phase coupling we collapsed the rising and the falling part of the θ cycle. Therefore, the y-axis ranges from 0 (θ peak) to ±π (θ trough). The x-axis gives the number of trial bins. The upper plot shows the average and the standard error of mean (SEM) of coupling phases across subjects for each trial bin. To better visualize this dependency of the SEM on the cognitive control we inserted the course of SEM over trial bins (red line) shows the standard error. This line demonstrates that the standard error across subjects is low in trial bins of HCC and high in trial bins of LCC.

Relation between PAC and behavioral performance) of HCC (long reaction times and a low error rate as at the beginning of the experiment and during random sequence trials) subject's coupling phase is the same, namely around the trough of the θ oscillation (see **Figure 10B**). In contrast, during phases of LCC (during late trials of the fixed sequence and during self-paced sequence trials) subjects show a great variation of the coupling phase. This is indicated by the greater errorbars during trialbins of LCC (see **Figure 10B**). In each trial bin we grouped the high gamma amplitude according to the 30 θ phase bins for the temporal interval ranging from 0 to 200 ms. We fitted a cosine function to the resulting 30 high gamma amplitude values. The coupling phase of the θ oscillation was defined as the phase at which the high gamma amplitude was maximal. This leads to 3 coupling phases one per each subject in each trial bin. To better illustrate the in-phase coupling we collapsed the rising and the falling part of the θ cycle. Therefore, the y-axis in **Figure 10B** ranges from 0 (θ peak) to ±π (θ trough). The x-axis gives the number of trial bins. The upper plot in **Figure 9B** shows the average and the standard error (error bar) of coupling phases across subjects for each trial bin. The red line shows the standard error. This line demonstrates that the standard error across subjects is low in trial bins of HCC and high in trial bins of LCC.

3.6. θ PHASE RE-ALIGNMENT

We tested for each subject whether PAC results can be a mere result of theta phase re-alignment. Here, we compared the phase concentration of the θ oscillation with an empirical distribution (see Materials and Methods). We did not find a statistically significant phase re-alignment in none of the subjects neither following the stimulus nor the motor response (see **Figure 11**).

3.7. SPECIFICITY OF θ-HIGH γ COUPLING

We tested whether θ and high gamma activity exclusively show coupling or whether other frequency combinations also show coupling. We found the variance of the high frequency bands (≈100–140 Hz) across the phase of the θ (4–8 Hz) band was higher than any other frequency combination (see **Figure 12**).
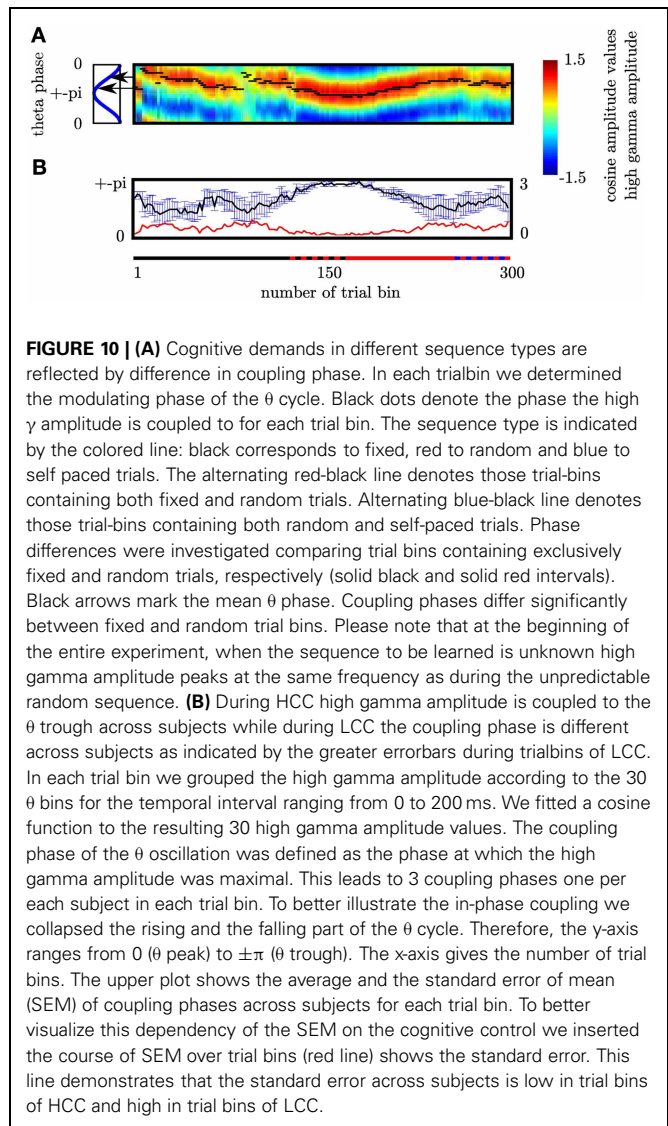
This yields a comparable narrow frequency interaction as found by Tort et al. (2008).

4. DISCUSSION

4.1. SUMMARY OF RESULTS

We investigated the dynamics of PAC in the human NAcc and show, that in the NAcc contralateral to a movement the θ phase modulates the high gamma amplitude (≈100–140 Hz) following a motor response. Importantly, this previously undescribed oscillatory pattern in the human NAcc increases with cognitive control and predicts behavioral adaptation as reflected in the reduction in error rates. Compared to reaction times the error rates show a more sluggish change which may explain the resemblance of the error rate if averaged across blocks. This means that changes in terms of RTs are more closely confined to the definition of blocks while the error rate changes with a greater time lag. However, the temporally resolved course revealed strong changes during the course of the experiment. We observed the strongest PAC in the first part of a task in which subjects responded to an unfamiliar
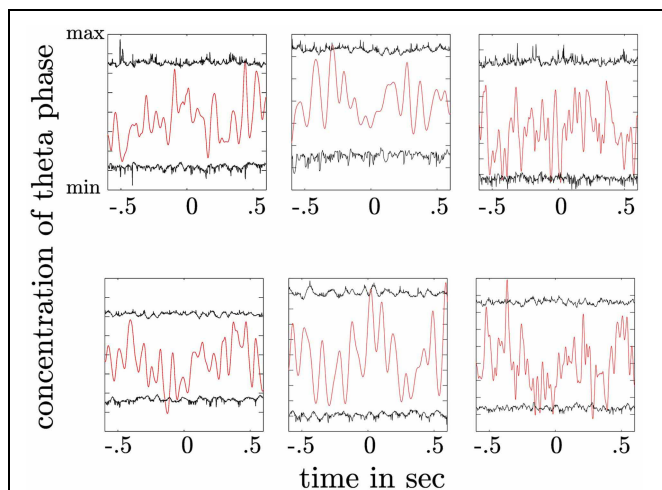
FIGURE 11 | Depiction of theta phase concentration as a function of time (red line) together with the confidence intervals derived from a permutation procedure (black lines). The upper plot shows the concentration parameter κ as a function of time for trials aligned to the stimulus. The lower plot shows the same for trials aligned to the response. High concentration values indicate a preferred θ phase across trials at a given time point. Concentration values exceeding the upper confidence interval would indicate a statistically significant alignment of the θ phase across trials. In both plots no significant θ phase alignment can be observed.
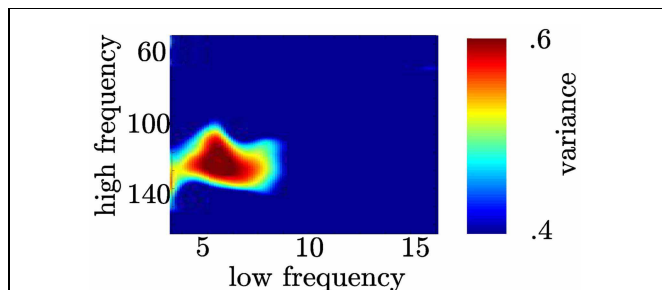
FIGURE 12 | Coupling following the motor response is restricted to the θ and high γ range. In the time range between 0 and 200 ms (see A right column) we calculated coupling strength between narrow high frequency bands (centerfrequencies: 50 to 180 Hz, bandwidth: 30 Hz, step size: 2 Hz) and narrow low frequency bands (centerfrequencies: 3 to 16 Hz, bandwidth: 4 Hz, step size: 1 Hz).

FIGURE 13 | Depiction of subject specific MIs in the contralateral NAcc following the motor response. Each line represents the modulation index as a function of time of one subject. 0 marks the response time. Following the motor response in each subject an increase of modulation strength is observable. The black bars represent the upper confidence intervals derived from a permutation procedure in each subject. Following the motor response in each subject a statistically significant coupling was found.

fixed order stimulus sequence, and during responses to stimuli presented in a random order that required high load of cognitive control. In contrast, in periods with low cognitive control demands, i.e., when subjects responded to already learned stimulus sequences and during self-paced sequences, PAC was reduced. This pattern of response locked PAC cannot be accounted for reaction time differences since analyzed epochs were locked to the subject's responses, and no PAC was observed when epochs were locked to the stimulus presentations. Hence, coupling takes place in the temporal interval following a decision. This pattern is consistent with coupling patterns observed in rats by Tort et al. (2008). These investigators found enhanced coupling between θ

and high gamma (80–120 Hz) within and between the striatum and the hippocampus. Coupling was strongest in epochs where a decision had to be made and thus were related to cognitive demands. Tort et al. (2008) hypothesized that PAC is a mechanism coordinating striatal and hippocampal learning circuits. As mentioned above, the hippocampus is strongly connected with the NAcc and a selective strengthening of this connection is assumed to be important for rapid facilitation of goal-directed behavior (Goto et al., 2005). The result that PAC decreases with learning indicates that PAC is related with the facilitated goal-directed behavior as proposed by Goto et al. (2005). That PAC occurs whenever a high level of cognitive control has to be applied supports the notion that PAC qualifies for facilitation. Thus, our data indicate that PAC can be a mechanism of information integration, since it occurs during high cognitive control supporting the hypothesis that PAC provides an effective mechanism to recruit local networks from functional related global networks to gate information (Buzsaki et al., 2004; Canolty et al., 2006).

4.2. INTERPLAY OF FREQUENCIES FOR INTEGRATION OF INFORMATION

It is assumed that the control of motor behavior in NAcc is accompanied by release of dopamine (Wilson et al., 1983). Münte et al. (2007) found the human NAcc involved in error-related modulation which preceded scalp error-related negativity (ERN). On a behavioral level NAcc activity inhibits specific conditioned motor behavior (Wilson et al., 1983). In the present study the patients probability of making errors systematically varies during the course of the experiment. This variation matches with the course from HCC to LCC to HCC and again to LCC. We hypothesize that the variation of making errors signals a change in motor behavior and hence points to adaptation to the external demands as a result of learning. The error probability was especially low at

the start of the experiment and during the random sequence task. The PAC in the contralateral human NAcc correlates with this change, which suggests that theta/high gamma coupling strength might be related with adaptation of behavior in later trials. This gains support by the PAC modulation occuring in early trials followed by behavioral adaptation. Once adapted in terms of reaction times and error rate no PAC modulation takes place. Thus, we speculate that the control for a specific action or motor routine as during an unknown or random sequence can be provided by enhanced coupling of θ-high gamma oscillations in the NAcc. This increased coupling becomes important when a subject has to switch from a previously established and automized motor routine to an unpredictable motor sequence. In contrast, a reduction in coupling, as observed during the tracking of the learned sequence, might facilitate automization. In our study enhanced action monitoring is especially important during learning of the fixed sequence and during the random sequence, since automatic behavior has to be interrupted. To achieve this, the NAcc has to integrate information between different cerebral units. This could be the information necessary to control the gating into the motor system from the limbic system and the prefrontal cortex (Mogenson et al., 1980). The NAcc neuronal activity is mutual depend on hippocampal input (O'Donnell et al., 1995) as well as PFC activity (French et al., 2002). Thus, the complex connections with limbic, prefrontal and motor structures make the NAcc an ideal site for the integration of information which is supported by the phase-amplitude cross-frequency coupling mechanism.

4.3. PAC IS STRONGEST FOLLOWING A DECISION

Tort et al. (2008) reports that in the rat's striatum and hippocampus PAC was strongest during the decision phase while rats navigated through a maze. In contrast, in our experiment the period of movement was short because there was only a single button press. This can explain differences in the timing of PAC patterns. In the present study, PAC occurred shortly after the decision was made and correlated with the probability of making an error, suggesting that changes in response selection based relative to past experiences calls for the coordination of information carried by different frequencies. Based on our results, we propose that the human NAcc signals the unpredictability of a future external event to which a response will have to be given, thereby indicating the necessity of stopping an automated response. This is accomplished by integrating information in the θ and high gamma band. In support of this contention Berns et al. (2001) found the reward system and especially the human NAcc responsive to different levels of predictability. In particular, the NAcc was more active during an unpredictable sequence, in line with our finding that PAC was elevated at the beginning of learning and during the tracking of the random sequence. Further, O'Donnell et al. (1995) found differences in activity in the striatum, especially in the putamen and the nucleus caudatus adjacent to the NAcc, for automated vs. unfamiliar motor behaviors. The increased coupling following a decision under a condition of high cognitive control might represent a type of associative memory which combines information about events (button press) and the context (stimulus presentation) (Tort et al., 2009). Here one can

image that the association which is acquired more easily under higher cognitive control provides the subject with the possibility to respond faster. Furthermore, we observed two patterns of the course of coupling. In the first, coupling decreased during fixed trials and in the second coupling increased during random trials and both differ with respect to the predictability of the upcoming event and hence which finger to move. This says that during fixed trials the subjects are informed based on the memory of past trials which finger is to move and hence the finger movement options are limited to one finger. In contrast in the random trials the subject has to hold up three finger movement options (3 since 4 different stimuli are presented with the constraint that no stimulus was consecutively repeated twice). This might also explain why PAC increases constantly during random trials. Alternatively, this pattern can be a result of the monitoring of the recent action which is underscored by the temporal relation. This interpretation is supported by the involvement of the human NAcc in action monitoring—the error detection and correction (Münte et al., 2007). The correlation of the modulation strength with the error rate indicates that NAcc activity is involved in action monitoring. Action monitoring in turn involves a comparison between the representations of an appropriate response and the response actually made (Scheffers and Coles, 2000). These diverge if a response error was committed. Error monitoring is accompanied by prominent scalp potentials (Nieuwenhuis et al., 2001) and the activity in the NAcc is involved in error-related modulations (Münte et al., 2007) . The authors have shown that the early surface potential which indicated the error detection was preceded by NAcc activity. Accordingly, activity in the NAcc should contribute to ERN when the error rate is high. Moreover, the NAcc activity involved in error detection should occur earlier than the PAC modulation since the error signal on the scalp level is evoked around 100 ms and is delayed by the NAcc by about 40 ms (Münte et al., 2007). Importantly, PAC modulation occurs when the error rate is small. This makes the PAC a complementary event to the error-related modulation. We speculate that PAC modulation occurs when the comparison process between the appropriate and the actual response revealed that no error was made. Therefore, PAC could be the signal involved in confirmation of the correct response which facilitates goal-directed behavior in later trials. Due to the vicinity to the motor response one could argue that PAC is a mere mechanical artifact, however coupling is observed only in one region and shows a tight functional correlation with behavioral measures. Furthermore, in case of an artificial result we expected coupling to be represented across a broad band of low coupling and high coupled frequencies. However, coupling was restricted to the θ – high gamma range. Hence, we precluded PAC to be a result of an artifact as a possible explanation. Based on this, we speculate that PAC in the NAcc signals a deviation from expectancy: a negative reinforcement that implies the need to stop an automated motor routine in which learned responses are pre-activated to reduce reaction times.

4.4. DIFFERENCES IN COUPLING PHASE

During the course of the experiment the coupling phase of θ oscillations varied systematically, with coupling close to the θ trough

during early learning and tracking the random sequence (high cognitive control), and coupling to the descending part of the θ cycle during tracking a well-learned fixed sequence (low cognitive control). A comparable result was found in a study conducted by Belluscio et al. (2012). In this study high γ activity (90–150 Hz) peaked near the θ trough during running but was coupled to the peak of the θ oscillations during REM-sleep. The authors hypothesized that modulation of the high gamma band by the θ band is state dependent. Here, we show that coupling in the human NAcc is also state dependent. The average coupling phase varies as a function of cognitive control applied by the subjects and parallels the results of Belluscio et al. (2012). This strengthens our hypothesis that PAC might provide a mechanism to integrate information. Hasselmo et al. (2002) highlighted the functional importance of different phases in the θ cycle for memory with the descending phase necessary for retrieval of memory and the trough for encoding of new information. They state that encoding of new information is facilitated if θ activity shifts in phase to accelerate the process of encoding. In our study when new information has to be encoded and the motor response has to be adjusted due to the new environmental

requirements we observe strong coupling of the high gamma activity to the θ trough. The epochs in which new information has to be encoded are the trials in the early part of the fixed sequence and the random sequence which differ from the trials late in the fixed sequence with respect to the possibility of memory retrieval. Retrieval is only possible when the fixed sequence has been learned distinguishing between the two distinct cognitive states.

5. CONCLUSION

Together these results show that motor learning is accompanied by a complex interplay of θ and high gamma activity. In the NAcc contralateral to the performing hand the coupling of these frequencies varies systematically with the experimental conditions which allowed the participants to perform differently.

REFERENCES

Axmacher, N., Henseler, M. M., Jensen, O., Weinreich, I., Elger, C. E., and Fell, J. (2010). Cross-frequency coupling supports multi-item working memory in the human hippocampus. *Proc. Natl. Acad. Sci. U.S.A.* 107, 3228–3233. doi: 10.1073/pnas.0911531107

Barcelo, F., Escera, C., Corral, M. J., and Periez, J. A. (2006). Task switching and novelty processing activate a common neural network for cognitive control. *J. Cogn. Neurosci.* 18, 1734–1748. doi: 10.1162/jocn.2006.18.10.1734

Belluscio, M. A., Mizuseki, K., Schmidt, R., Kempter, R., and Buzski, G. (2012). Cross-frequency phase-phase coupling between θ and γ oscillations in the hippocampus. *J. Neurosci.* 32, 423–435. doi: 10.1523/JNEUROSCI.4122-11.2012

Belujon, P., and Grace, A. A. (2008). Critical role of the prefrontal cortex in the regulation of hippocampus-accumbens information flow. *J. Neurosci.* 28, 9797–9805. doi: 10.1523/JNEUROSCI.2200-08.2008

Berns, G. S., McClure, S. M., Pagnoni, G., and Montague, P. R. (2001). Predictability modulates human brain response to reward. *J. Neurosci.* 21, 2793–2798.

Buzsáki, G., and Draguhn, A. (2004). Neuronal oscillations in cortical networks. *Science* 304, 1926–1929. doi: 10.1126/science.1099745

Canolty, R. T., Edwards, E., Dalal, S. S., Soltani, M., Nagarajan, S. S., Kirsch, H. E., et al. (2006). High gamma

power is phase-locked to theta oscillations in human neocortex. *Science* 313, 1626–1628. doi: 10.1126/science.1128115

Canolty, R. T., Ganguly, K., Kennerley, S. W., Cadieu, C. F., Koepsell, K., Wallis, J. D., et al. (2010). Oscillatory phase coupling coordinates anatomically dispersed functional cell assemblies. *Proc. Natl. Acad. Sci. U.S.A.* 107, 17356–17361. doi: 10.1073/pnas.1008306107

Chrobak, J. J., and Buzsáki, G. (1998). Gamma oscillations in the entorhinal cortex of the freely behaving rat. *J. Neurosci.* 18, 388–398.

Cohen, M. X., Axmacher, N., Lenartz, D., Elger, C. E., Sturm, V., and Schlaepfer, T. E. (2009). Good vibrations: cross-frequency coupling in the human nucleus accumbens during reward processing. *J. Cogn. Neurosci.* 21, 875–889. doi: 10.1162/jocn.2009.21062

Finch, D. M. (1996). Neurophysiology of converging synaptic inputs from the rat prefrontal cortex, amygdala, midline thalamus, and hippocampal formation onto single neurons of the caudate/putamen and nucleus accumbens. *Hippocampus* 6, 495–512.

Fitts, P. M., and Posner, M. I. (1973). *Human Performance*, Chapter 2, Learning and Skilled Performance. London: Wadsworth Publishing Company, 8–25.

French, S. J., and Totterdell, S. (2002). Hippocampal and prefrontal cortical inputs monosynaptically converge with individual projection

neurons of the nucleus accumbens. *J. Comp. Neurol.* 446, 151–165. doi: 10.1002/cne.10191

Goto, Y., and Grace, A. A. (2005). Dopamine-dependent interactions between limbic and prefrontal cortical plasticity in the nucleus accumbens: disruption by cocaine sensitization. *Neuron* 47, 255–266. doi: 10.1016/j.neuron.2005.06.017

Goto, Y., and Grace, A. A. (2008). Limbic and cortical information processing in the nucleus accumbens. *Trends Neurosci.* 31, 552–558. doi: 10.1016/j.tins.2008.08.002

Grace, A. A. (2000). Gating of information flow within the limbic system and the pathophysiology of schizophrenia. *Brain Res. Brain Res. Rev.* 31, 330–341. doi: 10.1016/S0165-0173(99)00049-1

Grace, A. A., Floresco, S. B., Goto, Y., and Lodge, D. J. (2007). Regulation of firing of dopaminergic neurons and control of goal-directed behaviors. *Trends Neurosci.* 30, 220–227. doi: 10.1016/j.tins.2007.03.003

Hasselmo, M. E., Bodeln, C., and Wyble, B. P. (2002). A proposed function for hippocampal theta rhythm: separate phases of encoding and retrieval enhance reversal of prior learning. *Neural Comput.* 14, 793–817. doi: 10.1162/089976602317318965

Knopman, D., and Nissen, M. J. (1991). Procedural learning is impaired in Huntington's disease: evidence from the serial reaction time task. *Neuropsychologia* 29, 245–254. doi: 10.1016/0028-3932(91)90085-M

MacDonald, A. W., Cohen, J. D., Stenger, V. A., and Carter, C. S. (2000). Dissociating the role of the dorsolateral prefrontal and anterior cingulate cortex in cognitive control. *Science* 288, 1835–1838. doi: 10.1126/science.288.5472.1835

Mai, J. K., Paxinos, G., and Voss, T. (2004). *Atlas of the Human Brain 2nd Edn.* San Diego, CA: Academic Press Elsevier.

Mogenson, G. J., Jones, D. L., and Yim, C. Y. (1980). From motivation to action: functional interface between the limbic system and the motor system. *Prog. Neurobiol.* 14, 69–97.

Morel, A. (2007). *Stereotactic Atlas of the Human Thalamus and Basal Ganglia.* New York, NY: Informia Health Care Inc. doi: 10.3109/9781420016796

Münte, T. F., Heldmann, M., Hinrichs, H., Marco-Pallares, J., Krämer, U. M., Sturm, V., et al. (2007). Nucleus accumbens is involved in human action monitoring: evidence from invasive electrophysiological recordings. *Front. Hum. Neurosci.* 1:11. doi: 10.3389/neuro.09.011.2007

Nieuwenhuis, S., Ridderinkhof, K. R., Blom, J., Band, G. P. H., Kok, A. (2001). Error-related brain potentials are differentially related to awareness of response errors: evidence from an anti-saccade task *Psychophysiology* 38, 752–760.

Nissen, M. J., and Bullemer, P. (1987). Attentional requirements of learning: evidence from performance

measures. *Cogn. Psychol.* 19, 1–32. doi: 10.1016/0010-0285(87)90002-8

Notebaert, W., Houtman, F., Opstal, F. V., Gevers, W., Fias, W., and Verguts, T. (2009). Post-error slowing: an orienting account. *Cognition* 111, 275–279. doi: 10.1016/j.cognition.2009.02.002

O'Donnell, P., and Grace, A. A. (1995). Synaptic interactions among excitatory afferents to nucleus accumbens neurons: hippocampal gating of prefrontal cortical input. *J. Neurosci.* 15(5 Pt 1), 3622–3639.

Poldrack, R. A., Sabb, F. W., Foerde, K., Tom, S. M., Asarnow, R. F., Bookheimer, S. Y., et al. (2005). The neural correlates of motor skill automaticity. *J. Neurosci.* 25, 5356–5364. doi: 10.1523/JNEUROSCI.3880-04.2005

Ridderinkhof, K. R., Ullsperger, M., Crone, E. A., and Nieuwenhuis, S. (2004). The role of the medial frontal cortex in cognitive control *Science* 306:443. doi: 10.1126/science.1100301

Scheffers, M. K., and Coles, M. G. H. (2000). Performance monitoring in a confusing world: error-related brain activity, judgments of response accuracy, and types of errors *J. Exp. Psychol.* 26, 141–151. doi: 10.1016/j.neuron.2005.02.028

Siapas, A. G., Lubenov, E. V., and Wilson, M. A. (2005). Prefrontal phase locking to hippocampal theta oscillations. *Neuron* 46, 141–151.

Sirota, A., Csicsvari, J., Buhl, D., and Buzsáki, G. (2003). Communication between neocortex and hippocampus during sleep in rodents. *Proc. Natl. Acad. Sci. U.S.A.* 100, 2065–2069. doi: 10.1073/pnas.0437938100

Staudigl, T., Zaehle, T., Voges, J., Hanslmayr, S., Esslinger, C., Hinrichs, H., et al. (2012). Memory signals from the thalamus: early thalamocortical phase synchronization entrains gamma oscillations during long-term memory retrieval. *Neuropsychologia* 50, 3519–3527. doi: 10.1016/j.neuropsychologia.2012.08.023

Sturm, V., Lenartz, D., Koulousakis, A., Treuer, H., Herholz, K., Klein, J. C., et al. (2003). The nucleus accumbens: a target for deep brain stimulation in obsessive-compulsive- and anxiety-disorders. *J. Chem. Neuroanat.* 26, 293–299. doi: 10.1016/j.jchemneu.2003.09.003

Tort, A. B. L., Komorowski, R. W., Manns, J. R., Kopell, N. J., and Eichenbaum, H. (2009). Theta-gamma coupling increases during the learning of item-context associations. *Proc. Natl. Acad. Sci. U.S.A.* 106, 20942–20947. doi: 10.1073/pnas.0911331106

Tort, A. B. L., Kramer, M. A., Thorn, C., Gibson, D. J., Kubota, Y., Graybiel, A. M., et al. (2008). Dynamic cross-frequency couplings of local field potential oscillations in rat striatum and hippocampus during performance of a T-maze task. *Proc. Natl. Acad. Sci. U.S.A.* 105, 20517–20522. doi: 10.1073/pnas.0810524105

Voges, J., Volkmann, J., Allert, N., Lehrke, R., Koulousakis, A., Freund, H.-J., et al., (2002). Bilateral high-frequency stimulation in the subthalamic nucleus for the treatment of Parkinson disease: correlation of therapeutic effect with anatomical electrode position. *J. Neurosurg.* 96, 269–279. doi: 10.3171/jns.2002.96.2.0269

Wilson, W. J. (1983). Nucleus accumbens inhibits specific motor but not nonspecific classically conditioned responses. *Brain Res. Bull.* 10, 505–515.6. doi: 10.1016/0361-9230(83)90148-X

6 APPENDIX

6.1 PROCEDURE: SURGERY AND DEEP BRAIN STIMULATION

We performed a bilateral stereotactically guided implantation of quadripolar brain electrodes (model 3387, Medtronic, Minneapolis, MI, USA) in the Nucleus Accumbens (NAcc) and in the anterior nuclear group of the thalamus (ANT) of 3 patients for treatment of a longterm pharmacoresistant epilepsy. General anesthesia was employed during the surgery. The implantation was conducted due to clinical reasons and as part of the treatment of the epilepsy.

Treatment planning standards and the surgical procedure are described elsewhere in detail Voges et al. (2002). Briefly, the target for the deep brain stimulation electrode was defined using standard coordinates as the point 2 mm rostral to the anterior border of the anterior commissure at the level of the mid-sagittal plane, 3–4 mm ventral and 6–8 mm lateral of the midline (Mai et al., 2004), with these coordinates modified according to individual planning MRIs. An important landmark is the vertical limb of Broca diagonal band, which can be clearly visualized in coronal MRI-scans. The target was placed 2-0.5 mm lateral to this structure. Using a deep fronto-lateral approach, the two distal contacts of the DBS-electrode were placed in the caudo-medial accumbens, the third contact within the transition-area medial to the border of the abutting internal capsule, and the fourth highest contact in the most medial part of the capsule or in the transition area to the caudate. The contacts within the NAcc are placed in the caudo-medial part, which according to histochemical criteria represents the remnant of the shell area in the primate (Sturm et al., 2003). In contrast to rodents, in the primate the shell area has regressed and is no longer clearly distinguishable, except by the typical receptors that it carries.

In addition, electrodes were implanted in the bilateral anterior nuclei of thalamus (ANT) of all the patients. The anterior thalamic nucleus is located 5 mm lateral to and 12 mm above the midcommisural point according to the Schaltenbrand atlas. Since the anterior nucleus of the thalamus is readily visible on the floor of the lateral ventricle in MRI images, the exact location of this target could be directly specified in each patient. Intraoperatively the localization of the leads was documented by stereotactic x-ray imaging using x-ray tubes installed in the OR.

In addition, we performed postoperative CT-examination (2 mm slice thickness). After a transformation of postoperative CT- and X-ray images to align them with the stereotactic treatment planning-MRI, we defined the stereotactic coordinates of each electrode lead contact and visualized these anatomical positions on corresponding sections of two stereotactic brain atlases of (Morel et al., 2007). The localization of the electrodes is depicted in **Figure A1**. To further indicate the coordinates of the most caudal NAcc electrode, we transformed all patients MRI images to MNI-space. The resulting individual MNI coordinates were (x, y, z): Pat 01: left (−6.9 5.2 −11.9), right (4.3 5.4 −10.4); Pat 02: left (−8.6 3.5 −8.6), right (9.6 3.7 −9.6); Pat 03: left (−8.3 7.5 −11.0), right (−6.2 7.3 −11.0). Postoperatively the electrode leads were externalized to allow electrical test stimulation with different parameters and recording from the depth contacts during different psychological tasks. Finally the four electrode-leads were connected to a single impulse-generator (IPG; Activa-PC, Medtronic)

Table A1 | Patient Information.

Patient	Gender, age, duration of epilepsy	Epilepsy Syndrome	lateralization	seizure onset	etiology	AEDs	IQ (HAWIE-R)	Verbal memory Immediate free recall (z-score)	Delayed free recall (z-score)	Recognition (z-score)	Figural memory (z-score)	Sustained Attention (z-score)
Pat 01	F, 52, 19	multifocal	bilateral	mesio-temporal	cryptogenic	LCM 400 mg LTG 200 mg	74.2	40 (−0.65)	5 (−1.6)	9 (−1)	8 (−1.6)	199 (−2.2)
Pat 02	M, 35, 9	focal	right	temporal	right temporal encephalocele	LEV 2000 mg ESL 1200 mg	124.9	57 (−0.65)	12 (0.2)	15 (1.1)	39 (−1)	486 (0)
Pat 03	F, 28, 12	multifocal	bilateral	temporal	cryptogenic	LTB 200 mg LCM 200 mg	94	53 (−0.4)	13 (0.2)	15 (1.1)	23 (−1)	424 (−0.8)

F, female; M, male, AED, antiepileptic drugs; LCM, Lacosamide; OXC, Oxcarbazepine; LTG, Lamotrigine; LEV, Levetiracetam; ESL, Eslicarbazepine acetate summarizes demographical and clinical information about the subjects

FIGURE A1 | Anatomical location of bilateral NAccs.
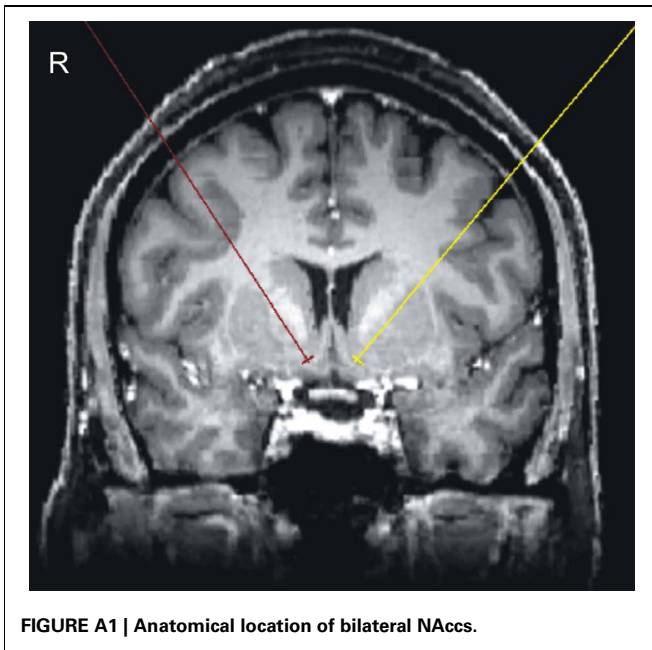
Table A2 | *post-hoc* statistical analysis of the error rate.

comparison	*p*-value
1–2	0.81
1–3	0.64
1–4	0.81
1–5	0.25
2–3	0.82
2–4	1
2–5	0.17
3–4	0.82
3–5	0.11
4–5	0.17

The p-values refer to the pairwise comparisons of frequency by means of the χ^2 of the summed number of errors across subjects per block.

placed subcutaneously beneath the right clavicle. To evaluate our hypotheses we analyzed data from the bilateral NAcc electrodes. To provide evidence of the specificity of our results for the NAcc we also performed a control analysis of the recordings from the bilateral thalamus. We found results described for the contralateral NAcc were not duplicated in the thalamus.

Oscillatory Dynamics Track Motor Performance Improvement in Human Cortex

Stefan Dürschmid[1,2]*, Fanny Quandt[2], Ulrike M. Krämer[3], Hermann Hinrichs[1,2,4], Hans-Jochen Heinze[1,2,4], Reinhard Schulz[5], Heinz Pannek[5], Edward F. Chang[6], Robert T. Knight[7,8]

1 Department of Neurology, Otto-von-Guericke University, Magdeburg, Germany, 2 Leibniz Institute of Neurobiology (LIN), Magdeburg, Germany, 3 Department of Neurology, University of Lübeck, Lübeck, Germany, 4 German Center for Neurodegenerative Diseases (DZNE), Magdeburg, Germany, 5 Epilepsiezentrum Bethel, Bielefeld, Germany, 6 Department of Neurological Surgery, University of California San Francisco, San Francisco, California, United States of America, 7 Helen Wills Neuroscience Institute, University of California, Berkeley, California, United States of America, 8 Department of Psychology, University of California, Berkeley, California, United States of America

Abstract

Improving performance in motor skill acquisition is proposed to be supported by tuning of neural networks. To address this issue we investigated changes of phase-amplitude cross-frequency coupling (paCFC) in neuronal networks during motor performance improvement. We recorded intracranially from subdural electrodes (electrocorticogram; ECoG) from 6 patients who learned 3 distinct motor tasks requiring coordination of finger movements with an external cue (serial response task, auditory motor coordination task, go/no-go). Performance improved in all subjects and all tasks during the first block and plateaued in subsequent blocks. Performance improvement was paralled by increasing neural changes in the trial-to-trial paCFC between theta (θ; 4–8 Hz) phase and high gamma (HG; 80–180 Hz) amplitude. Electrodes showing this covariation pattern (Pearson's r ranging up to .45) were located contralateral to the limb performing the task and were observed predominantly in motor brain regions. We observed stable paCFC when task performance asymptoted. Our results indicate that motor performance improvement is accompanied by adjustments in the dynamics and topology of neuronal network interactions in the θ and HG range. The location of the involved electrodes suggests that oscillatory dynamics in motor cortices support performance improvement with practice.

Introduction

Phase-amplitude cross-frequency coupling (paCFC) of oscillations in different frequency bands has been proposed as an effective mechanism to form functional networks that recruit local neuronal populations across a global spatial scale [1–4]. Phase-amplitude CFC between HG (80–150 Hz) amplitude to θ (4–8 Hz) phase was first described by [2] and later confirmed by other authors in rats [5,6] and humans [7]. During paCFC amplitudes of higher frequency oscillations, reflecting local cortical processing, are modulated by the phase of low frequency oscillations [8–12]. This mechanism has been proposed to engage and coordinate local processing modules across spatially distributed brain areas supporting cognition and motor performance [4,9,13–17].Further support for this proposal comes from recent clinical studies linking altered paCFC to debilitating psychiatric and motor disorders [18–21]. Moreover, paCFC is prominent during language and motor tasks [2,4] and the frequency of the slower phase coupling oscillation is task dependent [12]. However, beyond clinical studies evidence for a functional role of paCFC in the process of organizing human cognition and behavior is limited predominantly to the memory domain (see [22] for a review). Axmacher and colleagues [23] reported that inter-individual differences in

working memory performance correlated with differences in paCFC precision, supporting the functional relevance of CFC for memory processing. Tort and colleagues [6] examined the dynamic modification of functional relations between performance and CFC in rat hippocampus and found coupling strength between θ and gamma (γ: 25–100 Hz) correlated with maze learning.

A stronger link between paCFC and behavior in humans would be supported by a correlation between paCFC and trial-by-trial variations in performance. To address this, we examined the relation between paCFC and motor performance improvement. We recorded the electrocorticogram (ECoG) in human patients (N = 6; mean age = 20.5, std = 5.5; 2 female) undergoing epilepsy diagnosis while they learned skilled motor behaviors. To assess the link between paCFC and behavior we compared changes in paCFC to changes in performance over an extended time scale during motor skill acquisition, and correlated performance and paCFC at the single trial level. We show that paCFC in intracranial subdural recordings between θ (4–8 Hz) and HG (80–180 Hz) in the human cortex tracks level of motor performance across different motor tasks.

Results

Phase amplitude cross frequency coupling

We investigated potential links between paCFC and motor performance in six subjects each performing one of three repetitive motor tasks described next. The three different behavioral tasks (Figure 1) were a serial reaction time task (SRT 2 subjects), a go/no-go task (GNG 3 subjects), and an auditory motor coordination task (AMCT 1 subject). All three tasks required the coordination of finger movements with an external stimulus. We assessed motor performance as reaction time in the SRT and GNG tasks and as the temporal deviation from the target time point in the AMC task. The cognitive requirements for performance improvement are different in all three tasks: learning the motor sequence in the SRT, learning the stimulus-response association in the GNG and improving movement timing in the AMCT. However, the motor component is performance improvement with practice. The dynamics of the different performance measures were assessed in a group statistic, by comparing the average behavioral outcomes between fixed trial bins (see Figure 2). We recorded the ECoG while subjects performed two blocks of one of each task with the hand contralateral to the electrode grid. The ECoG-time series were filtered in the θ -band (4–8 Hz) and in the HG-band (80–180 Hz) yielding two separate filtered signals (see Methods). We calculated the analytic amplitude of the HG-band time series by taking the absolute value of the Hilbert transform of the filtered time series. The analytic amplitude is a new time series representing the amplitude envelope of the HG-oscillations at any moment in time. We performed the analysis on the 500 ms interval immediately following the stimulus onset. This interval includes the preparation of the responses indicated by the stimulus and includes approximately three θ-cycles.

We first asked whether the amplitude envelope of the local HG oscillations is phase coupled to the local θ-band oscillations. Figure 3A shows the time course of sine waves fitted to the single
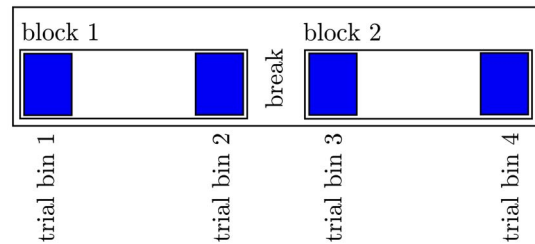
experimental session

Figure 2. Here we depict the separation of the whole experimental session into trial bins. The experimental session in each patient consisted of 2 blocks separated by a short break. In each block we defined two trial bins each containing 30 trials (blue). We compared the PLV across the four trial bins to assess the evolution of connectivity length of and HG activity during motor performance improvement.
doi:10.1371/journal.pone.0089576.g002

trial variations of HG analytic amplitude pooled across all electrodes in one subject. As predicted, HG analytic amplitude varied systematically over the θ-cycle. Figure 3B shows single subject sine wave fits to the HG analytic amplitude averaged over trials and electrodes. Each fit was significant (p < 0.001) and the HG amplitude variations were consistent over subjects with only a slight deviation of subject 1 (see Figure 3B). The frequencies of the fitted sine waves are in the θ band (.95 Hz, SE: .02 Hz) and the phase angle is .6 rad (SE: .23 rad, see Methods for an explanation of the sine wave parameters - frequency and phase angle). The maximum of the HG-analytic amplitude centers around the trough in the θ-cycle (mean = 2.56 rad, std = .56 rad, skewness = −.16).
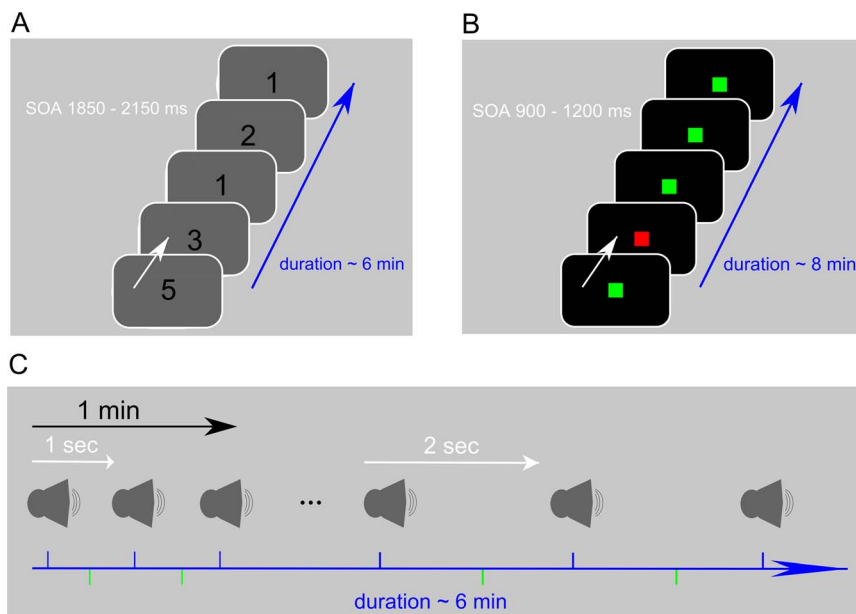
Figure 1. Paradigms employed (details described in Methods). A) Serial reaction time task: The numbers on the screen indicate the finger to be used for the key press. B) Go/no-go: Green indicates a go and red indicates a no-go trial. C) Auditory motor coordination: Subjects were instructed to press a key in the middle of the interval between two consecutive tones. The interval length was either one second or two seconds and was held fixed for one minute. Each subject carried out two blocks (see Methods).
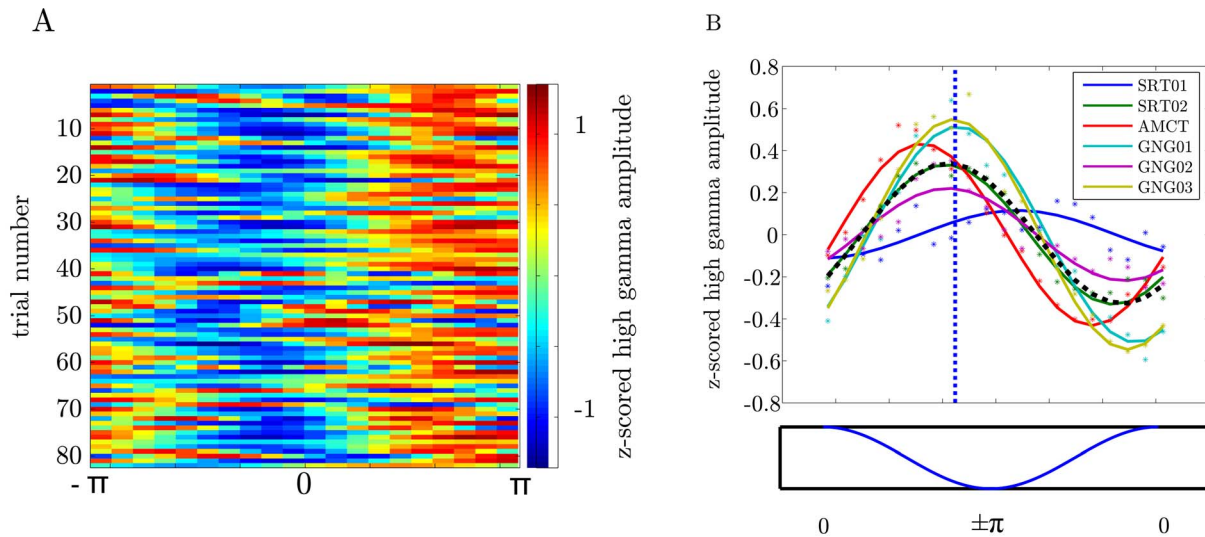doi:10.1371/journal.pone.0089576.g001

A

B

Figure 3. The amplitude of the HG oscillations is phase coupled to the θ-band (4–8 Hz) oscillations in all subjects across paradigms.
A) Time courses of sine wave functions fitted to the single trial amplitude envelopes of the HG oscillations of one subjects collapsed over electrodes.
B) Sine wave functions fitted to the trial-averaged HG oscillation amplitudes envelopes of each subject. Each solid line represents the fit for one subject. Each dot represents the individual trial average of the HG oscillation in one of 20 intervals equally spaced over a θ cycle. The black dashed line shows the averaged sine waves across subjects. The vertical blue dashed line denotes the averaged phase angle the HG amplitude peaks across subjects. The maximum of the θ cycle is at phase 0 and the minimum at $\pm\pi$.
doi:10.1371/journal.pone.0089576.g003

Covariation of paCFC with performance improvement

To investigate if cross frequency coupling (paCFC) covaries with motor performance variations, we first calculated the trough to peak ratio (θ-trough to HG peak ratio - TPR; see Methods) over all electrodes on the grids as a metric for paCFC and related it to behavioral performance. Figure 4A shows the development of TPR and motor performance over the time course of the two experimental blocks each subject completed. Both TPR and performance increased during the experiment, as indicated by the fitted exponential functions. A statistical test confirmed this finding. In this test, we first compared average motor performance in the initial 30 trials of the first block with performance in the final 30 trials and found a significant improvement (Wilcoxon rank sum test across all subjects: p < .05, Figure 4B, See Figure 2 for the structure of the experimental session and Table 1 for mean performance measures for each trial bin). However, performance plateaued in the second block as indicated by no significant difference (p = 0.18). The difference between the first and the second block is indicated by a significant block-by-trial-bin interaction in a two way ANOVA across subjects (F(1,20) = 11.28; p = .003, df$_{error}$ = (Nsubj -1)*Ntrialbin). The next question was whether TPR exhibits the same behavior (Figure 4C). In concordance with behavioral performance we found, that the TPR increased between the first and the last 30 trials of the first block (Wilcoxon rank sum test across all subjects: p < .05) but did not change between the first and the last 30 trials of the second block (p = 0.3). A significant block-by-trial-bin interaction in a two way ANOVA (F(1,20) = 5.95; p = .03) confirmed that TPR changed during the first block and plateaued during the second block. This suggests that, on average, paCFC covaries with motor performance with paCFC and motor performance increasing early in the first experimental block and both plateauing in the second block.

Support for a functional relation between paCFC and motor performance would be provided by a trial-by-trial TPR with performance correlation. In order (i) to test for this correlation and

(ii) to disentangle cortical regions showing varying paCFC with performance, we pooled the data in six anterior and frontal regions of interest (ROIs); the anterior and posterior medial frontal gyrus, the anterior and the posterior inferior frontal gyrus, and the superior and inferior sensorimotor cortex (see Figure 5) for all five subjects with a square 8×8 (N = 4)/16×16 (N = 1) grid implantation (see Figure S2). In each ROI we pooled the TPR values across electrodes and determined the p-values of the trial-by-trial correlation with performance of each ROI (Figure 5 for details see Methods and Figure S1). Significant correlation of TPR with motor performance (corrected for multiple comparisons) was observed in pre-/motor cortex and in anterior and posterior inferior frontal sulcus. We predicted two sources of variability in single trial correlation between TPR and motor performance: one that is performance improvement related and varies systematically over time and another one that is not related to performance improvement and varies randomly from trial to trial. The first analysis supported performance improvement related trial-by-trial correlations reflecting the co-evolution of coordination between brain networks and improvements of motor performance. We then calculated in the same ROIs the partial correlation of TPR with performance. This analysis factored out the fraction of correlation between TPR and performance which can be attributed to random trial-by-trial covariations and is performance improvement unrelated. This performance improvement unrelated correlation of TPR with motor performance was observed in sensorimotor cortex and in premotor cortex, in the posterior middle temporal sulcus (corrected for multiple comparisons) and overlaps with the performance improvement related correlation.

Discrimination of performance improvement from Random Performance Fluctuations

To disentangle these two potential and functionally distinct causes of paCFC-performance covariations and disentangle the spatially wide ROIs we performed two different correlation analyses separately for each recording electrode. First, we
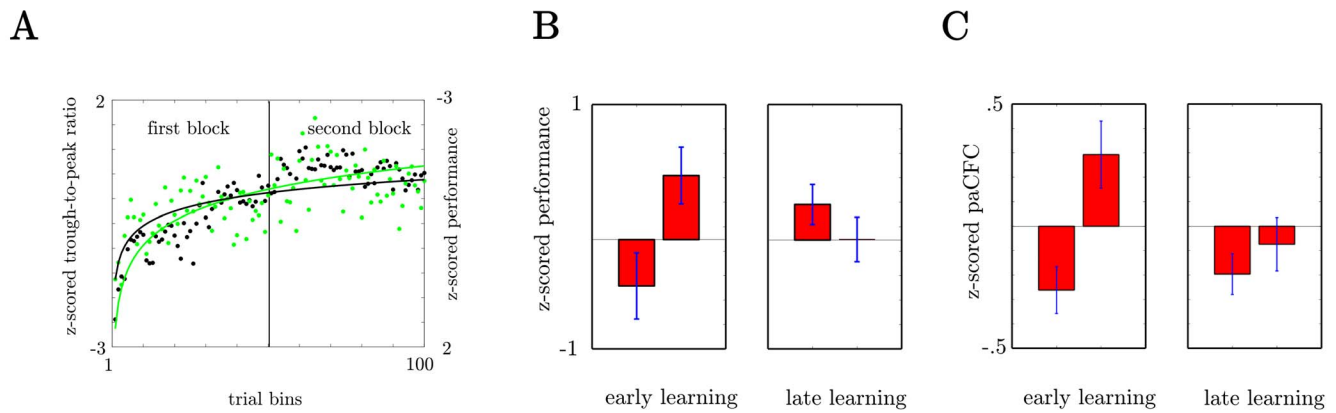
Figure 4. Covariation of average paCFC with performance over the time course of the experiment. A) The development of TPR and motor performance during the time course of the experiment. Results are collapsed across all six subjects/three experiments. Data for the first block and second block are shown in the left and second half of the plot. Each point represents the average in one of 100 time bins. Exponential functions fitted to the data z-scored over both blocks indicate a similar time course for performance and TPR. B) Subject averaged motor performance during the first and last sets of 30 trials in the first (early learning) and the second (late learning) experimental block. C) Subject averaged TPR. Data was z-scored within blocks and TPR was averaged over all electrodes.
doi:10.1371/journal.pone.0089576.g004

calculated the partial correlation of TPR with performance. Second, we calculated the standard Pearson correlation between TPR and motor performance. Pearson correlation captured the performance improvement related plus the performance improvement unrelated correlation. Combined with partial correlation this was used to distinguish between the two effects. Electrodes that capture performance improvement related TPR with performance correlations should show a partial correlation different from zero and a Pearson correlation different from the partial correlation (see Methods). Importantly, we reasoned that if we observed a significant Pearson correlation in an electrode that significantly changes if we discount time related correlations (in partial correlation), then the TPR - performance correlation in this electrode is partly due to performance improvement related TPR - performance correlations. Figure 6A shows the electrodes where random trial-by-trial fluctuations of TPR correlated with motor performance (significant partial correlation - uncorrected for multiple comparisons). Clusters of electrodes showing high

correlations are located in sensorimotor cortex, in premotor cortex, in lateral prefrontal cortex and in ventral anterior temporal cortex. Figure 6B shows the distribution of electrodes with performance improvement related trial-by-trial correlations between TPR and motor performance. Clusters of performance improvement related electrodes were apparent in premotor cortex, in lateral prefrontal cortex and in ventral anterior temporal cortex. Importantly, the variation of TPR with performance improvement was not a result of a shift of the HG amplitude peak relative to the θ trough and hence the coupling phase remained stable during performance improvement (see Appendix S1).

Discussion

Phase-amplitude cross-frequency coupling has been proposed to support interaction within functional networks [4]. Here we show that fluctuations of θ and HG paCFC are tightly linked to motor performance improvement at the single-trial level and show robust performance improvement clusters over pre-motor and motor cortices.

Performance improvement and theta and high gamma activity

During motor performance improvement θ and HG activity show a clear development of coupling that asymptotes in strength as motor behavior performance improvement plateaus. paCFC is highly dynamic and task-specific [4,24] and it has been proposed that paCFC enables adaptive behavior [2]. Here we report data from three different motor behavior experiments showing that paCFC dynamics reflect adaptive behavior supporting a relationship between paCFC and motor performance improvement on a trial-to-trial level. Notably, despite the differences in tasks similar cortical regions associated with performance improvement or random trial-to-trial performance are identified by paCFC evolution. The dynamic nature of paCFC and the task-specific coupling patterns have been shown in a variety of studies with task dependent differences in coupling frequencies and coupling phase [12,24–27]. Here, we add an important paCFC characteristic. We show that even though the preferred phase as indicated by coupling phase stability does not change the activity pattern of both frequencies varies with behavioral changes.

Table 1. Behavioral data.

Paradigm		trial bin			
	Patient	**1**	**2**	**3**	**4**
SRT					
	SRT01	917 (271)	767 (227)	748 (219)	707 (161)
	SRT02	1472 (300)	1017 (284)	859 (207)	966 (232)
AMCT					
	AMCT01	117 (66)	98 (65)	147 (197)	142 (129)
Go/No-Go					
	GNG01	343 (46)	323 (117)	331 (109)	302 (128)
	GNG02	426 (185)	301 (42)	260 (28)	301 (66)
	GNG03	433 (168)	379 (178)	286 (40)	393 (89)

For SRT (serial reaction time task) and GNG (Go/No-Go) task reaction time is shown (standard deviation) in msec. For AMCT (auditory-motor coordination task) the absolute deviation from precision is shown also in msec. Each trialbin encompasses 30 trials.
doi:10.1371/journal.pone.0089576.t001
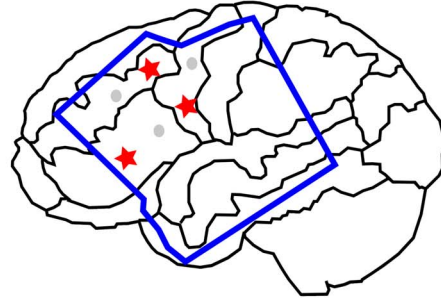
A   Pearson correlation
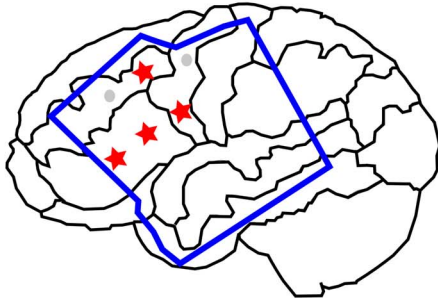
B   Partial correlation

Figure 5. Depiction of the results from the ROI-analysis. A) ROIs with significant performance improvement unrelated TPR/performance correlations. B) ROIs with significant performance improvement related TPR/performance correlations. ROIs with significant correlations (Bonferroni correct for six comparisons) are marked with an asterisk. The 6 ROIs are the anterior and posterior medial frontal gyrus, the anterior and the posterior inferior frontal gyrus, and the superior and posterior sensorimotor cortex. The blue margin shows the grid coverage across all subjects with a square grid implanted.
doi:10.1371/journal.pone.0089576.g005

Biological mechanism

Oscillatory dynamics are proposed [1] to be inherent to the interplay of brain regions for cognitive control in memory and learning [21]. For example θ activity observed in hippocampal and neocortical regions varies as a function of the state of the subjects [28]. The neocortex exhibited more prominent θ activity during wakefulness compared to REM sleep. Performance improvement during practice can be achieved by distributed θ networks - which are up-regulated during wakefulness - by integrating or coordinating local activity. Here, the concept of information integration means that θ oscillatory activity accumulates and integrates the results of local processing as reflected in HG activity in the premotor/motor region. HG activity, either an indication of spiking activity or very fast network oscillations [25,29], may be involved in planning and initiation of motor responses [30]. This frequency possibly reflects the activation of cortico-subcortical networks involved in the feedback control of discrete movements [31]. Taken together we speculate that information on planning of motor responses is integrated into memory by paCFC which results in performance improvement during the process of performance improvement.

Conclusion

We identified cross-frequency coupling in the human cortex which is associated with motor performance variability per se. In this network a smaller area is integrated whose oscillatory dynamics reflect the progress in performance improvement. This learning related network suggests the establishment of a memory trace which is accumulated during practice and which is represented in a mutually adapted level of activity of θ and HG activity [16,32–34]. In this respect paCFC provides a mechanism subserving motor memory formation [2].

Materials and Methods

Patients

Six epilepsy patients undergoing pre-surgical monitoring with subdural electrodes participated in the experiments after providing their written informed consent. Experimental and clinical recordings were taken in parallel. Recordings took place at the University of California San Francisco (UCSF), CA, USA (4 Patients), Johns Hopkins University, Baltimore, USA (1 Patient) and the Epilepsy Center Bethel (ECB), Bielefeld (1 Patient), Germany and were approved by the local ethics committees ("Committee for the Protection of Human Subjects at UC Berkeley", "Johns Hopkins Medicine Institutional Review Board" and "Ethical Committee of the University of Magdeburg").

Experimental Paradigms

We carried out three different motor tasks (serial reaction, go/ no-go, auditory-motor coordination) with six different patients (Fig. 1). Each patient participated in one of the tasks. All paradigms required coordination of key presses on a computer keyboard to an external stimulus. Patients performed the task sitting upright in their bed using the hand contralateral to the grid.

Serial Reaction Task. The serial reaction task (SRT) consisted of a series of visually cued finger taps. The subjects had their fingers placed on different keys of a laptop keyboard (right hand: space bar, j, k, and ; - left hand: space bar, f, d, and a). Trials started with one of the numbers 1, 2, 3, or 5 appearing on a laptop-screen cueing the movement of thumb, index finger, middle finger, or little finger, respectively. Numbers were presented until a key was pressed but maximally for 2 seconds. In each subject the four numbers were presented in a fixed sequence (six items long) or random order depending of the block number but only fixed blocks were used. Each block took approximately 10 minutes. Two patients participated in this task (SRT01 - 02). They were instructed to press keys as fast and accurate as possible. One block took approximately six minutes.

Auditory-Motor Coordination Task. The second motor-paradigm was an auditory-motor coordination task (AMCT). One patient participated and was instructed to respond as accurately as possible halfway between successive auditory clicks presented at a constant rate. Seven click sequences, each 60 s long, were presented in a block. The inter-click-interval in a sequence was either 500 ms, 1000 ms or 2000 ms and the participant was
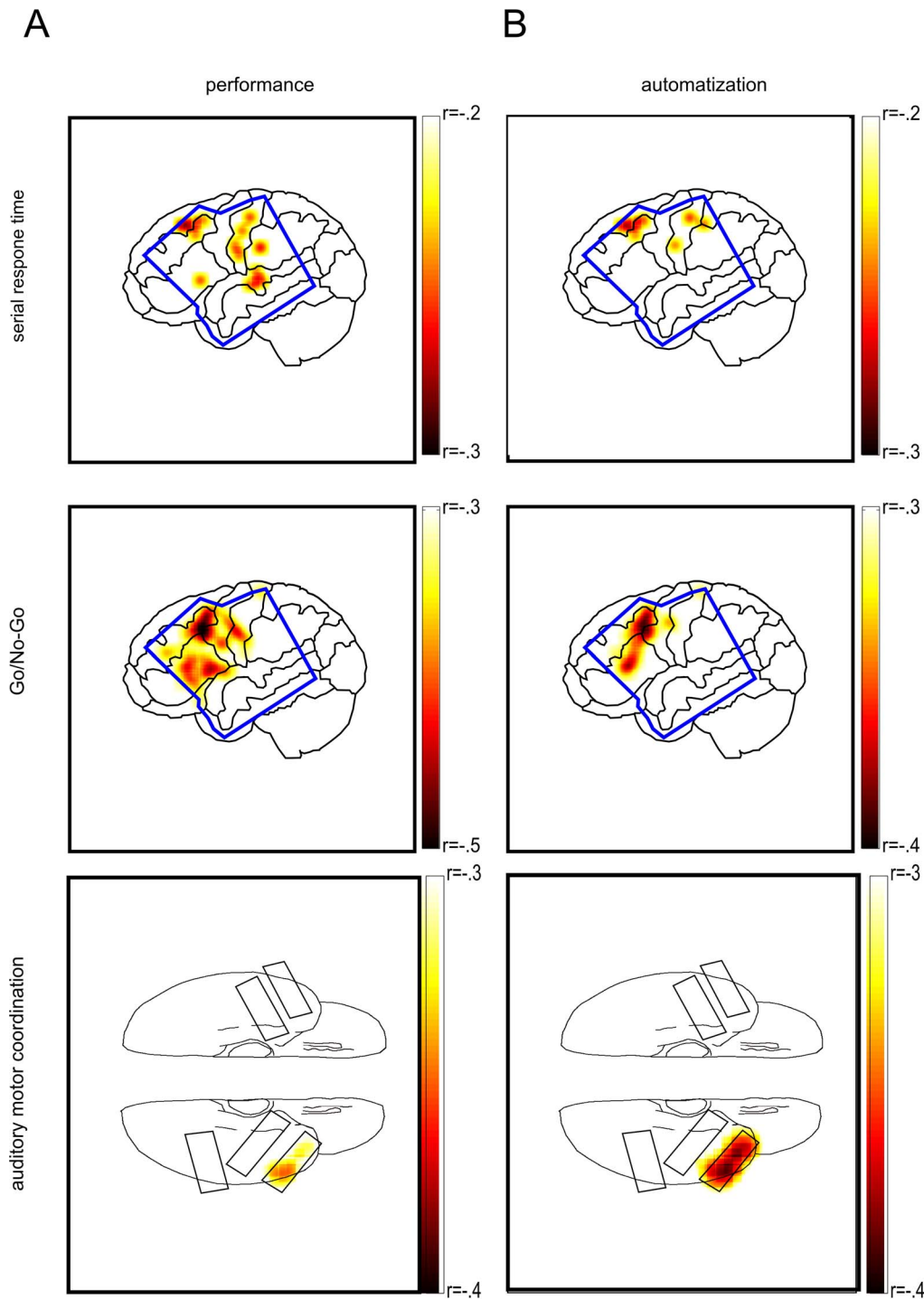
Figure 6. Electrodes with significant trial-by-trial correlations of TPR with performance. The significance threshold was determined in a permutation procedure (see Methods) A) Learning unrelated correlations of TPR with performance. B) Learning related correlations of TPR with performance. Darker colors indicate stronger correlations. See Methods for calculations on separating performance and learning related effects. The blue shape in the first and second row show the outline of all superimposed square grids. The black shapes in the third row denotes the grid locations for the participant in the AMCT. Spatial distortions result from the projection onto the cortex (for details see Figure S2).
doi:10.1371/journal.pone.0089576.g006

informed that the interclick-interval changes. The seven click sequences with the differing interclick-interval were presented randomly within each block. Only sequences with a interclick-interval of 1000 and 2000 ms entered the analysis. The clicks were presented with speakers plugged into the laptop's sound card and

placed in front of the patient at 1 m distance. One block lasted 7 min.

Go/No-Go task. Three patients participated in the go/no-go (GNG) task (GNG01 - 03). In each trial the patients were presented with either a green or red square of 100 ms duration

and 900 - 1200 ms stimulus onset asynchrony. The subjects were instructed to respond as quickly as possible to green squares by pressing a key on a laptop keyboard but to withhold responses when a red square was presented (in block 1–3: 20% of the trials; in block 4: 50% of the trials). The participants were familiarized with the task in an initial short practice session. Only correct Go-trials of the first two blocks entered the analysis. Each block lasted approximately eight minutes.

Data recording

At UCSF the electrocorticogram (ECoG) was recorded either from 64 platin-iridium-electrode grids arranged in an 8×8 array with 10 mm center-to-center spacing (FTT01, FTT02, GNG01, GNG02 GNG03) or from a 256 electrode grid (both Ad-Tech Medical Instrument Corporation, Racine, Wisconsin) arranged in a 16×16 array with 4 mm center-to-center spacing (GNG02). Exposed electrode diameter was 2.3 mm in the 64 electrodes grid and 1.8 mm in the 256 electrodes grid. The electrode signals were recorded with a 256 channel preamplifier (PZ2-256, Tucker-Davis Technologies (TDT), Inc) with the electrode furthest from the motor cortex used as a reference. The data from the pre-amplifier were sampled at 3051.7 Hz on a digital signal processor (RZ2 4 DSP, Tucker-Davis Technologies (TDT), Inc) with 16-bit resolution and stored to hard disk. Trigger signals indicating button presses and stimulus onsets were sent from the stimulus laptop via a USB-1208FS DAQ (Measurement Computing, Norton, MA) plus a photodiode attached to the screen and recorded on the DSP synchronized to the brain data. Trigger timing was additionally recorded on the stimulus laptop by querying the computers performance counter using the Psychophysics Toolbox (www. psychtoolbox.org). In Bielefeld (AMCT) the ECoG signal was recorded at 1000 Hz sampling frequency (16 Bit resolution) with a Nihon Kohden system (Tokyo, Japan) equipped with auxiliary analogue channels for synchronous recording of the trigger signals and the output from the sound card. Here 5 stripes were implanted each equipped with two parallel rows of 5 electrodes each (see Figure 6).

Data analysis

We used Matlab 2008a (Mathworks, Natick, USA) for all offline data processing. We first preprocessed the recorded brain data and then we derived measures quantifying adaptation of oscillatory neural dynamics during motor skill learning. All filtering was done using IIR filters (Butterworth filter of order 4). Preprocessing served to remove non-physiological artifacts from the recorded data and to prepare them for further analysis. First we excluded channels exhibiting ictal activity or excessive noise from further analysis. In the remaining good channels we then excluded time intervals containing artifactual signal distortions such as steps of pulses by visual inspection. Finally, we re-referenced the remaining electrode time-series by subtracting the common average reference

$$x_{CAR}(t) = \frac{1}{n}\sum_{c=1}^{n} x_c(t) \qquad (1)$$

calculated over the n good channels c from each channel time series. The resulting time series were then used to characterize brain dynamics over the time course of motor behavior performance improvement in terms of the TPR:

For each trial starting at stimulus onset we calculated the TPR to quantify the evolution of phase-amplitude cross-frequency interactions of cortical oscillations during motor skill learning.

Therefore, we band-pass filtered each electrode's time series at two frequency bands, in the θ-range (4–8 Hz) and in the HG (80–180 Hz) range since coupling was task relevant between these frequencies across a variety of experimental tasks [2]. We detected θ-troughs, the local minima, in the θ-range filtered time series in the interval between 0 to 500 ms after stimulus onset (Figure 7). We obtained the HG analytic amplitude $A_{HG}(t)$ by Hilbert-transforming the HG filtered time series. For each detected θ-trough we then estimated the depth of the through D_θ and the simultaneous HG amplitude as the average of the θ-filtered and the A_{HG} time series over an interval of 83 ms (half θ oscillation) centered on the trough. Note that multiple θ troughs fit into the 500 ms analysis leading to multiple estimates per trial. We averaged the individual estimates $D_\theta(t)$ and $A_{HG}(t)$ to obtain one measure for θ trough depth $\overline{D}_\theta$ and one for HG amplitude $\overline{A}_{HG}$ for each trial j. From these values we calculated TPR for each trial j as:

$$TPR_j = \log\frac{\overline{D}_{\theta,j}}{\overline{A}_{HG,j}} \qquad (2)$$

Taking the log of the ratio makes the distribution of TPRs symmetric. Note that the TPR includes both stimulus-locked and non-stimulus-locked brain activity. It summarizes the global cross frequency interaction on the grids.

Phase-Amplitude Coupling

paCFC was tested by splitting the θ oscillations of the 500 ms analysis window into 20 equally spaced phase bins ranging from -π to π (18° or 0.314 rad) in each subject and each electrode. In each phase bin we averaged the amplitude envelope of the local HG. A cosine wave function
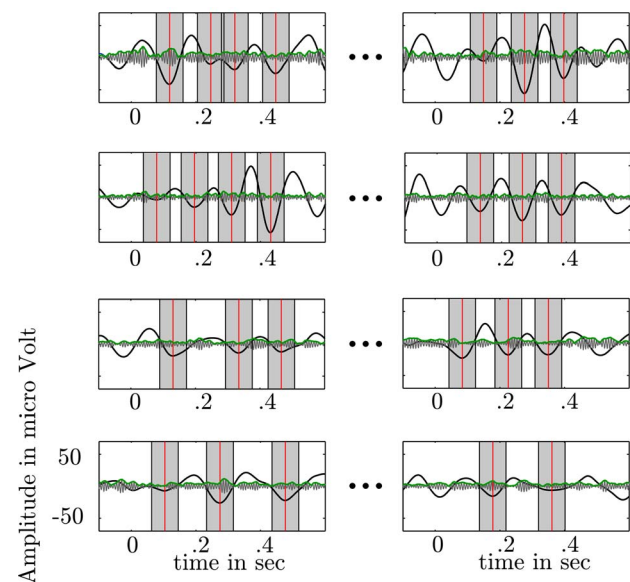

Figure 7. Calculation of the trough to peak ratio (TPR). We quantified paCFC as the ratio between θ trough (local minima of the θ time series - red vertical lines) and HG amplitude at the corresponding θ trough. Around each detected trough we spanned a window (half θ cycle - gray bars) in which θ activity (black bold line) and HG amplitude (green line) was averaged.
doi:10.1371/journal.pone.0089576.g007

$$\hat{y} = \alpha * \cos(\omega * HG + \phi) \tag{3}$$

with α representing the amplitude, ω representing the frequency and ϕ representing the phase angle was fitted to the resulting 20 HG amplitude (y) values. ω close to 1 indicates that HG amplitude variation is accounted for the θ cycle.

ROI analysis

In each patient we grouped electrodes according to the same anatomical landmarks in 6 regions of interest (see Figure S1): The anterior (in sum 34 electrodes across subjects) and posterior (44 electrodes) medial frontal gyrus, the anterior (49 electrodes) and the posterior inferior frontal gyrus (81 electrodes), and the superior (48 electrodes) and inferior (46 electrodes) sensorimotor cortex. We averaged the TPR-values within each ROI across electrodes. In each patient we determined the p-value for Pearson's correlation coefficient r and the partial correlation coefficient rho (ρ) between the averaged TPR values and behavioral performance across trials. Each ROI in which the mean p-value across subjects fell below the p-value corrected for multiple comparisons ($p_{corr} = \frac{.05}{6}$) was considered statistically significant.

Separating performance from learning effects

We separated performance from learning effects by applying a permutation test statistic. The reasoning for applying a permutation test was two-fold. First, we sought to correct the p-values for each electrode due to the many individual correlation tests applied. We tested this against a distribution which did not rely on the same temporal interval (500 ms following the stimulus presentation) for which the correlation coefficient was calculated. Second, we wanted to identify electrodes in which Pearsons correlation coefficient r was significantly higher than the partial correlation coefficient ρ. This means that we looked for electrodes with a significant difference between r and ρ. Since the significance can only be determined in relation to a distribution we estimated this distribution from our data. Hence, the null hypothesis to be rejected was that the difference between electrodes r and ρ was derived from a random distribution. The recorded time series were filtered in the θ (4–8 Hz) and in the HG (80–180 Hz) frequency. Subsequently, we calculated the HG envelope of the HG time series in each electrode and each trial by taking the absolute value of the Hilbert transform of the filtered time series. The analytic amplitude is a new time series representing the amplitude envelope of the HG-oscillations at any moment in time. We then determined 20 time windows around the stimulus onset each with a width of 500 ms and 400 ms overlap. In order to conduct the TPR permutation test statistic we calculated $\overline{D}_\theta$ and $\overline{A}_{HG}$ (see above) around each θ trough in the time window in each electrode and trial which yields

20 $\overline{D}_\theta$ and 20 $\overline{A}_{HG}$ values in each trial from which one $\overline{D}_\theta$ and one $\overline{A}_{HG}$ value was randomly chosen in each permutation. In each trial the TPR was calculated from the random $\overline{D}_\theta$ and $\overline{A}_{HG}$ values and correlated (partial correlation) with behavioral measures. In 500 permutation we estimated a distribution of partial correlation which served to assess the significance of the observed partial correlation coefficient. Electrodes exceeding the 95% percentile were considered significantly predictive for performance. In a comparable way learning effects were obtained. In general we tried to find the subset of electrodes within the pool of electrodes which are correlated with performance. Specifically we sought to find those electrodes whose Pearson's correlation coefficient is significantly greater than the partial correlation coefficient (ρ). Therefore we again chose randomly one $\overline{D}_\theta$ and one $\overline{A}_{HG}$ value per trial and correlated (Pearson's correlation – r) the randomly obtained TPR values with behavioral measures. In each permutation we calculated the difference $d_{r-\rho}$ between the randomly obtained r and ρ. In 500 permutations we estimated a distribution of $d_{r-\rho}$ which served to assess the significance of the observed $d_{r-\rho}$. Electrodes exceeding the 95% percentile were considered significantly predictive for performance improvement. Note that this analysis results in spatially more limited clusters than in the ROI-analysis since in the ROI-analysis Pearson's r was used and not the difference of $r - \rho$.

Supporting Information

Appendix S1 Supplementary Material.
(PDF)

Figure S1 Prediction of behavior changes as a function of the phase. Red and black asterisks show the number of signicant electrodes for each of the 20 phase bins for the performance/paCFC correlation and partial correlation, respectively.
(TIF)

Figure S2 We grouped electrodes into 6 regions of interest. Each outline denotes the grid coverage of one subject. The bold outline shows the summed coverage across all subjects. The anterior and posterior medial frontal gyrus (FMa, FM), the anterior and the posterior inferior frontal gyrus (FIa, FI), and the superior and inferior sensorimotor cortex (MI,MII). The outline of the grid location of the AMCT participant is given in Figure 5.
(TIF)

Author Contributions

Conceived and designed the experiments: SD FQ UK RTK. Performed the experiments: SD FQ UK. Analyzed the data: SD RTK. Contributed reagents/materials/analysis tools: HJH HH RS HP EC. Wrote the paper: SD RTK HH UK.

References

1. Buzsáki G, Draguhn A (2004) Neuronal oscillations in cortical networks. Science 304: 1926–1929.
2. Canolty RT, Edwards E, Dalal SS, Soltani M, Nagarajan SS, et al. (2006) High gamma power is phase-locked to theta oscillations in human neocortex. Science 313: 1626–1628.
3. Canolty RT, Ganguly K, Kennerley SW, Cadieu CF, Koepsell K, et al. (2010) Oscillatory phase coupling coordinates anatomically dispersed functional cell assemblies. Proc Natl Acad Sci U S A 107: 17356–17361.
4. Canolty RT, Knight RT (2010) The functional role of cross-frequency coupling. Trends Cogn Sci 14: 506–515.
5. Tort ABL, Kramer MA, Thorn C, Gibson DJ, Kubota Y, et al. (2008) Dynamic cross-frequency couplings of local field potential oscillations in rat striatum and

6. Tort ABL, Komorowski RW, Manns JR, Kopell NJ, Eichenbaum H (2009) Theta-gamma coupling increases during the learning of item-context associations. Proc Natl Acad Sci U S A 106: 20942–20947.
7. Axmacher N, Cohen MX, Fell J, Haupt S, Dmpelmann M, et al. (2010) Intracranial eeg correlates of expectancy and memory formation in the human hippocampus and nucleus accumbens. Neuron 65: 541–549.
8. Klausberger T, Magill PJ, Márton LF, Roberts JDB, Cobden PM, et al. (2003) Brain-state- and cell-type-specific firing of hippocampal interneurons in vivo. Nature 421: 844–848.
9. Jensen O, Colgin LL (2007) Cross-frequency coupling between neuronal oscillations. Trends Cogn Sci 11: 267–269.

hippocampus during performance of a t-maze task. Proc Natl Acad Sci U S A 105: 20517–20522.

10. Cardin JA, Carln M, Meletis K, Knoblich U, Zhang F, et al. (2009) Driving fast-spiking cells induces gamma rhythm and controls sensory responses. Nature 459: 663–667.

11. Haider B, McCormick DA (2009) Rapid neocortical dynamics: cellular and network mechanisms. Neuron 62: 171–189.

12. Voytek B, Canolty RT, Shestyuk A, Crone NE, Parvizi J, et al. (2010) Shifts in gamma phaseamplitude coupling frequency from theta to alpha over posterior cortex during visual tasks. Front Hum Neurosci 4: 191.

13. Grafton ST, Woods RP, Tyszka M (1994) Functional imaging of procedural motor learning: Relating cerebral blood ow with individual subject performance. Human Brain Mapping 1: 221–234.

14. Jueptner M, Stephan KM, Frith CD, Brooks DJ, Frackowiak RS, et al. (1997) Anatomy of motor learning. i. frontal cortex and attention to action. J Neurophysiol 77: 1313–1324.

15. Jueptner M, Frith CD, Brooks DJ, Frackowiak RS, Passingham RE (1997) Anatomy of motor learning. ii. subcortical structures and learning by trial and error. J Neurophysiol 77: 1325–1337.

16. Brovelli A, Lachaux JP, Kahane P, Boussaoud D (2005) High gamma frequency oscillatory activity dissociates attention from intention in the human premotor cortex. Neuroimage 28: 154–164.

17. Aron AR (2010) From reactive to proactive and selective control: Developing a richer model for stopping inappropriate responses. Biol Psychiatry.

18. Uhlhaas PJ, Singer W (2010) Abnormal neural oscillations and synchrony in schizophrenia. Nat Rev Neurosci 11: 100–113.

19. Allen EA, Liu J, Kiehl KA, Gelernter J, Pearlson GD, et al. (2011) Components of cross-frequency modulation in health and disease. Front Syst Neurosci 5: 59.

20. Crowell AL, Ryapolova-Webb ES, Ostrem JL, Galifianakis NB, Shimamoto S, et al. (2012) Oscillations in sensorimotor cortex in movement disorders: an electrocorticography study. Brain 135: 615–630.

21. de Hemptinne C, Ryapolova-Webb ES, Air EL, Garcia PA, Miller KJ, et al. (2013) Exaggerated phase-amplitude coupling in the primary motor cortex in parkinson disease. Proc Natl Acad Sci U S A 110: 4780–4785.

22. Lisman JE, Jensen O (2013) The - neural code. Neuron 77: 1002–1016.

23. Axmacher N, Henseler MM, Jensen O, Weinreich I, Elger CE, et al. (2010) Cross-frequency coupling supports multi-item working memory in the human hippocampus. Proc Natl Acad Sci U S A 107: 3228–3233.

24. Yanagisawa T, Yamashita O, Hirata M, Kishima H, Saitoh Y, et al. (2012) Regulation of motor representation by phase-amplitude coupling in the sensorimotor cortex. J Neurosci 32: 15467–15475.

25. Scheffer-Teixeira R, Belchior H, Leo RN, Ribeiro S, Tort ABL (2013) On high-frequency field oscillations ($>$100 hz) and the spectral leakage of spiking activity. J Neurosci 33: 1535–1539.

26. Miller KJ, Hermes D, Honey CJ, Hebb AO, Ramsey NF, et al. (2012) Human motor cortical activity is selectively phase-entrained on underlying rhythms. PLoS Comput Biol 8: e1002655.

27. Belluscio MA, Mizuseki K, Schmidt R, Kempter R, Buzski G (2012) Cross-frequency phase-phase coupling between and oscillations in the hippocampus. J Neurosci 32: 423–435.

28. Cantero JL, Atienza M, Stickgold R, Kahana MJ, Madsen JR, et al. (2003) Sleep-dependent theta oscillations in the human hippocampus and neocortex. J Neurosci 23: 10897–10903.

29. Ray S, Maunsell JHR (2011) Different origins of gamma rhythm and high-gamma activity in macaque visual cortex. PLoS Biol 9: e1000610.

30. Crone NE, Miglioretti DL, Gordon B, Sieracki JM, Wilson MT, et al. (1998) Functional mapping of human sensorimotor cortex with electrocorticographic spectral analysis. i. alpha and beta eventrelated desynchronization. Brain 121 (Pt 12): 2271–2299.

31. Cheyne D, Bells S, Ferrari P, Gaetz W, Bostan AC (2008) Self-paced movements induce highfrequency gamma oscillations in primary motor cortex. Neuroimage 42: 332–342.

32. Brashers-Krug T, Shadmehr R, Bizzi E (1996) Consolidation in human motor memory. Nature 382: 252–255.

33. Muellbacher W, Ziemann U, Wissel J, Dang N, Koer M, et al. (2002) Early consolidation in human primary motor cortex. Nature 415: 640–644.

34. Simon SR, Meunier M, Piettre L, Berardi AM, Segebarth CM, et al. (2002) Spatial attention and memory versus motor preparation: premotor cortex involvement as revealed by fmri. J Neurophysiol 88: 2047–2057.

Supplementary Material

Interpretation of partial and Pearson correlation

A geometric interpretation is given by the fact that Pearson correlation, as a similarity measure between random variables, is closely related to the angle between two vectors. The two vectors are the two possible regressions between the two variables. Correlation is high when the angle between the regressions is small. Partial correlation introduces a third variable, in our case time. It measures the angle of the two regression lines in the plane perpendicular to the third variable. Thus, in a 3D space spanned by TPR, performance, and time the plane in which the two possible regressions between TPR and performance can have different orientations with the time axis. If the time axis is orthogonal to the plane, then the correlation between TPR and performance is fully independent of time and unrelated to learning. On the contrary, if the two regression lines are in the same plane as the time axis, then the correlation between TPR and performance is fully time dependent and due to learning. In practice, we can expect to most likely observe mixed effects with regressions oriented between the extremes, indicating mixed contributions of learning and learning unrelated correlations. Importantly, our reasoning is that if we observe a significant Pearson correlation in an electrode that significantly changes if we discount time related correlations (in partial correlation), then the TPR with performance correlation in this electrode is at least partly due to learning related TPR with performance correlations. With this combination of partial and Pearson's correlation we also discount the possibility that the correlation effects are only due to a paCFC variation over time. One prerequisite to conduct the correlation approach described here is that motor performance is linearly independent across trials. We assessed this by estimating the autocorrelation function for the performance measures in each subject. We found the autocorrelation function exceeding the 95 percent confidence interval with a time lag greater than 1 only for the one subject in the AMC task. This is likely a result of the task itself since the subject is required to respond within the same temporal frame. To verify that the significance of the correlation coefficients is not prone to an inter-trial dependency of performance (autocorrelation) we tested in each subject for each electrode showing a significant Pearsons correlation whether it was drawn from a random distribution. In 500 runs we randomly shuffled both the TPR values and performance measures of each trial and calculated the correlation coefficient r. Then we estimated the probability that the observed r values could have been derived from the random distribution. The p-values were all smaller than .002 indicating that the observed r values are not a result of a possible inter-trial dependency of the performance measures.

Stability of coupling phase

The previous analyses showed that performance covaries with paCFC. However, calculating the paCFC at one phase (see Section 4.2) the changes with performance can either be a result of a shift of the HG amplitude peak relative to the θ trough or the result of simultaneous adaption of both frequency components. To test the hypothesis that the covariation is not a result of the HG peak shift we used the fitted phase angle of the trial-wise sine fit functions (see Figure 2) . By means of a linear regression we tested whether there are systematic changes of the phase angle over time. In each subject we compared the slope of the linear regression with an empirical distribution of slopes derived from randomizing the order of trials 500 times. Both for the channels showing correlation and partial correlation no systematic change was found as indicated by slopes within the confidence intervals. This suggests that performance/paCFC covariation is a result of simultaneous adaptation of both frequency components rather than a shift of the HG amplitude peak.

Specificity of θ-HG interaction

We investigated whether HG nested to the θ trough is exclusively predictive for performance. In the three experimental tasks we additionally assessed the specificity of the θ/HG coupling compared to θ/β or θ/γ coupling. For a broad frequency range encompassing β, γ, and high θ range we extracted all frequencies with a band width of 6 Hz and a resolution of 2 Hz; center frequencies: 13-190 Hz). For each sub band ($N_{subbands} = 89$, 13 belonging to the β band, 21 the γ and 65 to the HG range) we calculated the paCFC with the θ activity and assessed the correlation with behavior for each channel across subjects. The number of electrodes showing a significant (p < .05, uncorrected) performance/paCFC correlation varied as a function of frequency band ($N_{\theta/\beta} = 193$, $N_{\theta/\gamma} = 187$, $N_{\theta/H\gamma} = 289$; $\chi^2 = 29.4$; p < .0001). The corresponding r-values were compared using a one-way ANOVA with the factor frequency band. The frequency bands predicted behavior differently (F(2,666) = 10.9, p < .0001). Posthoc tests revealed that the prediction of behavior by the θ/HG coupling was better than the prediction by θ/β coupling or θ/γ coupling (p corrected for Nsubbands < .0001), suggesting a specific effect of the θ/HG coupling for the prediction of motor behavior. Necessity of Interaction We then tested whether θ or HG alone predicted behavior. We compared performance/θ, performance/HG, and performance/paCFC correlation coefficients. As for the specificity analysis, we calculated for each electrode the Pearson's r for correlation of performance with θ, HG, and paCFC and compared r-values of electrodes showing significant correlation. Since Pearsons r is not a metric measure we transformed r values using the inverse hyperbolic tangent

$$\operatorname{arctanh}(r): \frac{1}{2} \ln \frac{(1+r)}{(1-r)} for |r| < 1 \tag{1}$$

The levels covaried differently with behavior (F(2,501) = 19.67, p < .0001). Post-hoc tests revealed a significant difference between paCFC and θ (t(373) = -4,81; p < .0001) and paCFC and HG (t(416) = -4.7; p < .0001) at a Bonferroni corrected significance level. We did not find such difference comparing HG with θ (p = .5). Hence, paCFC predicted performance better than θ or HG activity alone. This indicates that the motor performance improvement variation of θ-HG coupling is a result of cooperative modulation of neuronal activity in the two frequency bands rather than the result of a variation of either θ or HG band activity alone.

We next asked whether the trial-by-trial correlation strength depends on the θ phase at which the paCFC is calculated. The previous analysis showed that HG-amplitude varies with the θ phase. Importantly, a variation of performance/paCFC correlation strength as a function of θ phase, could underscore the neurophysiological relevance of paCFC for behavioral adaptation. Therefore, we determined trial-by-trial performance/paCFC correlations at 20 different equally spaced θ phase bins. To test the hypothesis we compared the probability to detect significant electrodes across θ phase bins for correlation and partial correlation. We compared the phase specificity by fitting a cosine function to the probability of significant electrodes (see Figure S1). Both for correlation and partial correlation the fit was highly significant (p < .001) with the maximum of significant electrodes close to the trough ($\phi_{correlation} = .4$, $\phi_{partialcorrelation} = .6$). Figure S1 shows the probability of significant correlations both for the performance/paCFC correlation and partial correlation.

ORIGINAL ARTICLE

Mind-wandering Is Accompanied by Both Local Sleep and Enhanced Processes of Spatial Attention Allocation

Christian Wienke [1,†], Mandy V. Bartsch[3,†], Lena Vogelgesang[3], Christoph Reichert[2,3,4], Hermann Hinrichs[1,2,3,4,5], Hans-Jochen Heinze[1,2,3,4,5] and Stefan Dürschmid[1,3]

[1]Department of Neurology, Otto-von-Guericke University, Leipziger Str. 44, 39120 Magdeburg, Germany, [2]Forschungscampus STIMULATE, Otto-von-Guericke University, Universitätsplatz 2, 39106 Magdeburg, Germany, [3]Department of Behavioral Neurology, Leibniz Institute for Neurobiology, Brenneckestr. 6, 39118 Magdeburg, Germany, [4]CBBS – center of behavioral brain sciences, Otto-von-Guericke University, Universitätsplatz 2, 39106 Magdeburg, Germany and [5]German Center for Neurodegenerative Diseases (DZNE), Leipziger Str. 44, 39120 Magdeburg, Germany

Address correspondence to Stefan Dürschmid, Department of Behavioral Neurology, Leibniz Institute for Neurobiology, Brenneckestr. 6, 39118 Magdeburg, Germany. Tel: 0049 391 626392531; Email: sduersch@lin-magdeburg.de.
[†]These authors contributed equally to this work.

Abstract

Mind-wandering (MW) is a subjective, cognitive phenomenon, in which thoughts move away from the task toward an internal train of thoughts, possibly during phases of neuronal sleep-like activity (local sleep, LS). MW decreases cortical processing of external stimuli and is assumed to decouple attention from the external world. Here, we directly tested how indicators of LS, cortical processing, and attentional selection change in a pop-out visual search task during phases of MW. Participants' brain activity was recorded using magnetoencephalography, MW was assessed via self-report using randomly interspersed probes. As expected, the performance decreased under MW. Consistent with the occurrence of LS, MW was accompanied by a decrease in high-frequency activity (HFA, 80–150 Hz) and an increase in slow wave activity (SWA, 1–6 Hz). In contrast, visual attentional selection as indexed by the N2pc component was enhanced during MW with the N2pc amplitude being directly linked to participants' performance. This observation clearly contradicts accounts of attentional decoupling that would predict a decrease in attention-related responses to external stimuli during MW. Together, our results suggest that MW occurs during phases of LS with processes of attentional target selection being upregulated, potentially to compensate for the mental distraction during MW.

Key words: high-frequency activity, local sleep, mind-wandering, N2pc, visual spatial attention

Introduction

Depending on the time spent awake and the richness of experiences rodents and humans enter local sleep-like states, which manifests both as high amplitude slow wave activity (SWA) in the delta/theta range (1–6 Hz) and brief neuronal silencing (Vyazovskiy et al. 2011). Local sleep (LS) refers to the occurrence of use-dependent, sleep-like slow oscillations in neuronal populations while being awake. These slow oscillations are temporally and spatially isolated and occur more often with sustained cortical use or prolonged wakefulness. On a neuronal level, LS is accompanied by neuronal silencing, i.e., short periods where neurons interrupt and then resume their firing pattern. The occurrence of these offline periods in behaviourally relevant cortical areas, e.g., motor cortex during a reaching task, can lead to performance errors (Vyazovskiy et al. 2011). Electrophysiologically, LS leads to localized peaks in slow wave oscillations (1–6 Hz, increased SWA), which served as a proxy for LS in previous human EEG studies (Murphy et al. 2011; Bellesi et al. 2014; Castelnovo et al. 2016). Recent intracranial recordings in nonhuman primates indicate that local epicortical high-frequency activity (HFA) consists of both infragranular single-unit and supragranular calcium-dependent dendritic processes (Leszczyński et al. 2020) and is a key marker of cortical activation (Ray et al. 2008). When local neuronal assemblies interrupt and then resume their firing patterns (LS), this interruption leads to a reduction of amplitude in the HFA range. In humans, increased SWA as well as worsened performance have been observed after extended practice and prolonged wakefulness (Hung et al. 2013; Bernardi et al. 2015). Phenomenologically, LS is assumed to unearth mind-wandering (MW) (Andrillon et al. 2019), during which attention shifts inwards to self-centered matters (Smallwood and Schooler 2006). MW encompasses that (i) we retrieve episodic memory while (ii) we are occupied with another task, and (iii) that we become aware of this episodic material (Smallwood and Schooler 2006). However, becoming aware of something cannot be confused with directing attention to it. But in practice it is challenging to disentangle consciousness and attention. Hence, in this study, we also pursue the question how tightly consciousness is coupled with attention or whether attention can be allocated elsewhere while we are conscious of a different matter. Andrillon et al. (2019) proposed that LS, occurring in attentional networks, might trigger the deactivation of those networks and the recruitment of the default mode network (DMN), which in combination then leads to MW. Whether LS indeed leads to MW is not clear. Here, we provide an initial study in which we test whether and how LS and MW are related. Both LS and MW increase behavioral errors (Carriere et al. 2008; Smallwood et al. 2008; Bernardi et al. 2015; Seli 2016; Leszczynski et al. 2017) promoting the prediction of perceptual and attentional decoupling (Schad et al. 2012; Christoff et al. 2016). Perceptual decoupling is attested by reduced electrophysiological responses to the perceptual input during MW (Smallwood et al. 2008; Kam et al. 2011, 2018; Christoff et al. 2016). However, reduced electrophysiological responses are often interpreted as evidence for a reduction in attention ("attentional decoupling" - Smallwood 2011; Schad et al. 2012) even if the respective EEG components are not associated with attention. Importantly, since off periods (LS and MW) during waking are potentially harmful (He et al. 2011; Kucyi et al. 2013; Yanko and Spalek 2014; Brandmeyer and Delorme 2018) the survival in general would be endangered if the brain´s need for rest is met entirely during waking at the expense of the ability to flexibly shift attention to key features in the environment (Vyazovskiy and Harris 2013). Here, we explicitly ask how the brain's ability

to shift attention varies during off periods (LS and MW) and whether MW leads indeed to an attentional decoupling.

To this end, we employ an established electrophysiological response attributed to the focusing of visual attention onto a target searched among distractors, the EEG component N2pc (Luck and Hillyard 1994a; Eimer 1996; Luck et al. 1997; Hopf et al. 2000; Mazza et al. 2009; Boehler et al. 2011). The N2pc is characterized by a more negative deflection at posterior EEG channels contralateral to the visual field in which the target was presented. Theoretically there are at least 2 principal scenarios which can be tested using the N2pc. On the one hand, the attentional decoupling account predicts that the N2pc as an index of attentional selection gradually decreases with MW. On the other hand, it could be hypothesized that the N2pc increases with MW. That is, MW and external distractors are assumed to share a common underlying mechanism (Forster and Lavie 2014; Unsworth and McMillan 2014) and the N2pc is known to increase with an increasing amount of distracting information (Mazza et al. 2009).

Using the high spatiotemporal and spectral resolution of magnetoencephalographic recordings (MEG) we investigated how cortical dynamics varied with self-reports ranging from being ON (uninterrupted focus on the external environment) to OFF (MW) the task. The task was to search for a color-defined pop-out (target) among task-irrelevant distractors. Moreover, we hypothesized that if associated with LS, MW leads to SWA and neuronal silencing. The latter we would expect to be reflected in a reduction in HFA (80–150 Hz). HFA is a correlate of population neural firing rate (Mukamel et al. 2005; Liu and Newsome 2006; Manning et al. 2009; Miller et al. 2009; Ray and Maunsell 2011) and preferred proxy for asynchronous areal activation (Miller et al. 2009; Privman et al. 2013; Coon and Schalk 2016; Kupers et al. 2017) and thus ideally suited to test neuronal silencing.

Materials and Methods

Participants

A total of 16 subjects (5 female, range: 18–39 years, M: 27.13, SD: 5.85) participated after providing their written informed consent. One subject who did not experience MW was excluded, resulting in 15 subjects in the final analyses. All participants reported normal or corrected-to-normal vision and none reported any history of neurological or psychiatric disease. All recordings took place at the Otto-von-Guericke University of Magdeburg and were approved by the local ethics committee ("Ethical Committee of the Otto-von-Guericke University Magdeburg") and each participant was compensated with money. The sample size in our study was chosen according to previous studies examining the N2pc (e.g., Boehler et al. (2011): N = 15; Hopf et al. (2000): N = 12). Since our analytical approach for the N2pc is in part based on these studies, we required a similar sample size. Regarding the HFA, previous studies often used intracortical recordings. Here, sample sizes are typically limited to similar numbers of subjects (e.g., Tallon-Baudry et al. (2005): N = 14; Golan et al. (2016): N = 14).

Paradigm

Participants were presented with a stimulus array of red, green, and blue grating patterns each consisting of 3 colored and 2 gray stripes viewed through a circular aperture (Fig. 1). The gray stripes matched the gray of the background. While either of the green and red gratings served as target, blue gratings always
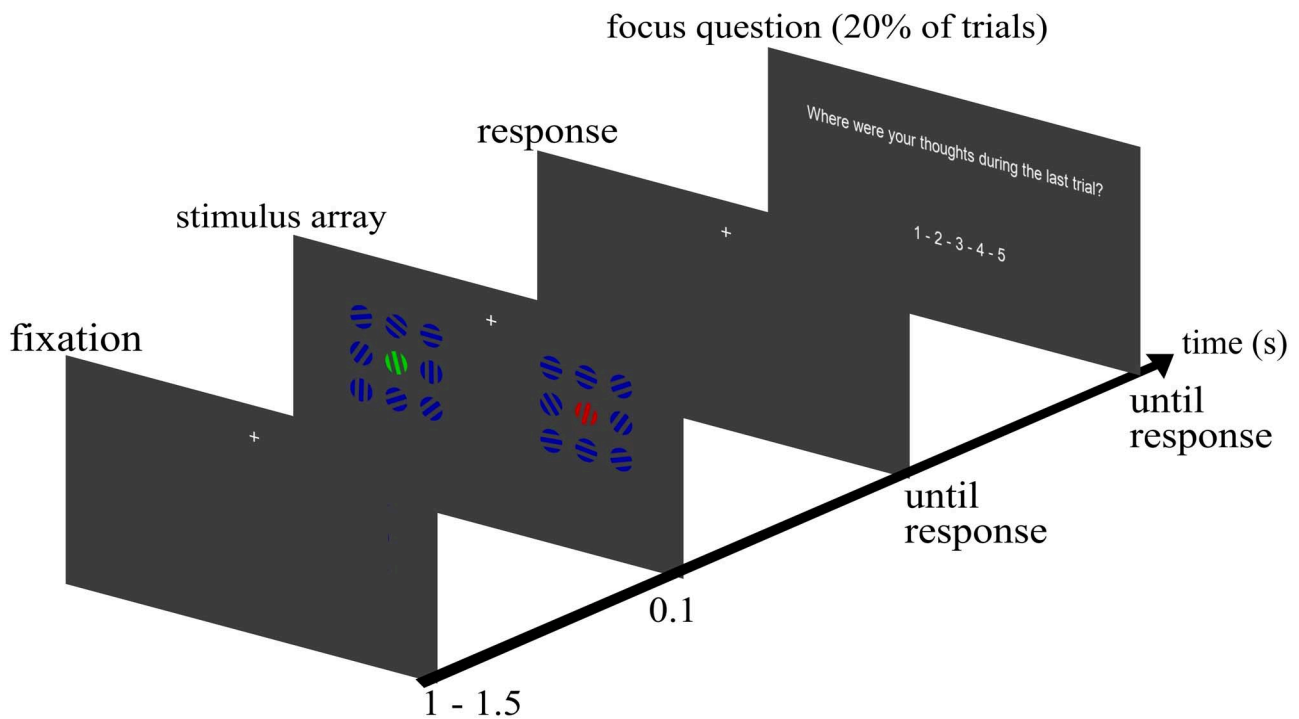
Figure 1. Single trial with focus question (see text for detail).

served as distractor items. Stimulus arrays consisted of 18 gratings arranged in 2 blocks of 9 gratings left and right below the fixation cross. Stimuli were placed below fixation since it has been shown that search displays evoke a stronger N2pc amplitude when displayed in the lower visual field (Luck et al. 1997; Hilimire et al. 2011). Participants were instructed to keep fixation on the fixation cross located at 1.9° visual angle (va) above the stimulus array. The size of each grating was 1.15° va, distance between single gratings (edge-to-edge) was 0.69° va. The left and right block of gratings each had a size of 4.83° by 4.83° va, the horizontal distance between both blocks (inner edges) amounted to 5.15° va. Diagonal distance between the fixation cross and the center of the nearest upper grating was 2.81° va. Target gratings could be tilted left or right in 10 steps of 1.5°, with the smallest tilt being 1.5° and the maximal tilt being 15° from the vertical axis. Orientation and tilt angle of the nontarget and distracter gratings varied randomly. Stimulus generation and experimental control was done using Matlab R2009a (Mathworks, Natick, USA) and the Psychophysics Toolbox (Brainard 1997; Pelli 1997; Kleiner et al. 2007). Colors were matched for isoluminance using heterochromatic flicker photometry (Lee et al. 1988).

Procedure

At the beginning of each of the 12 blocks, participants were instructed to attend either only to the red or green grating and report via button press toward which side it was tilted (left: index finger, right: middle finger of the right hand). Target color assignment alternated blockwise. In blocks with the red grating as target the green grating served as nontarget which had to be ignored and vice versa. The target could appear at each of the 18 locations. The location of the nontarget was constrained to the mirrored location in the opposite grating block to keep equal distances to the fixation cross for both target and nontarget

gratings. Each trial started with a fixation period of 1250 ms (±250 ms) before the stimulus array was presented for 100 ms. Participants were asked to respond as fast and accurately as possible. Afterwards the next trial started. The experiment started with a training block of 20 trials to familiarize participants with the procedure. After 20 consecutive trials, a blinking pause allowed participants to blink and rest their eyes. These pauses lasted 7 s. Each block consisted of 100 trials.

Experience Sampling

Throughout the experiment we presented thought probes in pseudorandomly chosen trials (20% of all trials) asking participants to rate their attentional focus, in the single trial immediately preceding the probe, on a 5-point scale from 1 ("thoughts were anywhere else"—OFF) to 5 ("thoughts were totally at the task"—ON). The experience sampling approach allows the analysis of only a limited number of trials since more focus queries would prevent MW. Responses to focus questions were given with all 5 fingers of the left hand (thumb: 5, index finger: 4, middle finger: 3, ring finger: 2, little finger: 1). The probes were presented following orientation discrimination, with the restriction that 2 probes were separated by a minimum of one intervening search trial (this minimal distance of one intervening trial between probes occurred only for 7% of the focus queries). The probes were initiated by an auditory stimulus (500 Hz, ca. 85 dB for 200 ms). To increase statistical power, we grouped the 5 MW ratings in 3 groups of mental state (OFF: 1&2, MID: 3, ON: 4&5). Statistical analyses between mental states were performed on this subset of trials immediately preceding the focus query. Note that an increased number of thought probes (>20%) would lead to a decrease in time between single probes. This would leave little to no time for participants to let their minds wander, especially since the single trial duration in our experiment was only a few seconds.

MEG Recording

Participants were equipped with metal-free clothing and seated in a dimmed, magnetically shielded recording booth. Stimuli were presented via rear projection onto a semi-transparent screen placed at a viewing distance of 100 cm in front of the participants with an LCD projector (DLA-G150CLE, JVC, Yokohama, Japan) that was positioned outside the booth. Responses were given with the left and right hand via an MEG compatible LUMItouch response system (Photon Control Inc., Burnaby, DC, Canada). Acquisition of MEG data was performed in a sitting position using a whole-head Elekta Neuromag TRIUX MEG system (Elekta Oy, Helsinki, Finland), containing 102 magnetometers and 204 planar gradiometers. Sampling rate was set to 2000 Hz. Vertical EOG was recorded using one surface electrode above and one below the right eye. For horizontal EOG, one electrode on the left and right outer canthus was used. Preparation and measurement took about 2 h.

Preprocessing and Artifact Rejection

We used Matlab 2013b (Mathworks, Natick, USA) for all offline data processing. The 102 magnetometers were involved in our analyses. All filtering (see below) was done using zero phase-shift IIR filters (fourth order; filtfilt.m in Matlab). First, we filtered the data between 1 and 200 Hz. To discard trials of excessive, nonphysiological amplitude, we used a threshold of 3pT, which the absolute MEG values must not exceed (−1 to 2 s around stimulus onset—sufficiently long to prevent any edge effects during filtering). We then visually inspected all data, excluded epochs exhibiting excessive muscle activity, as well as time intervals containing artifactual signal distortions, such as signal steps or pulses. We refrained from applying artifact reduction procedures that affect the dimensionality and/or complexity of the data like independent component analysis. Time series of remaining trials were used to characterize HFA (80–150 Hz), SWA (1–6Hz), and the N2pc (1–30 Hz, main frequency range for cognitive event-related-potential (ERP) components, see Luck (2014)). Resulting time series were used to characterize brain dynamics over the time course of visual target detection. Each trial (−1 to 2 s around stimulus onset) was baseline corrected relative to the 100 ms interval prior to the stimulus onset.

Statistical Analysis

Statistical analyses between mental states were performed on the trials immediately preceding the probe. Under the assumption that MW might comprise several trials, the focus query could have interrupted participants in the beginning, the middle, or at the end of an MW episode. Hence, including more than the trial directly preceding the focus question would have weakened the separation of mental states. To determine statistical significance, we compared each statistical parameter against a surrogate distribution, which was constructed by randomly yoking labels of the trials and repeating the analysis of variance (ANOVA), t-tests, and calculation of Pearson's correlation coefficient. Consequently, reported P values represent the statistical significance relatively to the constructed surrogate distribution. We tested for statistically significant temporal intervals in 4 analyses: stimulus response of HFA, difference of the HFA between mental states, the N2pc, and difference of the N2pc between mental states. We considered only intervals with consecutive sample points exceeding 10 ms as significant (see Maris and Oostenveld (2007)).

To correct statistical significance for multiple comparisons we applied Bonferroni correction. Since activity at each time point t linearly depends on activity at time point t-1, 2 adjacent tests cannot be regarded as independent. Hence, we determined how many individual components are contained in both the grand average HFA and N2pc and corrected the alpha value by the number of components that significantly explained variance. We carried out a principal component analysis (PCA) and determined the eigenvalues of the resulting components. Components with an eigenvalue larger than 1 were considered to explain a significant amount of variance within our data. In the HFA activity we found 5 and in the N2pc 4 individual components. Hence, the corrected P value for the HFA is 0.05/5 = 0.01 and for the N2pc 0.05/4 = 0.0125.

I – Behavioral Results

We tested whether the ratio of ON and OFF ratings changed across the experiment to rule out the possibility that changes in cortical dynamic are a result of a change across the experiment and not of fluctuations of the mental state throughout the experiment. We divided the 12 experimental blocks in 4 parts by averaging ratings in 3 consecutive blocks since individual subjects did not make use of each of the 5 ratings in single blocks and compared the number of ON and OFF ratings across these 4 parts with a 4×2 ANOVA with the factors block (I, II, III, and IV) and mental state (ON vs. OFF).

Performance, measured as percent correct responses, was averaged across tilt angles for each subject and compared between mental states with a one-way ANOVA. Performance during focus trials was then correlated with N2pc amplitude (see below) to test whether N2pc strength predicts performance.

Reaction times (RTs) were grouped for the 3 mental states and averaged across subjects. The averaged RTs where then compared using a one-way ANOVA with the factor mental state (OFF, MID, ON).

II – HFA Response (Neuronal Silencing)

We then obtained the HFA response. For each trial we band-pass filtered each magnetometer´s time series in the broadband high-frequency range (80–150 Hz). We obtained the analytic amplitude $A_f(t)$ of this band by Hilbert-transforming the filtered time series. In the following, HFA refers to this Hilbert transform. We smoothed the HFA time series such that amplitude value at each time point t is the mean of 25 ms around each time point t. We then baseline-corrected by subtracting from each data point the mean activity of the 100 ms preceding the stimulus onset in each trial and each channel. Afterwards, we identified stimulus-responsive channels showing a significant (compared to an empirical distribution, see below) amplitude modulation in the HFA following the onset of the visual search array. Since we expected an HFA amplitude modulation within the first 300 ms following the stimulus presentation, we first calculated the average HFA modulation, averaged across the 300 ms following the stimulus onset, from which we then subtracted the baseline activity preceding the stimulus onset. Second, after stimulus-responsive channels were determined, a one-way ANOVA (OFF, MID, ON) was conducted at each time point between 100 ms prestimulus and 600 ms poststimulus to test for HFA differences between mental states. To facilitate interpretability, we report F-values after stimulus presentation. The F-value of the main effect "mental state" parameterizes neuronal silencing in the

HFA response, with high F-values indicating a large difference in HFA amplitude between mental states. To set a threshold for significant difference, an empirical distribution of the main effect was constructed by randomly reassigning the labels (OFF – MID – ON) to the single trials in 1000 permutations. Peak responses (maximal average HFA response following stimulus onset) in each of the mental states were compared against a surrogate distribution. In each iteration, time series of each channel were circularly shifted time series of participants between -500 and 300 ms separately, and new (surrogate) trial averages were calculated. From these trial averages we calculated the peak value in the time range of 0 to 300 ms following stimulus onset. Mental states exceeding the 97.5th percentile were classified as showing significant HFA modulation.

The HFA is a frequency band, whose amplitude is modulated by stimulus presentation both in the auditory (Crone et al. 2001) and visual modality (Lachaux et al. 2005). Hence, the HFA is a stimulus-responsive band. The usual 2-step approach is to (i) assess stimulus-responsive channels and then (ii) test for condition differences. The prediction from recent MW literature is that the sensory representation of an onsetting stimulus is low when subjects report that their minds wandered. Using the HFA, we can test which regions are stimulus-responsive. Slow wave oscillations, in contrast, are instantaneous in the sense that they occur locally but might travel across cortical regions during sleep. These occasionally appearing SWA peaks are different from ongoing activity that should be modulated by stimulus onsets. Hence, SWA-peaks are not assumed to carry stimulus information. Instead, synchronized occurrences of OFF periods result in the high-amplitude electro- or magnetoencephalogram (EEG/MEG) slow waves that are typical for early, nonrapid eye movement sleep. The electrographic manifestation of sleep—high-amplitude EEG/MEG slow waves—arises from such synchronized alternation between on and off periods across large cortical neuronal populations.

III – High-Amplitude Slow Wave Oscillation

For each trial we band-pass filtered each magnetometer´s time series in the frequency range of slow wave oscillations (1–6 Hz) and z-scored the obtained analytic amplitude $A_f(t)$ of this band by Hilbert-transforming the filtered time series. In the following text, SWA refers to this Hilbert transform. We used z-scoring for the SWA for 2 reasons. First, SWA peaks are single temporally and spatially isolated events (Vyazovskiy et al. 2011), while the HFA is an ongoing time series (Crone et al. 2001). Second, unlike the HFA, the SWA is not stimulus-responsive. SWA pattern can occur even in the baseline period. In contrast to the HFA, we did not expect the number of SWA peaks to be modulated by the stimulus onset. Hence, the z-score method allows to assess the local occurrence of SWA independently of stimulus onset across the entire recording time. We then counted the number of peaks of the SWA defined as local maxima exceeding 3 SD in each trial at each channel in the time from 500 ms prestimulus to 500 ms poststimulus. Next, we identified channels with a high number of SWA peaks. To account for the occurrence of SWA peaks local in time, a surrogate distribution was constructed by randomly exchanging channel labels in each subject and calculating new (surrogate) channel averages across participants. In each of 1000 iterations we randomly exchanged channel labels in each subject and new (surrogate) channel averages were calculated across participants. Channels exceeding the 97.5th percentile of the channel-specific surrogate distribution were classified as showing a significant SWA modulation (SWA channels). The number

of SWA peaks was averaged separately for the 3 mental states across SWA channels in each participant. We then carried out a one-way ANOVA with factor mental state (OFF – MID – ON) at each time point, with single participants as random variable. The F-value of the main effect "mental state" parameterizes the occurrence of SWA with high F-values indicating a large difference in the number of SWAs between mental states. To set a threshold for significant difference, an empirical distribution of the main effect was constructed by randomly reassigning the labels (OFF – MID – ON) to the single trials in 1000 permutations.

The rationale for the different analytic approaches for SWA and HFA, even though they reflect presumably similar processes, is the following: Modulation of the HFA is usually assessed as its variation across time. In contrast, SWA are single events local in time. The difference in analytic approaches is also due to the fact that low-frequency characteristics can be detected easier in macroscopic recordings than high-frequency patterns which is why they can be localized more feasible in time (i.e., as single events in time). However, both measures are strongly related since an increase of SWA in the rodent's LFP is paralleled by neuronal silencing. In our study we can assess SWA but not multiunit activity that could directly index neuronal silencing. The neural signature closest to the MUA, however, is the HFA, which has been regarded a good measure of neuronal spiking (Liu and Newsome 2006; Berens et al. 2008) and consists of both infragranular single-unit and supragranular calcium-dependent dendritic processes (Leszczyński et al. 2020). This is also consistent with the idea that HFA reflects aggregated local neuronal output (Buzsáki et al. 2012) due to reliably high correlations between HFA and multiunit activity. Hence, the HFA became a classical indicator of cortical activation.

IV – N2pc

To assess the allocation of spatial attention, we employ the so-called N2pc, which is a marker of attentional selection in visual search paradigms (Luck and Hillyard 1994a; Eimer 1996; Luck et al. 1997; Hopf et al. 2000). The N2pc is an event-related component of the EEG and MEG response that is elicited contralateral to the target when subjects covertly (i.e., without eye-movements) shift their spatial attention to the respective target presented in the left or right visual field. Specifically, shifting the focus of attention to the left visual hemifield will lead to an enhanced response—typically around 200–300 ms after stimulus-onset—at right-hemisphere sensors and vice versa. Importantly, a stronger N2pc (higher amplitude) is associated with a stronger focusing to the respective target item and/or better suppression of surrounding distractor items (Luck et al. 1997; Mazza et al. 2009). The N2pc is recorded at sensors showing a maximum difference in response to left versus right visual field targets, typically at parietal/occipital recording sides. For EEG, there is usually a single maximum (negativity) contralateral to the target. For MEG, the respective dipole creates both an efflux and an influx maximum contralateral to the target that will be combined (Hopf et al. 2000; Boehler et al. 2011). The N2pc can then be displayed as the respective left-minus-right difference waveform with the signal often being averaged across both hemispheres for simplification (i.e., only one single waveform for the N2pc combining attended left and right visual field targets) (e.g., Mazza et al. 2009; Lagroix et al. 2015; Donohue et al. 2018). Extraction of the N2pc waveform was adapted from Boehler et al. (2011). For each participant, 4 channels were selected. One in each hemisphere reflecting the efflux maximum and one in each

Table 1. Mean number and percentage of thought probes, categorized as ON, MID, or OFF

	Mean %	SD %	Mean N	SD N
ON	51.25	27	107.14	46.75
MID	33.1	18.7	76	42.64
OFF	15.67	16.8	34.92	36.27

hemisphere reflecting the influx maximum. Selection of channels was limited to an occipital-parietal region of interest (ROI) which is in line with the N2pc ROI in the previous literature (e.g., Hopf et al. 2000; Boehler et al. 2011; Donohue et al. 2016). Efflux and influx channels of both hemispheres were combined by subtracting the signal of the influx channel from the signal of the efflux channel. To extract the N2pc, we subtracted this combined signal for targets in the right visual field from the combined signal for targets in the left visual field, again separately for both hemispheres. The final N2pc waveform was generated by averaging together the N2pc generated over the left and right hemisphere. In the next step we tested whether the N2pc was significantly elevated over baseline. We baseline-corrected the N2pc time series of each subject by subtracting from each data point the mean activity of the 200 ms preceding the stimulus onset. We then tested whether the average N2pc shows a significant (compared to an empirical distribution, see below) amplitude modulation following the onset of the visual search array. We first calculated the average activity modulation $\overline{A}_{N2pc}$ averaged across the 200–300 ms following the stimulus onset from which we subtracted the baseline activity $\overline{B}_{N2pc}$ preceding the stimulus onset. The difference between $\overline{B}$ and $\overline{A}$ was compared against a surrogate distribution. In each iteration, time series of each subject were circularly shifted between −500 and 300 ms separately, and new (surrogate) trial averages $(\overline{B}$ and $\overline{A})$ were calculated. Time points exceeding the 97.5th percentile of the channel-specific surrogate $\overline{A}_{N2pc} - \overline{B}_{N2pc}$ distribution were classified as showing a significant N2pc modulation following stimulus onset. The first time point of significant N2pc modulation in each subject was used as N2pc onset. Using a time point-by-time point ANOVA between -100 and 600 ms with the factor mental state (OFF, MID, ON) we tested whether the N2pc differs between focus conditions. The F-value of the main effect "mental state" parameterizes the variation of the N2pc as a function of mental states with high F-values indicating a large difference in N2pc amplitude between mental states. To set a threshold for significant difference, an empirical distribution of the main effect was constructed by randomly reassigning the labels (OFF – MID – ON) to the single trials in 1000 permutations.

V – Local Sleep-N2pc Correlation

First, HFA and N2pc onset times were compared via t-test to analyze temporal discrimination between both. Second, to examine the interaction between HFA and N2pc over the different mental states, HFA and N2pc time series were averaged separately for the 3 mental states in each participant for the interval between onset and offset (interval between significant elevation over baseline). We then carried out a 2-way ANOVA with factor MEG response (N2pc – HFA) and mental state (OFF – MID – ON) at each time point, with single participants as random variable. Third, for each mental state N2pc (averaged across the interval of significant

amplitude modulation for all trials) was correlated with HFA response (averaged across the interval of significant amplitude modulation for all trials). The resulting Pearson's correlation values were tested against a surrogate distribution. This surrogate distribution was constructed by randomly assigning the HFA values of each participant with the N2pc values from another participant in 1000 iterations.

Results

I – Behavioral results

Excluding times for individual pauses, thought probes were presented on average every 10.34 s (SD = 5.09; range: 3.7–29.6 s). MW ratings differed in frequency ($F_{2,42} = 10.11$, $P < 0.001$; ON 51.25% (SD: 27%), MID 33.1% (SD: 18.7%), and OFF 15.67% (SD: 16.8%); Table 1) with more ON than MID ratings ($t_{14} = 2.21$, $P = 0.035$) and more MID than OFF ratings ($t_{14} = 2.56$, $P = 0.016$). The ratio of ratings did not vary across blocks: main effect of block ($F_{3,112} = 0.03$, $P = 0.99$) and interaction ($F_{3,112} = 0.6$; $P = 0.6$) were not significant (Fig. 2A). While ON ratings did not vary across blocks (all P's > 0.1), OFF ratings increased from block I to II ($t_{14} = 2.5$; $P = 0.02$) but remained constant afterwards. Performance varied with mental state ($F_{2,42} = 5.14$, $P = 0.01$) with worse performance during OFF trials (M: 70.2%, SD: 18.8%) than during MID trials (M: 80.2%, SD: 7%; $t_{14} = 2.62$, $P = 0.01$) or ON trials (M: 84.7%, SD: 7%; $t_{14} = 2.09$, $P = 0.03$). No differences were observed between ON and MID trials ($t_{14} = 1.76$, $P = 0.1$; Fig. 2B). Performance varied also as a function of tilt angle. Participants made more errors at small angles and performance increased fast with increasing angles. To increase statistical power, we averaged trials across all tilt angles (Fig. 2C). Also, reaction times differed significantly between mental states ($F_{2,42} = 2.75$ $P = 0.003$) with longer RTs during OFF (M: 898 ms, SD: 1028 ms) compared with ON (M: 433 ms, SD: 146 ms; $t_{14} = 1.72$, $P = 0.04$), a trend of statistical significance between OFF and MID trials (M: 489 ms, SD 212 ms; $t_{28} = 1.48$, $P = 0.07$), but no differences between ON and MID trials ($t_{28} = 0.87$, $P = 0.38$; Fig. 2D).

II – HFA Response (Neuronal Silencing)

A total of 15 occipital magnetometers showed stimulus response in the HFA between 81 and 234 ms poststimulus (HFA$_{max}$ = 1.24fT at 161 ms, $P < 0.001$, Fig. 3A,B,C). The HFA differed between mental states between 145 and 171 ms poststimulus ($F_{crit} = 2.74$; $F_{max} = 3.18$ at 151 ms, $P = 0.02$, Fig. 3D) with smaller HFA in OFF (M: .47fT, SD: .93fT) versus ON (M: 1.24fT, SD: .82fT; $t_{14} = 2.16$, $P = 0.02$) and versus MID trials (M: 1.25fT, SD: 1.28fT; $t_{14} = 2.04$, $P = 0.03$) but no difference between ON and MID ($t_{14} = 0.53$, $P = 0.69$). Importantly, in contrast to ON (critical peak amplitude = 0.63fT, HFA$_{max}$ = 1.29fT at 149 ms; $P < 0.001$) and MID trials (HFA$_{max}$ = 1.33fT at 152 ms; $P < 0.001$), HFA did not show a significant peak response in OFF trials (HFA$_{max}$ = 0.5fT at 151 ms, $P = 0.15$). We then tested whether the HFA is simply not different from but equals baseline activity. Specifically, we estimated the Bayes factor (BF) to determine the amount of evidence for a change over baseline (amplitude values across all time points and subjects in the 100 ms prior to stimulus onset). The BF was estimated at each time point separately for the ON and OFF condition. We found no evidence for the H$_1$ and therefore no evidence for a change (BF$_{max}$ = 0.76 at 142 ms) in the OFF condition. But strong evidence in the ON condition (BF$_{max}$ = 43.01 at 152 ms; see Fig. 3D).
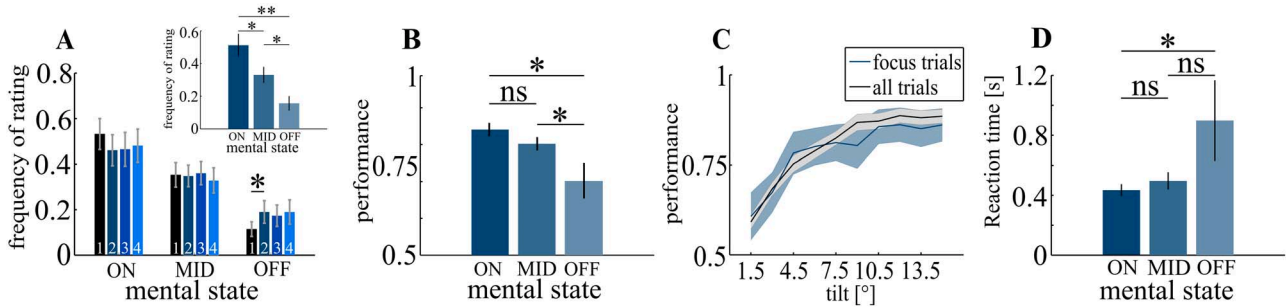
Figure 2. Behavioral data, A: participants made more ON and MID than OFF ratings (small inset). Only between the first and the second quarter of the experiment was a significant increase in OFF ratings, which then remained constant. Numbers at the bottom of bar graphs indicate the corresponding quarter (i.e., first, second, third or fourth) of the experiment. B: subjects made more errors during OFF trials than during ON and MID trials. C: Performance was lowest at small tilt angles and increased with increasing angles. This pattern was identical for all trials (black) as well as for the trials in which a thought probe was presented (blue), irrespective of mental state. D: Reaction times were significantly longer in OFF vs. ON trials. The error bars and shaded areas represent the standard error of the mean (SEM). * $P < 0.05$, **$P < 0.01$.

III – High-Amplitude Slow Wave Oscillations

A total of 28 MEG sensors covering a frontal-parietal (N_{crit} = 0.3 Hz; N_{SWA} = 0.43 Hz; $P < 0.0001$) and an occipital channel cluster (N_{SWA} = 0.38; $P < 0.0012$, Fig. 3E) showed a significant number of SWA. In frontal-parietal sensors we observed a trend toward differences in frequency of SWA between mental states ($F_{2,42}$ = 2.7; $P = 0.07$, Fig. 3E), but a highly significant difference in occipital sensors ($F_{2,42}$ = 5.9; $P < 0.0001$, Fig. 3E) with more SWA peaks in OFF (N_{SWA} = 0.51) versus ON (N_{SWA} = 0.27; t_{14} = 3.4; $P = 0.004$) and versus MID trials (N_{SWA} = 0.25; t_{14} = 2.6; $P = 0.02$) in the boccipital region.

IV – N2pc

Attentional target selection elicited an N2pc between 179 and 319 ms poststimulus (N2pc$_{crit}$ = 4fT, N2pc$_{max}$ = 61.7fT at 258 ms, $P < 0.001$; Fig. 4A,B) with no differences between hemispheres (t_{crit} = ±2.74, t_{max} = -1.74 at 71 ms, $P = 0.94$). The N2pc differed between mental states between poststimulus (F_{crit} = 3.53, F_{max} = 7.62 at 256 ms poststimulus, $P < 0.001$; Fig. 4C) with a larger amplitude in OFF (M: 78.69fT, SD: 46.16) versus MID (M: 50.65fT, SD: 28.89; t_{14} = 3.44, $P = 0.01$) and versus ON (M: 38.82fT, SD: 19.73; t_{14} = 4.1, $P = 0.002$) but no significant difference between ON and MID trials (t_{14} = 0.39, $P = 0.69$).

V – Local Sleep-N2pc Correlation

The number of SWA peaks correlated with the N2pc in OFF trials both in the fronto-parietal and the occipital channel cluster (rcrit = 0.53, fronto-parietal: r = 0.71; $P = 0.0044$; occipital: r = 0.6; $P = 0.014$) but not in ON (fronto-parietal: $r = -0.29$, $P = 0.13$; occipital: r = 0.45, $P = 0.04$) or MID trials (fronto-parietal: $r = -0.04$, $P = 0.56$; occipital: r = 0.19, $P = 0.22$; Fig. 5A). Note that peaks of SWA and the N2pc were both well separable from each other, though their topographies did show some overlap at occipital sensors. Specifically, the SWA peaks were evenly distributed across time intervals before and after stimulus onset and were not time-locked to the N2pc, which could have confused measures of SWA peaks with the occurrence of the N2pc amplitude. A respective analysis was performed for the occipital SWA peaks. We compared the number of SWA occurrences in the N2pc interval (200–300 ms) against that of a prestimulus interval (-100–0 ms) and that of a later poststimulus interval after the N2pc (400–500 ms) and found no difference in neither comparison (t_{14} = 1.66;

$P = 0.12$ and t_{14} = 0.93; $P = 0.37$). That is, the SWA peaks do not correlate in time with stimulus onset or N2pc emergence.

Importantly, the HFA (reflecting initial visual response) showed a significantly earlier onset than the N2pc (HFA: 83 ms poststimulus, SD: 14 ms; N2pc: 198 ms poststimulus, SD: 17 ms; t_{14} = 20.1, $P < 0.001$, Fig. 5B, left). Average HFA and N2pc showed a strong interaction with mental states with the N2pc increasing with decreasing HFA ($F_{2,87}$ = 11.17, $P < 0.001$; Fig. 5B, right). Similarly to SWA, only in OFF trials HFA correlated with the N2pc (r_{crit} = ±0.42, r = -0.54, $P = 0.04$), indicating that a low HFA amplitude is associated with an increased N2pc amplitude but not in ON (r = 0.07, $P = 0.71$) or MID trials (r = 0.31, $P = 0.27$, Fig. 5C). This enhancement of the N2pc appeared to be behaviorally relevant as in OFF trials, the N2pc was correlated to performance (r_{crit} = ±0.53, r = 0.57, $P = 0.02$) but not in ON (r = -0.14, $P = 0.29$) or MID trials (r = -11, $P = 0.33$; Fig. 5D).

Discussion

We examined how indicators of LS, cortical processing, and attentional selection change during MW. Participants performed a visual search paradigm, yielding robust increases in the HFA response in occipital MEG sensors, followed by the N2pc responses reflecting attentional target selection. The onset of the HFA increase in occipital MEG sensors was as early as ~90 ms and depended on how focused participants were on the task. Specifically, under MW, the HFA response was strongly decreased (i.e., no significant difference from baseline). But what caused the reduced HFA response during MW? If changes in the activation of the attention network would be the cause for the HFA reduction, we would also expect to observe a modulation at fronto-parietal sensors. Hence, we think that this very early occipital HFA reduction most likely corresponds with neuronal silencing (Vyazovskiy et al. 2011) reflecting local sleep. In parallel, the number of SWA periods increased with MW, consistent with participants experiencing phases of local sleep. In line with previous studies, the performance decreased under MW with manual reaction times being substantially prolonged. In contrast, neural markers of attentional selection were even more pronounced during MW and closely linked to behavioral responses. That is, even though low in performance during OFF trials, subjects that showed a higher N2pc amplitude performed better than those with a less pronounced N2pc. In general, processes of attentional target selection, as indexed by the N2pc,
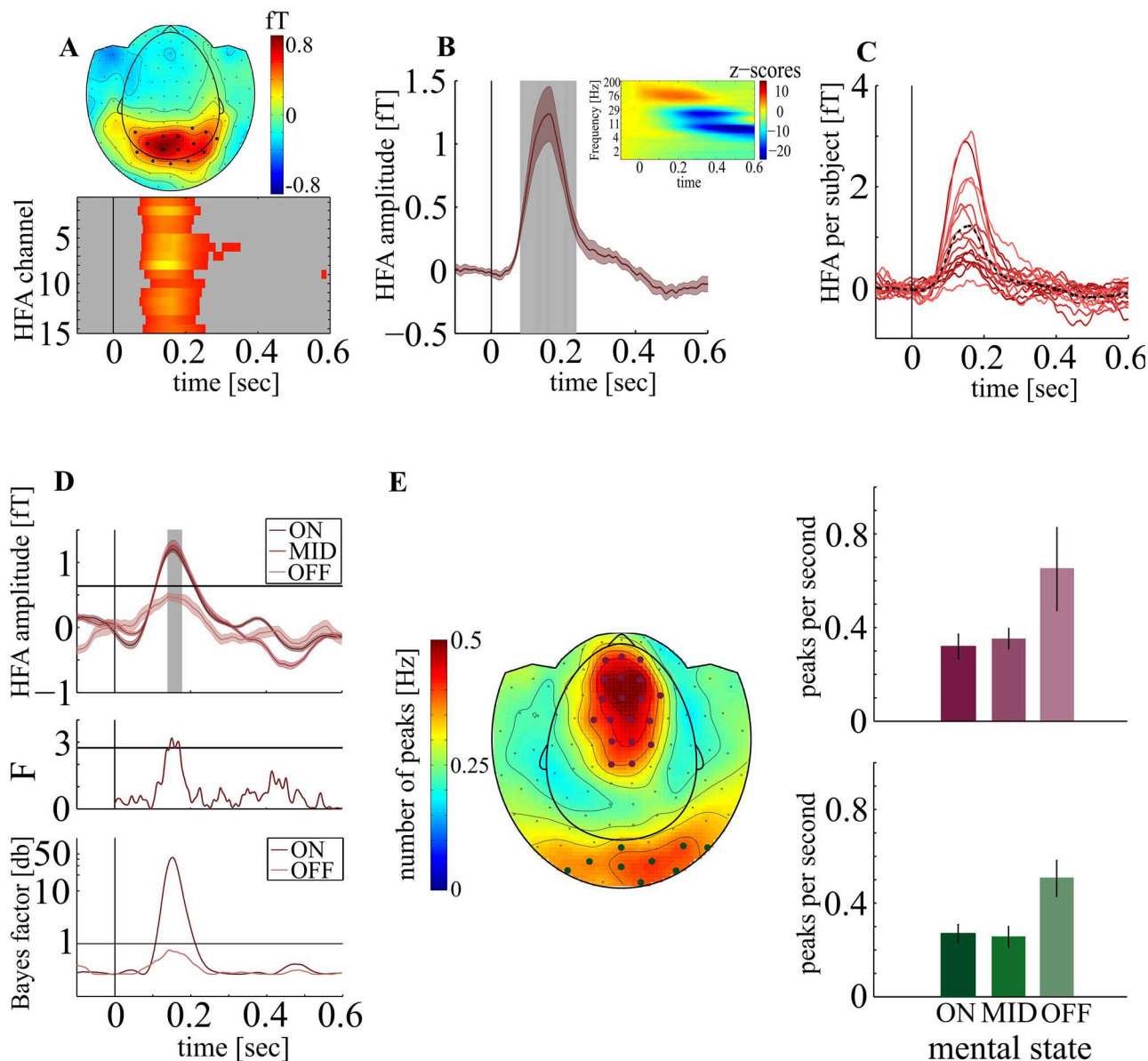
Figure 3. HFA A: Grand Average event related magnetic field (ERMF, 80–150 Hz) averaged across all focus trials and subjects between 0 and 300 ms poststimulus (top) shows 15 occipital sensors with significant response after stimulus onset. HFA onset and time course (bottom) are highly similar. B: Averaged across all trials and subjects, we found an HFA between 81 and 234 ms poststimulus (gray shaded area). The inset shows the time frequency representation averaged across all 15 MEG sensors. C: HFA response averaged across significant sensors for each subject. The dotted black line represents average across subjects. D top: HFA for each mental state, averaged across subjects. Gray inset represents time of significant differences in amplitude between mental states. The horizontal line represents critical peak amplitude modulation. D middle: Time course of F-values. The horizontal line represents critical F-value for statistical significance. D bottom: Bayes factor for amplitude modulation above baseline for ON and OFF condition. E: 28 Sensors showed significant SWA (left). The number of SWA peaks in occipital sensors (green, lower right) was significantly elevated during OFF trials (red: frontal sensors). The vertical lines represent stimulus onset. The shaded areas around curves represent SEM.

were rather increased during MW, potentially compensating for mental distraction.

Grating stimuli reliably evoked high-frequency activity in our noninvasive MEG recordings strongly resembling HFA responses in intracranial recording in early visual cortex with a modulation over baseline between 50 and 350 Hz, a fast increasing flank peaking around 200 ms, and a slowly decreasing flank in early visual cortex (Burke et al. 2014; Szczepanski et al. 2014; Golan et al. 2016, 2017; Gerber et al. 2017; Helfrich et al. 2018; Bartoli et al. 2019). The high similarity of the HFA response across subjects indicates that MEG in contrast to EEG can reliably pick up HFA

responses to visual stimuli, which even has been shown at the single trial level (Westner et al. 2018).

The HFA reduction during MW might not result from attentional decoupling but rather reflects neuronal silencing. Previous studies showed reduced electrophysiological responses during MW (Christoff et al. 2016) potentially due to attentional decoupling during MW but without deciphering the causal relation between MW and reduced cortical responses. The authors assumed that MW attenuates the cortical response (Christoff et al. 2016)—the HFA—since attentional resources are shifted inwards (Smallwood and Schooler 2006) in line with an
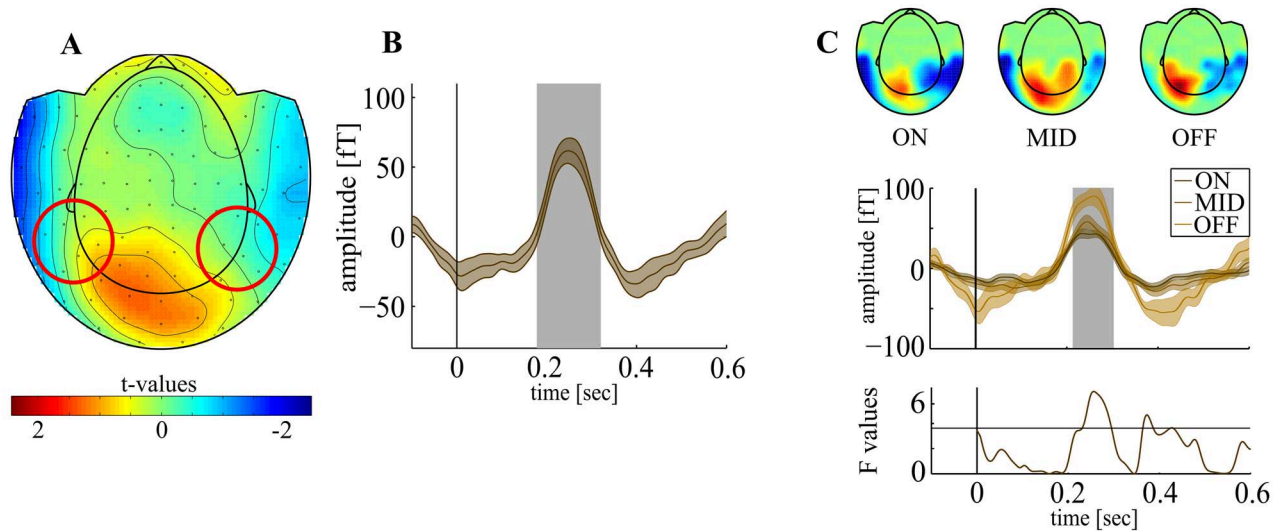
Figure 4. N2pc A: Grand average event related magnetic field (ERMF; 1–30 Hz) averaged across analyzed trials between 200 and 300 ms poststimulus. The circles represent probable location of underlying dipoles. B: N2pc averaged across analyzed trials and subjects. We found a significant N2pc between 179 and 319 ms poststimulus (gray inset). C top: Grand average ERMF between 200 and 300ms for the 3 mental states. Please note that the topographical field distribution and sensor locations are well in line with the literature with an occipito-temporal maximum evolving between 200 and 300 ms (Hopf et al. 2000; Boehler et al. 2011) and are highly consistent across the mental states. C middle: N2pc for each mental state, averaged across subjects. We found significant differences in N2pc amplitude between mental states (gray inset) between 213 and 298 ms poststimulus. C bottom: time course of F-values. The horizontal line represents critical F-value. The vertical lines represent stimulus onset. The shaded areas around curves represent SEM.

attentional decoupling account. However, we hypothesize that participants experience MW, since use-dependent neuronal silencing reduces sensory representation of the visual environment in the first place. First, any attentional reduction of the HFA should also predominantly be found in fronto-parietal structures (Szczepanski and Kastner 2013; Szczepanski and Knight 2014; Perrone-Bertolotti et al. 2020) where we did not find any strong stimulus-driven modulation in our study. Second, and most importantly, attentional modulations of cortical responses are amply attested with a reduction of responses (Smallwood et al. 2008; Kam et al. 2011, 2018) often using a contrast between task relevant versus irrelevant stimuli (Müsch et al. 2014). But task-irrelevant stimuli still evoked a comparable HFA response even though smaller in amplitude. Also, in audition even though ignoring the stimulation and attending a second task, clear stimulus-driven responses can be seen in frontal and temporal cortex (Dürschmid et al. 2016). Hence, although modulated by attention, ERPs and HFA response in previous studies were preserved. In contrast, the here observed HFA increase in occipital MEG sensors was virtually absent under MW (no significant difference from baseline). Hence, we assume the strong reduction in HFA during MW is most likely not driven by attention but rather corresponds with neuronal silencing (Vyazovskiy et al. 2011) reflecting local sleep.

Importantly, only local sleep would potentially allow for independent regulation of attentional resources. A global state change, in contrast, would downregulate attentional resources concomitantly. Hence, the strong interaction between N2pc and HFA speaks in favor of the occurrence of brief periods of local sleep, which is typically observed for single units during NREM sleep (Vyazovskiy et al. 2011; Siclari et al. 2017) even in the absence of signs of drowsiness. The HFA, a localized index of functionally selective activity (Crone et al. 1998; Miller et al. 2007) and most likely reflecting multiunit activity, seems almost completely absent during MW in regions strongly responding to stimulation. In addition, in sleep-restricted humans, the

waking EEG typically shows increased low-frequency power (SWA) reflecting the duration of prior wakefulness (Finelli et al. 2000; Leemburg et al. 2010; Vyazovskiy et al. 2011). Moreover, a homolog phenomenon to neuronal silencing can be observed in brain regions that were disproportionately used during waking (Rector et al. 2009) and involved in prior learning (Hung et al. 2013). Both strong signatures of local sleep—i.e., HFA reduction and SWA increase—did not overlap spatially but occurred locally (Bellesi et al. 2014), which points at different functions.

SWA could serve as a carrier wave that allows or drives the transfer of information between structures such as the hippocampus and neocortex. It occurred over centro-parietal, sensory, and motor area regions relative to the rest of the brain in a previous study (Castelnovo et al. 2016). In line with those results, we found an increase in centro-parietal and in occipital cortex. The parallel SWA increase between these regions argues strongly for a common plasticity-dependent component to sleep regulation (Murphy et al. 2011). Importantly, these signatures of local sleep occur even in subjects which are not sleep deprived (Quercia et al. 2018). The here observed SWA does probably indicate sleep need (Huber et al. 2004) but it varies locally in time, since subjective ON and OFF task ratings were evenly distributed across the entire experiment. Hence, we can rule out the possibility that the observed signatures of LS only increased with time and thus without any strong relation to MW.

Local sleep periods are of behavioral relevance since they are associated with cognitive lapses (Nir et al. 2017) that are marked by prolonged reaction times (Bernardi et al. 2015; Nir et al. 2017). The response time prolongation during such lapses probably arises due to reduced stimulus-triggered activity in visual areas causing a lower quality perceptual representation of the target stimulus (Weissman et al. 2006). Consistent with subjects experiencing attentional lapses, we also found reaction times to be substantially longer during MW. The observed motor slowing might in part explain behavioral errors in previous studies on MW as well. MW manifests behaviorally
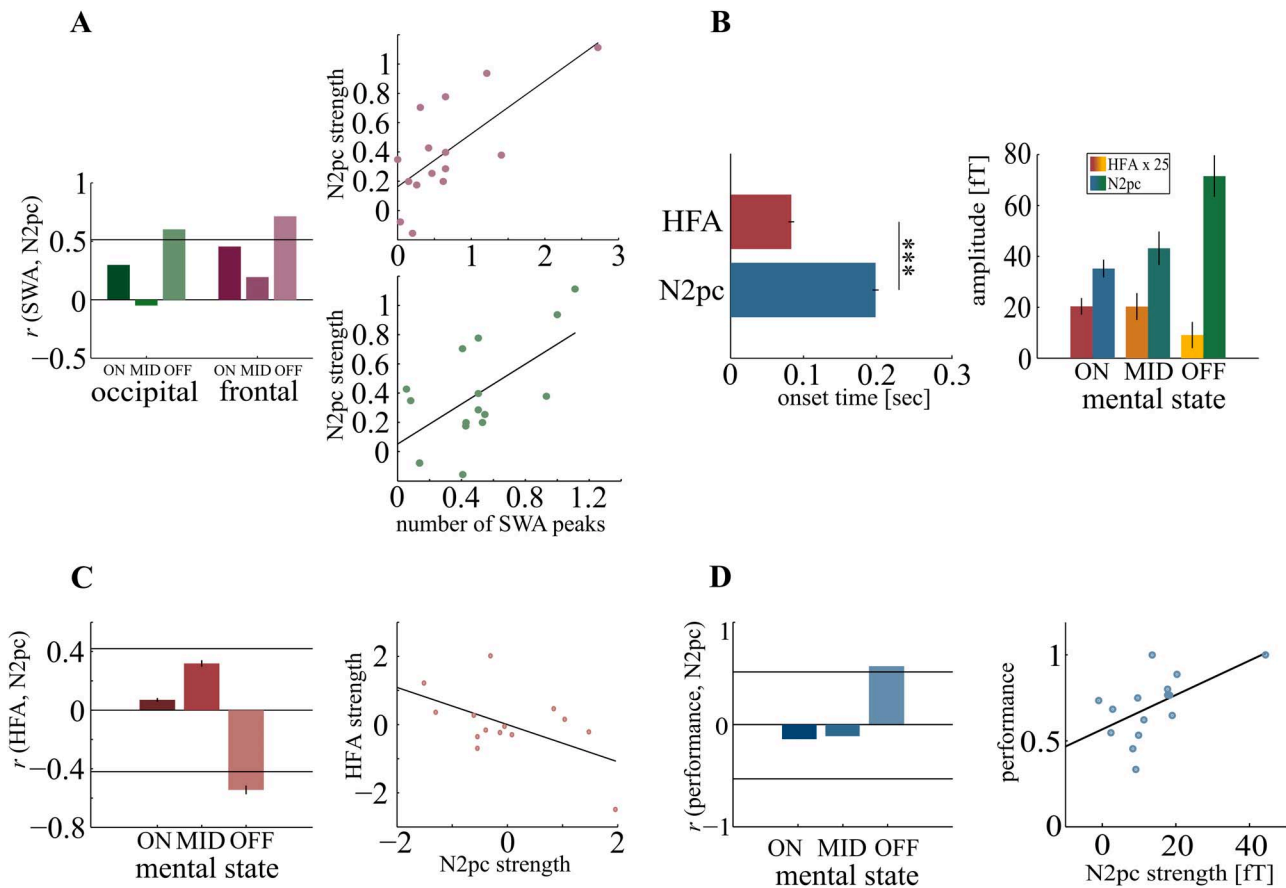
Figure 5. Local sleep-N2pc correlation A: Correlation between SWA count and N2pc amplitude was significant only during OFF trials. The horizontal line represents critical correlation value (left). Scatterplots showing the correlation between SWA count and N2pc for OFF trials in frontal (red, upper) and occipital sensors (green, lower right). B: Onset times for HFA and N2pc differed significantly (left). Average HFA and N2pc amplitude for each mental state. Note that the HFA is scaled up in this plot to compensate for lower amplitudes (right). C: Correlation between HFA and N2pc reached significance only during OFF trials. The horizontal lines represent critical correlation values (left). Scatterplot showing the correlation between HFA and N2pc during OFF trials (right). D: Correlation between performance and N2pc reached statistical significance only during OFF trials. The horizontal lines represent critical correlation values (left). Scatterplot showing the correlation between performance and N2pc strength during OFF trials (right). The error bars represent the SEM. ***$P < 0.001$.

especially in highly automated task like reading or the Sustained-Attention-to-Response-Task (SART) (Smallwood et al. 2008; Seli 2016). Hence, behavioral decrements in SART experiments could result from a slowing of a general control of manual responses which could hypothetically be beneficial to prevent overhasty decisions when sensory evidence is low. Lower sensory evidence on MW trials would also be in line with an upregulation of the N2pc attention allocation response. That is, though low in performance, subjects with stronger N2pc perform better, underscoring the behavioral relevance of an upregulation of attentional resources to keep performing the task under MW.

Indeed, our major finding is that during local sleep the strength of SWA and neuronal silencing predicts how attentional reallocation is modulated. Previously, MW was found to positively correlate with task-irrelevant distraction indicating that MW reveals individual susceptibility to task-irrelevant distraction including both internal and external sources (Forster and Lavie 2014). Specifically, it was suggested that MW and external distraction reflect distinct, yet correlated constructs related to working memory (Unsworth and McMillan 2014). Hence, the N2pc increase is in line with previous studies showing that target-distractor disambiguation increases with distractor load (Mazza et al. 2009) and suggesting a stronger influence of

distractors under momentary attention lapses (Weissman et al. 2006). These results indicate that MW does not inflict attentional decoupling (Smallwood and Schooler 2006). Given the earlier onset of HFA compared to the N2pc, the reduction in HFA during MW (worse stimulus representation) might consequently lead to the upregulation of the N2pc (more target enhancement and/or distractor suppression needed). Since experience sampling can only be applied in a subset of trials, a trial-wise measure of MW cannot be provided. Hence, we cannot dissolve the number of trials by which neuronal silencing is ahead the N2pc upregulation.

The N2pc was originally interpreted as suppression of distractors (Luck and Hillyard 1994b), but others argued that the N2pc reflects target selection (Eimer 1996) and is now considered a composition of overlapping processes of both target processing (target negativity, Nt) and distractor suppression (distractor positivity, Pd) (Hickey et al. 2009; Hilimire et al. 2012; Gaspar and McDonald 2014). Since we presented the target simultaneously with a color pop-out nontarget in the opposite visual field, both the target selection (Nt contralateral to the target) as well as distractor suppression (Pd contralateral to the pop-out nontarget) will contribute to the amplitude of the observed N2pc waveform. Importantly, we observed an enhanced N2pc when the subjects

were in a state of MW. Since our stimuli always contained both laterally presented targets and distractors, we cannot unambiguously decide as to whether the enhanced N2pc was caused by a stronger target enhancement, increased distractor suppression, or both, or whether the N2pc would be rather generally suppressed in the focused state. In general, the N2pc component seems to strongly depend on stimulation parameters, showing larger activation differences between hemispheres when more than one item per visual field is presented, the discrimination task is more complex (e.g., a feature conjunction task), and the target is in the lower visual field (Luck et al. 1997). Hence, we chose our visual search display accordingly to maximize the observed N2pc amplitudes with the target being located in the lower visual field, multiple surrounding irrelevant distractor items, and a task requiring high spatial scrutiny. Most importantly, the target was always an easily detectable color pop-out item, requiring no time-consuming search process that might have smeared out N2pc responses over time. In fact, the N2pc was elicited at the expected time range of 200 ms irrespective of the mental state. That is, the initial target selection was not delayed under conditions of MW as it has been previously reported when target saliency was low (Töllner et al. 2011), during periods of attentional blink or shortly after task switches (Corriveau et al. 2012; Lagroix et al. 2015). Still, there was a substantial increase in response time (about 400 ms), when subjects reported to be "OFF" task which might have reflected lower sensory evidence, a delayed processing of the information provided by the N2pc, or could be caused by parallel interfering processes of MW. In fact, Lagroix et al. (2015) suspected that a response time increase caused by the attentional blink (about 300 ms) was not fully accounted for by N2pc latency differences (about 30 ms). However, later steps of information processing which might be impacted by MW—such as extraction of information or response planning—might play a role. Importantly, only when participants experienced MW (OFF task), the amplitude of the N2pc was positively correlated with performance. That is, a larger N2pc, typically associated with a stronger focusing onto the target and potentially reflecting better distractor suppression (Mazza et al. 2009; Donohue et al. 2016), might have partially compensated for the MW. Alternatively, it is reasonable to assume that the enhancement of the N2pc amplitude might not reflect a stronger selective distractor suppression but the participation of more neurons in the attention process. One might speculate that the attentional tuning is less strict and, hence, broader under MW with more (less selective) neurons responding to the attention focusing process, and in consequence leading to a larger N2pc. Since we have no baseline measure (MW without N2pc increase), it is difficult to determine how much the enhancement of the N2pc might have helped performance under MW. Still, at the between-subjects level, under MW, a higher N2pc amplitude was associated with a better performance speaking for a behavioral relevance of the N2pc increase.

When investigating MW, a major challenge is how to reliably capture phases of reduced focusing on the task. Frequently prompting thought probes during the course of the experiments will most likely discourage MW, hence, we chose to assess the participants mental state on only 20% of the trials. As a consequence, trial numbers are inherently limited for comparing neural responses between mental states. Furthermore, participants reported for the majority of trials (51%) to be "on task", which might be caused by the perceptually rather demanding discrimination task, or also be influenced by participants trying to respond in a socially desirable way. Nevertheless, the markers of local sleep (SWA increase, HFA reduction) match participants

self-reports with being "off the task" and might also provide future measures depending less on self-report.

Our critical conclusion is that MW is strongly linked to cortical dynamics associated with local sleep and that attentional resources needed for visual search are upregulated to circumvent restrictions caused by limited sensory evidence. Occipital HFA, which shows a strong stimulus response comparable to intracranial recordings, falls out when participants have the subjective impression of being off the task, commensurate with an increase in periods of SWA increase. Attentional decoupling as predicted for being off the task is expected to produce a decrease in the N2pc (Schad et al. 2012; Christoff et al. 2016). But reduced sensory evidence compels stronger attentional allocation to key features in the environment and hence a stronger target-distractor disambiguation during MW. Hence, these results indicate that MW does not lead to a global blackout of HFA but cortical regions generating the target-distractor disambiguation also flexibly react to internal distractions. These functional explanations indicate that expected input to visual stimulation is tracked and stronger reallocation of spatial attention is generated when sensory evidence is scarce, presumably by frontal cortical areas. In sum, we provide evidence that MW is strongly related to local sleep and establish a direct link between boosted attentional resources due to local sleep during waking.

Notes

Funding

References

Andrillon T, Windt J, Silk T, Drummond SPA, Bellgrove MA, Tsuchiya N. 2019. Does the mind wander when the brain takes a break? Local sleep in wakefulness, attentional lapses and mind-wandering. *Front Neurosci*. **13**:1–10.

Bartoli E, Bosking W, Li Y, Beauchamp MS, Yoshor D, Foster B. 2019. Distinct Narrow and Broadband Gamma Responses in Human Visual Cortex. *bioRxiv*. https://doi.org/10.1101/572313.

Bellesi M, Riedner BA, Garcia-Molina GN, Cirelli C, Tononi G. 2014. Enhancement of sleep slow waves: underlying mechanisms and practical consequences. *Front Syst Neurosci*. **8**:1–17.

Berens P, Keliris GA, Ecker AS, Logothetis NK, Tolias AS. 2008. Comparing the feature selectivity of the gamma-band of the local fi eld potential and the underlying spiking activity in primate visual cortex. *Front Syst Neurosci*. **2**:199–207.

Bernardi G, Siclari F, Yu X, Zennig C, Bellesi M, Ricciardi E, Cirelli C, Ghilardi MF, Pietrini P, Tononi G. 2015. Neural and Behavioral correlates of extended training during sleep deprivation in humans: evidence for local, task-specific effects. *J Neurosci*. **35**:4487–4500.

Boehler CN, Tsotsos JK, Schoenfeld MA, Heinze H-J, Hopf J-M. 2011. Neural mechanisms of surround attenuation and distractor competition in visual search. *J Neurosci*. **31**:5213–5224.

Brainard DH. 1997. The psychophysics toolbox. *Spat Vis.* **10**:433–436.

Brandmeyer T, Delorme A. 2018. Reduced mind wandering in experienced meditators and associated EEG correlates. *Exp Brain Res.* **236**:2519–2528.

Burke JF, Long NM, Zaghloul KA, Sharan AD, Sperling MR, Kahana MJ. 2014. Human intracranial high-frequency activity maps episodic memory formation in space and time. *Neuroimage.* **85**:834–843.

Buzsáki G, Anastassiou CA, Koch C. 2012. The origin of extracellular fields and currents-EEG, ECoG, LFP and spikes. *Nat Rev Neurosci.* **13**:407–420.

Carriere JSA, Cheyne JA, Smilek D. 2008. Everyday attention lapses and memory failures: the affective consequences of mindlessness. *Conscious Cogn.* **17**:835–847.

Castelnovo A, Riedner BA, Smith RF, Tononi G, Boly M, Benca RM. 2016. Scalp and source power topography in sleepwalking and sleep terrors: a high-density EEG study. *Sleep.* **39**:1815–1825.

Christoff K, Irving ZC, Fox KCR, Spreng RN, Andrews-Hanna JR. 2016. Mind-wandering as spontaneous thought: a dynamic framework. *Nat Rev Neurosci.* **17**:718–731.

Coon WG, Schalk G. 2016. A method to establish the spatiotemporal evolution of task-related cortical activity from electrocorticographic signals in single trials. *J Neurosci Methods.* **271**:76–85.

Corriveau I, Fortier-Gauthier U, Pomerleau VJ, McDonald J, Dell'Acqua R, Jolicoeur P. 2012. Electrophysiological evidence of multitasking impairment of attentional deployment reflects target-specific processing, not distractor inhibition. *Int J Psychophysiol.* **86**:152–159.

Crone N, Miglioretti DL, Gordon B, Lesser RP. 1998. Functional mapping of human sensorimotor cortex with electrocorticographic spectral analysis. II. Event-related synchronization in the gamma band. *Brain.* **121**:2301–2315.

Crone NE, Boatman D, Gordon B, Hao L. 2001. Induced electrocorticographic gamma activity during auditory perception. *Clin Neurophysiol.* **112**:565–582.

Donohue SE, Bartsch MV, Heinze HJ, Schoenfeld MA, Hopf JM. 2018. Cortical mechanisms of prioritizing selection for rejection in visual search. *J Neurosci.* **38**:4738–4748.

Donohue SE, Woldorff MG, Hopf JM, Harris JA, Heinze HJ, Schoenfeld MA. 2016. An electrophysiological dissociation of craving and stimulus-dependent attentional capture in smokers. *Cogn Affect Behav Neurosci.* **16**:1114–1126.

Dürschmid S, Edwards E, Reichert C, Dewar C, Hinrichs H, Heinze HJ, Kirsch HE, Dalal SS, Deouell LY, Knight RT. 2016. Hierarchy of prediction errors for auditory events in human temporal and frontal cortex. *Proc Natl Acad Sci U S A.* **113**:6755–6760.

Eimer M. 1996. The N2pc component as an indicator of attentional selectivity. *Electroencephalogr Clin Neurophysiol.* **99**:225–234.

Finelli LA, Baumann H, Borbély AA, Achermann P. 2000. Dual electroencephalogram markers of human sleep homeostasis: correlation between theta activity in waking and slow-wave activity in sleep. *Neuroscience.* **101**:523–529.

Forster S, Lavie N. 2014. Distracted by your mind? Individual differences in distractibility predict mind wandering. *J Exp Psychol Learn Mem Cogn.* **40**:251–260.

Gaspar JM, McDonald JJ. 2014. Suppression of salient objects prevents distraction in visual search. *J Neurosci.* **34**: 5658–5666.

Gerber EM, Golan T, Knight RT, Deouell LY. 2017. Cortical representation of persistent visual stimuli. *Neuroimage.* **161**:67–79.

Golan T, Davidesco I, Meshulam M, Groppe DM, Mégevand P, Yeagle EM, Goldfinger MS, Harel M, Melloni L, Schroeder CE et al. 2016. Human intracranial recordings link suppressed transients rather than "filling-in" to perceptual continuity across blinks. *Elife.* **5**:1–28.

Golan T, Davidesco I, Meshulam M, Groppe DM, Mégevand P, Yeagle EM, Goldfinger MS, Harel M, Melloni L, Schroeder CE et al. 2017. Increasing suppression of saccade-related transients along the human visual hierarchy. *Elife.* **6**:1–15.

He J, Becic E, Lee YC, McCarley JS. 2011. Mind wandering behind the wheel: performance and oculomotor correlates. *Hum Factors.* **53**:13–21.

Helfrich RF, Fiebelkorn IC, Szczepanski SM, Lin JJ, Parvizi J, Knight RT, Kastner S. 2018. Neural mechanisms of sustained attention are rhythmic. *Neuron.* **99**:854–865.e5.

Hickey C, Di Lollo V, McDonald JJ. 2009. Electrophysiological indices of target and distractor processing in visual search. *J Cogn Neurosci.* **21**:760–775.

Hilimire MR, Hickey C, Corballis PM. 2012. Target resolution in visual search involves the direct suppression of distractors: evidence from electrophysiology. *Psychophysiology.* **49**:504–509.

Hilimire MR, Mounts JRW, Parks NA, Corballis PM. 2011. Dynamics of target and distractor processing in visual search: evidence from event-related brain potentials. *Neurosci Lett.* **495**:196–200.

Hopf J-M, Luck SJ, Girelli M, Hagner T, Mangun GR, Scheich H, Heinze H-J. 2000. Neural sources of focused attention in visual search. *Cereb Cortex.* **10**:1233–1241.

Huber R, Felice Ghilardi M, Massimini M, Tononi G. 2004. Local sleep and learning. *Nature.* **430**:78–81.

Hung C-S, Sarasso S, Ferrarelli F, Riedner B, Ghilardi MF, Cirelli C, Tononi G. 2013. Local experience-dependent changes in the wake EEG after prolonged wakefulness. *Sleep.* **36**:59–72.

Kam JWY, Dao E, Farley J, Fitzpatrick K, Smallwood J, Schooler JW, Handy TC. 2011. Slow fluctuations in attentional control of sensory cortex. *J Cogn Neurosci.* **23**:460–470.

Kam JWY, Solbakk AK, Endestad T, Meling TR, Knight RT. 2018. Lateral prefrontal cortex lesion impairs regulation of internally and externally directed attention. *Neuroimage.* **175**:91–99.

Kleiner M, Brainard D, Pelli D, Ingling A, Murray R, Broussard C. 2007. What's new in Psychtoolbox-3. *Perception.* **36**:1.

Kucyi A, Salomons TV, Davis KD. 2013. Mind wandering away from pain dynamically engages antinociceptive and default mode brain networks. *Proc Natl Acad Sci.* **110**:18692–18697.

Kupers E, Wang H, Amano K, Kay K, Heeger D, Winawer J. 2017. A non-invasive, quantitative study of broadband spectral responses in human visual cortex. *PLoS One.* **13**:e0193107.

Lachaux J-P, George N, Tallon-Baudry C, Martinerie J, Hugueville L, Minotti L, Kahane P, Renault B. 2005. The many faces of the gamma band response to complex visual stimuli. *Neuroimage.* **25**:491–501.

Lagroix HEP, Grubert A, Spalek TM, Di Lollo V, Eimer M. 2015. Visual search is postponed during the period of the AB: an event-related potential study. *Psychophysiology.* **52**:1031–1038.

Lee B, Martin P, Valberg A. 1988. The physiological basis of heterochromatic flicker photometry. *J Physiol.* **404**:323–347.

Leemburg S, Vyazovskiy VV, Olcese U, Bassetti CL, Tononi G, Cirelli C. 2010. Sleep homeostasis in the rat is preserved during chronic sleep restriction. *Proc Natl Acad Sci U S A.* **107**:15939–15944.

Leszczyński M, Barczak A, Kajikawa Y, Ulbert I, Falchier AY, Tal I, Haegens S, Melloni L, Knight RT, Schroeder CE. 2020. Dissociation of broadband high-frequency activity and neuronal firing in the neocortex. *Sci Adv.* **6**:1–13.

Leszczynski M, Chaieb L, Reber TP, Derner M, Axmacher N, Fell J. 2017. Mind wandering simultaneously prolongs reactions and promotes creative incubation. *Sci Rep.* **7**:1–9.

Liu J, Newsome WT. 2006. Local field potential in cortical area MT: stimulus tuning and behavioral correlations. *J Neurosci.* **26**:7779–7790.

Luck SJ. 2014. *An Introduction to the Event-Related Potential Technique.* 2nd ed. Cambridge, MA: MIT Press.

Luck SJ, Girelli M, McDermott MT, Ford MA. 1997. Bridging the gap between monkey neurophysiology and human perception: an ambiguity resolution theory of visual selective attention. *Cogn Psychol.* **33**:64–87.

Luck SJ, Hillyard SA. 1994a. Spatial filtering during visual search: evidence from human electrophysiology. *J Exp Psychol Hum Percept Perform.* **20**:1000–1014.

Luck SJ, Hillyard SA. 1994b. Electrophysiological correlates of feature analysis during visual search. *Psychophysiology.* **31**:291–308.

Manning JR, Jacobs J, Fried I, Kahana MJ. 2009. Broadband Shifts in Local Field Potential Power Spectra Are Correlated with Single-Neuron Spiking in Humans. *J Neurosci.* **29**:13613–13620.

Maris E, Oostenveld R. 2007. Nonparametric statistical testing of EEG- and MEG-data. *J Neurosci Methods.* **164**:177–190.

Mazza V, Turatto M, Caramazza A. 2009. Attention selection, distractor suppression and N2pc. *CORTEX.* **45**:879–890.

Miller KJ, denNijs M, Shenoy P, Miller JW, Rao RPN, Ojemann JG. 2007. Real-time functional brain mapping using electrocorticography. *Neuroimage.* **37**:504–507.

Miller KJ, Sorensen LB, Ojemann JG, Den Nijs M. 2009. Power-law scaling in the brain surface electric potential. *PLoS Comput Biol.* **5**:e1000609.

Mukamel R, Gelbard H, Arieli A, Hasson U, Fried I, Malach R. 2005. Neuroscience: coupling between neuronal firing, field potentials, and fMRI in human auditory cortex. *Science.* **309**:951–954.

Murphy M, Huber R, Esser S, Riedner BA., Massimini M, Ferrarelli F, Felice Ghilardi M, Tononi G. 2011. The cortical topography of local sleep. *Curr Top Med Chem.* **11**:2438–2446.

Müsch K, Hamamé CM, Perrone-Bertolotti M, Minotti L, Kahane P, Engel AK, Lachaux JP, Schneider TR. 2014. Selective attention modulates high-frequency activity in the face-processing network. *Cortex.* **60**:34–51.

Nir Y, Andrillon T, Marmelshtein A, Suthana N, Cirelli C, Tononi G, Fried I. 2017. Selective neuronal lapses precede human cognitive lapses following sleep deprivation. *Nat Med.* **23**:1474–1480.

Pelli DG. 1997. The VideoToolbox software for visual psychophysics: transforming numbers into movies. *Spat Vis.* **10**:437–442.

Perrone-Bertolotti M, El Bouzaïdi Tiali S, Vidal JR, Petton M, Croize AC, Deman P, Rheims S, Minotti L, Bhattacharjee M, Baciu M et al. 2020. A real-time marker of object-based attention in the human brain. A possible component of a "gate-keeping mechanism" performing late attentional selection in the ventrolateral prefrontal cortex. *Neuroimage.* **210**:116574.

Privman E, Malach R, Yeshurun Y. 2013. Modeling the electrical field created by mass neural activity. *Neural Netw.* **40**:44–51.

Quercia A, Zappasodi F, Committeri G, Ferrara M. 2018. Local use-dependent sleep in wakefulness links performance errors to learning. *Front Hum Neurosci.* **12**:1–17.

Ray S, Maunsell JHR. 2011. Different origins of gamma rhythm and high-gamma activity in macaque visual cortex. *PLoS Biol.* **9**:e1000610.

Ray S, Niebur E, Hsiao SS, Sinai A, Crone NE. 2008. High-frequency gamma activity (80–150Hz) is increased in human cortex during selective attention. *Clin Neurophysiol.* **119**:116–133.

Rector DM, Schei JL, Van Dongen HPA, Belenky G, Krueger JM. 2009. Physiological markers of local sleep. *Eur J Neurosci.* **29**:1771–1778.

Schad DJ, Nuthmann A, Engbert R. 2012. Your mind wanders weakly, your mind wanders deeply: objective measures reveal mindless reading at different levels. *Cognition.* **125**:179–194.

Seli P. 2016. The attention-lapse and motor decoupling accounts of SART performance are not mutually exclusive. *Conscious Cogn.* **41**:189–198.

Siclari F, Baird B, Perogamvros L, Bernardi G, LaRocque JJ, Riedner B, Boly M, Postle BR, Tononi G. 2017. The neural correlates of dreaming. *Nat Neurosci.* **20**:872–878.

Smallwood J. 2011. Mind-wandering while reading: attentional decoupling, mindless reading and the Cascade model of inattention. *Lang Linguist Compass.* **5**:63–77.

Smallwood J, Beach E, Schooler JW, Handy TC. 2008. Going AWOL in the brain: mind wandering reduces cortical analysis of external events. *J Cogn Neurosci.* **20**:458–469.

Smallwood J, Schooler JW. 2006. The restless mind. *Psychol Bull.* **132**:946–958.

Szczepanski SM, Crone NE, Kuperman RA, Auguste KI, Parvizi J, Knight RT. 2014. Dynamic changes in phase-amplitude coupling facilitate spatial attention control in Fronto-parietal cortex. *PLoS Biol.* **12**:e1001936.

Szczepanski SM, Kastner S. 2013. Shifting attentional priorities: control of spatial attention through hemispheric competition. *J Neurosci.* **33**:5411–5421.

Szczepanski SM, Knight RT. 2014. Insights into human behavior from lesions to the prefrontal cortex. *Neuron.* **83**:1002–1018.

Tallon-Baudry C, Bertrand O, Hénaff M-A, Isnard J, Fischer C. 2005. Attention modulates gamma-band oscillations differently in the human lateral occipital cortex and fusiform gyrus. *Cereb Cortex.* **15**:654–662.

Töllner T, Zehetleitner M, Gramann K, Müller HJ. 2011. Stimulus saliency modulates pre-attentive processing speed in human visual cortex. *PLoS One.* **6**:e16276.

Unsworth N, McMillan BD. 2014. Similarities and differences between mind-wandering and external distraction: a latent variable analysis of lapses of attention and their relation to cognitive abilities. *Acta Psychol (Amst).* **150**:14–25.

Vyazovskiy VV, Harris KD. 2013. Sleep and the single neuron: the role of global slow oscillations in individual cell rest. *Nat Rev Neurosci.* **14**:443–451.

Vyazovskiy VV, Olcese U, Hanlon EC, Nir Y, Cirelli C, Tononi G. 2011. Local sleep in awake rats. *Nature.* **472**:443–447.

Weissman DH, Roberts KC, Visscher KM, Woldorff MG. 2006. The neural bases of momentary lapses in attention. *Nat Neurosci.* **9**:971–978.

Westner BU, Dalal SS, Hanslmayr S, Staudigl T. 2018. Across-subjects classification of stimulus modality from human MEG high frequency activity. *PLoS Comput Biol.* **14**:1–14.

Yanko MR, Spalek TM. 2014. Driving with the wandering mind: the effect that mind-wandering has on driving performance. *Hum Factors.* **56**:260–269.